
The Department of Bioengineering

# The development of a Miniaturised and Integrated ECMO system

Christopher John Lynn

Submitted in 2012

‘This thesis is the result of the author’s original research. It has been composed by the author and has not been previously submitted for examination which has led to the award of a degree.’



Signed:

Date:

***Abstract***

**Background:** Extracorporeal membrane oxygenation (ECMO) is a treatment used to temporarily replace the function of the heart and/or lungs over an extended period of time to allow for organ recovery. The first successful use of an extracorporeal life support system over an extended period of time was achieved in 1972. Since then ECMO has been responsible for saving the lives of many thousands of patients, particularly in the neonatal population. Despite this technical success, ECMO is associated with high morbidity and mortality rates due to the invasive nature of the treatment and the technical complexity of the system. Complications associated with ECMO can be considered in two categories; patient related and technical complications or failures. These complications include but are not limited to haemolysis, thrombosis and inflammatory response. After extensive review of the medical literature and consideration of ECMO system design requirements it was determined that a miniaturized and integrated system represents a natural evolution of life support technology, addressing the failings of current system designs. Such a system should allow for reduced blood contact surface area, reduce priming volume, increased accessibility of the patient to other treatments and should allow for rapid deployment of the system, which has been shown to be essential in improving patient outcomes.

**Materials and Methods:** The work strategy adopted throughout employed the following steps: concept development, computational design and simulation, physical testing and ultimately animal testing under clinically mimetic conditions. Computational simulation was used as a tool for design optimization and to provide quantitative and qualitative feedback on the performance of the physical prototypes. This allowed the number of design iterations to be reduced minimizing the time and cost associated with an iterative design based strategy. Physical testing was conducted under clinically mimetic conditions wherever possible to ensure that the performance of each component and the complete integrated design was satisfactory prior to animal testing.

**Results:** This project has produced a miniaturized blood pump, oxygenator and heat exchange system and corresponding computer models. Physical testing of each component indicated that the designs were capable of achieving acceptable hydrodynamic and haemodynamic performance. These results were verified with the computational models, which showed a close correlation.
Testing of the integrated strategy showed that the complete device was capable of meeting the performance requirements of a live animal experiment, producing acceptable levels of oxygen transfer, heat addition and overcoming significant pressure head over an extended period of time.
The results of the large animal testing indicated that the miniaturized and integrated design was capable of reliably producing acceptable gas exchange, temperature maintenance and blood flow rate allowing for the successful support of a live animal over an extended period of time.

**The following are the main achievements of this work;**

1) The use of computational models to reduce the iterative load associated complex device development was confirmed as viable.

2) We were able to utilize an integrated rapid prototyping approach to develop working prototypes of individual components for laboratory testing.

3) There was a clear correlation between the results predicted by computational methods and those obtained in the laboratory.

4) We were able to employ computational design approach to optimizing integration thereby reducing the number of rapid prototypes required for testing.

5) It is possible to produce a fully integrated low foot print, priming volume and blood-material contact surface area EMCO system with adequate performance characteristics suitable for clinical use.

6) The integrated ECMO system was proven computationally and in the lab was compatible with deployment under near clinical conditions.

7) The integrated ECMO design was proven capable of partially supporting a large animal under clinically mimetic conditions over an extended period of time.

8) A novel heat exchange technology was developed that allows the miniaturized and integrated system to be independent of a mains water supply.

***Table of Contents***

***Table of Figures***

***Table of Equations***

***Table of tables***

# 1. Background

# 1.1. Introduction

## 1.1.1. The ECMO Procedure

Extracorporeal membrane oxygenation (ECMO) is used to treat patients with life threatening pulmonary and/or cardiac failure. It is most commonly used in emergency situations after failure of another medical treatment (Marasco, Lukas et al. 2008). There are two types of ECMO treatment: veno-venous, which provides respiratory support and veno-arterial, which provides both cardiac and respiratory support. A diagram of a typical ECMO circuit can be seen within Figure 1 and a picture of a current ECMO system in use is shown within Figure 2.

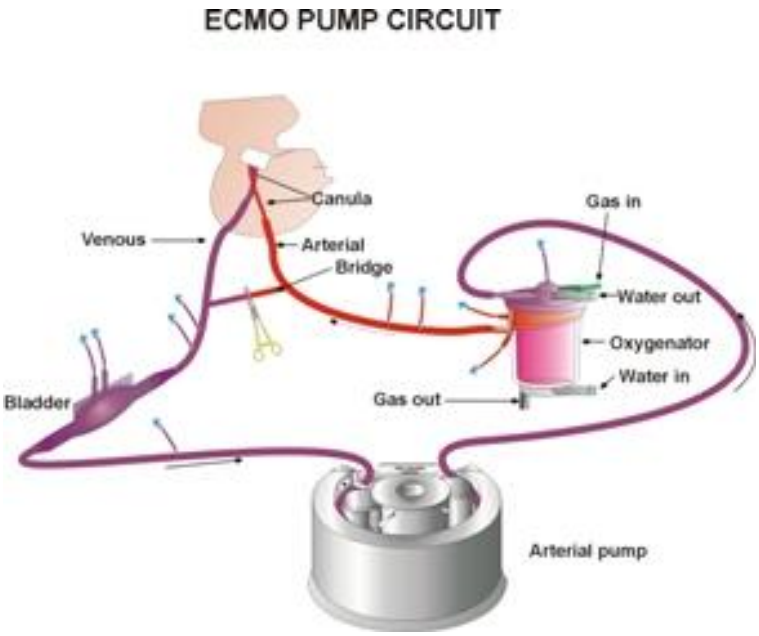


**Figure 1: A Diagram of an ECMO circuit taken from (Brown and Goldman 2008).**

**Figure 2: An ECMO circuit being used to treat a neonate. Taken from (Smith 2007)**

Venous cannulation of the patient is typically achieved through the right internal jugular vein to the right atrium. Blood is removed from the patient and, in a circuit driven by a roller pump, will enter a venous bladder. This bladder is used to ensure that the forward pump flow does not exceed the rate of blood drainage from the patient. If outflow exceeds inflow the bladder will collapse; an alarm will sound and cause the pump to slow down or switch off (Frenckner and Radell 2008).

From the pump the blood then enters a membrane oxygenator. Modern oxygenator designs incorporate membrane hollow fibres in an extra-luminal flow arrangement with blood flowing over the hollow fibres and oxygen passing through them. Oxygen diffuses into, and $CO_2$ is removed from, the blood.

Heat loss occurs throughout the circuit and therefore a heat exchanger is required in order to maintain normothermia of the patient. Some oxygenators have a heat exchanger built into the design; otherwise, and most commonly in ECMO, an independent heat exchanger is required. Blood is then circulated back to the patient. In VA ECMO blood is typically returned through the right common carotid artery to the aortic arch and for VV ECMO it is returned to the internal jugular vein or the inferior vena cava (Bartlett, Toomasian et al. 1986).

### 1.1.2. The Origins of ECMO

Extracorporeal circulation to temporarily support the heart and lung was first attempted by Gibbon in 1953 (Gibbon 1954). This extracorporeal support was known as cardiopulmonary bypass (CPB). The aim of CPB was to maintain life while the heart was stopped, providing surgeons with stationary operating conditions.

The concept of *prolonged* extracorporeal support was first attempted by Dr D. S. Melrose at the Hammersmith hospital in 1962. A patient was treated post cardiac surgery in the ward using a rotating disk film oxygenator for 4 days before, unfortunately, dying. Figure 3 shows Dr Melrose and his patient in the Hammersmith hospital.

**Figure 3: Dr D. S. Melrose performing prolonged extracorporeal support on the ward at Hammersmith hospital (Taken with permission form Professor T. Gourlay's personal Library).**

Early extracorporeal equipment could only offer short term support due to the large amount of damage caused to the patient's blood through protein denaturation (Dobell, Mitri et al. 1965; Sinard and Bartlett 1990). The first successful long term support was achieved in 1972 (Hill, O'Brien et al. 1972). The equipment used featured a newly developed membrane oxygenator and from that point on extended extracorporeal support was given the term extracorporeal membrane oxygenation (Bartlett 2005). ECMO has evolved from CPB principles; however there are subtle differences between the technique and equipment used:

- Cannulation

In CPB, cannulation is most frequently achieved through the open chest. The arterial cannulation site is typically the aorta but may also be through the auxiliary artery or

femoral artery and the venous cannulation site may be auxiliary vein, femoral vein, vena cava or right atrium. Cannulation sites depend upon the surgery to be performed and the patient's condition but ultimately it is the choice of the surgeon performing the treatment. In ECMO cannulation is most commonly achieved either cervically or femorally. With VA ECMO the venous cannula is usually inserted into the right atrium via the internal jugular vein and arterial cannula is inserted in to the aortic arch via the right common carotid artery. With VV ECMO blood is generally removed through cannulation of the right atrium and is returned to the right atrium via double lumen cannula placed within the internal jugular vein or to the inferior vena cava via cannula placed within a femoral vein (Lequier 2004).

- Cardiotomy reservoir, suction and microfiltration.

CPB is commonly used to allow surgeons to perform heart surgery. In this case blood must be removed from the operating field. Blood is removed via coronary suction device and is collected in a cardiotomy reservoir. The reservoir contains a defoaming chamber, storing chamber and filters (Chang 1998). The cardiotomy reservoir and suction set up of CPB is known to be a source of haemolysis, particulate and gaseous micro emboli, fat globule formation, cell aggregation, platelet loss and injury, and activation of coagulation and fibrinolysis (Estafanous, Barash et al. 2001). During ECMO suction of an operating field is unnecessary. For this reason the cardiotomy reservoir is not required. This eliminates some of the sources of damage to the patient's blood and also removes potential complications associated with the reservoir.

- Anticoagulation

ECMO requires much less anticoagulation in comparison to CPB. The higher flow rates associated with ECMO reduce the thromboembolic potential of the circuit (Sinard and Bartlett 1990). To determine the time taken for blood to clot and hence to monitor the effect of anticoagulation within the patient the activated clotting time (ACT) is the

standard test used (Graves, Chernin et al. 1996). In this test a blood sample is passed over a negatively charged surface activator, which causes activation of coagulation via the intrinsic pathway. The ACT is the time taken for a clot to form. Commonly accepted activated clotting time (ACT) with heparin in ECMO is around 180-200s, which is about twice the time of normal blood (Lequier and Chan 2005). In CPB the ACT must be a minimum of 400 seconds.

- Oxygenators

CPB oxygenators typically use hollow fibre micro porous membranes. These membranes are sufficient for short term usage; however prolonged use can result in plasma leakage (Eash, Jones et al. 2004). ECMO oxygenators require plasma tight hollow fibres. Such fibres typically have a nonporous outer skin, which prevents plasma leakage and allows gas transfer by diffusion only. The extra layer of material reduces the performance of the plasma tight fibres in comparison to the micro-porous fibres.

In general, CPB is a method of short term temporary support ranging from 30 minutes to 6 hours. It is employed in the operating room and is designed to give the surgeon a motionless and blood free environment to work on. CPB procedures most commonly run for under four hours (Brown, Moody et al. 2000).

ECMO is usually employed within the ICU and rarely involves an open chest. It is used to allow for organ recovery in patients with pulmonary and/or cardiac failure. ECMO circuitry is designed for long term operation with the duration of ECMO treatments ranging from hours to weeks (von Segesser 1999).

Figure 4 and Figure 5 show diagrams of a CPB and ECMO circuit, respectively.

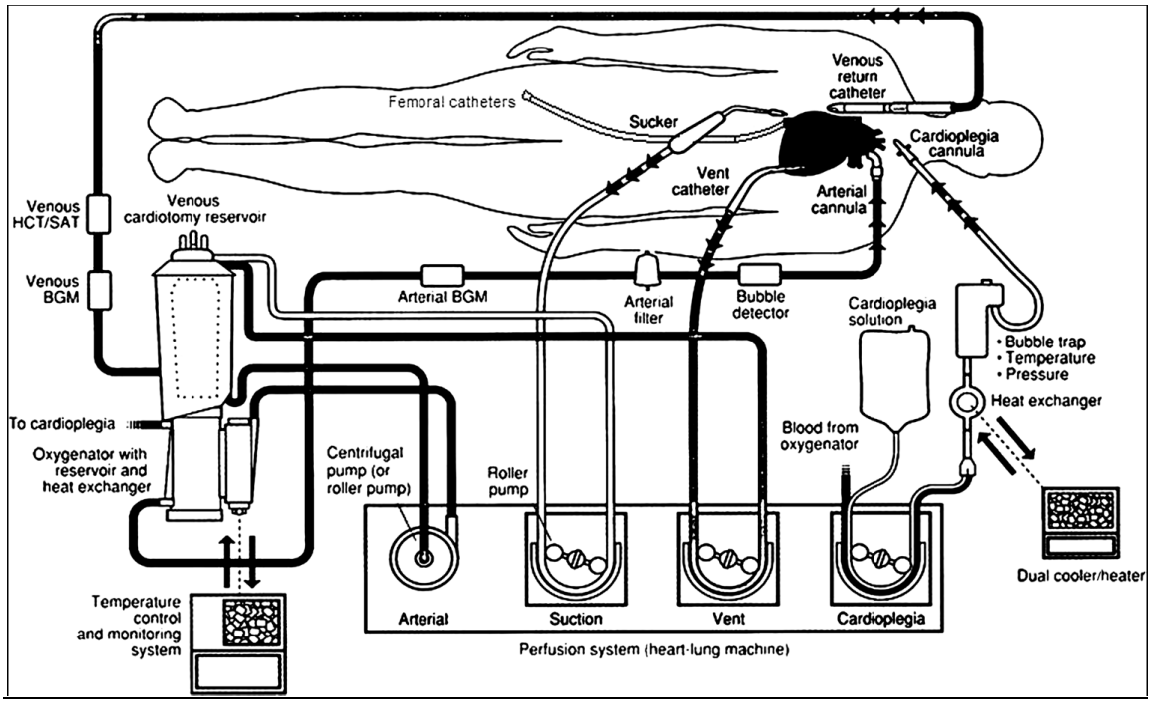


**Figure 4: Diagram of a Cardiopulmonary Bypass circuit. (Taken from www.cardiovascularperfusionists.com)**

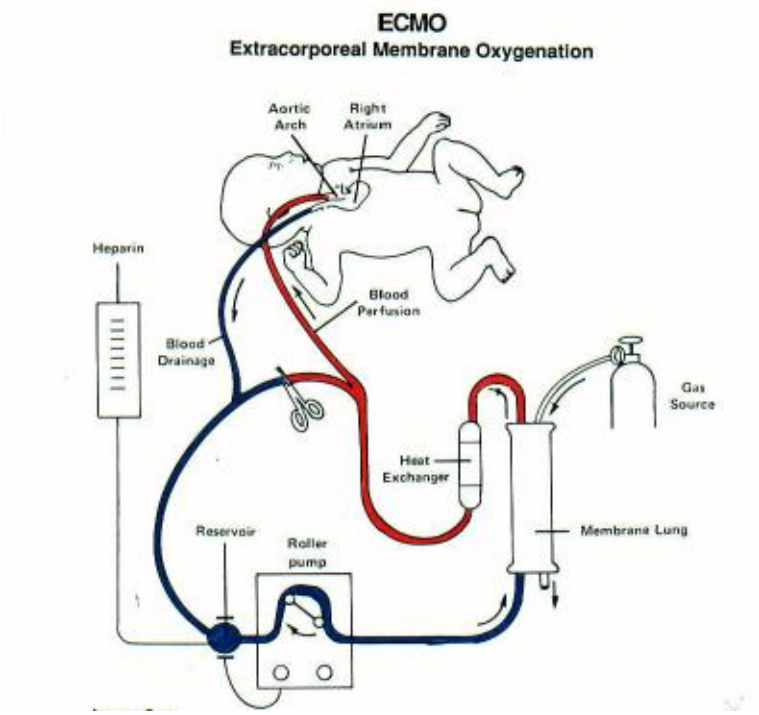


**Figure 5: Diagram of an Extracorporeal Membrane Oxygenation circuit. (Taken from www.mitchellmask.com).**

### 1.1.3. Indications for ECMO

ECMO is an invasive procedure and there is high risk associated with its use. For this reason it tends to be used only when absolutely necessary and as a last resort. Patient selection follows detailed criteria; however selection criteria vary between institutions implementing the treatment. Generally the following are considered to be good indications:

- An oxygenation index (Equation 1) of greater than 40 on two or more arterial blood gas measurements.

$$OI = \frac{F_iO_2 * M_{PAW}}{P_aO_2}$$

**Equation 1: Oxygenation Index.**

Where:
$F_iO_2$ = Fraction of inspired oxygen
$M_{PAW}$ = Mean Airway pressure
$P_aO_2$ = Partial pressure of oxygen in arterial blood.

- $PaO_2$ of less than 50 mmHg for four hours.
- Failure to react to maximal medical treatment.
- Persistent acidosis despite alkalization treatment, hyperventilation and $NaHCO_3$ infusion.
- Gestational age of greater than 35 weeks.
- Patient weight of greater than 2 kg.

(UCSF 2004; Smith 2007; Frenckner and Radell 2008)

The most common indication for ECMO is to support neonates with circulatory failure following cardiac surgery (Brown and Goldman 2008). Examples of other conditions that are typically treated by ECMO are:

- Immature lungs.
- Insufficient surfactant.
- Underlying persistent pulmonary hypertension.
- Meconium aspiration syndrome (MAS).
- Inability to come off CPB after operation.
- Congenital diaphragmatic hernia.
- Congenital heart defects such as:
    - Left to right shunt
    - Left or right side obstructed
    - Hypoplastic left heart syndrome
    - Cyanotic increased pulmonary blood flow
    - Cyanotic decreased pulmonary blood flow
    - Cyanotic increased pulmonary congestion

(ELSO 2007)

There are many other conditions that may also be treated by ECMO. Selection of a patient will depend upon the reversibility of their organ failure, organ function and the timing of the situation. In order to avoid irreversible damage and to maintain organ function ECMO must be initiated as early as possible (Di Russo and Martin 2005). It has been shown that patients unable to be weaned from cardiopulmonary bypass or that have undergone cardiopulmonary failure, placed on ECMO within the operating theatre rather than the intensive care unit, have a much better survival rate (Duncan, Ibrahim et al. 1998; Aharon, Drinkwater et al. 2001; Chaturvedi, Macrae et al. 2004).

More recently ECMO has been shown to be effective in the treatment of Influenza (H1N1) (Davies, Jones et al. 2009; Cianchi, Bonizzoli et al. 2011; Beurtheret, Mastroianni et al. 2012).

### 1.1.4. Contra-Indications for ECMO

ECMO is used to relieve the cardio and pulmonary systems to allow for organ recovery. Major contra-indications to its use are irreversible organ damage and major organ dysfunction, such as irreversible myocardial infarction, severe brain injury, central nervous system damage, chronic renal failure, hepatic dysfunction and residual cardiovascular lesions. Residual cardiovascular lesions place an additional hemodynamic load on the myocardium and will lead to deterioration. They must be surgically addressed before the patient is placed on ECMO (Chaturvedi, Macrae et al. 2004). Progressive multiple organ dysfunction results in decreasing chance of survival and after prolonged treatment could lead to termination of the ECMO treatment (Montgomery, Strotman et al. 2000).

### 1.1.5. Complications during ECMO

Complications that occur during ECMO can be considered in terms of mechanical and physiological complications. Typical mechanical complications are as follows:

- Oxygenator Failure
- Raceway rupture (for systems using roller pumps)
- Tubing rupture
- Heat exchanger complications
- Cannula problems
- Air within the circuit
- Pump malfunction

- Separation of connectors
- Electrical failures
- Kinking in the cannula

Each component of the ECMO circuit has the potential for mechanical failure. The frequency of failure typically varies with ECMO set-up and hence between institutions; however air emboli or clots within the circuit and oxygenator failure are most common (Bartlett, Toomasian et al. 1986; Shanley, Hirschl et al. 1994; Zwischenberger, Nguyen et al. 1994). Typical physiological complications are as follows:

- Haemorrhagic
- Neurological
- Renal
- Infectious
- Cardiopulmonary
- metabolic

Anticoagulation treatment is necessary for ECMO and the most common approach is systemic heparinization. Heparin acts by activating the enzyme inhibitor anti-thrombin. The anti-thrombin then inactivates thrombin and other proteases including factor Xa (Martini 2005).

Haemorrhagic complications are very frequent within ECMO treatment and this is typically because of the complex nature of a patient's condition. Many patients have pre-existing conditions, such as overt thrombosis or disseminating intravascular coagulation (DIC) that may cause bleeding or may be aggravated by ECMO (Muntean 1999). Many patients have clotting factor deficiencies and neonates in particular have decreased levels of clotting factors compared to children and adults (Andrew, Paes et al. 1990). During ECMO patients are likely to be given transfusions of packed red blood cells and platelets to reduce the risk of bleeding complications. The levels of

anticoagulation may be reduced in the presence of clinically significant bleeding (Lequier and Chan 2005).

Between 10 – 20 % of patients treated with ECMO experience some sort of neurological complications resulting in permanent neurodevelopmental disability (Robertson, Finer et al. 1995). It is difficult to determine the direct effect of the ECMO system because complications may be due to the underlying patient illness; however the most likely causes are through cerebral haemorrhage and infarction (Robertson, Finer et al. 1995; Rais-Bahrami, Wagner et al. 2000; Langenbacher, Nield et al. 2001). Patients suffering from congenital diaphragmatic hernia (CDH) treated with ECMO have a higher risk of suffering some sort of neurological complication (Stolar, Crisafi et al. 1995; Hamrick, Gremmels et al. 2003).

### 1.1.6. The Evolution of ECMO as a Treatment

#### *Veno-venous ECMO for Respiratory treatment*

The first successful treatment of neonatal respiratory disease was achieved by Bartlett in 1975 and this has remained the most common use for ECMO (Bartlett, Gazzaniga et al. 1976). ECMO for treatment of respiratory disease was found to be more successful with the neonatal population than with the adult population. The causes of respiratory failure within the new-born are thought to be more readily reversible. Furthermore the neonatal lung may have an increased capability for repair and regeneration (Wolfson 2003).

Figure 6 below shows the Extracorporeal Life Support Organisation (ELSO) records for annual respiratory neonatal runs in active ECMO centres around the world.

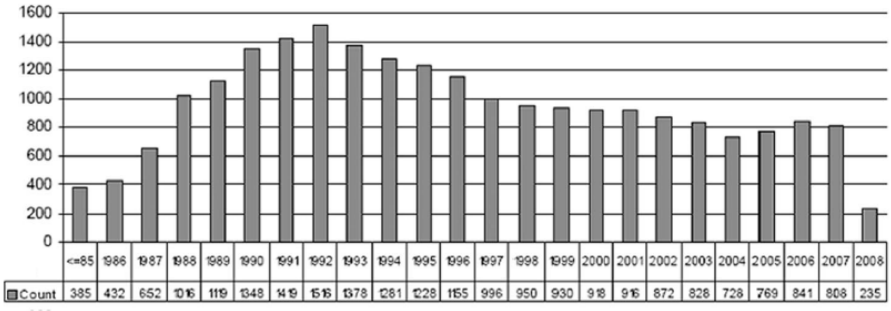


**Figure 6: Annual neonatal respiratory runs reported to the ELSO by active ECMO centers.**

From Figure 6 it can be seen that there was a peak in the number of runs in 1992. Since then there has been a decline in ECMO usage for respiratory failure. This is thought to be due to the use of alternative therapies, such as inhaled nitric oxide (iNO), high-frequency oscillatory ventilation (HFOV) and surfactant therapy, and also through improved in-house management, leading to a reduction in the number of patients that actually require ECMO (Wilson, Bower et al. 1996; Hintz, Suttner et al. 2000; Roy, Rycus et al. 2000). Table 1 below shows ELSO ECMO neonatal respiratory statistics for 2008.

| Primary Diagnosis | Total Runs | Number Survived | Survival |
|---|---|---|---|
| CDH | 5,411 | 2,780 | 51% |
| MAS | 7,247 | 6,790 | 94% |
| PPHN/PFC | 3,524 | 2,738 | 78% |
| RDS/HMD | 1,447 | 1,218 | 84% |
| Pneumonia/Sepsis | 2,831 | 2,074 | 73% |
| Air Leak Syndrome | 113 | 84 | 74% |
| Other | 1,624 | 1,035 | 64% |

**Table 1: ELSO ECMO neonatal respiratory statistics, total runs up to 2008.**

**CDH = congenital diaphragmatic hernia, MAS = meconium aspiration syndrome, PPHN = persistent pulmonary hypertension of the new-born, PFC = persistent fetal circulation, RDS = respiratory distress syndrome, HMD = hyaline membrane disease**.

### *Veno-arterial ECMO for Cardiac and respiratory treatment*

The frequency of neonates treated with cardiac ECMO is much less than those treated with respiratory ECMO. However unlike respiratory ECMO there has been a consistent increase in the number of cardiac cases each year as indicated by the ELSO records shown within Figure 7.

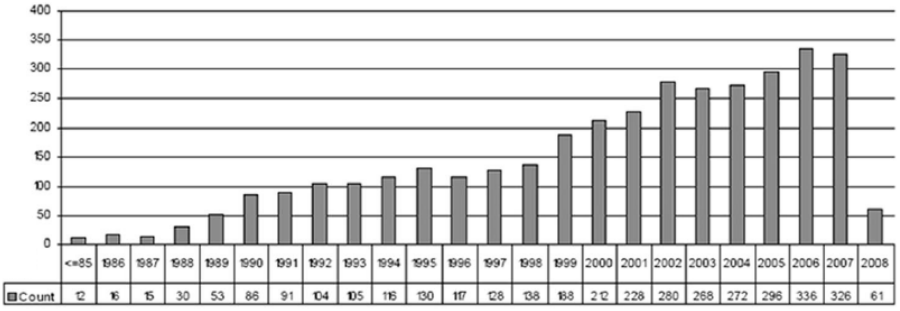


**Figure 7: Annual neonatal cardiac runs reported to the ELSO by active ECMO centers**

The increase in cases is attributed to an increase in access to ECMO centres. Also, evolving technology has allowed for more complex and diverse usage for cardiac ECMO (Haines, Rycus et al. 2009). Table 2 below shows the ELSO neonatal cardiac statistics for 2008.

| Primary Diagnosis | Total Runs | Number Survived | Survival |
|---|---|---|---|
| Congenital Defect | 3,114 | 1,062 | 36% |
| Cardiac Arrest | 44 | 10 | 23% |
| Cardiogenic Shock | 37 | 14 | 38% |
| Cardiomyopathy | 92 | 54 | 62% |
| Myocarditis | 41 | 20 | 49% |
| Other | 280 | 109 | 41% |

**Table 2: ELSO ECMO neonatal cardiac statistics, total runs up to 2008.**

In general the survival rates for cardiac patients are much less than that experienced by the respiratory patients.

### 1.1.7. Limitations of ECMO treatment

Although ECMO technology has been constantly evolving, mortality rates have been increasing. Patients with MAS and PPHN have a high success rate; however a large number of these patients are more frequently treated with alternative therapies. This combined with the increase in cardiac patients, which traditionally experience lower survival rates, has resulted in the general decreasing survival rate for the treatment (Wilson, Bower et al. 1996).

Significant improvements in patient outcome can be achieved by decreasing the time between a patient being diagnosed as eligible for ECMO and the institution of the treatment. Delay in the institution of ECMO is known to lead to a worse outcome with increased duration of hospital stay and decreased short and long term survival (Schumacher, Roloff et al. 1993; Duncan, Ibrahim et al. 1998; Aharon, Drinkwater et al.

2001; Gill, Neville et al. 2002; Chaturvedi, Macrae et al. 2004; Dalton, Rycus et al. 2005; Brown and Goldman 2008).

One of the main contributors to delay in the institution of ECMO is the clinical acceptance of the treatment. Currently ECMO is considered a 'last resort' to be used only when conventional therapy has failed to improve the condition of a patient. ELSO guidelines for physicians practicing ECMO state that the indications for the treatment are: "Acute severe heart or lung failure with high mortality risk despite optimal conventional therapy. ECLS is considered at 50% mortality risk, ECLS is indicated in most circumstances at 80% mortality risk."

A further complication leading to extended delays is the limited amount of ECMO centres available. ECMO systems are very expensive to buy, to operate and to maintain. They require a team of highly trained staff, typically consisting of nurses, perfusionist, technician, cardiothoracic surgeon and a respiratory therapist (Lequier 2004). ELSO guidelines for ECMO centres states that: "ECMO Centers should be located in geographic areas that can support a minimum of 6 ECMO patients per center per year. The cost effectiveness of providing fewer than 6 cases per year combined with the loss, or lack of clinical expertise associated with treating fewer than this number of patients per year should be taken into account when developing a new program."

The cost of establishing an active ECMO programme within an institution is not economically viable in many cases. This results in the development of specialised ECMO centres and hence reduced availability of the treatment. Lack in availability of ECMO means that transportation of patients is an inevitable requirement (Cornish, Gerstmann et al. 1986). This is a very expensive process with significant associated risk. Specialised transport systems are required along with a team of specialist staff, which typically consist of an anaesthesiologist, cardiac surgeon, ICU nurse and perfusionist (Wagner, Sangolt et al. 2008). Although this procedure has been shown to be successful, the cost and risk associated with its use mean that it should only be used

in the case of an emergency and should not replace early referral of a patient to an ECMO centre (Wilson, Heiman et al. 2002). Figure 8 below shows a diagram of a transport ECMO system.

**Figure 8: Diagram of a specialized Transport ECMO system. (Taken from www.Aerovaworld.com)**

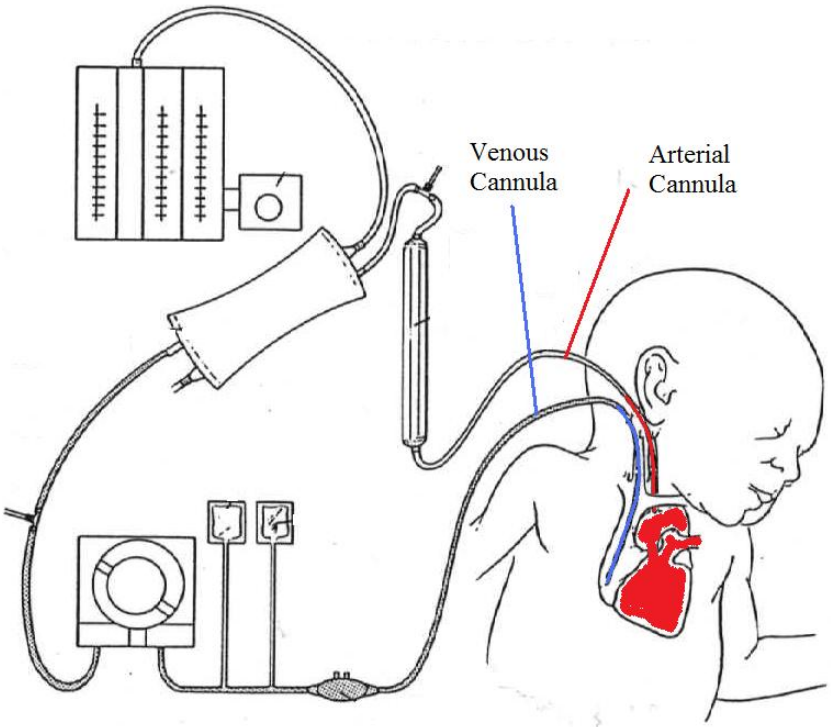


## The ECMO Circuit: Cannulation

## 1.2. Cannulation

Cannulation of a patient depends upon the method of ECMO adopted. The most common form of treatment for the neonatal population is VV ECMO using a double lumen catheter. Figure 9 below shows typical cannulation sites for VA (A), VV (B) and VV with double lumen catheter.

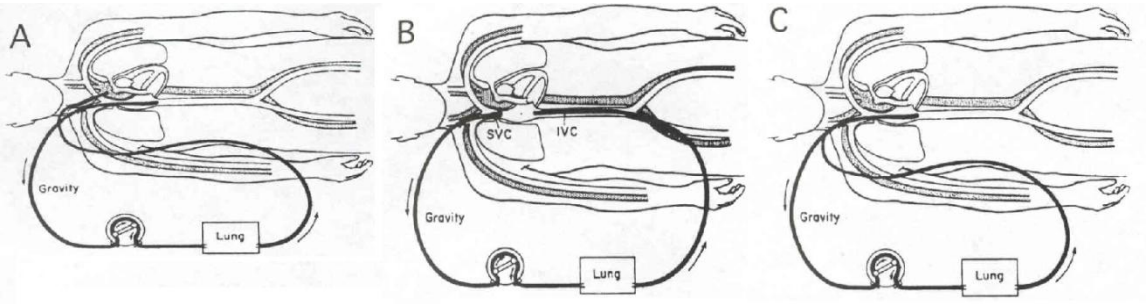


**Figure 9: Typical cannulation sites for VA (A), VV (B) and VV ECMO with double lumen catheter (C) (taken from surgery.med.umich.edu)**

Blood flow rate from the patient and hence the level of extracorporeal support is determined by the size of the venous cannula. The French scale is generally used to classify cannula sizes. The reinfusion size is not as critical as the venous; however it must be of sufficient size to tolerate maximum predicted blood flows at total support without generating high pressures (University of Michigan and Section of Pediatric Surgery 2007).

Commonly cannulation procedure results in permanent ligation of the common carotid artery (CCA) in VA ECMO and ligation of both the CCA and the internal jugular vein. Permanent ligation of these vessels results in reduced blood flow to the brain as shown within Figure 10.

In extracorporeal carbon dioxide removal (ECCR) arteriovenous cannlation is used. In this process blood is typically removed from the femoral artery and re-infused through the femoral vein.

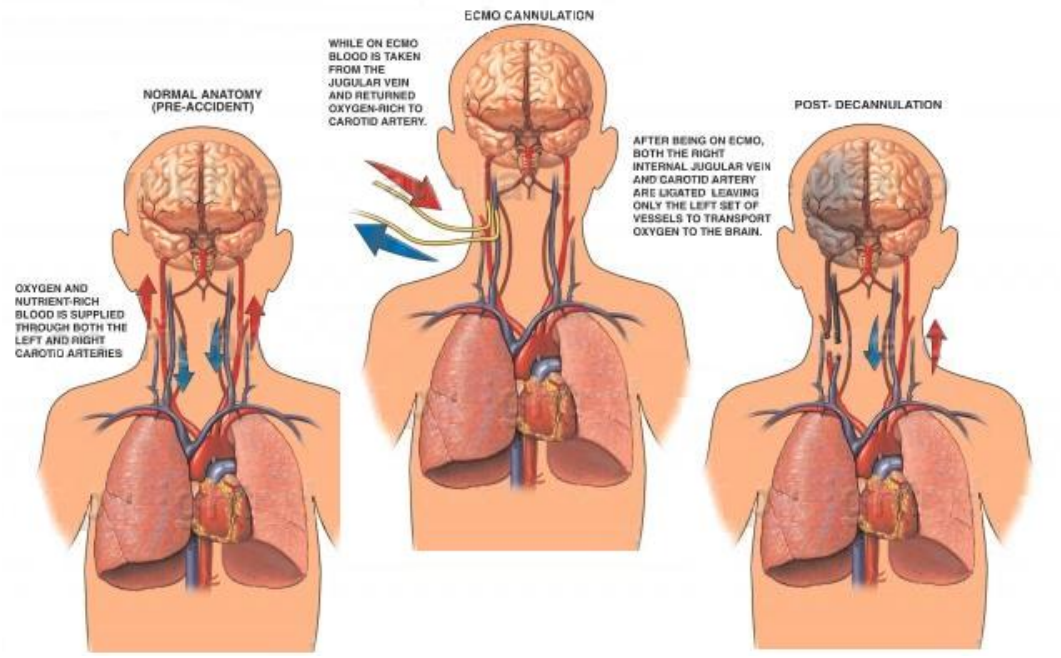


**Figure 10: Diagram of early cannulation procedure for VA ECMO (Image adapted from Nucleus Medical Media).**

More recently carotid artery reconstruction is being performed in order to increase perfusion to the brain. It has been shown that this procedure can be conducted safely with symmetrical flow to the brain successfully re-established (DeAngelis, Mitchell et al. 1992; Armainsson, Ilbawi et al. 1995; Levy, Share et al. 1995).

Development of the double lumen cannula has provided a system that is minimally invasive, prevents permanent ligation, is as safe as VA ECMO and provides adequate perfusion (Anderson and Bartlett 1993; Delius, Anderson et al. 1993).

Problems associated with the double-lumen cannula are that it can only be used with infants under 4-5 kg of weight and that recirculation of oxygenated blood into the

extracorporeal system results in reduced efficiency of the bypass and requires increased blood flow (Rais-Bahrami, Walton et al. 2002). Figure 11 and Figure 12 show a selection of commercially available catheters.

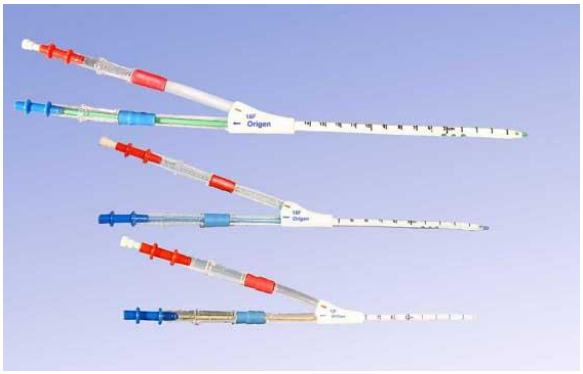

**Figure 11: Origen double lumen cannulae of various sizes (taken from www.origen.net).**

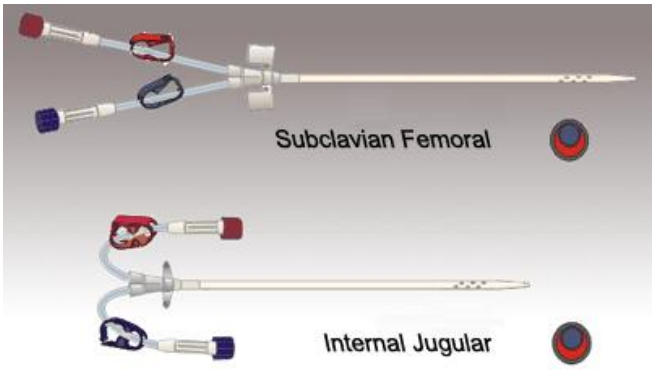


**Figure 12: Biometrix Subclavian femoral and internal double lumen catheters (taken from www.pinepharma.com)**

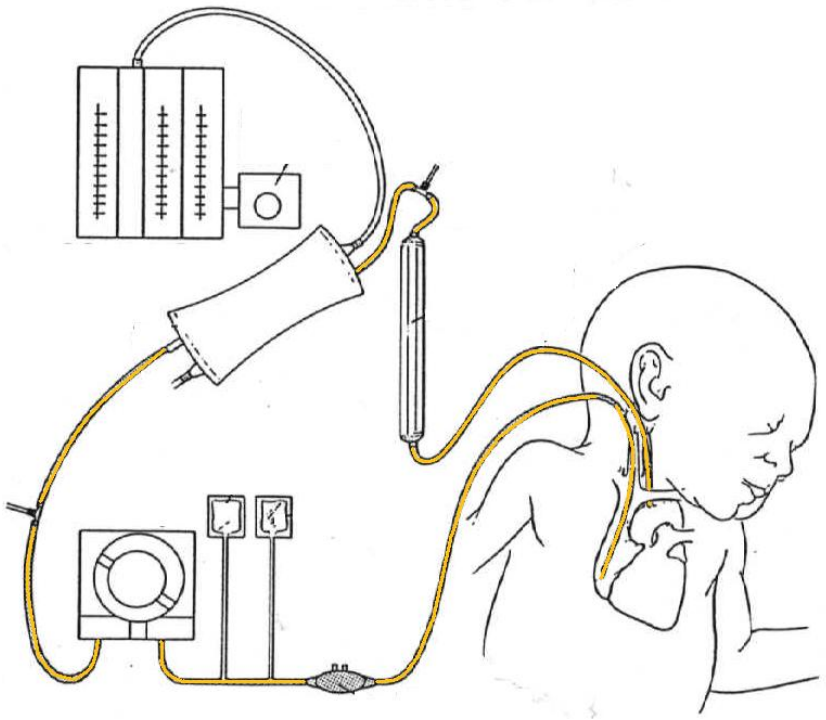

**The ECMO circuit: Tubing**

## 1.3. Tubing

Modern ECMO systems utilise PVC tubing. PVC is particularly attractive for use in medical devices because it is strong, flexible, and cheap, can be easily sterilised, is transparent and does not kink. PVC tubing is typically plasticised with di-(2-ethylhexyl) phthalate (DEHP). It has been shown that patients undergoing ECMO are exposed to levels of DEHP due to leaching of the plasticiser into the blood (Schneider, Schena et al. 1989). The levels of exposure are thought to be proportional to the surface area of tubing in the circuit (Karle, Short et al. 1997).

DEHP exposure in new-born animals has resulted in damage to reproductive systems; in males, reduced fertility and changes in sperm production and in females, ovarian dysfunction and decreased hormone production were observed. Respiratory distress and changes in kidney and liver function have also been associated with DEHP exposure (Rais-Bahrami, Nunez et al. 2004). Although DEHP has had an effect in animal reproductive organs, to date, no short-term or long-term effects have been observed in human reproductive organs (Karle, Short et al. 1997; Rais-Bahrami, Nunez et al. 2004). DEHP plasticized PVC has, however, been shown to be pro-inflammatory in human blood with the magnitude of response proportional to the level of exposure (Gourlay, Samartzis et al. 2003; Gourlay, Samartzis et al. 2003).

Heparin bonding on PVC tubing surfaces has been shown to significantly decrease levels of DEHP leaching (Karle, Short et al. 1997). Heparin is bonded to the surface by firstly treating it with an oxidiser to give it a negative charge. The surface is then exposed to a positively charged polymer that aggregates on the surface allowing for cross-linking. The final step is to covalently bond the heparin to the free terminal amino groups on the polymer side chains (Mahoney 1998). Another technique that reduces the levels of DEHP leaching is to wash the surface of the tubing with methanol (Gourlay, Stefanou et al. 2002).

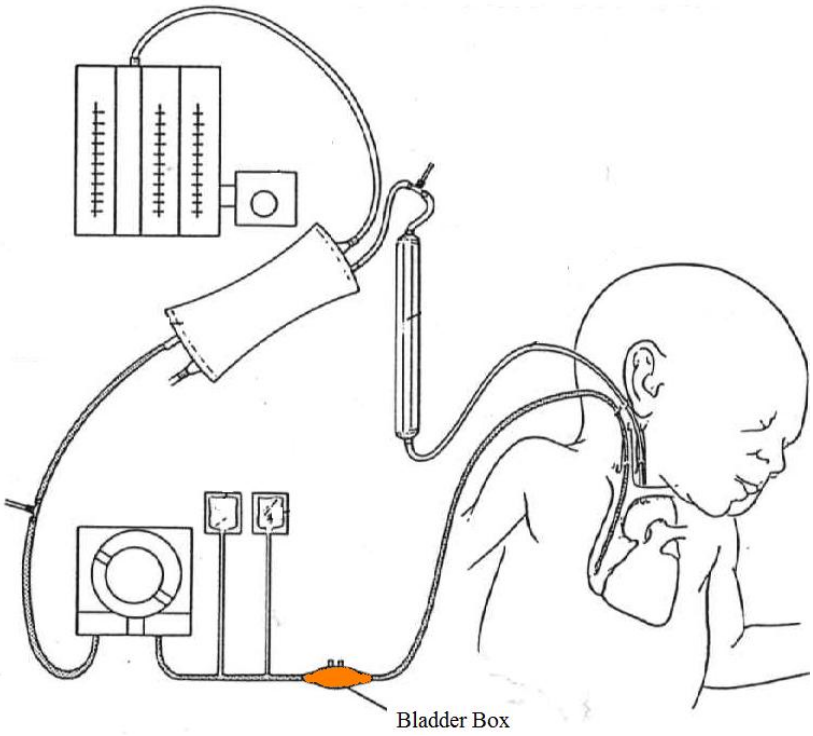


## The ECMO Circuit: The Bladder Box

## 1.4. Bladder Box

During ECMO treatment there is the possibility of negative pressure generation within the drainage circuit. This can occur if the blood flow from the patient is less than that of the forward flow of the blood pump used within the circuit (Setz, Kesser et al. 1992). This can be caused by incorrect cannula placement or kinking of the cannula. High negative pressure in the system can lead to haemolysis and leukocyte destruction (Pedersen, Videm et al. 1997) as well as damage to the endothelium of the right atrium or vena cava and cavitation of air (University of Michigan and Section of Pediatric Surgery 2007; Frenckner and Radell 2008). To prevent a negative pressure build up a pressure sensitive servo-regulation system is used. There are two systems that are typically employed: the bladder box and pressure monitoring. Both systems act as a slave to the pump.

### *The Bladder Box*

This system consists of a small collapsible bladder, typically made of silicone or PVC. The bladder sits within a box, which is connected to a switch that can directly influence the pump speed. If the bladder collapses the blood pump will stop or its speed will be reduced (Snyder, Weckerly et al. 1989).

### *Pressure monitoring*

In this system the inlet fluid pressure is monitored. This is compared to a pre-set pressure level and if there is a significant fluctuation the system will reduce the pump flow speed proportionally (Pedersen, Videm et al. 1997).

Pressure fluctuations are detected by each system and are used to control the pump speed. High pressure and the pump will increase in speed, low pressure and the pump will slow and in this manner a critical flow rate is maintained.

Figure 13 below shows a picture of a typical commercially available bladder box.

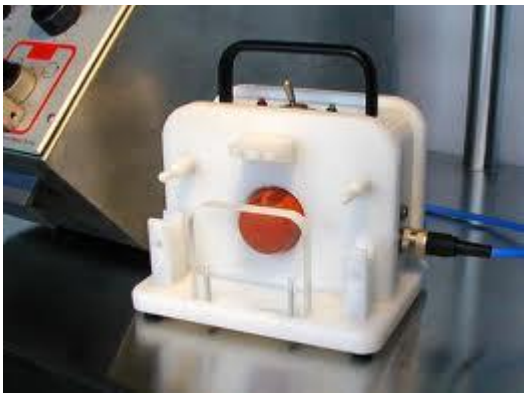

**Figure 13: Origen Bladder box. (Taken from www.Origen.net).**

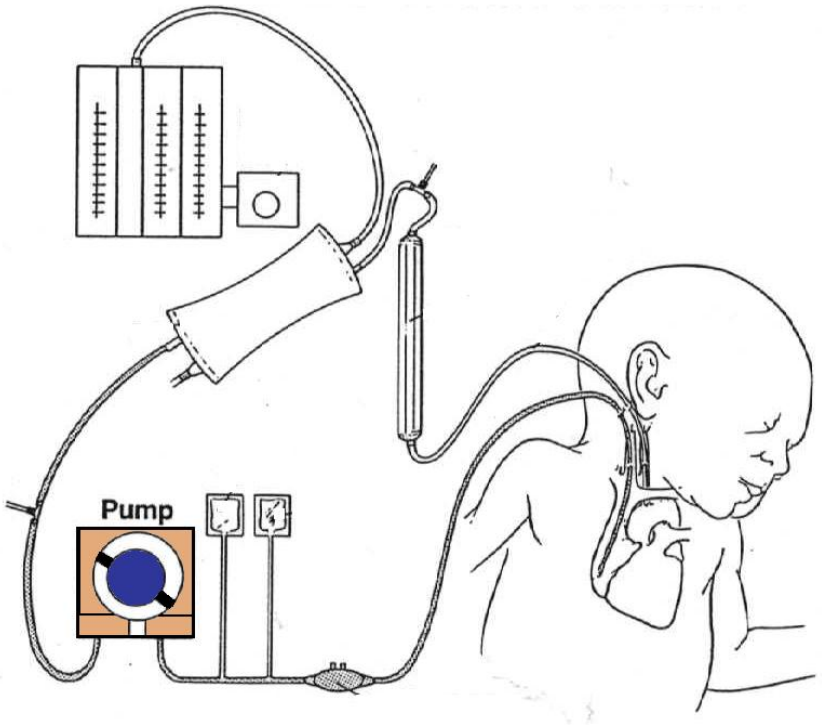


**The ECMO Circuit: The Blood Pump**

## 1.5. Pumping Systems

During VA ECMO treatment a patient's heart is temporarily relieved of its work load. By doing this the heart is allowed to rest and recover until it is once again able to successfully perfuse the body. During the recovery period a blood pump is used to maintain perfusion of the body.

The blood pump in the extracorporeal system must provide the membrane oxygenator with a sufficient volume of blood to maintain adequate perfusion within the patient. The pump must be easily controllable, reliable and must minimise haemolysis and thromboembolic potential. Currently there are several blood pumping systems available on the market. Typically these can be separated into two categories: non-pulsatile and pulsatile flow.

### 1.5.1. Non-Pulsatile Pumps

#### *Roller pumps*

The first roller pump system was patented by Porter and Bradley in 1855; however the roller pump, used for perfusion purposes, was developed by Dr Michael DeBakey in 1934. The roller pump was developed for use as short term support and is still employed clinically in treatments such as ECMO, CPB and dialysis.

Tubing is placed within the pump boot. A pump head, with rollers, compresses the tubing at the point of contact between the roller and the tubing. As the pump head rotates, fluid is propelled in front of the roller and moves out of the pumping system. A diagram of a double head roller pump can be seen within Figure 14.

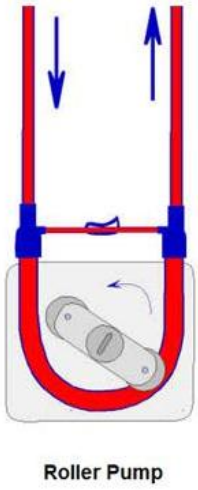


**Figure 14: Diagram of a double head roller pump (taken from media.photobucket.com).**

The level of haemolysis within the roller pump is influenced by occlusion settings of the rollers, tubing material and diameter, rotary speed of the pump head and the number of rollers used (Noon, Kane et al. 1985).

Blood flow can be controlled by varying the degree of occlusion of the pump system. By increasing occlusion it is possible to produce a more accurate blood outflow; however it also leads to an increase in haemolysis. A trade off must occur between the desired forward fluid output and haemolysis (Mongero, Beck et al. 1998). Increasing the rotary speed of the pump (Kurusz, Christman et al. 1980) and increasing the number of roller heads used (Cooley 1987) are both associated with an increase in haemolysis. During pump operation, tubing is continually subject to wear. Abrasion of the tubing inner surface leads to spallation (Kim and Yoon 1998). During prolonged treatment, such as ECMO, raceway tubing may rupture leading to air embolism and haemorrhage (Peek, Wong et al. 1999). The degree of spallation and durability of the tubing is determined by the material used, diameter and the calibration of the roller pump. Silicone rubber and PVC are the typical materials used as raceway tubing. Silicon rubber has been shown to produce less haemolysis (Bernstein and Gleason 1967).

Increasing the diameter of the raceway tubing used, has been found to decreases blood haemolysis (Crane, Brown et al. 1983). Tubing material and diameter selection will be a trade off in terms of desired pump settings, duration of operation and level of haemolysis. Figure 15 and Figure 16 below are both examples of commercially used roller pumps.

**Figure 15: Sarns 7000 perfusion system using Sarns roller pumps (Taken from www.dremedical.com).**

**Figure 16: Stockert perfusion system using Stockert roller pumps (Taken from www.pemed.com).**

### 1.5.2. Centrifugal blood pump

In 1979 the first clinical experiences with non-pulsatile blood pumps was performed (Murakami, Golding et al. 1979). The centrifugal blood pump was developed in the hope of producing a less traumatic pumping system. Centrifugal pump design also offers a number of advantages over the roller pump such as reduced size and weight, reduced power requirements, kinking of circuit tubing does not lead to a pressure blow out, increased reliability and simpler control (Leshchinskii, Itkin et al. 1990).

The main feature in a centrifugal pump is an impeller that is rotated by a motor. Blood enters and is accelerated outwards towards the pump casing by the impeller. The accelerated fluid leaves the device through the discharge outlet. A diagram of a centrifugal pump is given within Figure 17.

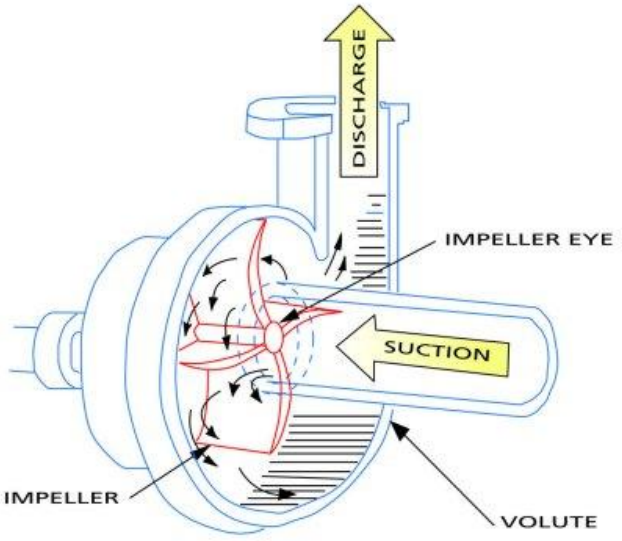


**Figure 17: Diagram of a Centrifugal blood pump (Taken from www.pumpfundementals.com).**

Haemolysis, due to the high shear stresses is a problem within these devices. However in several cases it has been shown that, during extended extracorporeal treatments, haemolysis in the centrifugal pump is less than that of the roller pump (Horton and Butt

1992; Curtis, Wagner-Mann et al. 1994; Moen, Fosse et al. 1994; Morgan, Codispoti et al. 1998).

One of the main limiting parameters with centrifugal pump design is the mechanical shaft/seal system used to suspend the impeller. This part of the design is in itself associated with haemolysis, thromboembolic complications and toxicity due to corroding mechanical bearings (Hoshi, Asama et al. 2005). To overcome this modern systems have been designed with magnetically levitated impellers to remove mechanical contact (Hoshi, Takatani et al. 2005). Flow from the centrifugal pump is dependent upon the preload and after load. If the patient pressure and the pressure head are greater than that of the pressure generated within the pump then no forward flow will occur. This can be problematic in that although the pump is still rotating the fluid stops flowing, which can cause severe haemolysis and make can make detection of the problem more difficult.

Figure 18 and Figure 19 both show examples of commercially available centrifugal blood pumps.

**Figure 18: Levitronix centrifugal pump head and drive (Taken from www.levitronix.com).**

**Figure 19: Medtronic Bio-pump centrifugal pump head (Taken from www.cardiomedical.com).**

### 1.5.3. The axial flow pump

The first clinical experiences with axial flow pumps was achieved using the DeBakey VAD in 2000 (Wieselthaler, Schima et al. 2000). The axial flow pump has been designed for long term implantable use for bridge to transplant, bridge-to-recovery and for permanent circulatory support (destination therapy).

Similar to centrifugal and roller pump design there are no valves present. Blood flows into the pump and is accelerated via an electromagnetically actuated impeller. Blood then passes over a diffuser, which decreases velocity and increases the pressure before the fluid leaves the device. A diagram of an axial pump system is shown within Figure 20.

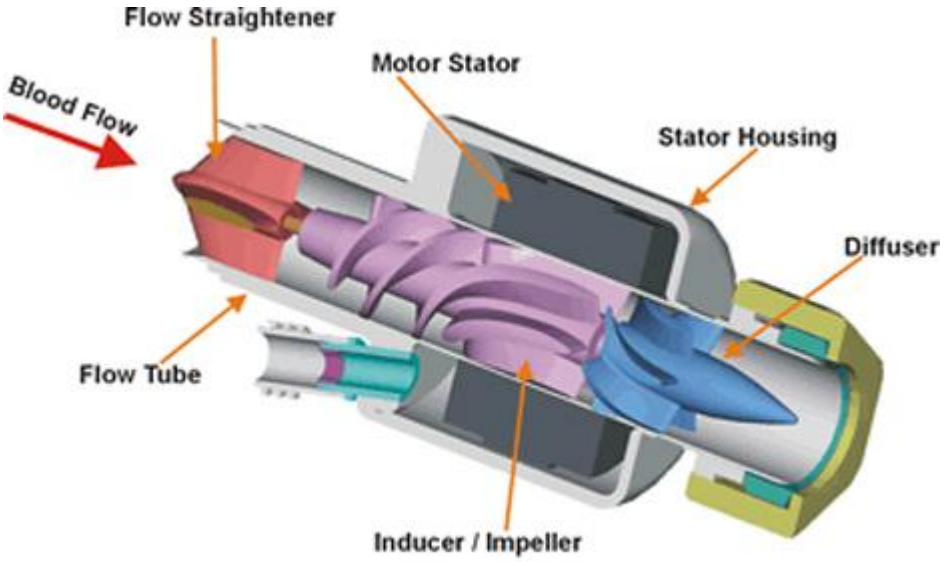


**Figure 20: Diagram of an Axial flow pump (Taken from www.medgadget.com).**

Axial flow blood pumps are the smallest of the three non-pulsatile blood pumps discussed. They produce high blood flows at low pressures, typically operating within a range of 8,000 to 12,000 rpm and producing blood flow of up to 6 L/min (Fraizier, Myers et al. 2002). They have been shown to produce less haemolysis than centrifugal pumps; however the level of haemolysis is determined by the operating conditions of the pump and by the corresponding shear stress levels and exposure time of the blood (Kawahito and Nose 1997). This pump design also requires a mechanical bearing between the rotating shaft and the rest of the device. Heat production due to friction can occur at the bearing sites. Heat production in areas of low wash out may lead to thrombosis formation (Reul and Akdis 2000); however most resent designs used blood immersed bearings, where blood flow is designed to continually wash over the bearings (Westaby, Katsumata et al. 1998).

Examples of axial flow pumps currently used within clinical practice are given within Figure 21 and Figure 22.

**Figure 21: Jarvik 2000 implantable left ventricle assist system (Taken from www.asaio.com).**


**Figure 22: DeBakey Heart Assist 5 ventricular assist device (Taken from www.micromedcv.com).**

### 1.5.4. Pulsatile pumps

The pulsatile blood pumps are most commonly used as an implantable long-term support system. The treatment is typically used as a bridge-to-transplantation and is not used in ECMO. The pulsatile pumping system simulates the workings of the natural heart. Blood will enter a compressible chamber through a one way valve. The chamber is compressed forcing the blood out of the device through another one way valve and into the body. A diagram of a typical pulsatile pump is given within Figure 23.

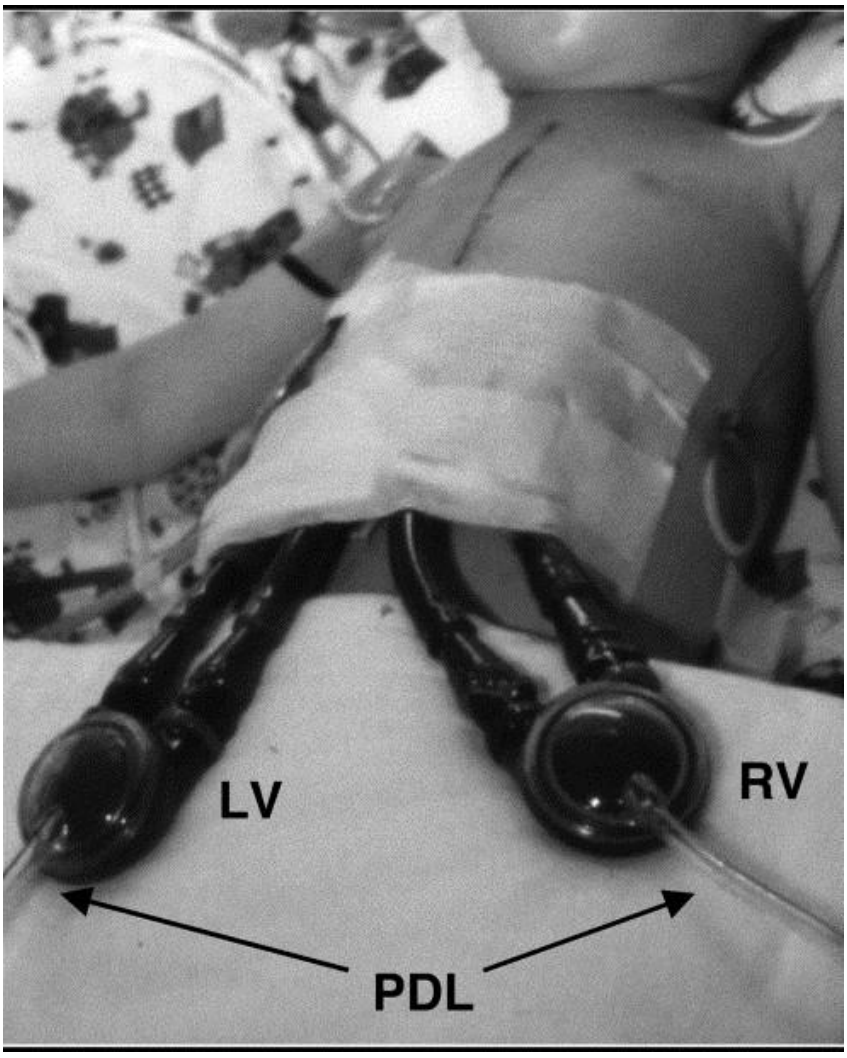


**Figure 23: Diagram of the HeartMate Pneumatic pulsatile blood pump (Taken from sciencedirect.com).**

Early generation pulsatile blood pumps were associated with high degrees of blood trauma and thromboembolic potential (Di Bella, Pagani et al. 2000). Advancement in the design and surface properties of these devices has led to significant improvements in thromboembolic potential (Slater, Rose et al. 1996). However there are many other short comings associated with these pumps; the systems are large and bulky, which limits the size of patient that they are available to, they including many moving parts, which make them susceptible to mechanical failure, they require large inflexible transcutaneous power and air lines (Olsen 2000; Goldstein 2003). In general pulsatile flow is used exclusively in VAD technology and although available tends not to be used in the ECMO setting; however there may be some advantage in using this flow variant in long term support. The mechanical complexity and interaction of other circuit components may render this flow modality unusable for the ECMO setting. Figure 24 below is an example of a commercially used pulsatile blood pumps.

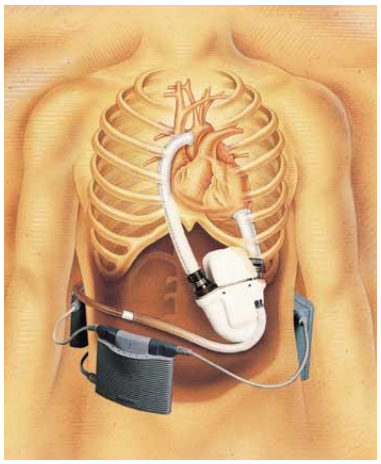

**Figure 24: World Heart Novacor pulsatile blood pump (Taken from www.memagazine.com).**

### 1.5.5. The problems associated with pulsatile and non-pulsatile flow

The heart operates through positive displacement. Blood enters the heart, the heart then contracts, ejecting blood and then relaxes to begin the cycle. This leads to pulsatile blood flow. There is a debate as to the most appropriate for of blood flow generated by blood pumps – pulsatile or non-pulsatile flow. The physiological impact of pulsatile compared to non-pulsatile pumping must be considered in both acute and chronic terms. Cardiopulmonary bypass (CPB) is an example of acute support. It has been shown that non-pulsatile flow leads to an increase in peripheral vascular resistance (PVR). This is thought to be due to increases in plasma renin and angiotensin II levels (Taylor, Bain et al. 1979). Pulsatile support has also been shown to reduce systemic vascular resistance, reduce the catecholamine response and improve splanchnic, renal and myocardial perfusion (Saito and Nishinaka 2005). Pulsatile systems have a much higher degree of LV volume unloading compared to non-pulsatile system. The effects of complete unloading on cardiac recovery are unknown; however it has been presumed that unloading may increase myocardial perfusion and recovery (Klotz, Deng et al. 2004). There is much debate as to the actual physiological effects of chronic non-pulsatile support (CNPS) and ultimately the effect on normal end-organ function using non-pulsatile flow is not yet fully known (Saito, Westaby et al. 2002). Vasku *et al* suggest that CNPS leads to permanent impairment of capillaries and could also lead to the permanent impairment of organ microvessles and hence results in poor organ perfusion. It was also suggested that lack of pulse could have a negative impact on the peripheral tissues and vital organs (Undar 2004; Vasku, Wotke et al. 2007); however several authors have suggest that CNPS does not impair end organ function (Sakaki, Taenaka et al. 1994; Wieselthaler, Schima et al. 2000; Saito, Westaby et al. 2002; Goldstein 2003). Although there is no definitive conclusion to the effect of non-pulsatility, due to the advantages mentioned and their ability to be easily implanted, non-pulsatile pumps are being employed more frequently in clinical practice. To date the longest surviving patient with a non-pulsatile ventricular assist device - the Jarvik LVAD - was Peter Houghton, who survived for 7.5 years.

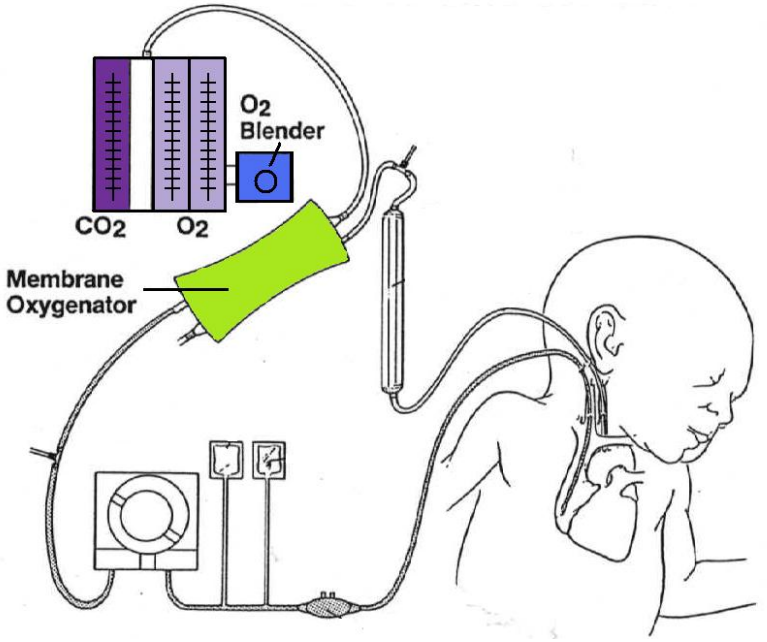


## The ECMO Circuit: The Membrane Oxygenator

## 1.6. Membrane Oxygenator

In Extracorporeal membrane oxygenation, it is the function of the oxygenator to oxygenate blood and remove carbon dioxide, providing long term support to the failing lungs of a critically ill patient.

In the respiratory system, air enters and makes its way to the lungs. Within the lungs the air is distributed throughout the branch structures of the bronchi. The final destination of the air in the lungs is in the alveoli; each alveolus is surrounded by a network of capillaries. Diffusion occurs across respiratory membranes with oxygen transferred to the blood and carbon dioxide removed (Martini 2005).

Human lungs are extremely efficient; replicating their function efficiently in an artificial device is a complicated and challenging task. To support an adult, an oxygenator must provide sufficient oxygenation and carbon dioxide removal from blood at a flow rate of approximately 5 L/min (Drummond, Braile et al. 2005). Surface contact must be kept to a minimum to avoid inflammation and coagulation and priming volume must also be as low as possible.

Since the 1950's various different technologies and techniques have been applied to oxygenator development leading to the design of the modern oxygenator. There have been three main types of oxygenators developed – the film oxygenator, the bubble oxygenator and the membrane oxygenator - with many variations of each.

### 1.6.1. Film Oxygenators

The first generation of oxygenators were known as film oxygenators. The main principle behind their design was to create a fine film of blood that is exposed to a supply of oxygen. In 1953 Gibbon used a sheet oxygenator to successfully support a patient (Gibbon 1954). The design functioned by allowing blood to enter a venous reservoir with vertical slits in the bottom which lead to stationary vertical screens. The blood flowed into the reservoir and down the screens. The chamber that held the screens was filled with oxygen and diffusion occurred through the direct exposure of the blood to oxygen as it flowed down the screens. The screens were made of mesh to encourage turbulence in the blood flow and hence mixing of the blood. Oxygenated blood was collected at the bottom of the device and returned to the patient. DeBakey roller pumps were used to drive the blood through the system and heat was provided by submerging parts of the apparatus within a water bath (Gibbon 1997).

Figure 25 and Figure 26 below show the screens of the Gibbon Oxygenator and the Model II prototype developed by IBM, respectively.

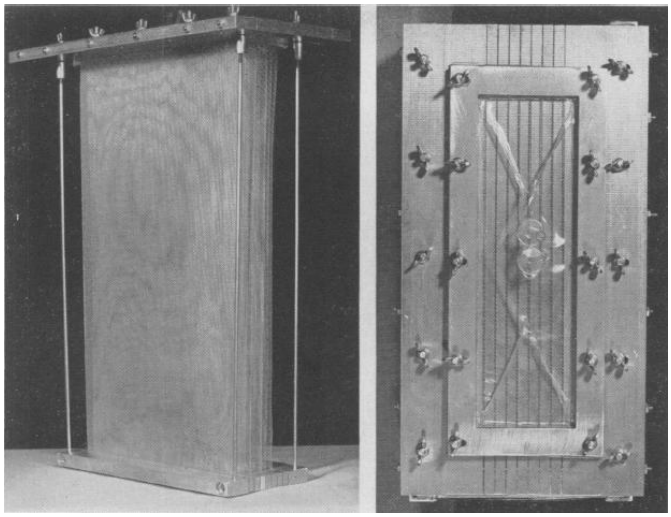

**Figure 25: Vertical screens of the Gibbon film oxygenator (Taken from (Diettert, Bercu et al. 1958))**

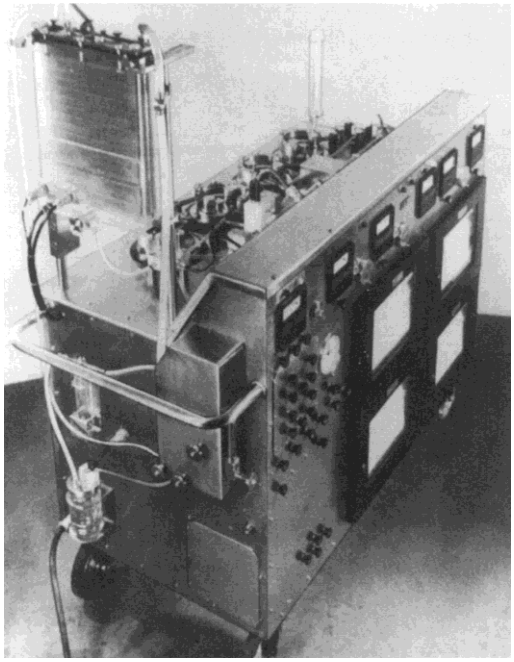

**Figure 26: Model II prototype of the Gibbon Oxygenator developed with IBM (Taken from (Cohn 2003)).**

There were several practical problems associated with the design. Firstly, in order to operate efficiently the entire surface area of the sheet had to be covered in a film of blood. Providing a complete and constant film cover over the sheets was challenging as rivulets tended to form. The blood film did not spontaneously reform if broken, therefore requiring the machine to be initially wetted and continually run (Clowes 1960). The success of the design relied upon sufficient exposure of the blood, which meant that large surface areas exposed to the oxygen were required. The system therefore had large blood volume requirements, which through the use of the vertical sheets increased with increasing flow rate (Melrose 1959). It was also large and could not be sterilised by autoclave, making the design impractical for clinical use (Diettert, Bercu et al. 1958).

Along with Gibbon in 1953, Melrose was developing a film oxygenator however Melrose's design used a rotating disk configuration rather than vertical sheets. In the design blood entered a large cylindrical vessel. The cylinder included a succession of plates and washers compressed together to create compartments, within which the blood

would pool. As the cylinder rotated a thin film of blood was formed on the plate surfaces. The chamber that housed the rotating device was filled with oxygen. After one rotation the blood moved down into the next compartment and so on until it left the device. The oxygenator was kept under a transparent hood which included space heat lamps to heat the device and ensure that blood was kept at body temperature (Melrose 1953). Figure 27 and Figure 28 show a cross section of the cylinder/washer configuration of the Melrose N.E.P oxygenator and the actual oxygenator and control system, respectively.

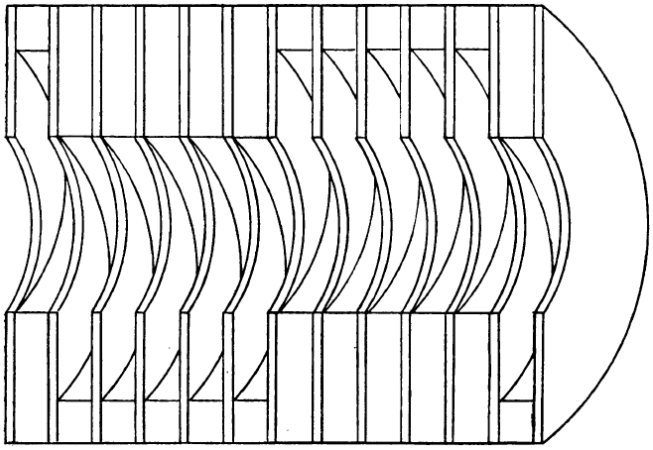

**Figure 27: Cross-section of cylinder washer arrangement within the rotating disk film oxygenator (Taken from (Melrose 1953)).**

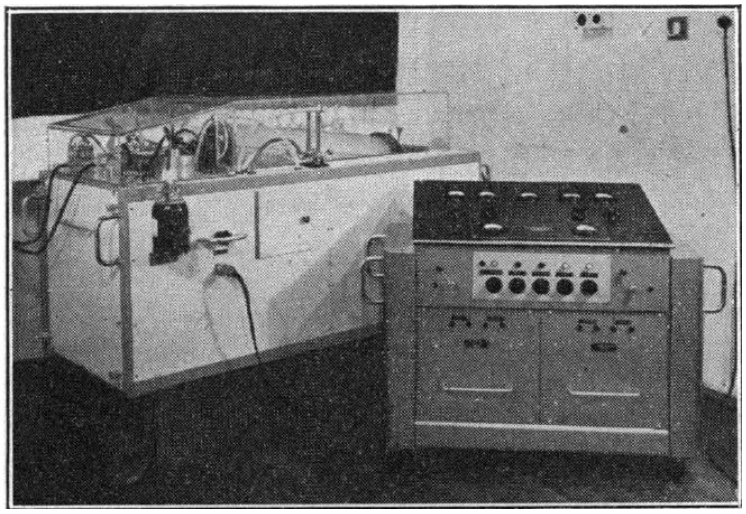

**Figure 28: The Melrose N.E.P oxygenator with control system (Taken from (Melrose 1953)).**

The main practical problem with this device was that if the discs were rotated at too high a speed foaming of the blood would occur (Nixon, Grimshaw et al. 1960). Initially the system used Perspex components in the oxygenator; however these were replaced with stainless steel in order to allow sterilization by autoclaving.

Kay and Cross developed a similar rotating disc design in 1956 that used Teflon on the rotating disks to reduce the haemolysis within the system (Cross, Berne et al. 1956).

Levels of haemolysis were low enough to be clinically acceptable at the time; however, this along with the immune response due to the exposure of blood to large surface areas of artificial material, limited these systems to very short term support.

### 1.6.2. Helical Reservoir Bubble Oxygenator

The first clinical use of a helical reservoir bubble oxygenator was in May 1955. The design was attributed to Dr Richard A DeWall. Blood was removed from the patient using a Sigmamotor finger pump. It was pumped up a long vertical PVC tube, through which pressurised oxygen was bubbled and hence oxygenation and carbon dioxide removal was again achieved through direct exposure of the blood to the gas. As the blood reached the top of the oxygenation tube it was then redirected to a debubbling chamber. The chamber was lined with silicone which acted as a defoaming agent. As a safety feature the blood was then passed down a helical reservoir to remove any remaining bubbles and was then passed through a filter prior to reinfusion. The helical coil bubble trap was submersed in a water bath to compensate for heat loss and heat lamps outside the device were used to reduce heat loss of the blood within the system (DeWall 2003; DeWall 2003). This helical reservoir bubble oxygenator was very successful and variations have been used clinically for over 50 years (Iwahashi, Yuri et al. 2004). Due to the fact that it was made of PVC, the system was disposable and could be autoclaved if sterilisation was required. Direct exposure of the blood to the oxygen bubbles caused a higher level of haemolysis when compared to other designs (Clowes

1960). The system was also limited to reasonably low blood flow rates, with the maximum achievable being around 3 L/min (Abrams 1959). Figure 29 and Figure 30 below show a diagram of the helical reservoir bubble oxygenator and a picture of Dr DeWall with an operating oxygenation system respectively.

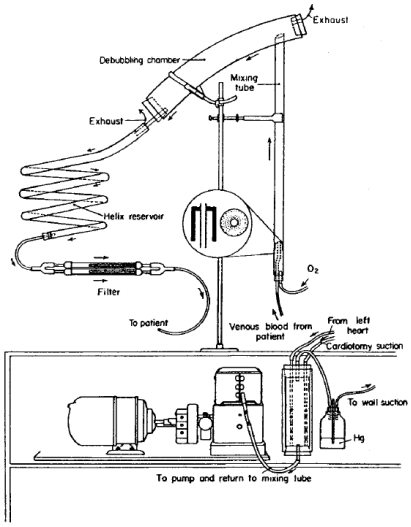


**Figure 29: Diagram of the Helical Reservoir Bubble Oxygenator (Taken from (DeWall 2003)).**

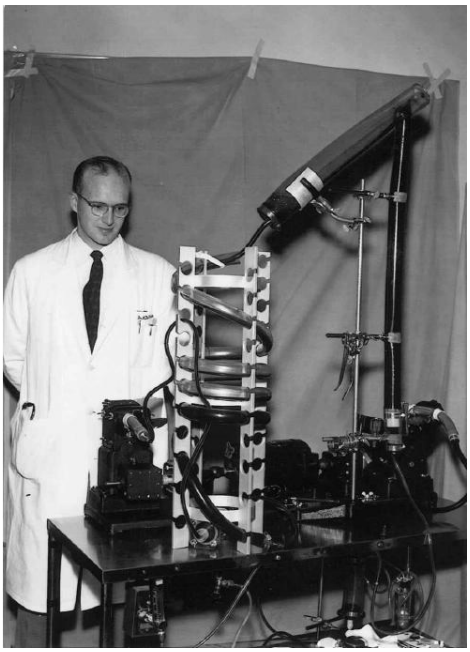

**Figure 30: Picture of Dr DeWall observing an oxygenator in the operating theatre (Taken from (DeWall 2003)).**

### 1.6.3. Membrane oxygenators

In 1956 Gorge H Clowes developed the first plate type membrane oxygenator. This device was based on the Skeggs-Leonard dialyzer developed in 1949 (Skeggs 2000). Clowes' device used multiple layers of gas-permeable Teflon membrane to achieve oxygenation of the blood (Iwahashi, Yuri et al. 2004). It was soon realised that the efficiency of such devices were limited by the rate at which gas transferred through the membrane. Clowes researched the effectiveness of different materials to act as membranes; his work indicated that silicone rubber was the most effective followed by Teflon, ethyl cellulose, polyethylene and cellophane (Clowes and Neville 1958).

The problems associated with Clowes' device were that it was prone to leaking and was difficult to assemble, mount and to sterilise (Drummond, Braile et al. 2005).

During experimentation linked with the development of an artificial kidney, Dr W J Kolff noted that blood became red as it passed through cellophane tubing. He associated this with gas exchange across the cellophane and subsequent oxygenation of the blood (Kolff 1997). This discovery led to the development of the coil membrane oxygenator. This design featured polyethylene tubing wound around a can. An oxygenation chamber was created by containing the device in a gallon bag filled with oxygen. Unlike previous designs oxygenation and carbon dioxide removal was not achieved through direct exposure of the blood but via diffusion through the tubing membrane. To achieve satisfactory oxygenation eight coil units were required (Kolff, Watschinger et al. 1956).

Ultimately the performance was limited by the high resistance to flow through the device. The configuration required large priming volumes and so to function efficiently large flow rates were required, which could not be achieved (Clowes 1960). Figure 31 and Figure 32 below show a single Kolff lung coil (left) and a full sized clinical oxygenator respectively.

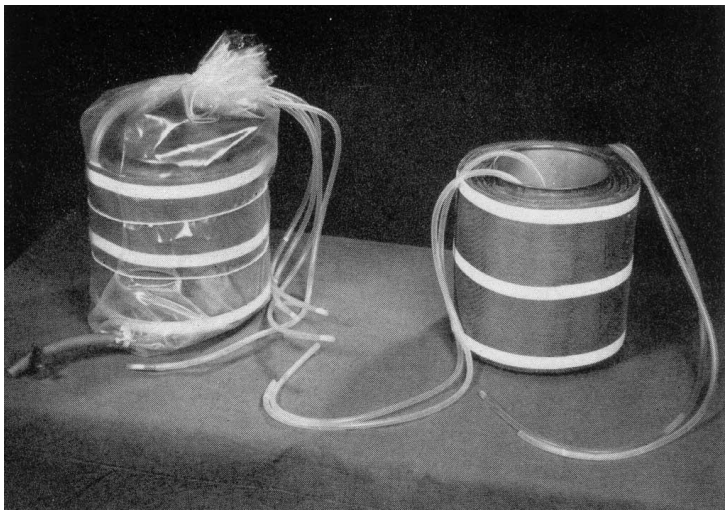

**Figure 31: Kolff artificial lung coil (right) and a sealed lung coil ready for clinical use (left).**

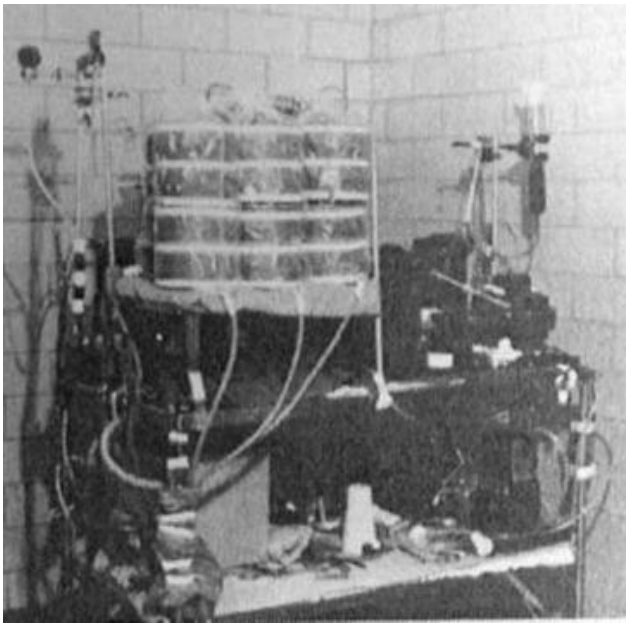

**Figure 32: Complete oxygenation system using and array of Kolff artificial lung coils (Taken from (Iwahashi, Yuri et al. 2004)).**

In 1963 Theodor Kolobow published data relating to his spiral membrane oxygenator design. The oxygenator consisted of a vinyl coated fibreglass mesh screen, which was enveloped by a Silastic coated Dacron screen. The envelope was sealed with oxygen inlet and outlets at either end of the device. Oxygen at negative pressure entered the

device creating a vacuum. This caused the Dacron to adhere to the fibreglass and assume the configuration of the mesh. The membrane was wrapped around a central cylinder and blood flow was parallel to the cylinder axis between individual layers of membrane. The irregular membrane surface induced mixing of the blood flow increasing efficiency. The intraluminal hypobaric pressure could also be changed to alter the membrane surface and hence provide continuous movement of the blood. The entire oxygenator was surrounded with a Silastic jacket, which eliminated the need for bolts or screws (Kolobow and Bowman 1963).

The oxygenator was evolved by Kolobow through the use of a silicone membrane (Kolobow, Spragg et al. 1971). This design allowed prolonged usage, and was the first oxygenator to be used successfully in adult (Hill 1977) and neonatal ECMO treatments (Bartlett, Gazzaniga et al. 1976). Figure 33 and Figure 34 below show a diagram of the Kolobow oxygenator and a picture of a clinical oxygenator respectively.

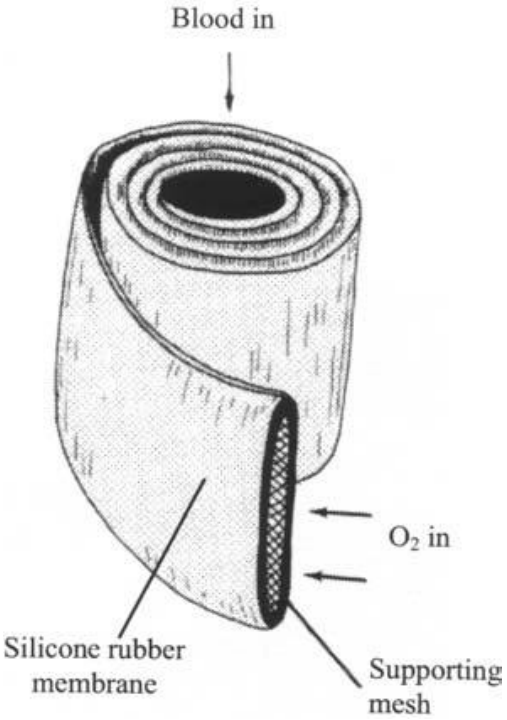


**Figure 33: Diagram of the inside of the Kolobow oxygenator (Taken from (Iwahashi, Yuri et al. 2004)).**


**Figure 34: Picture of a clinical Kolobow Oxygenator (Taken from (Iwahashi, Yuri et al. 2004)).**

Figure 35 shows a picture of 'Esperanza', survivor of the first neonatal ECMO treatment.

**Figure 35: Esperanza, first neonatal patient to be treated with ECMO, at the age of 21 with Dr Bartlett (Taken from www.surgery.med.umich.edu).**

### 1.6.4. Hollow Fibre Membranes – Development of the Modern Oxygenator

Membrane oxygenators offer advantages over film and bubble oxygenators in that they are more physiological, offer less haemolysis and didn't have the same danger of particulate or gaseous emboli (Clowes 1960); however a major restriction in membrane oxygenator design is that carbon dioxide partial pressures are particularly low in blood. Although early membrane designs had a high permeability to carbon dioxide, in order to maintain normal arterial carbon dioxide partial pressure a large surface area for gas exchange was required. This meant that the earlier generation of membrane oxygenators had large priming volumes and because of this their application in open heart surgery was limited (Clowes 1960; Sirotkina, Osipov et al. 1970; Heimbecker 1977).

The design of the modern oxygenator is based on satisfying the following criteria:

1. Physiological oxygen and carbon dioxide exchange.
2. Low priming volume.
3. Capability for extended use.
4. Haemocompatibility.
5. Ease of operation.
6. Low Cost. (Gaylor, Hickey et al. 1994)

A major step forward for membrane oxygenators was in the development of hollow fibre membranes. Hollow fibre membranes offer a high surface area to volume ratio and can be packed together within an oxygenator structure. This allows the designer to reduce the overall volume of the device and hence reduce priming volume. Early hollow fibre oxygenators were associated with impaired carbon dioxide removal, thrombus formation within the header, fall off in performance with scale-up of small units and non-uniform tube perfusion (Gaylor and Mockros 1978). These problems were due to poorly designed oxygenators and because the initial monolithic fibres produced did not have efficient gas exchange properties (Perepechkin and Perepechkina 1999).

In 1972 Y. Nose was developing the microporous membrane. In this design, gas exchange occurred through micorpores in the membrane structure that encourage direct exposure of the blood to the gas. However, the membranes were insufficiently hydrophobic and this resulted in the design being unsuccessful (Nose and Malchesky 1981). The first commercial oxygenator using the microporous membranes was not produced until 1981 (Suma, Tsuji et al. 1981). Microporous fibres are created by spinning and stretching polymers to produce a hollow cylinder with typical dimensions of approximately 300 μm outer diameter and 200 μm inner diameter. Micropores within the membrane structure are of around 0.2 μm in size. Several companies such as Celanese, Mitsubishi Rayon and Membrana produce these membranes.

Figure 36 shows scanned electron microscopy (S.E.M) images of the inner surface, cross section and outer surface of Membrana's Oxyphan polypropylene microporous membrane.

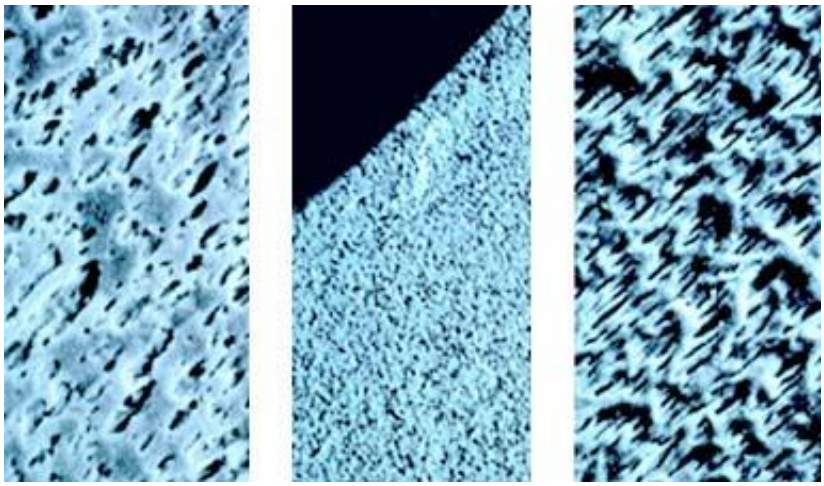

**Figure 36: S.E.M of inner surface, cross section and outer surface of a Membrana Hollow Fiber (Taken from www.membrana.com).**

The early hollow fibre oxygenator designs involved blood passing through the membrane capillaries and having oxygen circulating over the capillaries; however the small cross-sectional areas resulted in high resistance to flow and high pressure

gradients across the oxygenator. Thrombus formation was also common in the narrow membranes, which compromised the function of the oxygenator (Drummond, Braile et al. 2005). To address these problems later oxygenator designs featured intraluminal gas flow and extra luminal blood flow. In this configuration the fibres also act as turbulizers, which act to break up the concentration boundary layers, enhancing the efficiency of gas transfer (Catapano, Papenfuss et al. 2001). This design allowed a reduction in the required membrane surface area and priming volume and as a result in less contact activation of inflammatory and coagulation factors (Haworth 2003; Khoshbin, Roberts et al. 2005). Figure 37 and Figure 38 below give examples of intraluminal and extra luminal blood flow arrangements respectively.

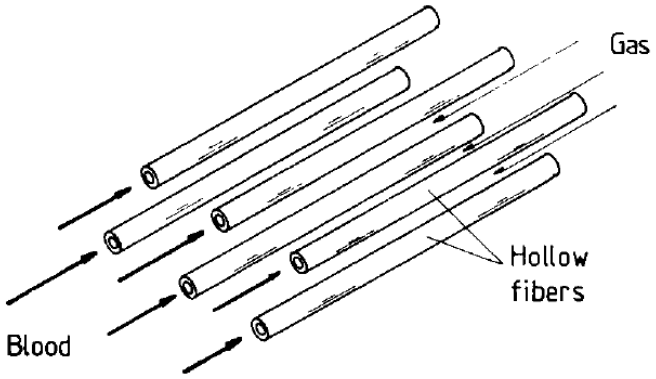


**Figure 37: Intraluminal blood flow arrangement (Taken from (Gaylor, Hickey et al. 1994)).**

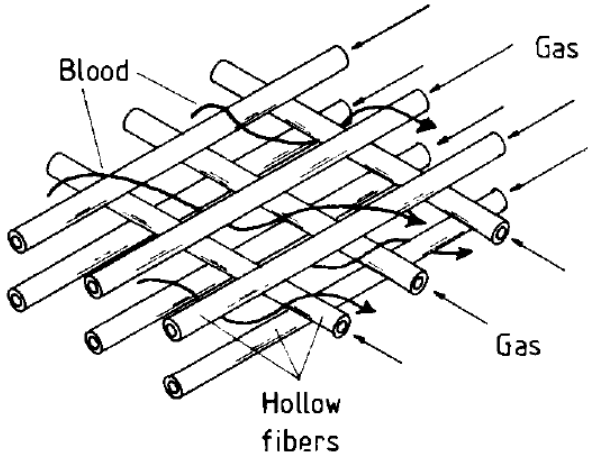


**Figure 38: Extra luminal blood flow arrangement (Taken from (Gaylor, Hickey et al. 1994)).**

In a hollow fibre membrane oxygenator with extra-luminal blood flow configuration uniformity of the blood flow through the device is essential to ensure sufficient performance. Uniform blood flow is achieved by accurate control of fibre position which also removes any areas of stagnant flow within the device (Gaylor and Mockros 1978). In modern oxygenators woven fibre mats are used to help control spacing. This combined with improved fibre stiffness gives satisfactory blood flow distribution (Haworth 2003).

Although microporous membranes provide oxygenators with efficient gas exchange whilst minimising priming volume, their use is limited to short term support due to plasma leakage. After 8 to 12 hours of contact between the fibre and blood, plasma will leak into the fibre wall. The micorpores are filled with liquid and the gas exchange efficiency is severely reduced (Eash, Jones et al. 2004). Plasma leakage is thought to be due to high driving pressures, absorption of phospholipids and condensation formation in the gas side (Meyns, Vercaemst et al. 2005). In order to successfully use hollow fibre technology for longer term applications, such as ECMO, plasma leakage needed to be addressed, particularly for neonatal and paediatric ECMO where patients are known to require longer durations of treatment (Motomura, Maede et al. 2003).

Plasma tight membrane hollow fibres feature a nonporous layer of membrane which completely isolates the blood and gas supplies addressing the plasma leakage issues of the microporous membrane (Eash, Jones et al. 2004). Two approaches to the design have been taken: skinned asymmetric or composite symmetric designs. Skinned asymmetric designs typically feature a microporous membrane, which have an outer nonporous skin; examples of this type of fibre are the Membrana Oxyplus and Dainippon Ink and Chemicals Separel fibre. Figure 39 and Figure 40 show S.E.M images of Membrana Oxyplus fibre and a diagram of the DIC Separel fibre, respectively.

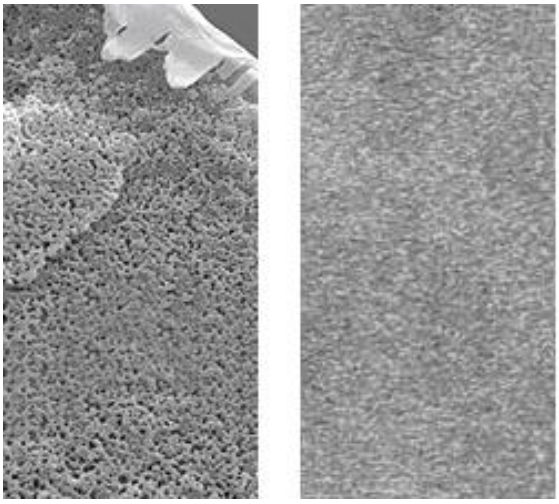

**Figure 39: SEM of cross section (left) and outer surface (right) of Membrana's Oxyplus Hollow Fiber (Taken from www.membrana.com)**

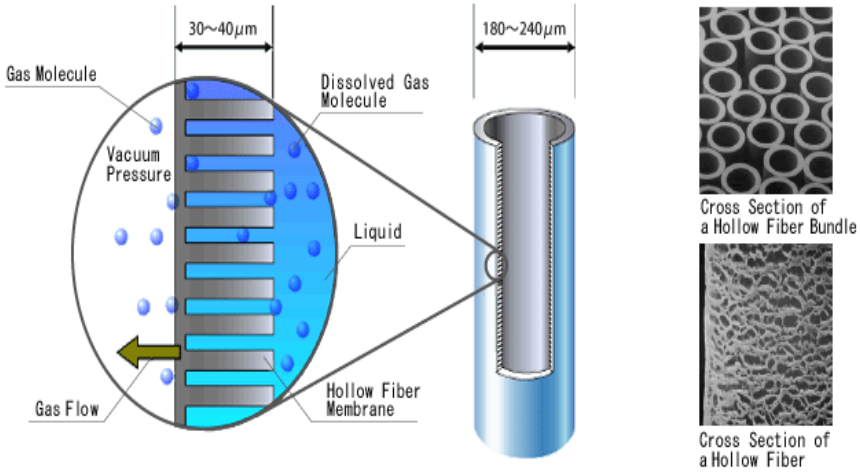


**Figure 40: Diagram of DIC Separel plasma tight hollow fibre (Taken from www.dic-europe.de).**

The composite symmetrical fibres are nonporous and are typically made from a base polymer and vinyl resin cross-linked using siloxane. Manufactures of these fibres include Senko (Mara) Medical Devices with the Mara Silox-S fibre and the Advanced Membrane Technology (AMT) fibre.

Currently there are over 50 different types of oxygenators that are commercially available. The design and performance of each system are all slightly different. The method of treatment of a patient varies between institutions and in each case is likely to be a complex combination of various modalities. The ideal choice of oxygenator therefore, similar to the method of treatment, will also vary between institution; no single solution for all applications exists; however it is widely agreed that the most efficient system to date is one, which incorporates hollow fibres in an extra luminal flow configuration (Gaylor, Hickey et al. 1994; Segers, Heida et al. 2001; Kawahito, Motomura et al. 2002; Leonard 2003; Drummond, Braile et al. 2005; Khoshbin, Roberts et al. 2005).

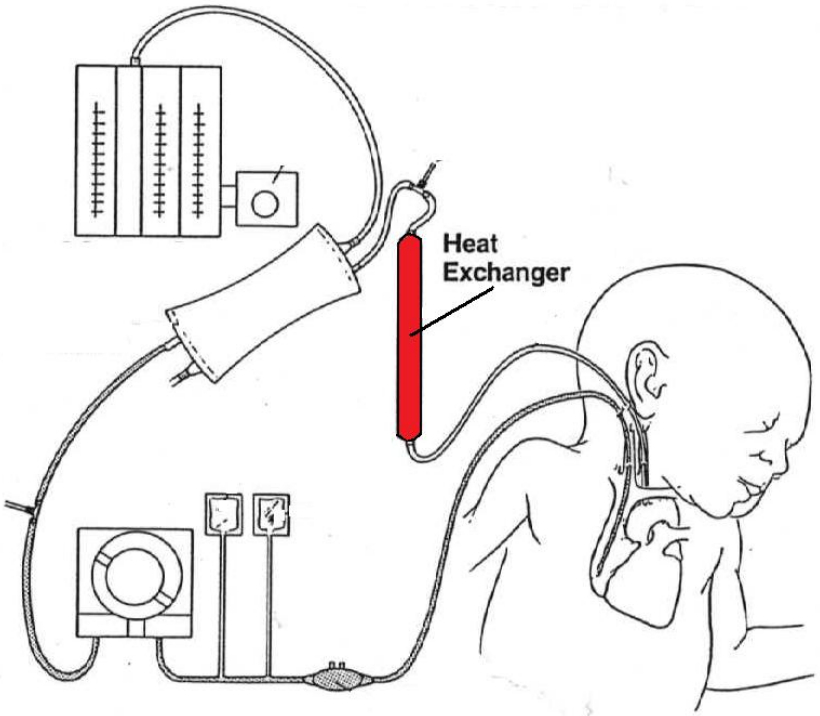


## The ECMO Circuit: The Heat Exchanger

## 1.7. Heat Exchangers

Blood removed from a patient will continually lose heat to the extracorporeal circuit and to the surroundings. In order to maintain normothermia of a patient blood must be heated prior to reinfusion. Heat exchangers are used to control the temperature of the body. They are typically placed after the membrane oxygenator (the final part of the circuit and typically the greatest source of heat loss) and heat the blood just before it is returned to the patient. In current systems the heat exchanger will either be an external component or will be built into the membrane oxygenator. In all cases heat transfer occurs through counter-current flow exchange between the blood and heated water as shown within Figure 41.

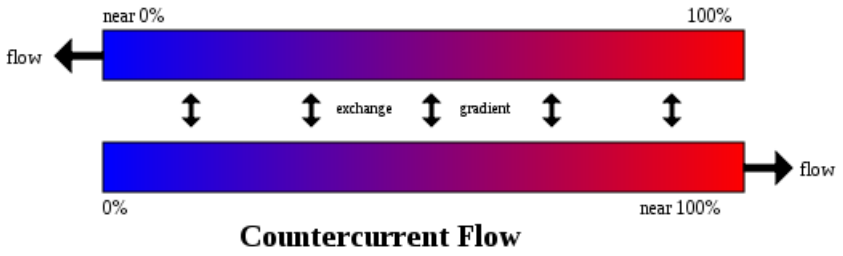


**Figure 41: Counter-current heat exchange configuration (Taken from en.wikipedia.org).**

Currently all heat exchange systems used incorporate a circulation system and a water bath. Design of the exchanger must be such that efficient heat transfer occurs without areas of localised heating, which may lead to haemolysis. Some designs, such as the Medtronic ECMOtherm, also act as a bubble trap. Figure 42 and Figure 43 show a diagram of a MEDOS oxygenator with built in heat exchanger and a Medtronic ECMOtherm external heat exchanger respectively.

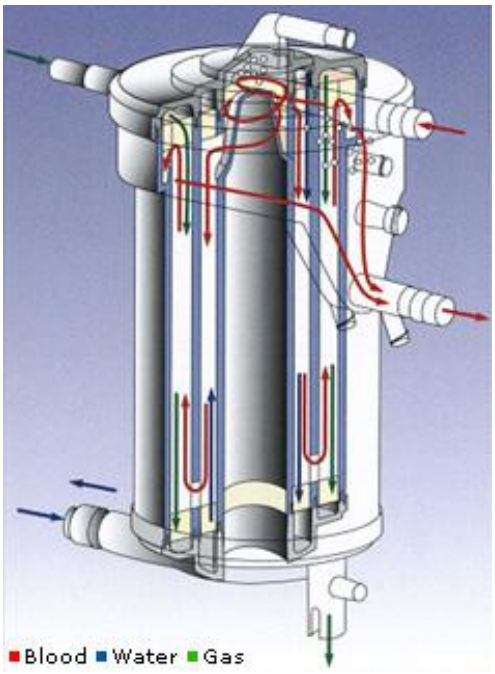


**Figure 42: Diagram of a Medos oxygenator with blood and water circulation systems (Taken from www.medos-ag.de)**

**Figure 43: Medtronic ECMOtherm external heat exchanger (Taken from www.medtronic.com).**

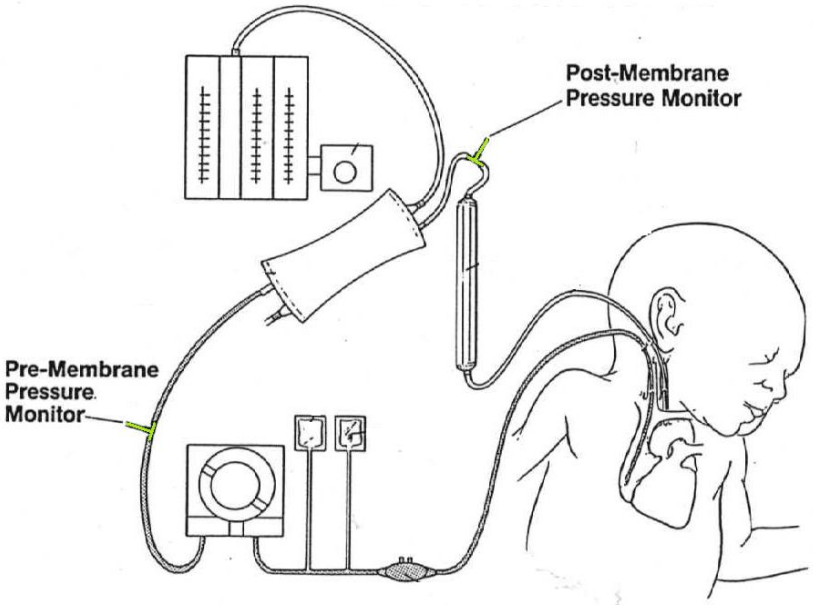


## The ECMO Circuit:

## Monitoring and Circuit Safety

## 1.8. Monitoring and Circuit Safety

Monitors within the ECMO circuit are essential to ensure that the system is working properly and to help provide early detection of/avoid circuit complications.

### 1.8.1. Pressure monitoring

Pressure monitoring is used pre-pump and pre and post oxygenator. Pre-pump pressure monitoring determines the pressure of the venous line drainage and is used to avoid negative pressure and to servo-regulate the pump system.

The oxygenator provides the highest resistance to flow within the circuit. Pre and post oxygenator pressure monitors are used to determine the pressure gradient across the oxygenator. A high pressure gradient is indicative of clot formation within the oxygenator. A pressure gradient above a certain value will result in an alarm sounding to let the clinicians know that there is a problem with the circuit.

### 1.8.2. Blood Flow

Blood flow is typically monitored using an ultrasonic detector. If a roller pump and standard tubing is used then flow can be calculated from pump capacity and the r.p.m of the blood pump. The flow rate will be proportional to the size and weight of the patient.

### 1.8.3. Oxyhaemoglobin Saturation

Oxyhaemoglobin saturation measurements are made pre and post membrane. A saturation of at least 95% is achieved in a fully functioning oxygenator. However venous saturation levels are typically used to monitor and manage the ECMO system.

Blood gases are also monitored pre and post oxygenator to determine the inlet and outlet $PCO_2$ and blood pH. Blood gases are measured either by continual inline monitoring or by batch sampling.

### 1.8.4. Bubble Trap

Many systems will have an independent bubble trap or will have bubble traps built into the oxygenator or heat exchanger; however bubble detectors are still used in the blood return line. Alarms will sound upon detection of a bubble and this can lead to a line being clamped or to the pump being switched off. Level sensors are also used to determine the capacitance of the system and ensure that air is not in the system.

## 1.9. Modern System Design

### 1.9.1. ECMO Design Considerations

The most important requirements in the design of a modern ECMO system are to offer safe and effective performance to the patient undergoing the treatment. The fundamental goal of the designer should be to improve patient outcomes; reducing morbidity and mortality rates through the application of modern technology and intelligent design. The sole function of an ECMO system is to manipulate human blood such that the system can temporarily replace the function of the heart and lungs of a patient to provide time for recovery. To achieve this task successfully the following criteria must be addressed:

### 1.9.2. Haemolysis

Haemolysis is the breaking down of a red blood cell with the haemoglobin content being released in to the surrounding medium. The breakdown of damaged or aging cells is common within the body and only around 10 % of the total cells recycled per day haemolyse in the blood stream (Martini 2005). Several mechanisms can lead to haemolysis, such as colloid osmotic lysis, perforation of the cell and erythrophagocytosis; however in an extracorporeal systems the main cause of haemolysis is through fragmentation of the red blood cells as a result of exposure to shear stress (Sharp 1998; Matsuda 1999; Gage 2002).

Haemolysis on a large scale results in increased levels of red blood cell constituents in the blood stream and this can have various clinical sequela such as hemoglobinuria, acute renal failure, increased systemic and pulmonary vascular resistance, altered coagulation profile, platelet dysfunction and increased mortality (Burgreen 2001; Qian 2006). In all extracorporeal systems each of the circuit components has the potential to cause haemolysis. Haemolysis within pumping systems (Curtis, Wagner-Mann et al.

1994; Moon, Ohtsubo et al. 1996; Morgan, Codispoti et al. 1998; Burda, Trittenwein et al. 2004; Thiara, Hoel et al. 2007) and oxygenators (Visser and de Jong 1997; Nakata, Maeda et al. 2000; Kawahito, Maeda et al. 2002; Kawahito, Motomura et al. 2002) is well documented. Although each of the components are designed to be free of or have clinically acceptable levels of haemolysis, problems can occur in the integration of the various components that make up the complete ECMO circuit (Burgreen 2001).

### 1.9.3. Thrombosis

Blood circulating around an ECMO circuit is exposed to a large surface area of foreign material. Platelets adhere to the surface and are activated, leading to the release of more enzymes and causing further platelet aggregation and activation of the clotting system (Lequier and Chan 2005). The clotting system is initially activated via the intrinsic pathway. This induces thrombin formation, which causes fibrinogen to be converted into fibrin and ultimately clot formation. Thrombin also causes the release of tissue factor and platelet factor – 3, which then initiates the extrinsic coagulation pathway and also accelerates the intrinsic pathway, hence a cascade effect is observed (Martini 2005). Excessive consumption of platelets during ECMO can lead to thrombocytopenia. Thrombocytopenia can lead to spontaneous bleeding or exacerbate bleeding and increases the risk of intracranial haemorrhage (ICH). ICH within neonates is associated with 62% mortality rate (Zwischenberger, Nguyen et al. 1994). As mentioned within section 1.1.5 (Complications during ECMO), the thrombolytic potential of the ECMO circuit results in the need for systemic anticoagulation of the patient.

### 1.9.4. Inflammatory Response

The treatment of a patient using an extracorporeal circuit has been widely associated with an inflammatory response (Chenoweth 1987; Wan, LeClerc et al. 1997; Gourlay, Stefanou et al. 2001; Graulich, Sonntag et al. 2002; Paparella, Yau et al. 2002). The inflammatory response induced is complex and is known to include compliment

activation, release of cytokines, leukocyte activation with expression of adhesion molecules and the production of oxygen-free radicals, platelet-activating factor, nitric-oxide, arachidonic acid metabolites and endothelins (Wan, LeClerc et al. 1997). The response is particularly complicated as there are a variety of ways in which the various elements that result in inflammation are activated. Firstly the patient may be predisposed to an inflammatory response due to their underlying condition. This has been shown to be the common with neonates suffering from respiratory failure (Fortenberry, Bhardwaj et al. 1996). During ECMO, inflammation can be caused through material dependent or independent factors. Intelligent design of an ECMO system can improve upon the factors that result in material dependent inflammation.

Blood exposed to a foreign surface has been shown to result in an inflammatory response (Gourlay, Stefanou et al. 2001) (Courtney, Lamba et al. 1994). Compliment activation occurs via the alternative pathway through exposure of blood to a foreign surface resulting in the formation of C3a and C5a (Chenoweth 1987; Utley 1990). C3a and C5a cause histamine release from mast cells and basophils, increase vascular permeability and stimulate white blood cells to release oxygen-free radicals and lysomal enzymes (Wan, LeClerc et al. 1997). C3a stimulates platelet aggregation and C5a stimulates neutrophil aggregation and adhesion to endothelial cells (Utley 1990). Neutrophil adhesion to endothelial cells is an important step in tissue injury leading to neutrophil migration and degranulation in the surrounding tissues. CD11b (mac-1) is an adhesion molecule that is expressed on the neutrophil cell surface. The concentrations of CD11b have been shown to increase during cardiopulmonary bypass (Rinder, Bonan et al. 1992) and have also been shown to be proportional to the surface area of the extracorporeal circuit that the blood is exposed to (Gourlay, Stefanou et al. 2001).

### 1.9.5. Clinical Requirements

The key characteristics of a successful ECMO system are:

- Performance
- Reliability
- Ease of use and accessibility
- Cost

As mentioned previously the performance and outcomes of ECMO depend heavily upon the time taken to initiate the treatment. An aggressive approach to the implementation of the treatment could significantly improve morbidity and mortality rates; however there is a stigma attached to ECMO such that it is most commonly used as a last resort after all other alternative therapies have been considered. ECMO is an invasive and complicated procedure used to treat patients in critical conditions. Maintaining the life of human being is extremely difficult and has only been made possible through the use of cutting edge technology. The complexity of the circuit and the duration of the treatment make mechanical complications almost guaranteed. The system also requires highly skilled operators available 24/7. The equipment and staff costs are high and as a result ECMO is restricted to specialised centres. Specialised centres reduce the accessibility of the treatment and hence the lack of availability increases the time between a patient requiring ECMO and the initiation of the treatment. For ECMO to be more successful the reliability issues must be addressed in order to improve the way in which medical professionals view the treatment. The complexity of the technology, although necessary, must be presented in a way such that the system is easier to use and maintain, without compromising on performance. By providing clinicians with a more reliable system that is easier to control and by improving accessibility more aggressive treatment strategies could be adopted. This would reduce the time taken to implement the treatment and ultimately improve patient outcomes.

## 1.10. Miniaturized and Integrated Extracorporeal Membrane Oxygenation

The development of a prolonged life support system is a complicated task. Multiple requirements exist that must be evaluated and prioritized. There is no single solution; however based upon evidence from the medical literature and consideration of the design requirements it is evident that a miniaturised and integrated system is a natural evolution of life support technology and one that represents the essentials of a modern system design. The benefits of such a system can be considered in terms of patient outcome and benefit to the clinicians operating the device.

### 1.10.1. Miniaturisation

A miniaturised system would provide the following:

- Reduced blood to foreign material surface contact area.

By reducing the surface area of foreign material to which the blood is exposed would reduce the magnitude of the inflammatory response (Gourlay, Stefanou et al. 2001). A reduction in the surface area would also have a direct impact on the thrombo-embolic potential of the system.

- Reduced priming volume.

A miniaturised device would require less blood to prime the system. A low prime volume ECMO system can be pre-primed with saline rather than donor blood. This can aid in rapid deployment of the system, reducing initiation times (Yamasaki, Hayashi et al. 2006) and the inflammatory response associated with use of foreign blood products (Hamada, Kohtani et al. 2001).

- Increased accessibility.

Reducing the foot-print of ECMO is essential in increasing the accessibility of the treatment. Currently specialised centres are limited as to the number of beds available due to the size of the equipment. Reducing the foot-print should also make the patient more accessible to both the clinician and family members.

- Increased manoeuvrability.

The logistics and risk involved in moving patients whilst on ECMO are significant. Limited mobility restricts ECMO patients in terms of other treatments they require, which cannot be accessed without transportation. This can impact on patient outcome and duration of hospitalization.

Although miniaturisation can provide several benefits a balance must be made between size, performance and device safety. A miniaturised system is likely to see higher pressures and faster moving flow. This will increase the requirements of the pump, which if miniaturised will have to rotate faster and hence the potential for haemolysis increases. An oxygenator must be able to perform to a certain standard through a range of conditions. Typically an oxygen saturation of approximately 95% with a venous saturation of 70% is deemed acceptable (Smith 2007). The rate at which oxygen diffuses into the blood depends upon the material properties of the fibres used, the surface area exposed for diffusion and upon the duration of the blood within the oxygenator. The performance of an oxygenator is therefore dependent upon its size and so the potential to miniaturise this component is limited. The safety of the device must also be considered. By reducing the volume of the device and increasing blood velocity the ability to remove air from the system is affected. A certain level of safety is required and so compromise for size must be compensated for in some other way. This could be through improved design of the system components or through the

addition/improvement of monitoring sensors. A further advantage of a miniaturised system would be in its ability for its component parts to be effectively integrated.

### 1.10.2. Integration

By integrating the system the following would be possible:

- Increased reliability.

ECMO systems typically consist of multiple components from various manufactures each with separate control systems. The composition of the system depends upon the institution implementing the treatment. This cocktail of devices increases the potential for mechanical complications and also increases the complexity of the system making it harder to maintain and to operate. A fully integrated system would significantly reduce these problems by having the components sourced from a single manufacturer. An integrated control unit could be used potentially reducing the training and level of maintenance required. These benefits would have a direct impact on the operating costs of the device along with patient outcomes. Furthermore, standardisation of the treatment could allow for more extensive research to be conducted and could allow hospitals offering the treatment to share experience and training more easily.

- Potential for a semi-intelligent system.

Having a single control unit influencing the entire system provides the potential for semi-intelligence and partial automation. An intelligent system could be configured to recognise clinically relevant situations based upon feedback of monitoring devices. The system could act on the information gathered or suggest a course of action to be taken. The system could also contact the relevant professionals through wireless communications. An integrated system would provide the most reliable format for a semi-intelligent control system giving the most potential for successful introduction of this established technology to applications in life support.

- Optimization of miniaturization.

An integrated system compliments full and efficient miniaturization. By focusing on the way all of the components are connected valuable savings in size can be made that can be used to increase the safety and performance of the each of the elements individually. A miniaturised and integrated system is one that addresses all of the significant design challenges. Improved performance and reliability combined with reduced operational and maintenance requirements will result in a system with considerably greater accessibility increasing the potential indications for ECMO. The system could be used with more aggressive treatment strategies and deployed in emergency situations, reducing the time to initiation and ultimately improving patient outcomes.

Miniaturization and integration has been shown to be an appropriate strategy to improve the performance, accessibility and ability of ECMO to be rapidly deployed (Arens, Schnoring et al. 2008; Gariboldi, Grisoli et al. 2011; Arlt, Philipp et al. 2012; Roncon-Albuquerque, Basilio et al. 2012).

## 1.11. Project Aims

ECMO involves an extracorporeal circuit temporarily replacing the function of the heart and lungs of a critically ill patient over an extended period of time. In temporarily replacing the function of the heart and lungs the treatment aims to allow the major organs time to recover from a critical condition.

It is a very invasive procedure and involves exposing blood to a highly complex artificial system. Exposure of the blood to foreign surfaces results in biological reactions that have negative impacts on the patient. The complexity of the circuit, although necessary, makes mechanical complications of some sort almost guaranteed during the treatment and also makes it expensive and difficult to operate, requiring a specialist staff available twenty four hours a day all year round. For these reasons ECMO is only available in specialist centers and hence accessibility of the treatment is limited.

The highly invasive nature of the treatment combined with the complex technology required makes ECMO a last resort technology. However after an extensive review of the literature it is quite clear that in order to improve the morbidity and mortality rates associated with ECMO the solution lies in the development of a miniaturized and integrated system.

The work within this thesis will specifically focus on the neonatal population. This patient population is being chosen as it reflects the most common usage of ECMO. Future work on the system should involve investigation into scaling of the technology to allow it to be used in pediatric and adult ECMO.

To this end the work within this project will focus on successfully meeting the following aims:

- To develop a miniaturized and integrated extracorporeal membrane oxygenation system, involving the development of an appropriate blood pump, membrane oxygenator and heat exchanger.

- To produce a system that has the potential to operate independent of main supplies and is therefore portable.

- To design the system such that aspects of the system that are in contact with blood are disposable allowing the device to be rapidly deployed.

- To test the technologies to demonstrate that they are capable of functioning in near clinical conditions.

- To use a combination of computational modeling and physical testing to optimize the design stage, reducing the time and cost associated with purely iterative physical prototyping and testing.

# 2. Concept Development

## 2.1. Introduction

In this project an iterative design philosophy will be adopted in which device development is split into four stages: concept development, computer modelling, laboratory testing and animal testing. At each of these stages the performance of the device will be measured and if satisfactory the device will evolve into the next stage. If the device fails, the feedback is used as an input into the previous step. Figure 44 below shows a flow chart of the project design philosophy.

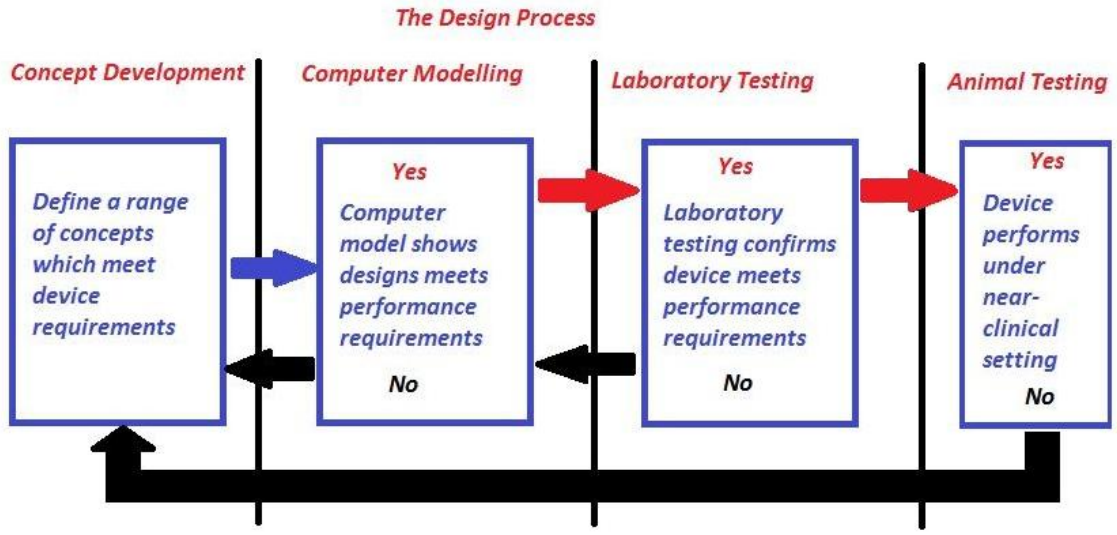


**Figure 44: A flowchart showing the design philosophy adopted within this project.**

Concept development is the foundation stage of this design philosophy. The purpose of concept development is to produce a set of designs to meet the requirements of a specific application. This is essentially an iterative process, taking a step-wise approach to meeting performance demands. The concepts provide approximate descriptions of the form, working principles, and product features of the device. Each of the design iterations is evaluated and the most suitable is selected for further refinement. Efficient concept development can aid all of the future steps of the device development, saving both time and money.

Thorough concept development is particularly essential for projects involving the integration of multiple components. Basing foundation designs on an integrated system ensures that the theme of integration is featured throughout the development process. Taking this approach in which the challenges of integration are considered from the outset and revised and reviewed throughout the design cycle the final integration of the refined components becomes a simpler task. The first step in concept development is to ensure that the application and requirements used to define the form and function of the device are fully established. To do this effectively, group creativity techniques such as brainstorming were used to allow the perspectives of all stakeholders involved to be considered. Figure 45 below shows an initial brainstorming session using a whiteboard.

**Figure 45: Initial whiteboard brain storming session to investigate the fundamental design requirements.**

In the present case the concept designs were formed to satisfy pre-existing qualitative requirements based upon clinical parameters which are well defined in terms of form and function. The geometries were not based upon any technical information; however, the size of each fundamental component was kept within a set of acceptable limits.

### 2.1.1. Review of the High-Level Design Requirements

The following points were highlighted in the review of the field as being the key considerations in the design of an ECMO system. These include both device requirements and desired characteristics – in essence addressing form and function.

- An oxygenator
- A blood pump
- A heat exchanger
- Minimised priming volume
- Minimised blood to foreign surface contact area
- Minimised haemolysis
- Minimised thromboembolic potential
- Biocompatibility
- Clinical acceptance

These requirements and characteristics should not be considered a complete design profile, rather, other factors such as manufacturability, maintenance, ease of access and aesthetics must be considered. The contribution of these factors to the overall form and function must also be taken into account.

In several cases the satisfaction of these requirements will come at the expense of another and therefore a compromise must be made in order to produce an efficient design. However in making these compromises the safety and efficacy of the end product of the design and conceptualization must remain of utmost importance. This is the principle factor underpinning this design work.

### 2.1.2. Initial Considerations

Some fundamental design requirements of the major components must be addressed prior to concept development.

#### *The Pumping System*

The most commonly used pumping systems within ECMO today are the roller pump and the centrifugal pump. Each system can produce sufficient flow rates, whilst overcoming high resistance with minimal haemolysis. However, when considering the design of a completely miniaturized and integrated ECMO system these pumping solutions are not appropriate as they would place unnecessary constraints on the potential geometry of the ECMO system.

Other pump systems are utilized in medical practice, including the axial flow pump (AFP). The most common application of the AFP is as a ventricular assist device (VAD). The AFP has shown to be efficient, consistent and reliable treating patients for many years (Goldstein 2003). The main challenge facing an AFP in an ECMO system is in overcoming the considerable resistances and producing sufficient flow rates without causing excessive haemolysis. The AFP is, however, well described in terms of its use in medical applications and its profile and general form fit well with a miniaturized and integrated system. For these reasons the concepts developed in this chapter will focus on utilizing an axial flow pump.

#### *The Heat Exchange System*

Current heat exchangers in ECMO are largely based upon water driven counter current exchange devices. This type of system is able to satisfy the performance requirements but is unable to meet the size restrictions of a miniaturised system. The water needs to

be heated or cooled and requires its own heat exchanger out with the device itself. Furthermore a separate circuit and pump is required to pump the water to the heat exchanger. The result is a significant increase in the size, cost and complexity of the ECMO system. This large footprint is one of the major challenges of current ECMO technologies.

The focus of the heat exchanger development process is to eliminate the water driven heat exchange system and replace it with a device of smaller foot print, reduced complexity and with minimal reliance on external components. The present work will focus on the development of a solid state solution to the provision of thermal control. A device of this nature will lend itself well to the integration process.

In all concept designs the modules have been based upon the geometries

## 2.2. Chapter Aims

The aims of this chapter are as follows:

- Develop a number of conceptual ideas based upon producing a miniaturised and integrated device that satisfies the fundamental design requirements previously established.

- Select the most efficient design from the concepts produced to be used as the foundation for the following, more detailed development chapters.

## 2.3. The Concepts

Before finalizing the design of the device for prototyping and subsequent performance testing a number of design configurations were considered. These range from the more conventional (Concept 1) to a design which meets the overall design rational in a more creative manner (Concept 3). The three concepts generated are considered in turn in the following sections and their degree of acceptability in terms of the major design, manufacture and application requirements were considered prior to concept selection and further development.

### *2.3.1.* Concept 1

Figure 46 below is a ProEngineer model showing the geometry and configuration of the components that form the Concept 1 integrated design.

**Figure 46: ProEngineer model showing the geometry and configuration of the components that form the Concept 1 integrated design.**

This model is based on a cylindrical design, which is featured in several currently available commercial oxygenators. The cylindrical design represents a fairly

conventional approach with limited novelty but one which can be easily understood by clinicians familiar with current ECMO technologies. Blood enters the AFP from the bottom of the system. In this configuration of the design space was made to accommodate an electromagnetic drive; however the design could be easily adapted to allow for direct drive of the pump. Figure 47 below shows a model of Concept 1, which has been sectioned down the center of the device. The location of the pump system geometry is highlighted in the cross-section in red.

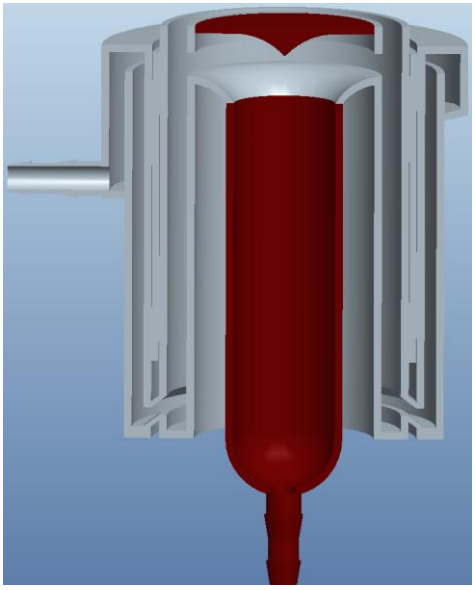

**Figure 47: ProEngineer model showing the cross-section of the concept 1 design highlighting the location of the pump component (in red).**

From the pump, blood is directed into the oxygenator and forced to move down and across the fibers. The gas flow is counter-current to the blood flow to increase the efficiency of oxygenation and carbon dioxide removal. Figure 48 below shows a cross-section of the system highlighting the location of the oxygenation system (in blue).

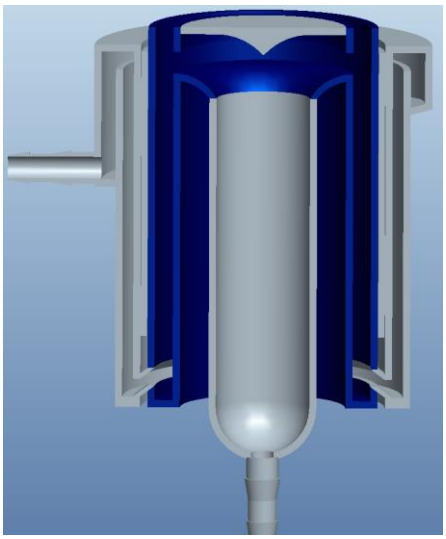

**Figure 48: ProEngineer model showing a cross-section of the Concept 1 design highlighting the location (in blue) of the oxygenation system.**

The blood moves from the oxygenator to the heat exchanger. A solid state heat source is sandwiched between the oxygenator bundle and the heat exchanger surface. This should transfer heat to the blood both within the exchanger and as it moves through the oxygenator bundle. Figure 49 below shows a cross-section of the system highlighting the location of the solid state heat source (in yellow).

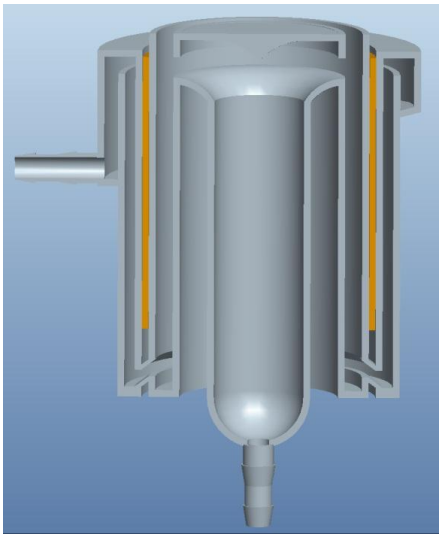

**Figure 49: ProEngineer model showing a cross-section of the concept 1 design highlighting the location (in yellow) of the solid state heat source.**

Figure 50 shows a cross-section with the location of the heat exchanger geometry and the blood path outlet from the device highlighted (in white).

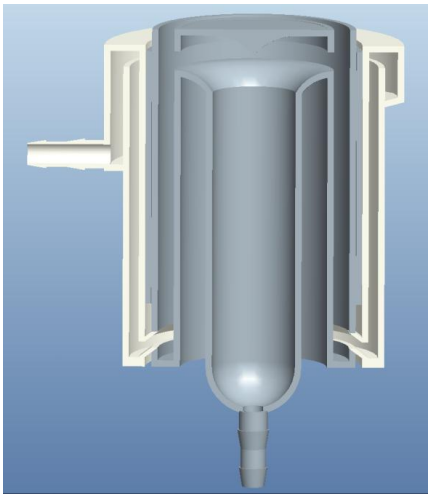

**Figure 50: ProEngineer model showing a cross-section of the concept 1 design highlighting the location (in white) of the heat exchanger.**

Figure 51 shows the complete concept model with an example of what a holder/control system might look like for the design. An early stage concept for the holder/controller is highlighted in black.

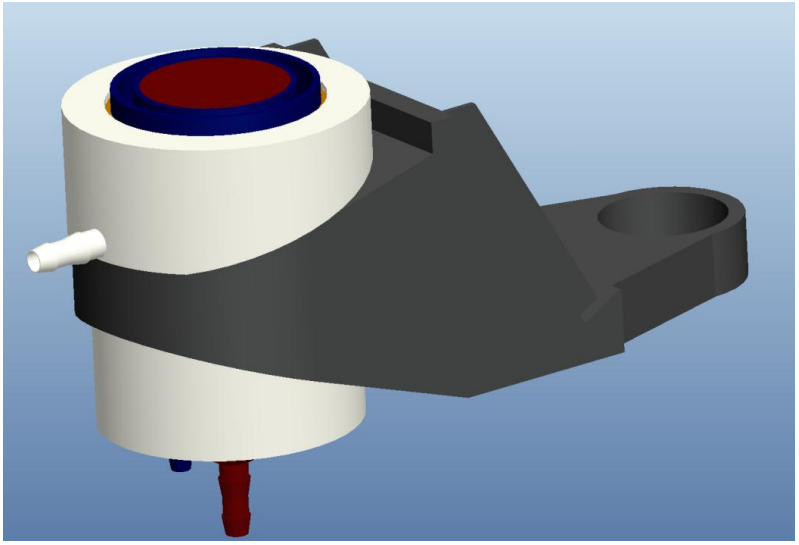

**Figure 51: ProEngineer Model showing the concept 1 design being held in an example of what a holder/control unit may look like for the system.**

### 2.3.2. Advantages of Concept 1 Design

- Conventional form

This design has been based upon conventional forms of the major components of the ECMO system. As such this design should be familiar to clinicians, making it easier to understand and more likely to gain acceptance.

- Compact encased components

This design is based on layers, with the pump on the inside, oxygenator in the middle and heat exchanger in the final outer layer. This configuration produces a compact cylinder and as such the device would not need an external casing, which could potentially reduce manufacturing costs.

- Thermal efficiency

The compact layers will ensure that heat loss to the surroundings is minimized and having the solid state heat source sandwiched between layers should make the thermal properties of the system particularly efficient.

### 2.3.3. Disadvantages of Concept 1 Design

- Manufacturability

The integration strategy used in this design was restricted by the conventional forms of the fundamental components of the system. As a result the compact layered design does not lend itself to a simple manufacturing process.

- Accessibility

Similar to manufacturability, accessibility is limited by the layered configuration. Access to the internal parts of this device will be impossible unless this is specifically addressed in future development of the design. This additional requirement could have significant implications on the cost and complexity of the final device configuration.

- Safety

The blood path is obscured in the internal structures of the devices. This could negatively impact upon the reaction time of a clinician to a bubble in the circuit reducing the overall safety of the device.

### 2.3.4. Concept 1 Design Summary

This design is based on components with a conventional form integrated in the most efficient manner possible. The resulting system is highly compact with familiar principles that should be easy for clinicians to understand and should inspire confidence.

Although the conventional form of the device should be familiar and inspire confidence it was not designed for efficient integration. As a result the concept has weaknesses in manufacturability, accessibility and the overall device safety.

### 2.3.5. Concept 2

Figure 52 below is a ProEngineer model showing the geometry and configuration of the components that form the Concept 2 integrated design

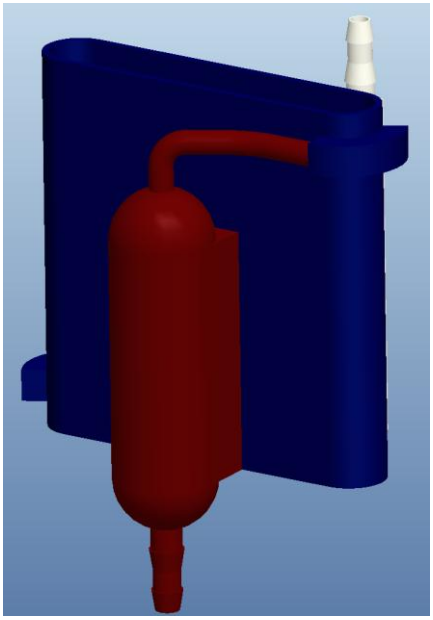

**Figure 52: ProEngineer model of the geometry and configuration of the components that form the concept 2 integrated design.**

This concept is based upon the simplest form of integration of the three fundamental components, which comprise an ECMO system. The oxygenator and heat exchanger have been flattened and all have been brought together in order to minimize the inter-connections between each element with the AFP at the most convenient location on the front of the oxygenator.

Similar to concept 1 blood enters the system through the bottom of the device train into the AFP, which is highlighted (in red) in Figure 53 below.

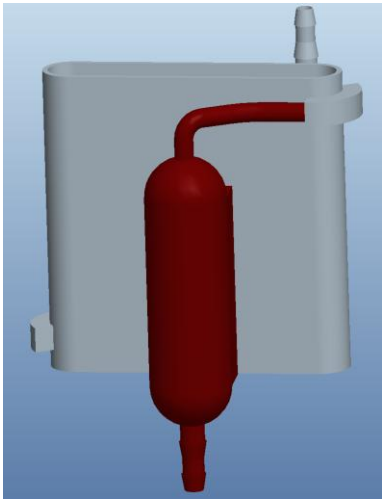

**Figure 53: ProEngineer model highlighting the location of the axial flow pump (in red) in the concept 2 design.**

Ideally the AFP would again be electro-magnetically driven, minimizing the need for bearings and shaft elements; however there is scope for direct drive. The blood leaves the pump and moves to the upper corner of the oxygenator. The blood is forced to move down and across the oxygenator bundle to the exit, which is diametrically opposed to the inlet. Gas flow enters at the bottom of the bundle and exits through the top ensuring counter-current flow. Figure 54 below highlights the location of the oxygenator bundle (in blue) in the concept 2 design.

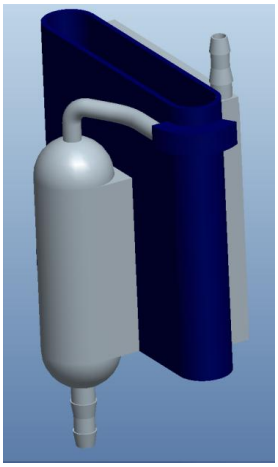

**Figure 54: ProEngineer model highlighting the location of the oxygenator bundle (in blue) in the concept 2 design.**

Upon exiting the oxygenator the blood enters the heat exchanger compartment. The blood is channeled through the heat exchanger to increase exposure to the heating element. The location of the heat exchanger in the concept 2 design is highlighted (in white) within Figure 55.

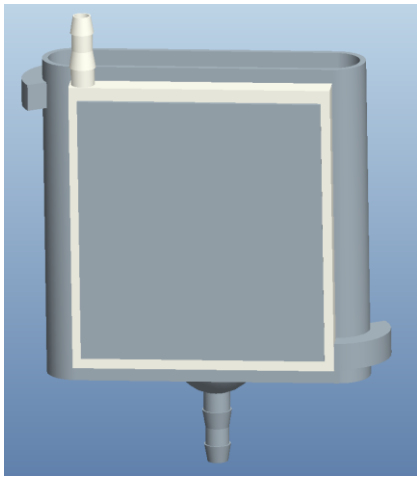

**Figure 55: Proengineer model highlighting the location of the heat exchanger (in white) in the concept 2 design.**

The heating element is located on the back of the heat exchanger as shown within Figure 56 below.

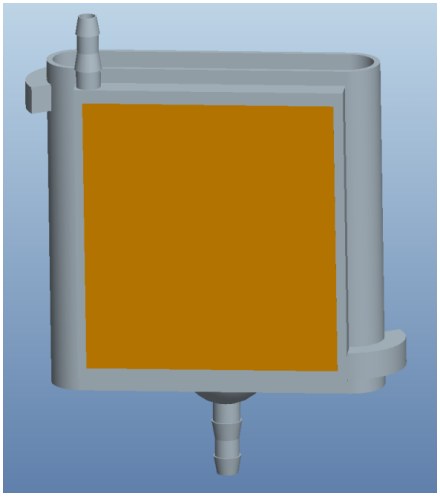

**Figure 56: Proengineer model highlighting the location of the solid state heat source (in yellow) in the concept 2 design.**

The blood exits the system from the top of the heat exchanger. This configuration would require an external casing in order to hold and protect each of the elements of the design. Figure 57 and Figure 58 below show a concept casing for the device and Figure 59 and Figure 60 show the complete design with concept casing connected to an example of a potential holder/controller configuration for the system.

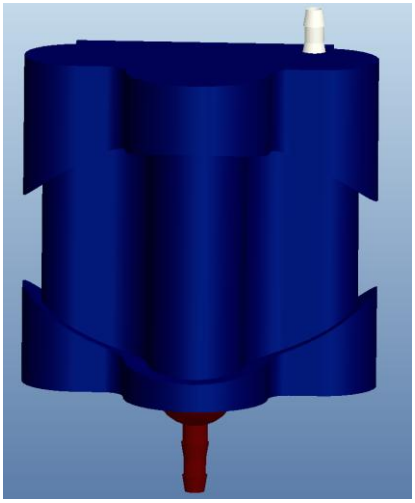

**Figure 57: ProEngineer model showing a front view of the complete concept 2 design with casing.**

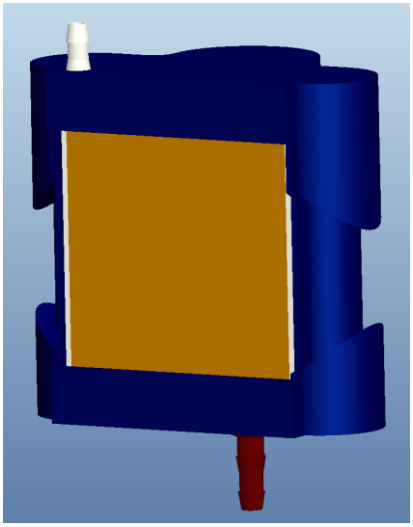

**Figure 58: ProEngineer model showing a rear view of the complete concept 2 design with casing.**

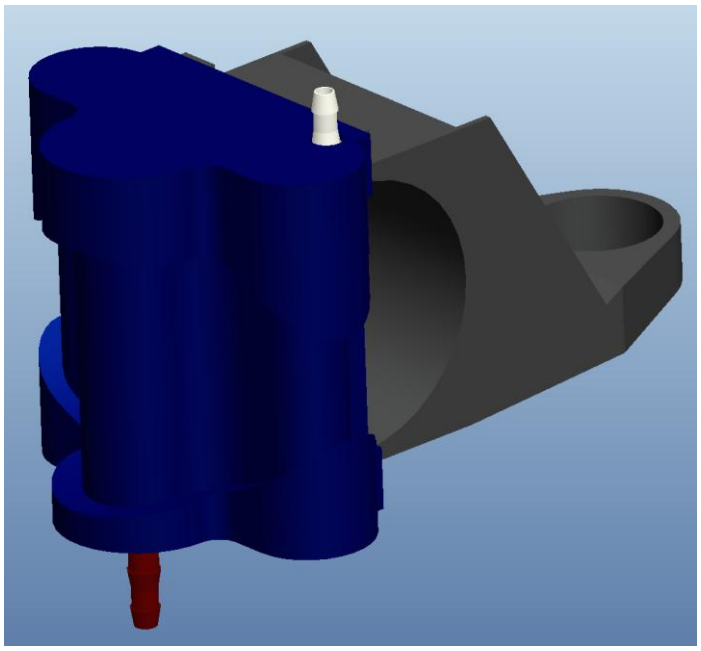

**Figure 59: ProEngineer model showing a front view of the complete concept 2 design with an example of a potential holder/controller for the system.**

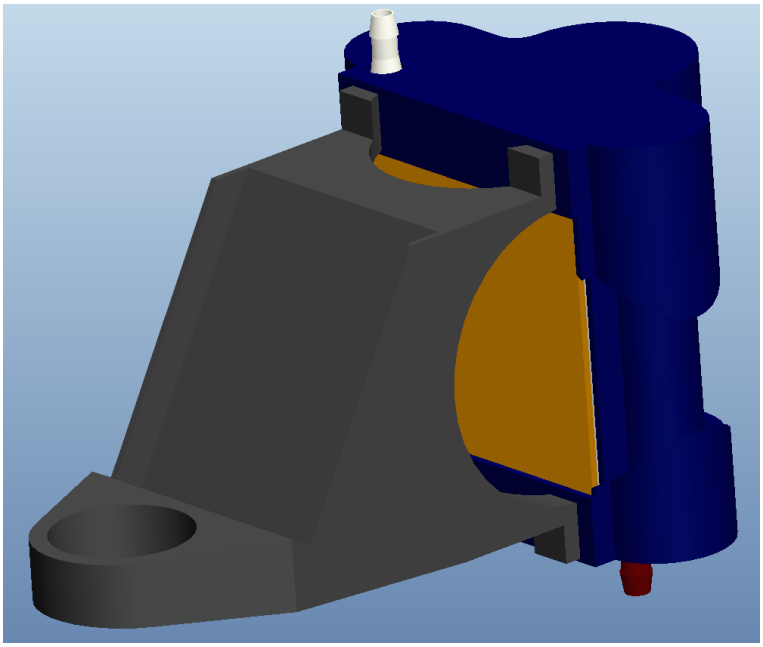

**Figure 60: ProEngineer model showing a front view of the complete concept 2 design with an example of a potential holder/controller for the system.**

### 2.3.6. Advantages of Concept 2 Design

- Manufacturability

In the Concept 2 design the integration strategy is based upon minimized interconnections and so in terms of the integration of the system this design features a more conventional approach. As a result each of the major components could be manufactured individually, considerably reducing the complexity of the manufacturing process in comparison to the concept 1 design.

- Accessibility

This device train should be considerably more accessible than Concept 1 as it is comprised of individual components. This configuration should also allow for much easier integration of the monitoring and control systems to be used.

- Safety

The flow path does not feature any layers and hence blood can be observed through the entirety of each aspect of the device, assuming that the external casing is transparent. This should increase the overall safety of the device.

### 2.3.7. Disadvantages of Concept 2 Design

- External casing

This configuration requires an external casing, which will add to the overall manufacturing costs. However by careful design the external casing can be used to

improve the practicality of the device making interfacing with a holder/controller unit a much simpler task.

- Foot print

This design is likely to have a lager foot print when compared with concept 1 as the integration of the components is less intimate and due to the requirement of an external casing. This could mean a higher priming volume and greater blood – foreign surface contact area and hence reduced performance.

### 2.3.8. Concept 2 Design Summary

The design of the major components of this system is less conventional when compared to Concept 1; however the integration approach is based upon optimizing the conventional method used in current ECMO systems. The resulting system is one which is simple to manufacture, is accessible and easy to understand.

### 2.3.9. Concept 3

Figure 61 below is a ProEngineer model showing the geometry and configuration of the components that form the Concept 3 integrated design.

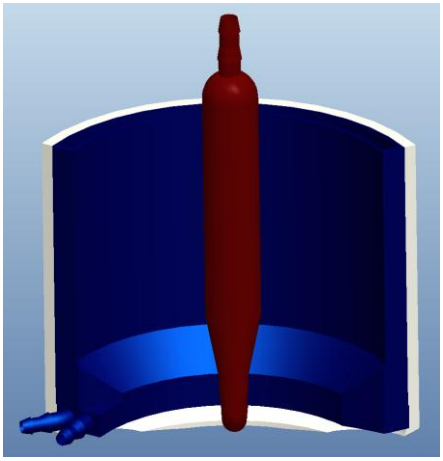

**Figure 61: ProEngineer model showing the geometry and configuration of the components that form the Concept 3 integrated design.**

This concept focuses on producing a system in which the main geometrical feature is an arc. Similar to the previous design a casing would be required to surround the elements. The principle upon which this concept is based is that the gas exchange bundle envelops the pump offering some protection. The result of this is a broader narrower fiber mat section which presents a large surface area upon which to directly apply a solid state heat exchanger. Unlike the previous designs blood enters from the top of the system. Figure 62 below highlights the location of the blood pump (in red) in the concept 3 design.

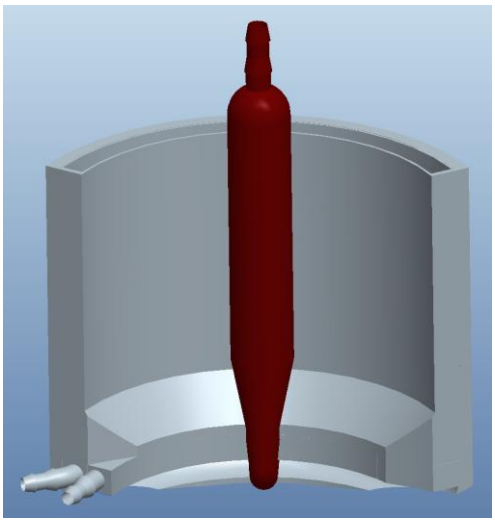

**Figure 62: ProEngineer model highlighting the location of the pump (in red) in the concept 3 design.**

Upon exiting the pump the blood is directed towards the heat exchanger. At this point the blood flow is spread out around the whole of the arc with the cross-sectional area gradually increasing to reduce velocity and to produce uniform flow distribution. The heat exchanger is located behind the oxygenator as shown (in white) within Figure 63 below.

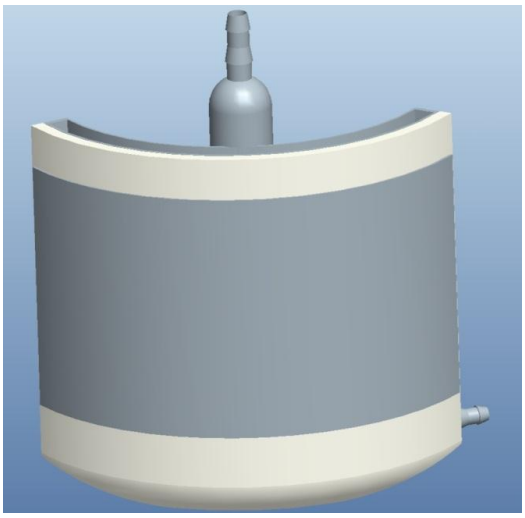

**Figure 63: ProEngineer model highlighting the location of the heat exchanger (in white) in the concept 3 design.**

Similar to concept 2 the solid state heat source is located on the back of the exchanger as shown (in yellow) within Figure 64.

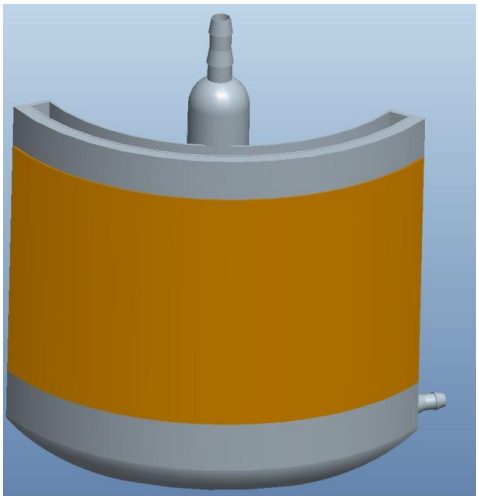

**Figure 64: ProEngineer model highlighting the location of the solid state heat source (in yellow) in the concept 3 design.**

The blood moves from the heat exchanger to the top of the oxygenator. The blood must move down and across the bundle to reach the exit reservoir. Gas flow enters from the bottom and leaves from the top of the bundle to once again achieve a counter-current arrangement. Figure 65 shows the location of the oxygenator bundle (in blue) with the blood outlet and gas inlet at the bottom.

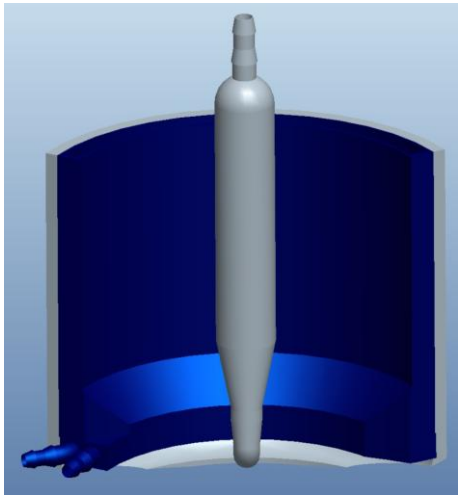

**Figure 65: ProEngineer model highlighting the location of the oxygenator bundle (in blue) in the concept 3 design.**

This concept also requires an external casing to hold and protect the components. The casing should allow for easy connection to a control system, while also ideally housing sensors and other control hardware. Figure 66 below shows the design with an external casing with the air vents and fans highlighted on the casing.

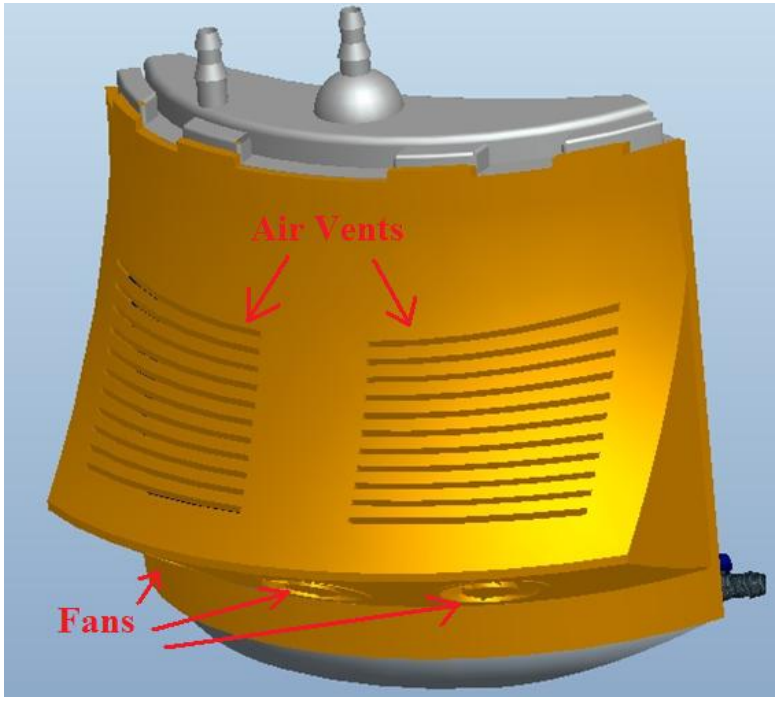


**Figure 66: ProEngineer model of the integrate concept 3 complete with external casing. Air vents and casing fans are highlighted in red.**

The fans and air vents on the external casing would be used to allow circulation of air throughout the device to aid the system in the event of it being used to cool the patient. Figure 67 and Figure 68 show the device including a potential configuration for a holder/controller for the concept 3 design.

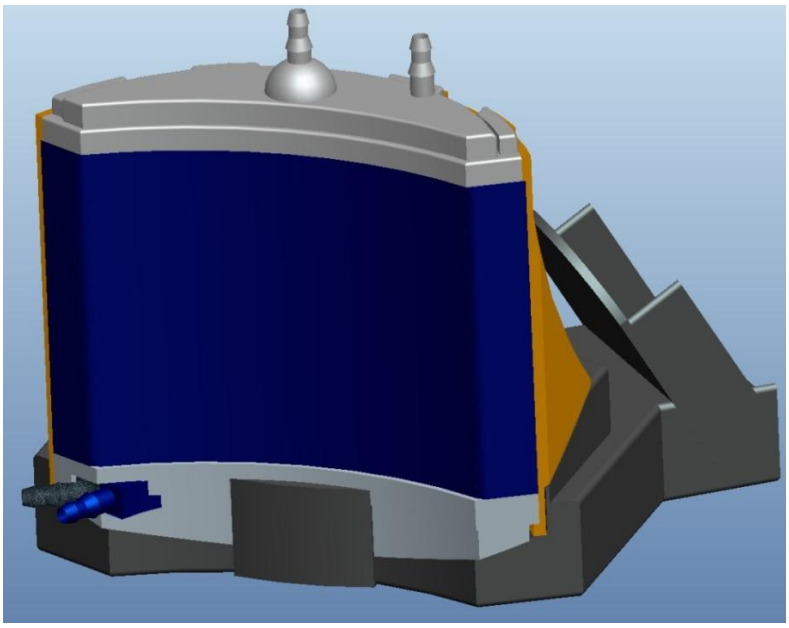

**Figure 67: ProEngineer model showing a front view of the concept 3 interfacing with a potential configuration of a holder/controller for the design.**

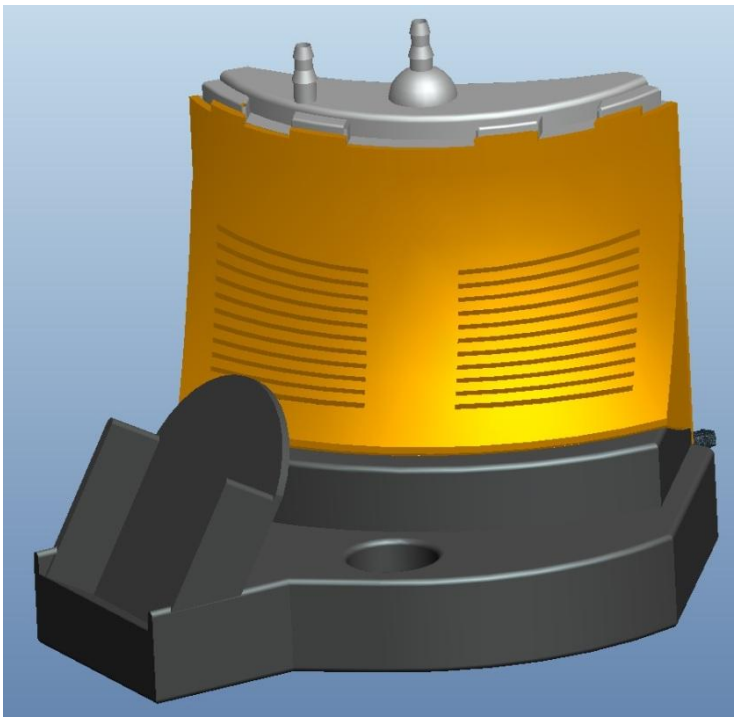

**Figure 68: ProEngineer model showing a rear view of the concept 3 interfacing with a potential configuration of a holder/controller for the design.**

### 2.3.10. Advantages of Concept 3 Design

- Novelty

This design focuses on a creative and innovative solution to a miniaturized and integrated ECMO system. Novelty can be used to allow the device to be differentiated from its competitors and let's potential users understand that this is something new, not simply an adaptation of conventional design.

- Foot Print

This design has actively adapted the fundamental components to allow for efficient miniaturization and has adopted a non-conventional integration strategy. This flexibility in the design has produced the smallest foot print of all of the concepts.

- Manufacturability

The manufacturing issues faced by concept 1 have been somewhat addressed in this design due to a non-conventional form being taken for the fundamental components. This design can be split naturally into four sections:

1. A top – holding the gas outlet and blood outlet.
2. A bottom – interfacing the pump with the heat exchanger and holding the blood outlet and gas inlet.
3. The AFP – standard design.
4. The oxygenator and heat exchanger.

This set-up would allow the oxygenator to be potted and then interfaced with the other components.

### 2.3.11. Disadvantages of Concept 3

- Location of the Heat exchanger

The configuration of the device train is such that the blood will enter the heat exchanger before the oxygenator. With the oxygenator the last aspect prior to reinfusion further heat loss could occur and would need to be compensated for. This could result in more complicated thermal control of the system.

- Safety

There is a degree of overlapping in this design and it would require a clinician to look at the device through 360 degrees to see the complete flow path. This could reduce the reaction time of a clinician to a bubble in the ECMO circuit, possibly impacting on the overall safety of the device.

### 2.3.12. Design Summary

Concept 3 is innovative and does not follow any of the guidelines of conventional design. This approach has produced a concept with a very small foot print, which can be easily broken down for manufacture. The wide arc of the oxygenator produces a large surface area which should improve the performance of both the oxygenator and the heat exchanger, whilst also enveloping the pump system offering protection and reducing the overall foot print.

## 2.4. Concept Evaluation

To enable evaluation of the concepts a concept selection matrix was established. This method involved evaluating each concept in terms of certain key design requirements – Aesthetics, Ergonomics, Manufacturability and Performance Requirements – and ranking them without weighting as to how well the design aspect was satisfied. The definition of each of aspect and the criteria against which the concepts were ranked are given below.

### 2.4.1. Aesthetics

Aesthetics relates to the senses and emotions of a person and the response someone has to an object. An aesthetically pleasing object is one which positively stimulates your senses giving you a pleasurable feeling. The opposite applies to an aesthetically displeasing object. A user's view of a device can encourage its use and presents a degree of satisfaction based on form and function. The importance of this element although subjective cannot be underestimated.

### 2.4.2. Ergonomics

Ergonomics refers to human interaction with a product, equipment, environment or system. An ergonomic design will result in optimized performance, whilst protecting the health, safety and well-being of individuals involved.

Satisfaction in terms of ergonomics is achieved by producing a system that can be easily operated and understood by the user, in this case clinicians. The system should be easy to handle, all aspects should be accessible and it should be operable in close proximity to a patient.

### 2.4.3. Manufacturability

Design for manufacturability considers the potential cost and ease of manufacturing of a product. Addressing the requirements of potential manufacturing methods early in the development process helps to avoid potentially expensive and time consuming redesign in the end stages.

In this project two phases must be considered. The first is for prototyping and the second for end-product manufacturing. Prototyping is iterative and parts that require complicated manufacturing techniques may restrict the quality of the development process; however parts designed for simplified manufacturing techniques may experience reduced quality. Satisfaction of this criterion will involve producing a simplified system that can undergo adaptation of some or all aspects without requiring significant redesign.

### 2.4.4. Performance Requirements

The performance requirements of the product must always be kept at the forefront of the design process to ensure clinical uptake. To do this effectively the requirements of the product must be sufficiently defined prior to design development.

A satisfactory design will have considered all of these requirements with compromise offset by some gain. In the present work an efficient design will be one that emphasizes miniaturization and integration with effective use of space and natural integration of the fundamental components, without compromise of safety or clinical performance demands.

### 2.4.5. Concept Selection Matrix

As discussed each concept was evaluated on a scale of 1 – 10 in each design criteria - 10 being highly effective and 1 being ineffective. Figure 69 below shows the concept selection matrix.

| Requirement | Concept Selection Matrix<br>Concept 1 | Concept 2 | Concept 3 |
|---|---|---|---|
| *Aesthetics* | 5 | 7 | 9 |
| *Ergonomics* | 8 | 7 | 6 |
| *Manufacturability* | 5 | 8 | 7 |
| *Performance Requirements* | 6 | 6 | 7 |
| **Total Score** | 24 | 28 | 29 |

**Figure 69: Concept Selection Matrix used to evaluate the concepts developed.**

All of the concepts have scored relatively highly; however there are notable differences in some criteria. A breakdown of the scoring rational is given below:

***Aesthetics***

In this area concept 1 has scored the lowest. This is because the outside of the device is defined by the geometry of the heat exchanger, which limits the scope for improvements on the aesthetics of the design. The other concepts require external casings and so an opportunity exists to consider aesthetics in the design of the outer shell. The third

concept scored marginally higher as the integration strategy used allows for more flexibility in the external casing design.

***Ergonomics***

In this criteria concept 1 scored the highest as it is based on conventional form and function. This should be the easiest design for the clinicians to understand. Although this design has layers, which make it difficult to observe bubbles there are several areas that could produce effective bubble traps.

Concept 2 scored second highest as the system integration is very basic and therefore the system should also be easily understood. The flexibility in the integration process should also help in producing efficient bubble traps.

The third concept scored the lowest as it is based on non-conventional design. This will therefore require clinicians spend some time to understand the system and how it works. This design also offers the least potential for a bubble trap, with the only realistic places being at the top of the heat exchanger and possibly in the reservoir at the outlet.

***Manufacturability***

In this criterion the ability to pot the oxygenator and integrate it with the rest of the system is one of the key aspects considered. Concept 2 scored the highest as the integration strategy used is the simplest which should result in the least complex manufacturing process.

The flexibility of the design and integration strategy used in the development of concept 3 has produced a design that can be easily split into major sections, which has a direct impact on the manufacturing process.

Concept 1 scored the lowest as it is based on non-conventional integration of conventional concepts. The inflexibility of the component design resulted in the concept failing to produce any obvious manufacturing strategies and therefore this design is likely to be the most complex and expensive to build.

***Performance Requirements***

In this case the third concept has again scored highest. This is due to the efficient miniaturization and integration that has been achieved through the flexibility of the design approach. As a result this concept has produced the smallest foot print.

Concept 2 has been scored at the same value as concept 1, although the latter has a smaller foot print. The layers of concept 1 shroud the blood path, possibly impacting on the overall safety of the device. Whereas the compromise in foot print of concept 2 has been off-set by a clearly defined blood path that enhances the safety of the design.

From the evaluation of all of the concepts the matrix has shown that concept 3 has scored the highest. The non-conventional design and integration has produced a concept that has the highest potential in terms of aesthetics and meeting the performance requirements without compromising manufacturability or ergonomics. The flexibility of this design approach should be particularly beneficial in early device development.

## 2.5. Concept Development

A fuse deposition rapid prototype was created of Concept 3 with external casing and control base as shown within Figure 70 below.

**Figure 70: Rapid prototype of concept 3 with a holder and example control device and connections.**

## 2.6. Chapter Conclusions

Concept development is an essential step in the evolution of a new device. It allows the designer to more freely engage in creative thinking to help produce exciting and innovative ideas. Considering requirements at all of the stages of a product life cycle allows for efficient design and should help in accurately defining the scope, cost and time required to achieve a suitable quality of device.

The evaluation method used allows for an impartial selection of the most suitable design. This provides a foundation for individual component development chapters ensuring that the initial requirements, aesthetics, ergonomics and manufacturability of the design have been considered from the very start of the development process. In theory this process will lead to a more effectively defined device, which meets the application needs with enhanced manufacturability. The veracity of this association will become clear as the project progresses.

# 3. The Pumping System

## 3.1. Introduction

The function of the heart is to perfuse the body with oxygenated blood. The heart is comprised of four muscular chambers; the left atrium, left ventricle, right atrium and right ventricle. The right atrium (RA) receives un-oxygenated blood from the systemic system. This un-oxygenated blood is passed from the RA to the right ventricle (RV). The RV them pumps the blood through the pulmonary circuit. Within the pulmonary circuit blood is passed through capillaries in the lungs. Here, gas exchange occurs; oxygen is transferred to the blood and $CO_2$ is removed. The oxygenated blood then moves to the left atrium (LA) via pulmonary venous return. From here it is passed into the left ventricle (LV). The LV is the largest section of the heart pumping oxygenated blood through the systemic circuit. The blood transfers oxygen to the tissues of the body and removes $CO_2$. It then returns to the RA via systemic venous return in order to start the cycle again. Each day the heart beats approximately 100,000 times and pumps 8000 litres of blood (Martini 2005).

During ECMO the function of the patient's heart is temporarily replaced by a blood pump. It is often considered desirable that the heart itself continues to pump during ECMO procedures . However much the heart contributes to the perfusion of the body during the ECMO procedure, the blood pump must be capable of augmenting this and providing the body with a normal systemic blood flow and critically for a mechanical system, it must be able to achieve this without compromising the integrity of the blood itself.

Over the past few decades, a number of pumping systems have evolved for ECMO applications. These include the roller and the centrifugal pumps, which according to the most recent survey of ELSO registered centres are the most commonly used pumps in the clinical setting (Lawson, Ellis et al. 2011). The roller pump typically produces non-pulsatile flow by the action of two rollers that compress tubing causing a positive displacement of fluid when rotated. The centrifugal pump features an impeller, which

when rotated draws fluid into the eye and then accelerates it outwards where it exits tangentially. Both systems are usually driven from the base and can provide sufficient flow rates, whilst overcoming considerable resistances. Although it is currently common practice to use one of these pumps in current ECMO circuits the configuration of these systems are impractical for efficient miniaturisation and integration. A more suitable option is the axial flow pump (AFP). This pump is most commonly used as an implanted ventricular assist device (VAD) supporting a patient for an extended period of time. The size and orientation of this pump design make it an ideal candidate for a fully miniaturised and integrated ECMO system.

## 3.2. Initial Considerations

The complicated fluid dynamics within pumping systems makes design particularly challenging. Traditionally an iterative design process is used based on extensive prototyping and experimentation. Theoretical fluid dynamics was limited to 1-D mean line analysis prior to the invention of computational fluid dynamics (CFD), which can provide the designer with detailed information of the flow field as it passes through the system. A combination of the traditional design approach with CFD as a tool for design optimization has been shown to be successful in producing cheaper and more efficient pumping systems (Sutera 1975; Sallam 1984; Chimenti 2004; Dehbahani 2009)

In ECMO the blood pump is responsible for removing blood from the patient, passing it through the components of the system and then pumping the treated blood back to the patient in order to perfuse the tissue. To do this the pump must provide a sufficient pressure head to overcome the resistance of the ECMO circuit, all of its components and the patient's vasculature resistance. This performance must be achieved without damaging the formed blood elements.

### 3.2.1. Mechanical Haemolysis

When fluid moves across a solid object, fluid particles are brought to rest on the surface. Figure 71 shows a diagram highlighting the action of the fluid particles at the solid surface.

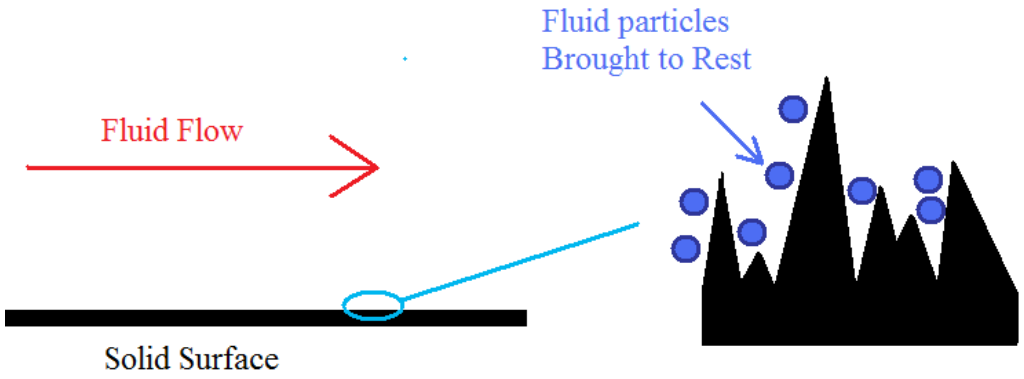


**Figure 71: Diagram showing fluid particles being brought to rest at a solid surface.**

The particles that are brought to rest influence neighbouring particles, reducing their momentum. The magnitude of reduction in momentum decreases with increasing distance from the solid surface. At a large enough distance the particles are no longer affected and are said to move at the free stream velocity. The distance from the solid surface to these unaffected particles is known as the boundary layer. Figure 72 below shows a diagram of the velocity profile of a fluid moving over a solid surface.

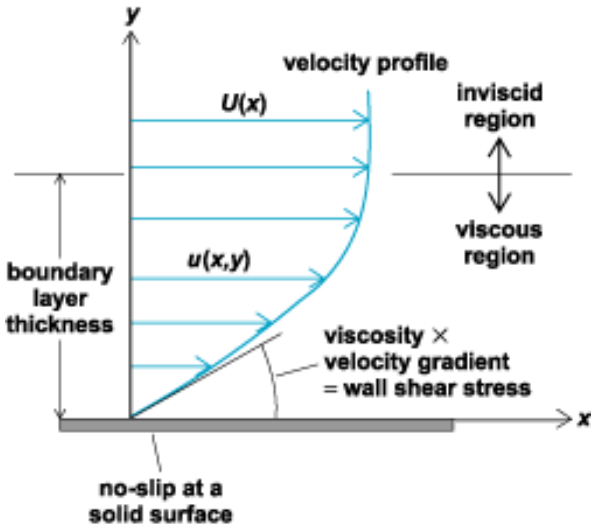


**Figure 72: Diagram of a laminar boundary layer. (Taken from McGraw-Hill Encyclopedia of Science and Technology).**

At the surface of the solid the fluid experiences a force acting to oppose its motion. The force per unit area is known as the wall shear stress. Shear stress in fluids is defined by Newton's law of viscosity given in Equation 2:

$$\tau(y) = -\mu \frac{du}{dy}$$

**Equation 2: Newton's law of viscosity.**

Where μ = dynamic viscosity (Pa.s)
u = fluid velocity along the boundary (m/s)
y = height above the boundary (m)

### 3.2.2. Blood Cells and Shear Force

Red blood cells (RBCs) have a biconcave disk shape, with thin central region and thicker outer margin as shown in Figure 73 below.

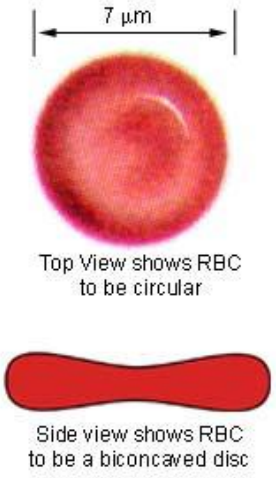


**Figure 73: Diagram showing the shape of a Red Blood Cell. (Taken from www.biosbcc.net)**

The shape of a red blood cell provides the following advantages:

- A large ratio of surface area to volume. This facilitates the rapid exchange of oxygen between the cells interior and the surrounding plasma.
- It enables the RBC's to form stacks. By stacking together larger number of cells can easily pass through narrow vessels. This would be difficult for the same number of individual cells as they would hit the walls and each other resulting in mechanical forces on the cell and potential blocking of vessels.
- The concave shape allows for a degree of bending and flexibility. The flexibility of the cells helps to absorb some of the forces that the cells are exposed to, increasing tolerance to shear stresses. It also allows them to contort their shape enabling them to pass through very narrow diameter vessels.

In the body the RBC's are exposed to high levels of mechanical stress. As a result the life span of the cell is short at approximately 120 days after which it will either rupture or be engulfed by phagocytic cells.

The upper limit of shear that blood can withstand before experiencing permanent damage has been shown in the literature to be approximately 1 – 3 mmHg (Sutera 1975; Sallam 1984; Sharp 1998). Above this threshold mechanical haemolysis can occur. Mechanical haemolysis is the releasing of haemoglobin into the plasma due to rupture of a cell's membrane induced by external forces. Other cells may respond differently to shear forces. For example, platelets will tend to become activated under high shear, forming platelet aggregates which may cause embolic injury under some circumstances.

The shear stresses in an extracorporeal circuit tend to be much greater than those present within the body (Lee, Ahn et al. 2004). In light of the understanding of the response of blood cells to forces applied to them, one of the main requirements in the design of artificial organs and extracorporeal systems is to minimise the exposure of blood cells to forces that could result in these inappropriate activation processes.

### 3.2.3. Resistance within the ECMO Circuit

As blood flows through a tube, shear forces act to resist the motion of the fluid. The magnitude of this resistance depends upon the cross-sectional area of the fluid path, the surface roughness and the velocity and viscosity of the fluid. A typical ECMO circuit consists of several components such as the oxygenator, the heat exchanger, cannulas and filters. Each of these components presents a resistance to blood flow; overcoming this requires increased pressure to drive the blood. High resistance and pressure systems will expose the blood to large mechanical forces.

Reducing the resistance within an ECMO circuit is complicated and requires assessment of each of the individual components. A compromise must be met between hydrodynamic performance and haemodynamic requirements.

### 3.2.4. Resistance within the Patient

Vascular resistance is the resistance to blood flowing through the vasculature of a patient. The resistance within the body is determined by the diameter of the vessels that the blood is passing through. At smaller diameters the blood is pumped faster and the resistance is higher. Vasodilation and vasoconstriction are ways in which the body expands and contracts blood vessels. Both actions can be influenced through medication; however a patient on ECMO can be suffering from a number of complicated conditions making control of vascular resistance a difficult task. Systemic vascular resistance (SVR) can be calculated from mean arterial pressure (MAP), central venous pressure (CVP) and cardiac output (CO) as shown within Equation 3:

$$SVR = \frac{(MAP - CVP)}{CO}$$

**Equation 3: Equation relating mean arterial pressure, central venous pressure and cardiac output to systemic vascular resistance.**

## 3.3. Device Performance Requirements

Typical protocols for ECMO treatment recommend a flow rate of approximately 100 – 120 ml/kg/min. For the neonatal population this would suggest an operating range of around 0 – 500 ml/min (Smith 2007). The pressure requirements of the system as discussed will depend upon the patient condition and the resistance of the circuit. The requirements of a miniaturised and integrated system should be less than that of the current commercial system. Taking these system requirements into consideration and from consulting with clinicians an operating pressure range of 0 – 120 mmHg was considered to be an acceptable performance range. The longevity of the blood pump is also essential. ECMO procedures can run from hours to weeks and so the pumping system must be able to operate reliably over an extended period of time.

## 3.4. Chapter Aims

The aims of this chapter are:

- To produce a functional axial flow pump for use within a miniaturised and integrated extracorporeal membrane oxygenation system.

- To use computational fluid dynamics as an optimization tool to improve design efficiency and to reduce the time and cost associated with design based solely on iterative prototyping and experimental data.

- To develop a prototype and experimental procedure to effectively bench test the blood pump to a standard that indicates the design is suitable for use in animal experimentation.

## 3.5. Impeller Designs

The foundation concept upon which the work within this chapter will be focused is based upon concept 3 of Chapter 2 – Concept Development. In this design it was established that in order to sufficiently miniaturise and integrate the ECMO system an axial flow pump design was required.

Figure 74 below shows concept 3 of Chapter 2 – Concept Development with the pump system highlighted in red.

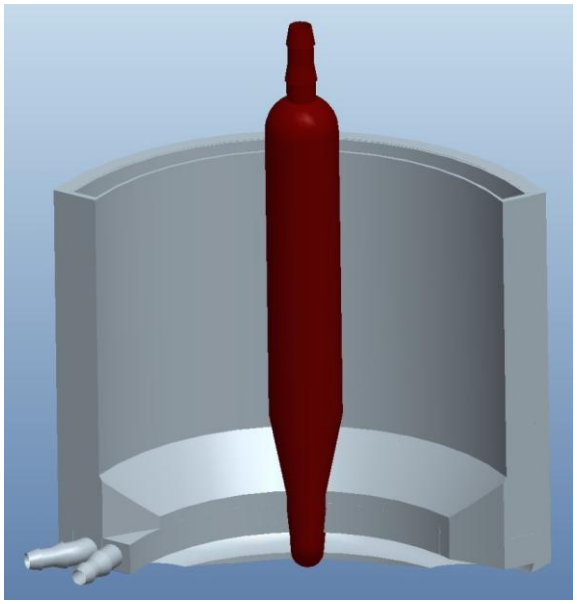

**Figure 74: Model of the foundation design with the pump system highlighted in red.**

An axial flow pump operates by moving the fluid in the direction parallel to the pump shaft. Typically the pump will feature an inducer, impeller and diffuser. The inducer features angled blades that upon rotation force the fluid forward to the impeller. The impeller rotates the fluid around the axis, increasing rotational velocity. The fluid moves to the stationary diffuser which converts the rotational velocity to pressure by changing the velocity vector.

To help visualise the concept Figure 75 shows a ProEngineer model of the proposed design with the inducer, impeller and diffuser highlighted.

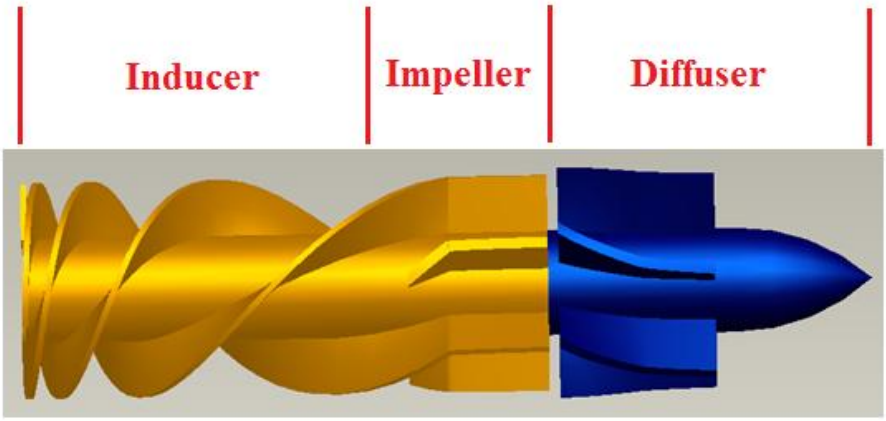


**Figure 75: ProEngineer model showing the inducer, impeller and diffuser of the initial axial flow pump design.**

This design was created with a variable pitch inducer to encourage acceleration of the fluid towards the impeller and a smooth transition in the direction of the velocity vector at the impeller. The diffuser features six angled blades that force a further change in the velocity vector; reducing the magnitude and changing the direction to result in an increased fluid pressure.

## 3.6. Inducer, Impeller and Diffuser Initial CFD

### *Aims*

The aims of this analysis were to use CFD to determine the performance characteristics of the proposed inducer, impeller and diffuser design and to determine effect of wall and impeller/diffuser gap on performance. This analysis should provide initial feedback as to the success of the design, which can be used to determine if the design is suitable for physical prototyping.

### *Methods*

A model of the flow path was developed to represent the geometry of the AFP generated in Concept 3 of Chapter 2 – Concept development. This fluid path was split into three volumes; the inlet (a static region of flow), the impeller fluid (a rotating region of flow) and the outlet (a static region of flow) and imported into Gambit for meshing. In this first analysis the gap distance between the impeller and the impeller casing and between the impeller and diffuser were to be analyzed. To do this several iterations of the model were created by changing the size and position of the impeller and diffuser, whilst maintaining the rest of the AFP geometry. Five iterations were created with the following defining features:

1. Wall gap of 0.5 mm and impeller/diffuser gap of 0.5 mm
2. Wall gap of 0.5 mm and impeller/diffuser gap of 0.75 mm
3. Wall gap of 0.5 mm and impeller/diffuser gap of 1 mm
4. Wall gap of 0.75 mm and impeller/diffuser gap of 1 mm
5. Wall gap of 1 mm and impeller/diffuser gap of 1 mm

Figure 76 below shows a diagram indicating the location of the wall gap and impeller/diffuser gap.

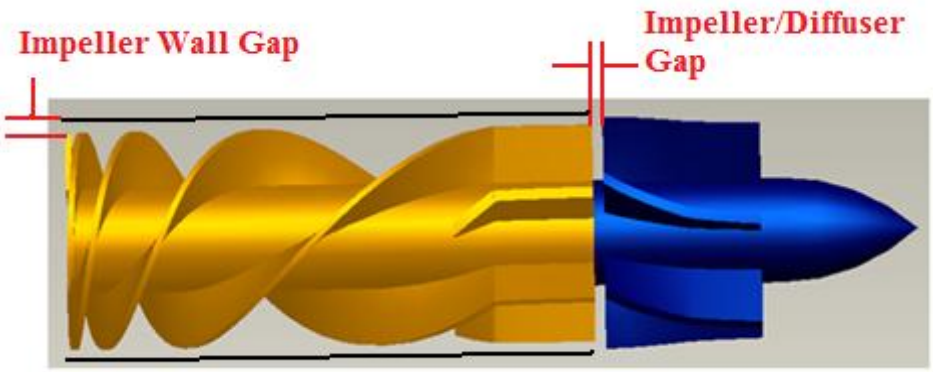


**Figure 76: Diagram indication the location of the wall and impeller/diffuser gaps.**

The mesh used on each model was a tetrahedral/hexagonal element hybrid mesh. Initially a mesh analysis was performed to determine the most suitable mesh with respect to run time and accuracy of the model. The most efficient mesh was calculated to be one with a spacing of 0.8. Figure 77 below shows the mesh for the model with a gap of 0.5 mm between the impeller and pump wall and of 0.75 mm between the impeller and diffuser. The mesh has a total of 391,987 nodes for all three volumes.

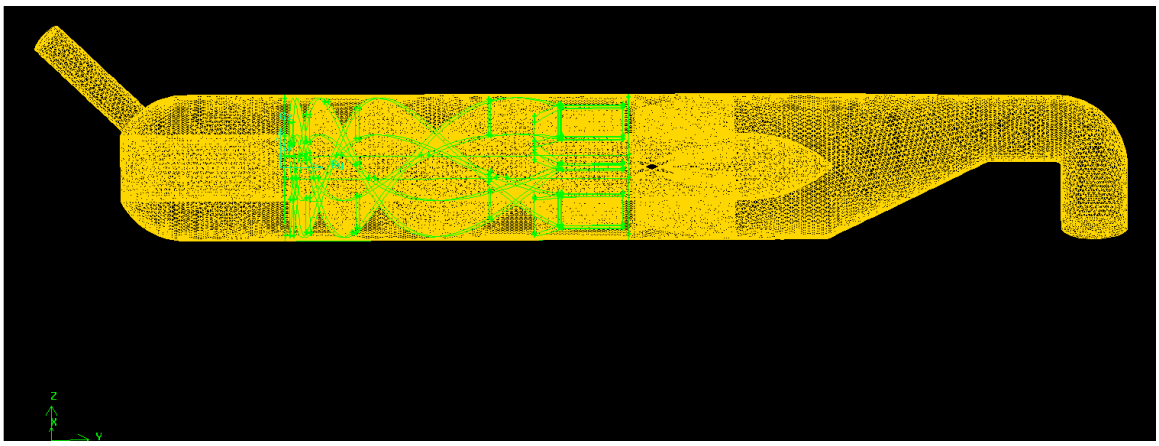

**Figure 77: Mesh of the impeller and diffuser pump system within Gambit.**

CFD analysis was run using Fluent Inc., Fluent version 6.3.26. The analysis was performed as a turbulent flow with the Reynolds averaged Navier Stokes equations solved for turbulent incompressible flow with a two equation k-epsilon model with enhanced wall treatment for turbulence closure. Turbulence was defined by providing a turbulence intensity and hydraulic diameter at the inlet to and outlet from the pump. In each analysis water was used as the domain fluid with constant viscosity of 0.001003 (Pa.s), specific heat of 4182 (J/kg.K), conductivity of 0.6 (W/m.K) and a density of 998.2 ($kg.m^{-3}$).

Performance analysis of the pump was conducted by running each model at 4000 r.p.m with the inlet and outlet boundary conditions set as open to atmospheric pressure. The most efficient combination was chosen and a further analysis was conducted on the model to determine the performance under the same boundary conditions at pump speeds of 500, 1000, 2000, 4000 and 6000 r.p.m.

### *Results*

The most appropriate characteristics to evaluate the performance of the pump under the conditions of the simulation were determined to be the flow rate induced and the resulting pressure drop across the module and area-weighted average wall shear stress on the impeller, diffuser and impeller casing. Table 3 below shows the pump characteristics determined from the simulation for each of the models.

| Pump Model | Flow rate (ml/min) | Preload (mmHg) | Area-weighted average Wall Shear Stress (mmHg) | | |
|---|---|---|---|---|---|
| | | | Impeller | Diffuser | Pump casing |
| 0.5 mm/0.5 mm | 2400 | -15.86 | 0.23 | 0.2 | 0.49 |
| **0.5 mm/0.75 mm** | **2412** | **-16.01** | **0.23** | **0.19** | **0.49** |
| 0.5 mm/1 mm | 2406 | -15.89 | 0.23 | 0.2 | 0.49 |
| 0.75 mm/1 mm | 2142 | -12.64 | 0.22 | 0.19 | 0.45 |
| 1 mm/1 mm | 1938 | -10.33 | 0.21 | 0.18 | 0.42 |

**Table 3: Table of pump characteristics for varying impeller/casing and impeller/diffuser gaps.**

The results show that a 0.5 mm wall gap and 0.75 mm gap between the impeller and diffuser is the most efficient configuration providing the greatest flow rate and pressure head with only slightly higher wall shear stresses. For these reasons this configuration was considered to be the optimum and was used in a more detailed performance analysis.

The results of the more detailed performance analysis were given in terms of the pressure head, the flow rate achieved and the wall shear stresses present at each pump speed. Figure 78, Figure 79 and Figure 80 show pressure head, flow rate and area-weighted average shear stress against pump speed for the 0.5 mm wall gap and 0.75 mm impeller/diffuser gap model respectively.

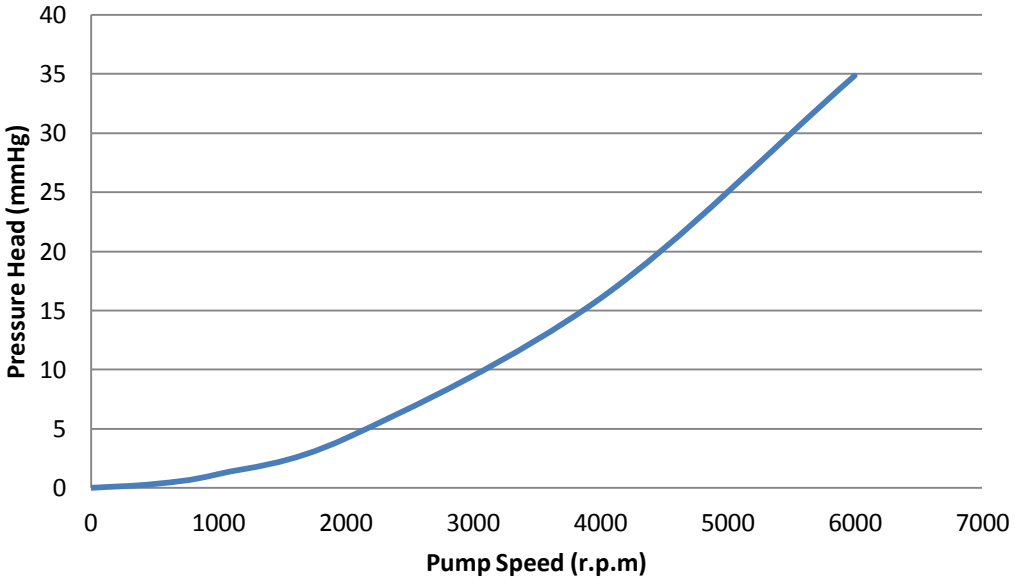


**Figure 78: Graph showing pressure head versus pump speed for the 0.5 mm wall gap and 0.75 mm diffuser/impeller gap pump configuration.**

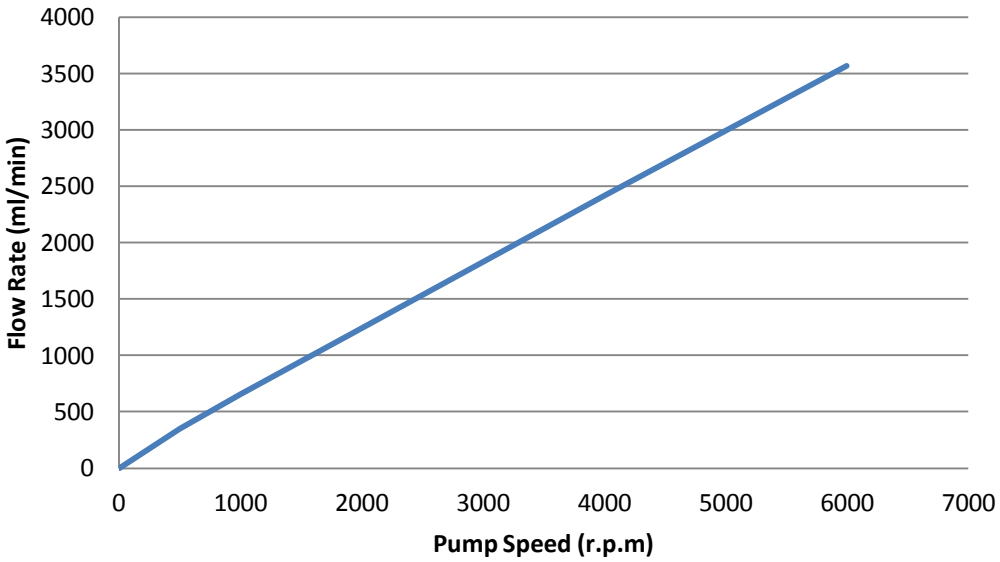


**Figure 79: Graph showing flow rate versus pump speed for the 0.5 mm wall gap and 0.75 mm diffuser/impeller gap pump configuration.**

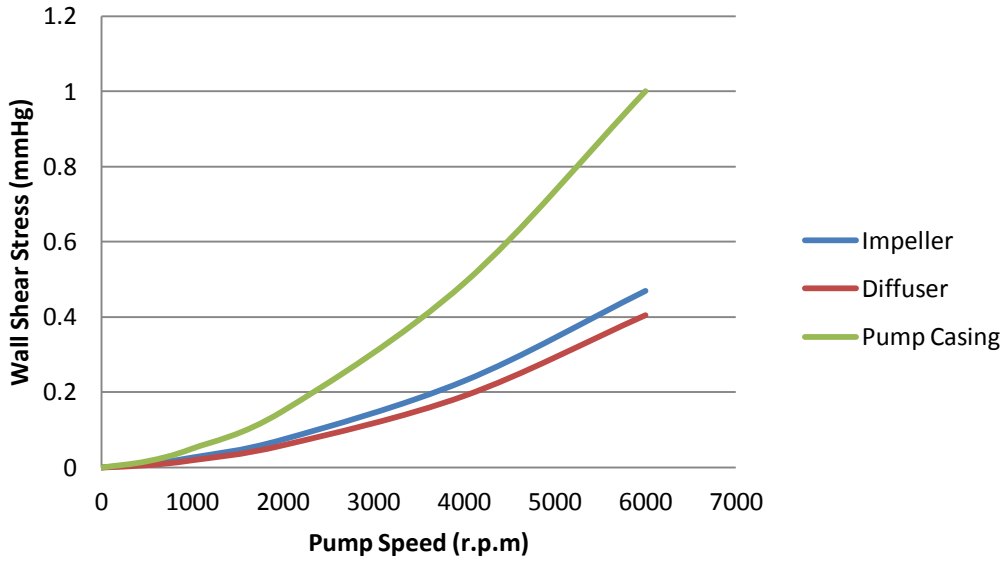


**Figure 80: Graph showing area-weighted average wall shear stress versus pump speed for the 0.5 mm wall gap and 0.75 mm diffuser/impeller gap pump configuration.**

## *Discussion and Conclusions*

This analysis has provided feedback of the initial design. The performance data obtained has been used to determine the most suitable configuration for the design geometry. The more detailed performance analysis of that design has indicated that this configuration is unable to perform adequately without operating at unacceptably high pump rotational velocity. Although this is the case, in order to validate the computational model and method used physical prototyping and experimentation is required. Comparison of the computational and physical experimentation will determine the accuracy of the simulation. Upon validation of the model qualitative and quantitative feedback as to the performance of the design can be made. Validation through physical experimentation also allows computational method to be used in future development of the pumping systems as a tool for design optimization.

## 3.7. Inducer, Impeller and Diffuser System Design

To ensure that the physical rig represented the model used within the CFD analysis as closely as possible the model geometry was used as the basis of the rig design. The flow path was inverted and modified to produce a practical rig for a directly driven pump. A cross-section of the proposed design can be seen in Figure 81 below with the main features of the design highlighted in red.

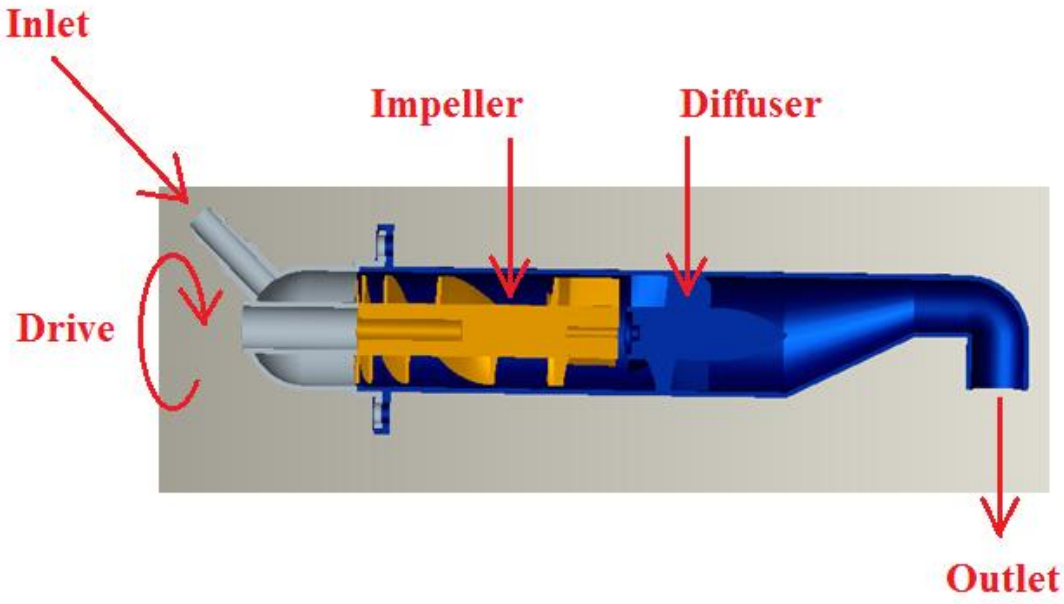


**Figure 81: Cross-section of the inducer/impeller and diffuser pump system design with the main features highlighted in red.**

This design was developed to be manufactured via rapid prototyping. The parts were printed on an Eden 350v 3D printer (Objet, Rehovot, Israel), which uses a polymer jetting technology. This manufacturing process can allow for rapid prototyping of complicated geometries; however the process places some configuration constrictions on the design, such as a minimum wall thickness of 0.7 mm but more notably in that the design must facilitate the removal of the soft support material used throughout the process to support the walls of the part. Upon completion this material is blasted away

using a high pressure water jet. Figure 82 below shows rapid prototype parts in the Objet machine after the printing process has been completed.

**Figure 82: Rapid prototyped parts in the Objet machine after printing prior to being cleaned and processed.**

Figure 83 provides a comparison between a prototype with support material attached and one that has been fully cleaned and is ready for use.

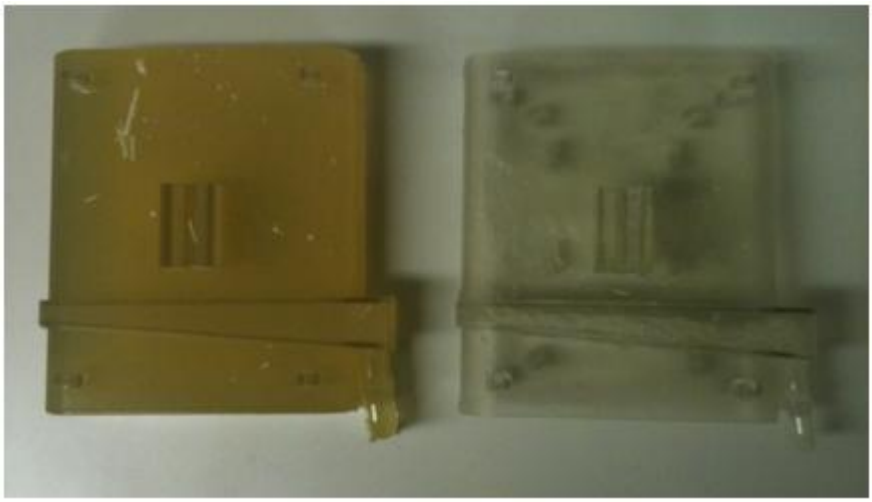

**Figure 83: Comparison of rapid prototyped parts with and without support material.**

In this design the impeller holds the drive shaft which exits through the upper section of the system. The impeller also holds a pin at the lower end, which rotates against a metal disk in the diffuser. The diffuser is designed to be printed with the lower casing as one piece. The manufacturing method used to construct the system was as follows:

- The pump shaft and pin were super-glued (RS components LTD, Northants, UK) into place in the impeller and the metal disk was super-glued into the diffuser.

- Bearings were glued into both ends of the upper section and an oil seal to the top of the pump casing.

- The drive shaft was placed through the upper section, which was then bolted to the lower section.

Figure 84 shows the completed components of the pump system prior to assembly.

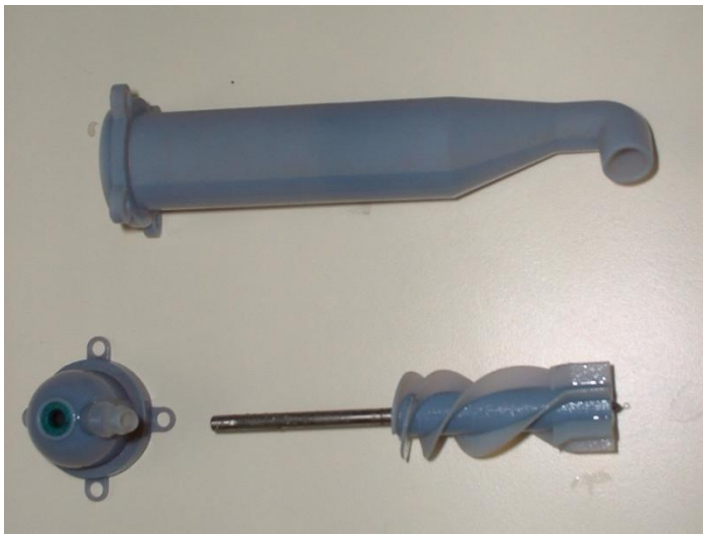

**Figure 84: Picture showing the finished components of the pump system ready to be assembled.**

The pump was connected to a commulathe 55T electric motor (Eagle Racing, Aichi-Ken, Japan) via a metal coupling. Both the pump and motor shafts were held in place in the coupling using grub screws as shown within Figure 85.

**Figure 85: Picture showing the coupling between the pump and the motor.**

The design has a priming volume 43.89 ml of and the blood is exposed to a surface area of 0.00428 $m^2$.

## 3.8. Inducer/Impeller and Diffuser Pump Testing

### 3.8.1. Aims

The aims of the following experiments were to determine the performance characteristics of the inducer/impeller and diffuser pump design and to use these results to validate the CFD analysis previously conducted.

### 3.8.2. Method and Materials

The principle components used to determine the performance characteristics of each of the systems are shown within Figure 86.

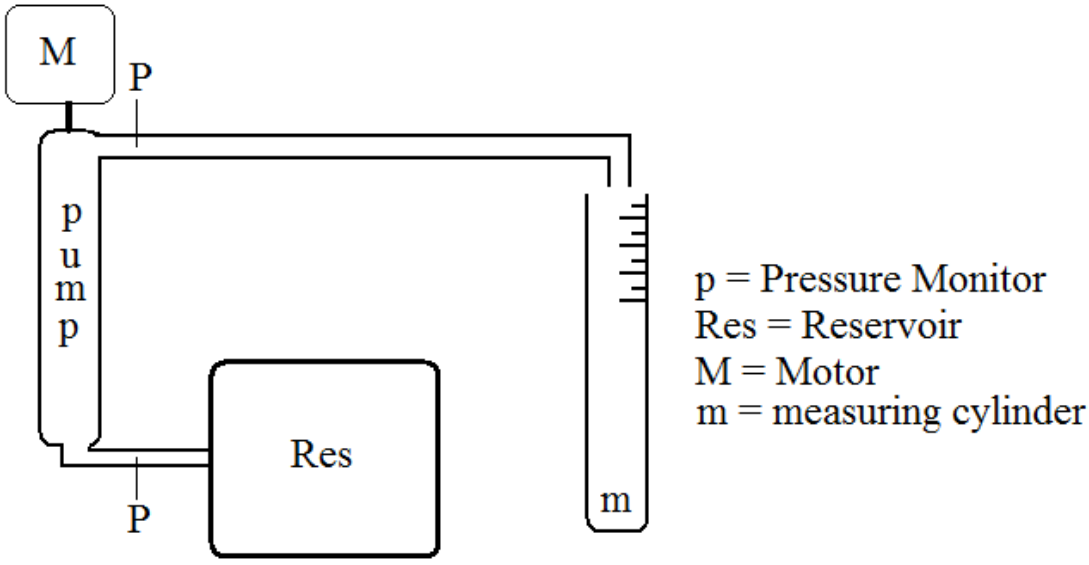


**Figure 86: Diagram showing experimental set-up for initial prototype testing.**

The impeller was driven via an electric motor powered by a HY3003-2 DC supply (Digimess instruments, Derby, UK). Pump impeller speed was recorded in (r.p.m) using a testo 460 tachometer (Testo Limited, Hampshire, UK). Reflective tape was placed on the coupling between the motor and the pump. The tachometer laser was aimed at this

tape and held stationary until a value was displayed. Figure 87 shows a picture of the pump system connected to the electric motor with the location of the reflective tape used by the tachometer highlighted in red.

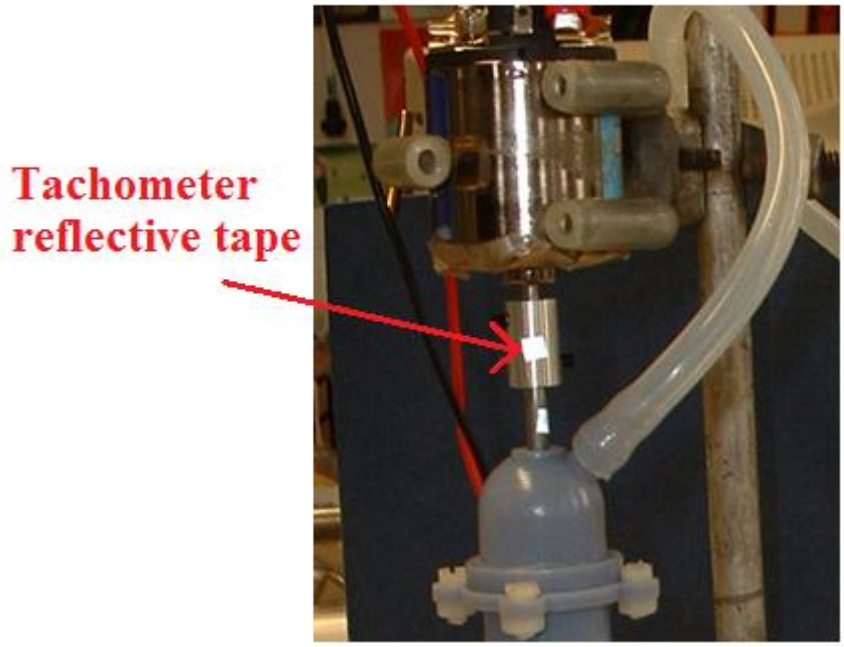


**Figure 87: Reflective tape used by the accelerometer to determine motor speed.**

TSD104A Blood pressure transducers (BIOPAC Systems Inc., California, USA) were positioned at the inlet to (pre-load) and outlet from (after-load) the pump. Pressure values were recorded in (mmHg). The pump system and pressure monitors were primed prior to running the motor. The motor power was increased in voltage increments of 0.5 v through a range of 0 – 7 v. At each voltage pump r.p.m, pre and after load pressures and flow rate were recorded. Flow rate was determined by recording the volume of fluid to flow into the measuring cylinder over a minute. The experiment was repeated three times. Figure 88 below shows the experimental configuration with each of the main elements numbered and labeled.

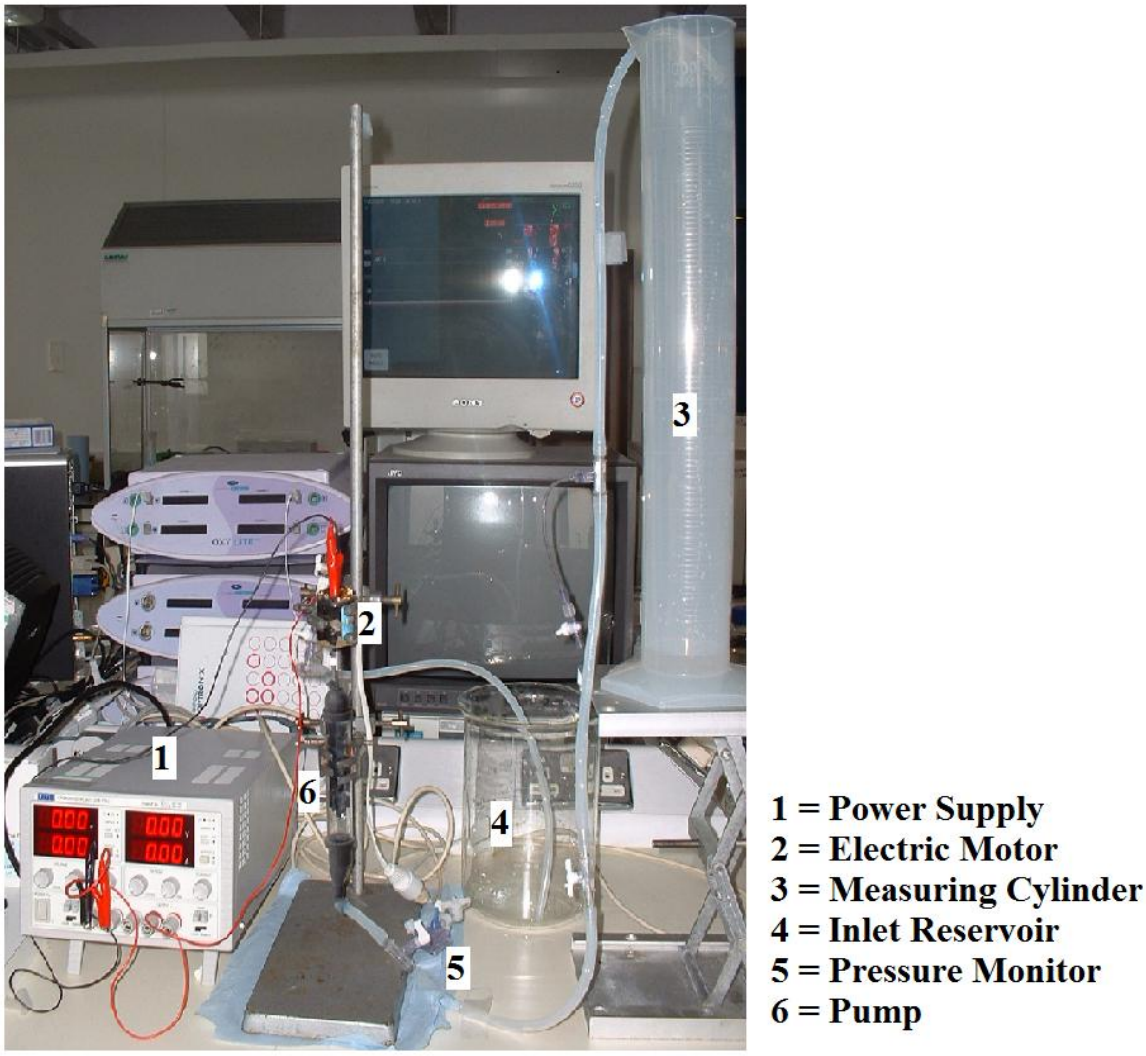


**Figure 88: Inducer, impeller diffuser pump system experimental configuration with the components of the experiment numbered and labeled.**

### 3.8.3. Results

To allow for a direct comparison to the CFD results, pressure head and flow rate versus pump rotational velocity were selected as the most appropriate performance characteristics. Figure 89 and Figure 90 below show pressure head and flow rate against pump speed respectively.

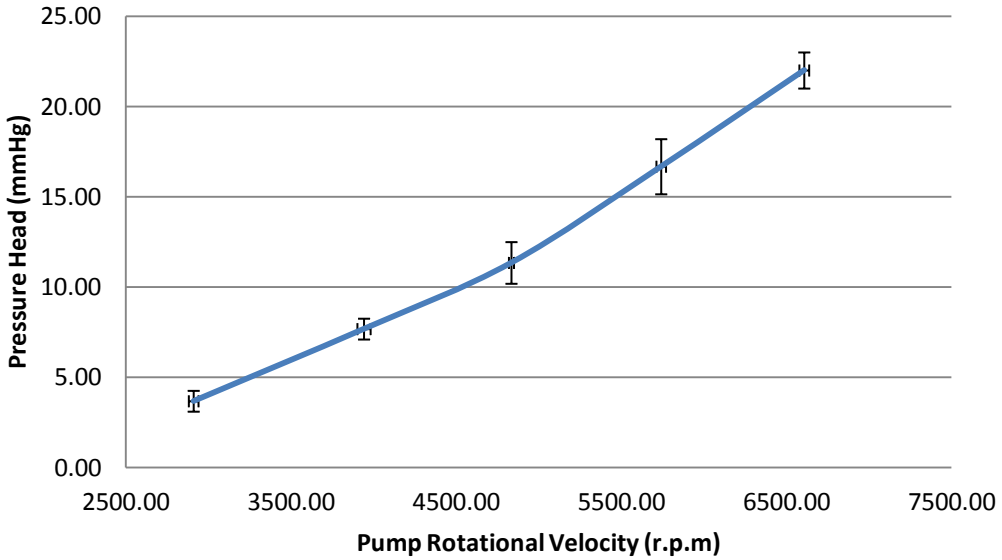


**Figure 89: Graph of pressure head vs. pump speed for the inducer/impeller pump system. ± 1 Standard Deviation.**

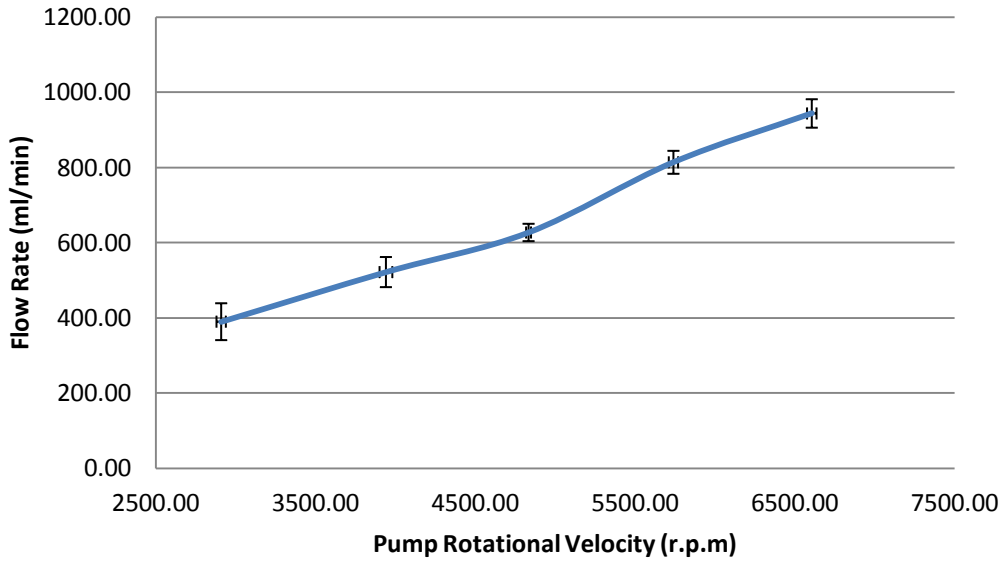


**Figure 90: Graph of flow rate vs. pump speed for the inducer/impeller pump system ± 1 Standard Deviation.**

### 3.8.4. Discussion

The results of this experiment show that the prototype is able to overcome a circuit induced pressure head and produce a positive flow rate. Pressure head and flow rate increase linearly with pump rotational speed. Comparison of the physical and computational results shows considerable differences. The performance in the physical experiment was particularly poor and may be attributed to both the pump design and the experimental set-up in the following ways:

1. ***Poor control of the motor.***

The system lacked a dedicated motor controller. The tachometer was difficult to use and there was a large amount of variance in readings at the same RPM. The coupling of the motor was also very primitive and slip between the motor shaft and the coupling could have occurred.

2. ***Air entering the system.***

The bearings used in the experiment were not air tight and even with oil seals, air could be seen in the pump chamber by shining a light at the back of the casing. A leak in the system would have a direct effect on the pressure head achievable through disruption of the flow field.

3. ***Misalignment of the pump.***

The lower end of the shaft featured a pointed end, which rotated on a metal disk secured to the diffuser. This configuration constrained the impeller in the vertical plane but not the horizontal. This could have resulted in misalignment, which would affect the flow path and performance of the pump.

### *4. Deformation of the impeller.*

The rapid prototype material was prone to deformation, particularly in the thin walled blades of the inducer. Upon examination post experimentation it was noted that the blades had deformed, bending closer together. This would have reduced the cross-sectional area at the inlet to the pump system and affected the flow path of the fluid.

To allow for further investigation of the results and for verification of the CFD process a further CFD analysis was ran using the pressure head and corresponding impeller rotational velocities from the physical experimentation.

## *CFD analysis of the impeller/diffuser System Experiment*

### *Aims*

The aims of this experiment were to validate the computational simulation of the pump system by using values obtained from the physical experiment. Upon validation the model will then be used to further investigate the results of the physical experiment and as a tool for optimization in future designs.

### *Methods*

The CFD model and fluid path used a similar set-up to the initial CFD analysis. The impeller was modified to include bending of the impeller blades as observed within the physical experiment. The boundary conditions were set using the impeller velocities and

the corresponding pressure head obtained from the physical experiment set as inlet velocity and after load. A model highlighting the modification made to the impeller blades can be seen within Figure 91 below.

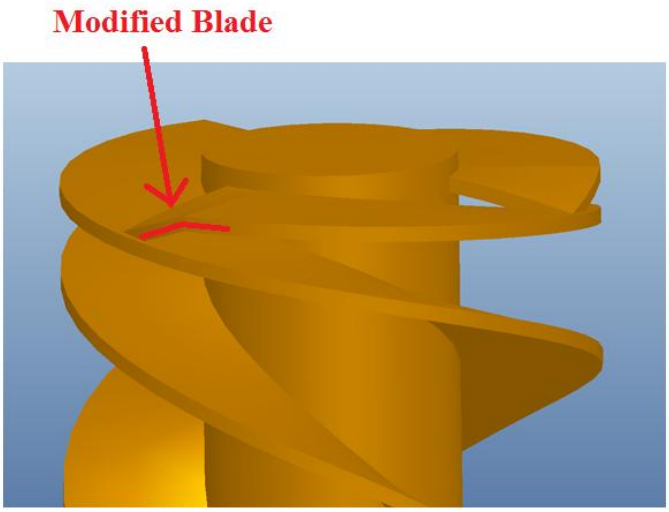


**Figure 91: ProEngineer model of the modified impeller blade.**

### *Results*

Figure 92 and Figure 93 below show graphs comparing the average experimental and computational results for pressure head and flow rate against impeller rotational velocity.

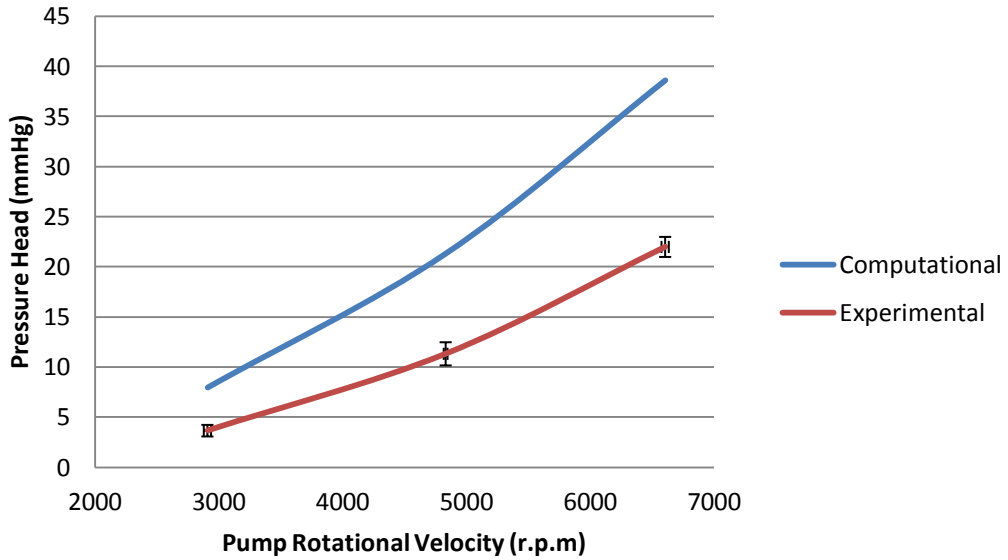


**Figure 92: Graph comparing experimental and computational pressure head vs. impeller rotational velocity. ± 1 Standard Deviation.**

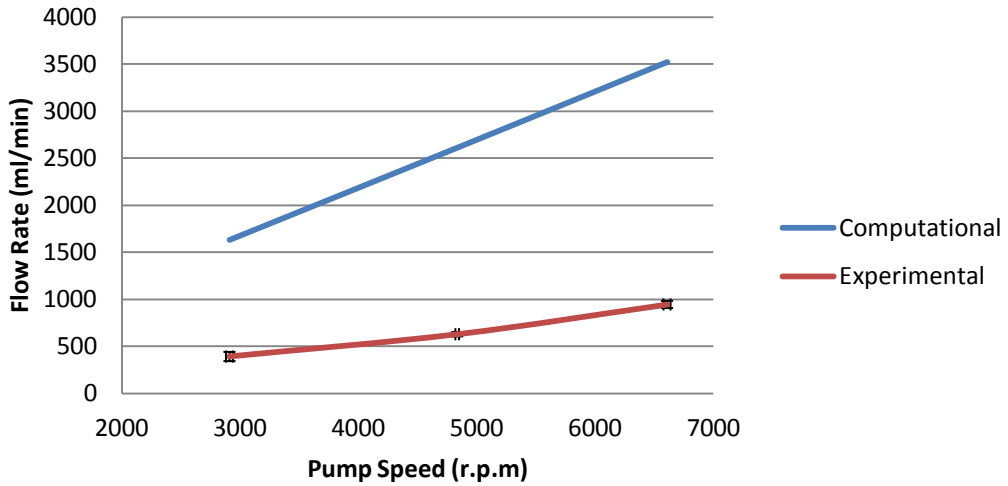


**Figure 93: Graph comparing experimental and computational flow rate vs. impeller rotational velocity. ± 1 Standard Deviation.**

***Discussion and Conclusions***

Comparison of the results shows that the CFD model is predicting higher performance in both pressure head and flow rate achieved. The difference between pressure head and flow rate is greatest at the lower rotational velocities with pressure head at 71 % and flow rate at 53 % of the computational value. As the rotational velocity increases the difference between the results also decreases with experimental pressure head at 83 % and flow rate at 73 % of that of the computational model.

Aside from the bending of the impeller blades, the CFD analysis represents a perfect set-up. The prototyped device had several problems associated with it that were impractical to model, such as air in the system. Considering the magnitude and complexity of the challenges met in the physical experimentation confidence in the efficacy of the model can still be maintained. As the quality of manufacturing and experimental procedure is improved the variance in the CFD model and physical experiment should also improve in future designs.

### 3.8.5. Conclusion

The initial CFD analysis of the pump design suggested that the system was unlikely to be able to meet the requirements of an ECMO device, with the system having to operate at high rotational speed to provide a moderate pressure head. At these speeds the wall shear stresses were such that mechanical haemolysis could occur. To help visualize the wall shear stress more effectively Figure 94 and Figure 95 below show contours of area-weighted average wall shear stress on the impeller and diffuser and on the impeller casing respectively for the modified model at a rotational speed of 6607 r.p.m..

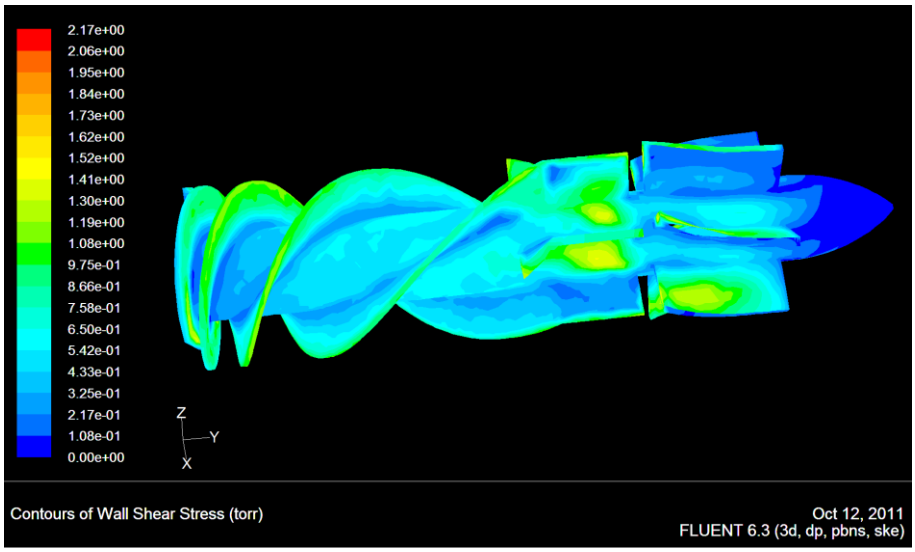


**Figure 94: Contours of wall shear stress on the impeller and diffuser for a pump speed of 6607 r.p.m.**

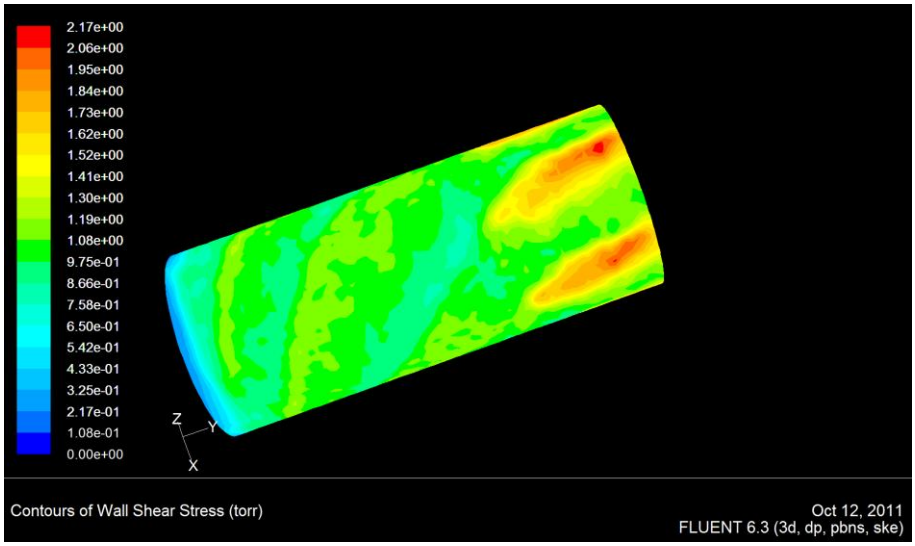


**Figure 95: Contours of wall shear stress on the impeller casing for a pump speed of 6607 r.p.m.**

Although the initial CFD evaluation predicted inadequate performance of the design, physical prototyping and testing were conducted in order to verify the CFD modeling technique used and to produce an effective test protocol for future iterations of the pump design. Overall the results of both the CFD analysis and physical testing of the system

suggest that both the pump design and the experimental set-up require redesign with a focus on addressing the following points:

1. Removing any air leaks from the pump casing.

2. Improving the flow path through the impeller and diffuser.

3. Replacing the variable pitch inducer with a constant pitch blade of greater thickness to prevent blade bending affecting the performance characteristics.

4. Redesigning the termination point of the impeller shaft within the pump to remove misalignment problems.

5. Improving the equipment used to control the pump.

## 3.9. Mark II Inducer/Impeller and Diffuser Pump Design

The redesign of the axial flow pump has focused on producing a more practical system that is easier to manufacture and operate. The failings of the previous design have been addressed in the following ways:

1. Redesign of the inducer, impeller and diffuser profiles.

The inducer profile was changed from a variable pitch blade to one with a constant pitch such that the total cross-sectional area of the flow path at the initial stages of the inducer was increased. This design allows for a greater volume of fluid to enter the inducer and reduces the risk of the blades bending and significantly occluding the flow path.

The impeller blades were lengthened, thickened and curved to increase axial velocity generated and to improve the fluid profiles on the top and bottom of the blades. The angles of the diffuser were also altered to encourage a smoother transition of the flow moving from the impeller to the diffuser. The diffuser blades were also streamlined to improve the downstream fluid profile.

2. Redesign of the prototype configuration.

The impeller was designed to have the drive shaft completely penetrate it. At the lower end of the impeller the drive shaft terminates within the diffuser, which was hollowed out to allow room for an additional bearing. This allowed for a much more accurate alignment of the impeller.

The system was designed in five pieces with the main body of the casing replaced with a transparent acrylic tube in order to provide visual feedback on the flow profile.

The previous motor and tachometer were replaced with an EC-Max Brushless DC motor controlled using an EPOS2 motor controller (Maxon Motor UK, Berkshire, UK).

Figure 96 below shows a ProEngineer model of the Mark II inducer/impeller and the diffuser.

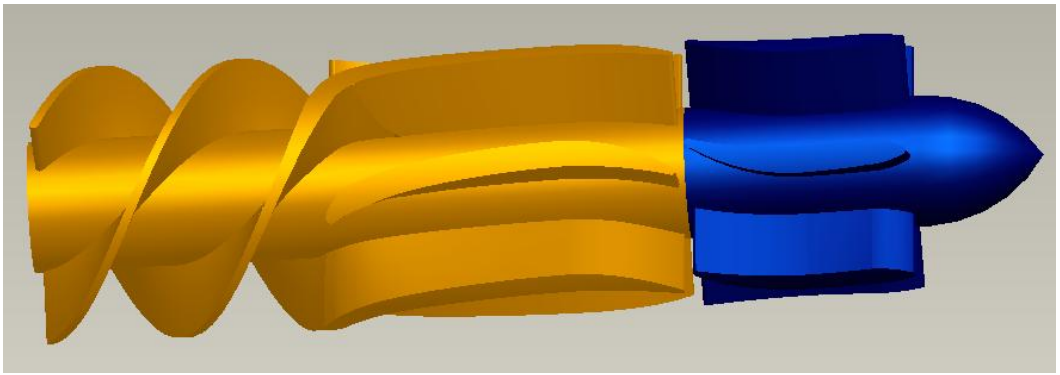

**Figure 96: ProEngineer model of the Mark II Inducer/Impeller and diffuser pump system.**

## 3.10. Inducer, Impeller and Diffuser Mark II Initial CFD

### *Aims*

The aims of this analysis were to use CFD to determine the performance characteristics of the redesigned inducer, impeller and diffuser and to compare the results to those of the previous design. The benefits of a flow straightener on performance will also be investigated.

### *Methods*

Two flow paths were generated for this analysis; one with a flow straightener and one without. The flow path used was very similar to that used in the analysis of the Mark I system with the exception of the redesigned geometry of the impeller and diffuser and with the addition of a flow straightener in the second model. Each model was imported into Gambit for meshing. The mesh used was a tetrahedral/hexagonal element hybrid mesh. For consistency both models were meshed in a similar manner to that of the Mark I system. The system without the flow straightener had a mesh with 173,873 nodes and the system with a straightener had 193,493 nodes. Figure 97 below shows the mesh for the system with a straightener.

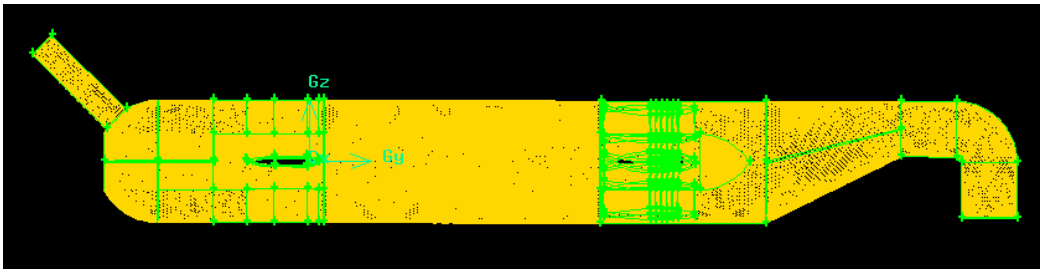


**Figure 97: Mesh of the Mark II inducer, impeller and diffuser with flow straightener.**

The CFD analysis was run with the same conditions as used in the previous analyses.

Performance analysis of the pump was conducted by running each model at 500, 1000, 2000, 4000 and 6000 rpm. Boundary conditions were set with the inlet and outlet defined as open to atmospheric pressure.

### *Results*

To allow for a suitable comparison of the systems the results are displayed in terms of the same performance parameters used in the testing of the Mark I system; that is pressure head and flow rate generated against the varying pump speed. As there are several components that are being evaluated area-weighted average wall shear stress is given in separate graphs for the Mark II system with and without a flow straightener respectively. Figure 98 and Figure 99 show graphs comparing the Mark I system and Mark II system with and without a flow straightener for pressure head and flow rate vs. impeller rotational velocity.

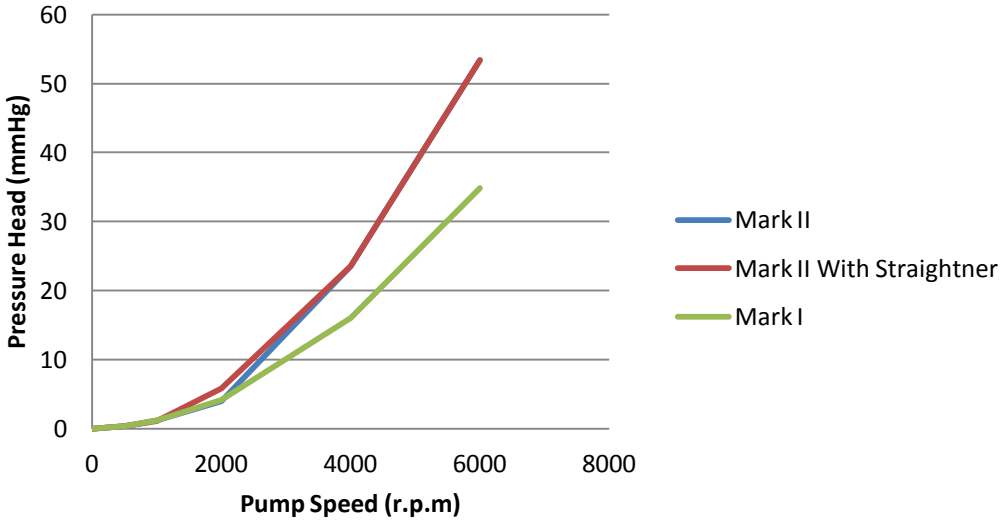


**Figure 98: Pressure head versus pump speed for the mark I pump and mark II pump with and without a flow straightener.**

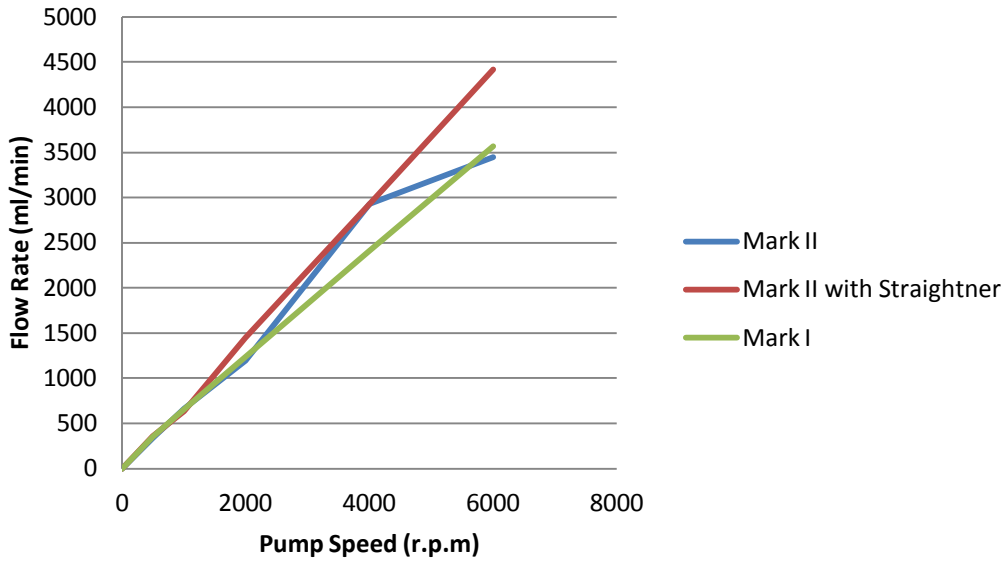


**Figure 99: Flow rate versus pump speed for the mark I pump and mark II pump with and without a flow straightener.**

Figure 100 and Figure 101 below show wall shear stress for the Mark II design with and without a flow straightener.

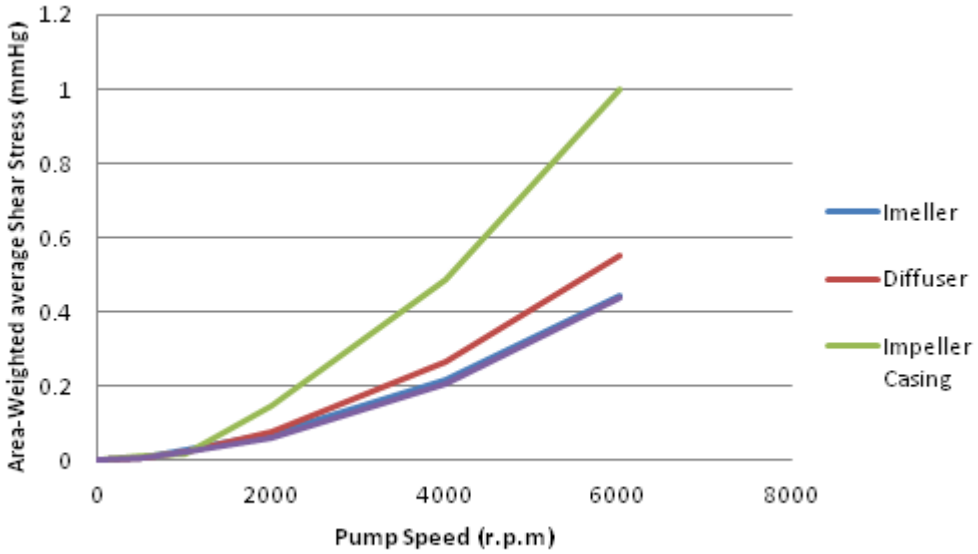


**Figure 100: Area-weighted average wall shear stress versus pump speed for the Mark II system with a flow straightener.**

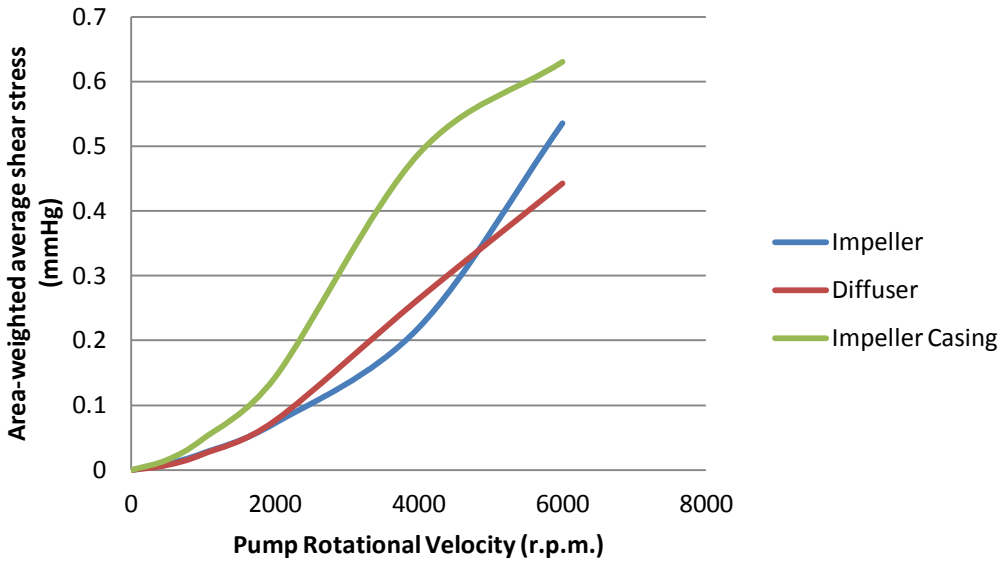


**Figure 101: Area-weighted average wall shear stress versus pump speed for the Mark II system without a flow straightener.**

### *Discussion and Conclusions*

The results of this analysis show that the Mark II pump with a straightener out performs the Mark II without straightener and the Mark I design in both pressure head and flow rate achieved. The shear stresses observed are similar to that of the Mark I impeller with the potential for shear at the impeller casing at rotational velocities above 6000 r.p.m.

The presence of a flow straightener can be seen to be very beneficial to the pump both in terms of performance and consistency and therefore should be incorporated into future pump designs. This design shows more promise than the previous Mark I system and is suitable for further investigation through physical prototyping and experimentation.

## 3.11. Inducer, Impeller and Diffuser Mark II System Design

The redesigned device was manufactured to be assembled from 5 parts. The manufacturing process was as follows:

1. A 4 mm steel shaft was measured and cut to size. The shaft was coated in super glue (RS components LTD, Northants, UK) and inserted through the impeller using a hammer.

2. Bearings and oil seals were glued into place using superglue at the top and bottom sections in the upper casing. A bearing was also glued into the diffuser.

3. The impeller and drive shaft were placed through the uppercasing and the acrylic tube glued into the upper section using silicone RVT adhesive (Dow Corning Toray Co., Ltd, Tokyo, Japan).

4. The diffuser was slid into place in the acrylic tube. To determine the position of the diffuser in the pump tube the impeller and top were slid into place. Once positioned correctly the impeller was removed and the diffuser was glued to the rig walls by applying super glue using a needle tip.

5. The upper section was then glued to the acrylic tube using the silicone adhesive.

Figure 102 and Figure 103 show a ProEngineer model of the system and a fully constructed prototype for use in the laboratory respectively.

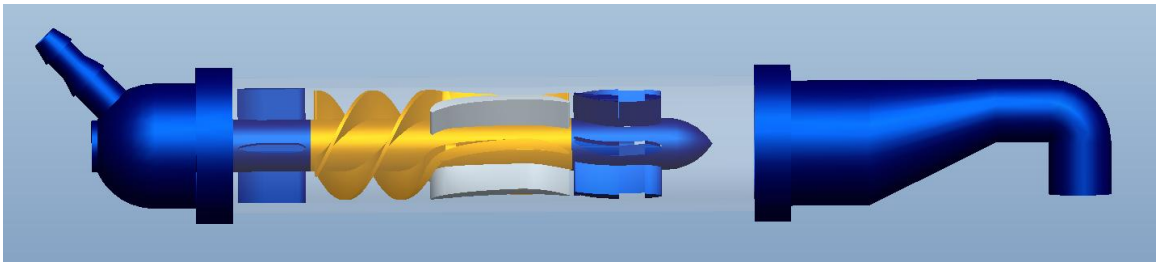

**Figure 102: ProEngineer model of the mark II inducer/impeller and diffuser pump system.**

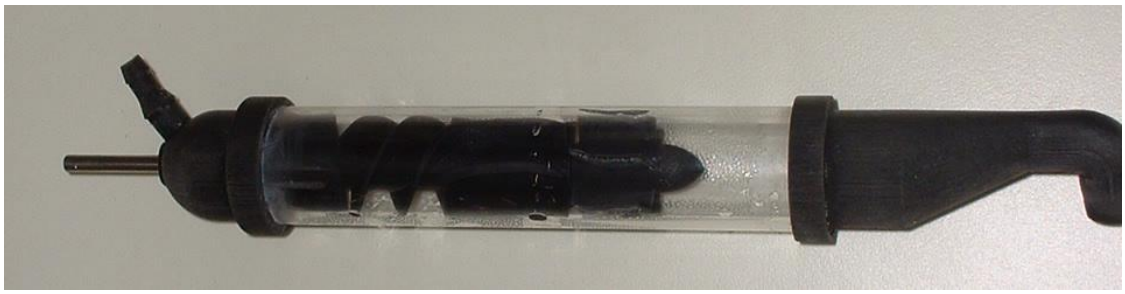

**Figure 103: Manufactured mark II inducer/impeller and diffuser system physical prototype assembled and ready for use within the laboratory.**

## 3.12. Mark II Inducer/Impeller and Diffuser Testing

### 3.12.1. Aims

The aims of the following experiments were to determine the performance characteristics of the Mark II inducer/impeller and diffuser pump design and to use these results to validate the CFD analysis previously conducted.

### 3.12.2. Method and Materials

In the same manner as with the Mark I system, this experiment focused on overcoming circuit generated resistance. The principle components used to determine the performance characteristics of each of the systems are shown within Figure 104.

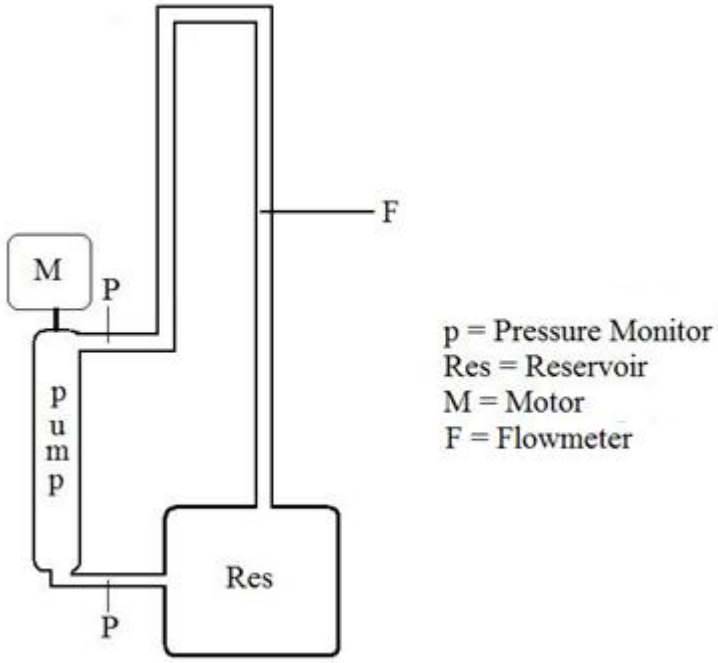


**Figure 104: Diagram of the experimental set-up used to test the Mark II pump system.**

The impeller was driven via an EC-Max Brushless DC motor controlled using a EPOS2 motor controller ((Maxon Motor UK, Berkshire, UK) which was powered by a CPX400A 60 v 20 A DC power supply (TTid, Cambridgeshire, UK). A 25 mm OD and 6 mm ID clamp style jaw coupling with torque disk was used to couple the motor to the pump shaft (Ruland Manufacturing Company, Inc., Marlborough, UK) as shown within Figure 105 below.

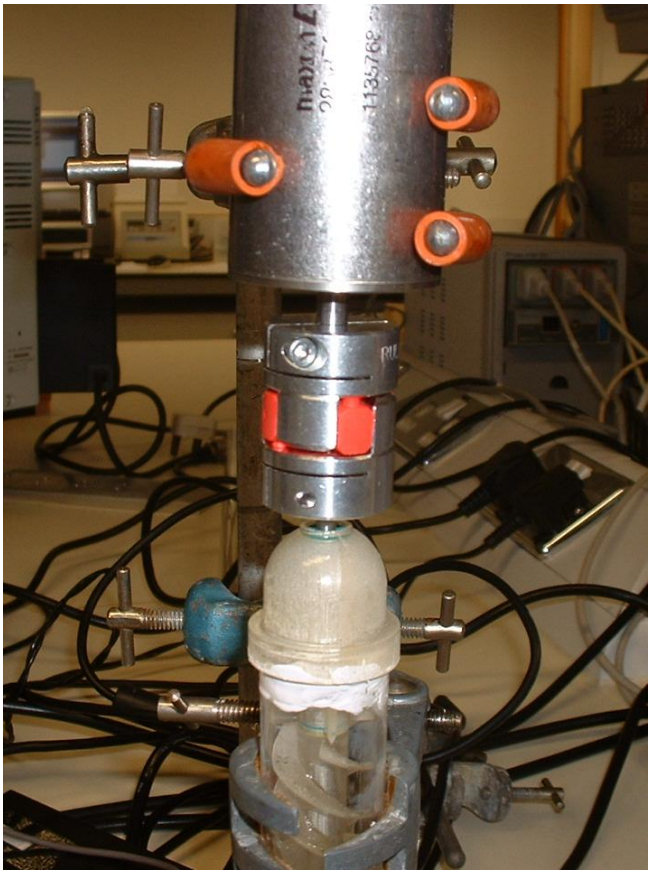

**Figure 105: Picture showing the motor and coupling in the Mark II prototyped used for physical experimentation.**

A TS410 flow meter (Transonic Systems Inc., New York, USA) was attached to the outlet tubing to determine the fluid flow rate in ml/min.TSD104A Blood pressure transducers (BIOPAC Systems Inc., California, USA) were positioned at the inlet to (pre-load) and outlet from (after-load) the pump. Pressure values were recorded in (mmHg). The pump prototype and pressure monitors were primed prior to running the motor. Motor r.p.m was controlled using the motor controller and increased in increments of 250 from 2000 to 3500 r.p.m. Flow rate and pressure recordings were made at each pump speed increment. This was then repeated again for pump speeds of 4500 – 6000 r.p.m. The entire experiment was repeated three times.

Figure 106 below show the set-up of the pump system within the lab with the various components used highlighted and labeled.

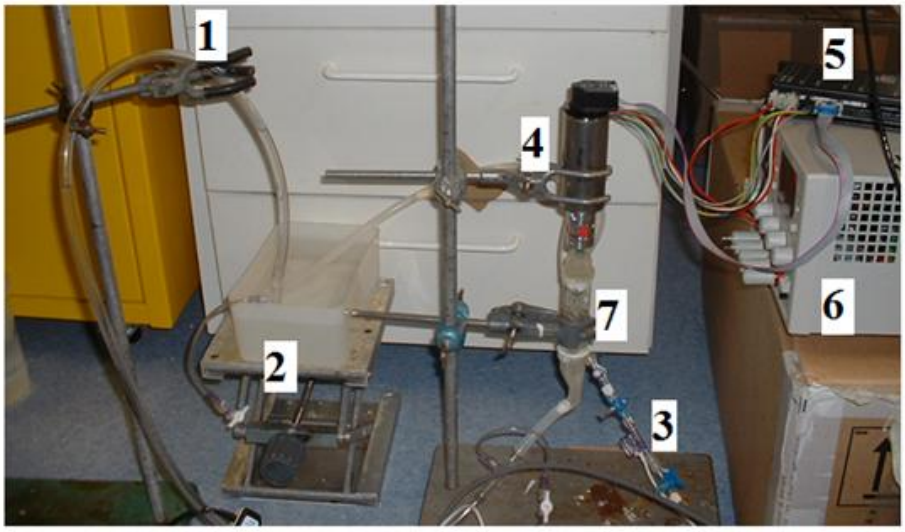


**Figure 106: Experimental set-up of the Mark II system with the components used highlighted and labeled.**

### 3.12.3. Results

The following results were presented in terms of the flow performance characteristics used to define performance of the previous system (pressure head and flow rate) against pump speed. As two different pump speed ranges were used the results are split between each pump speed range. Figure 107, Figure 108, Figure 109 and Figure 110 below show the pressure head and flow rate against pump speed for the 2000 – 3500 r.p.m and 4500 – 6000 r.p.m ranges respectively.

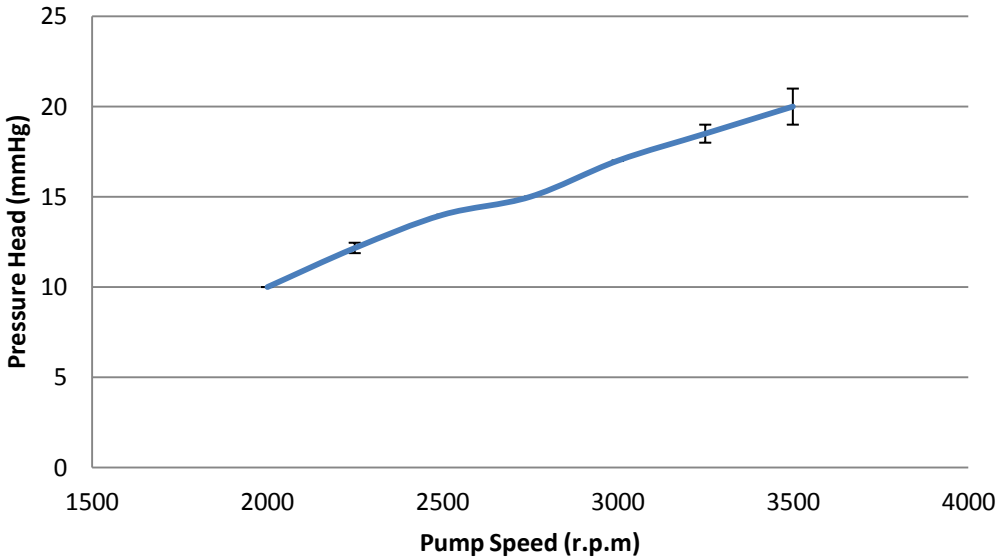


**Figure 107: Graph of pump pressures vs. pump speed through a range of 2000-3500 r.p.m for the Mark II pump system. ± 1 Standard Deviation.**

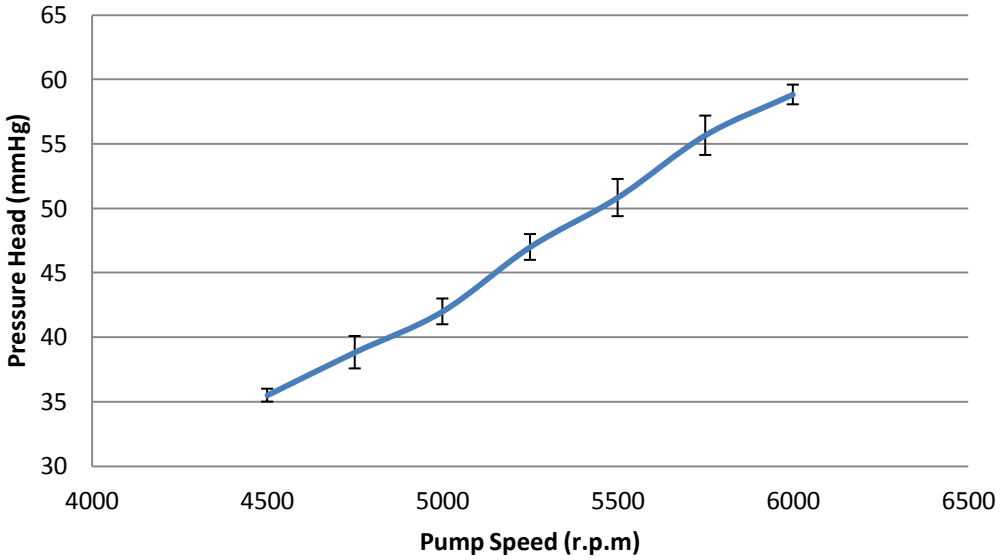


**Figure 108: Graph of pump pressures vs. pump speed through a range of 4500-6000 r.p.m for the Mark II pump system. ± 1 Standard Deviation.**

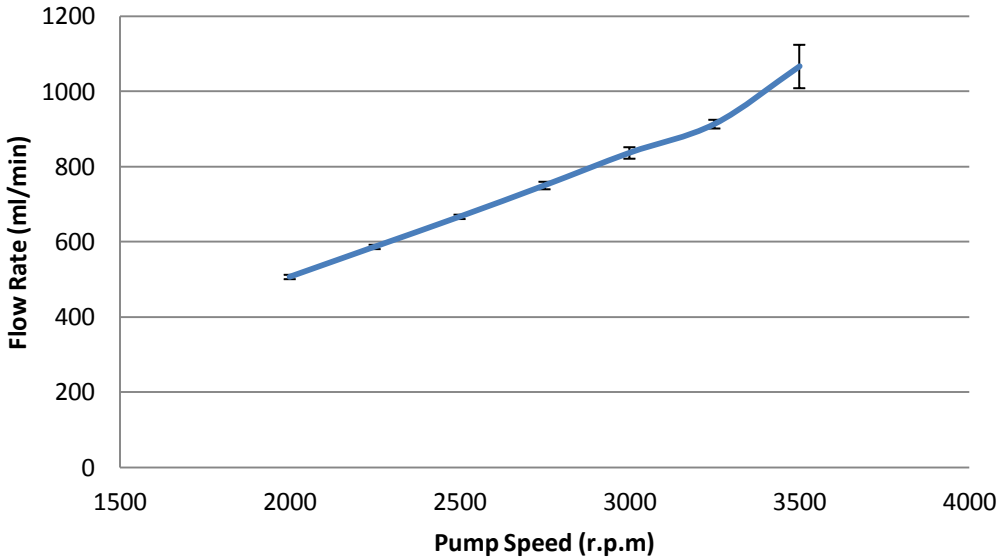


**Figure 109: Graph of flow rate vs. pump speed through a range of 2000-3500 r.p.m for the Mark II pump system. ± 1 Standard Deviation.**

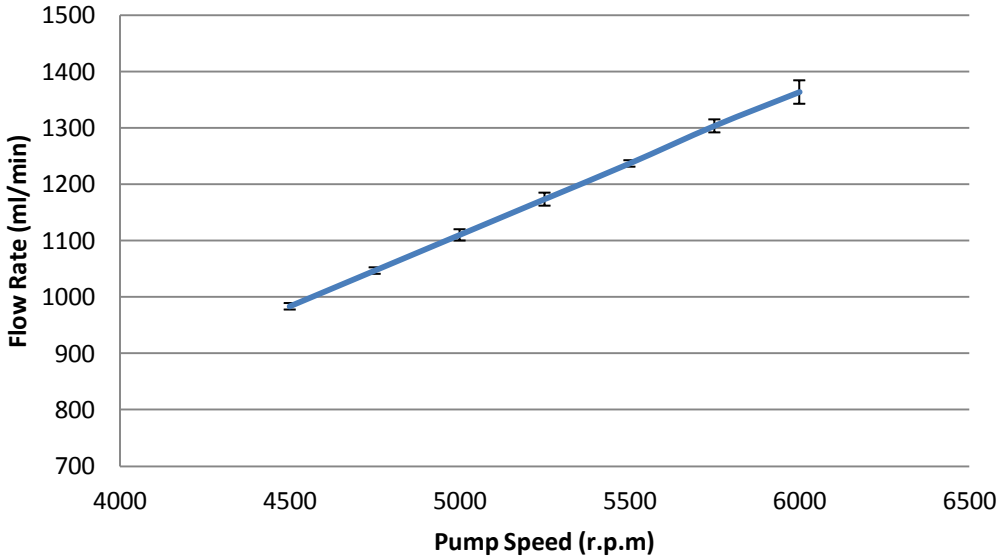


**Figure 110: Graph of flow rate vs. pump speed through a range of 4500-6000 r.p.m for the Mark II pump system. ± 1 Standard Deviation.**

### 3.12.4. Discussion

The results of this experiment show that the Mark II system can overcome considerably higher pressure heads and achieve more flow when compared to the Mark I system. Table 4 below compares the minimum and maximum values obtained by the Mark 1 and Mark II systems.

| Pump Design | Pump Speed (r.p.m) | Flow Rate (ml/min) | Pressure Head (mmHg) |
|---|---|---|---|
| Mark I (Min) | 2909 | 389 | 3.67 |
| Mark I (Max) | 6607 | 943 | 22 |
| Mark II (Min) | 2000 | 507 | 10 |
| Mark II (Max) | 6000 | 1363 | 59 |

**Table 4: Table comparing the results for the Mark I and Mark II systems.**

The improvement in performance can be attributed to the issues addressed in the design and the experimental set-up; however the haemodynamic performance must be evaluated. To do this the experimental results obtained previously were used as the boundary conditions for a CFD evaluation of the experiment.

## *CFD analysis of Mark II System Experiment*

### *Aims*

The aims of this experiment were to use the computational method developed and validated with the mark I system to produce a CFD analysis using values obtained within the physical experiment as boundary conditions. The results should determine if the computational simulation used in the previous analysis can be applied to alternative

geometries and if validated successfully the simulation should provide greater insight into the performance of the Mark II design.

### *Methods*

This simulation followed the protocol used to testing the Mark I system with the only difference being that the experimental values used to define the boundary conditions were taken from the Mark II physical experimentation. In the physical experiment the outlet tubing was placed inside the outlet of the prototype. This configuration reduces the cross-sectional area of the outlet flow path. To replicate this in the CFD model the outlet was similarly reduced in cross-sectional area as highlighted within Figure 111 below.

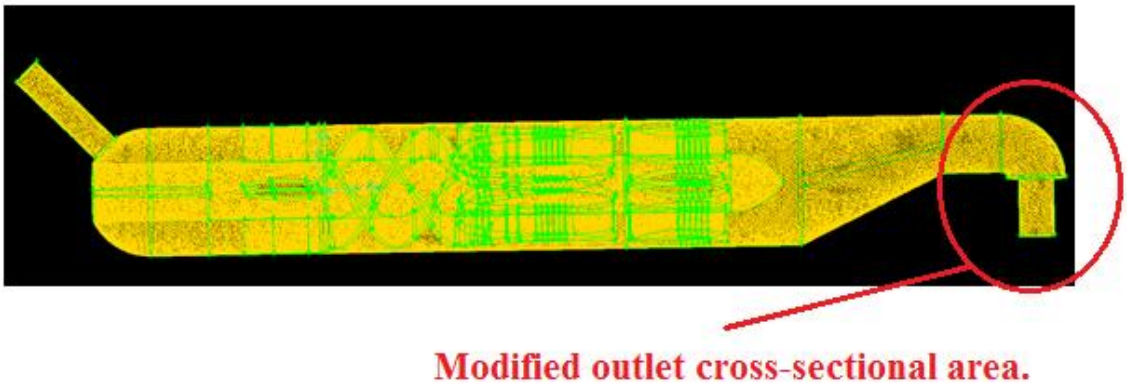


**Figure 111: Gambit mesh of the model highlighting the reduced cross-sectional area of the model to replicate the conditions of the physical experimentation.**

### *Results*

Figure 112 and Figure 113 below show graphs comparing the average experimental and computational results for pressure head against impeller rotational velocity through the ranges of 2000 – 3500 r.p.m and 4500 – 6000 r.p.m respectively.

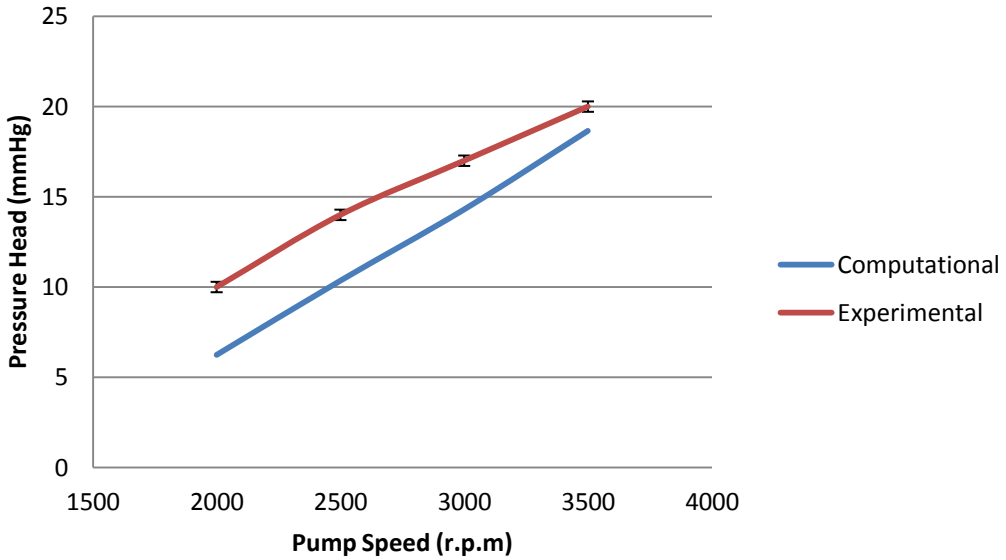


**Figure 112: Graph comparing experimental and computational pressure head vs. impeller rotational velocity for the range of 2000 – 3500 r.p.m. ± 1 Standard Deviation.**

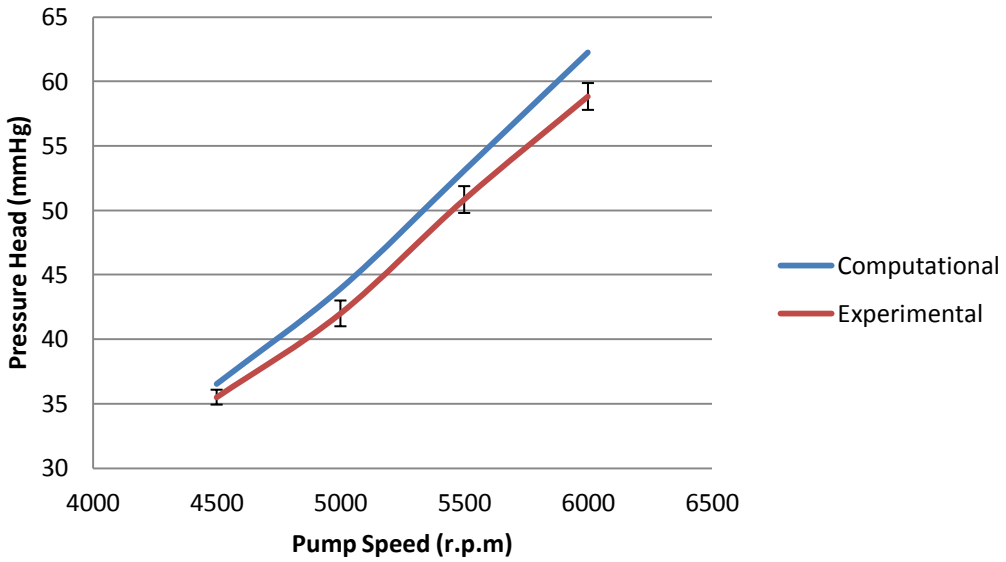


**Figure 113: Graph comparing experimental and computational pressure head vs. impeller rotational velocity for the range of 4500 – 6000 r.p.m. ± 1 Standard Deviation.**

Figure 114 and Figure 115 below show graphs comparing the experimental and computational results for flow rate against impeller rotational velocity through the ranges of 2000 – 3500 r.p.m and 4500 – 6000 r.p.m respectively.

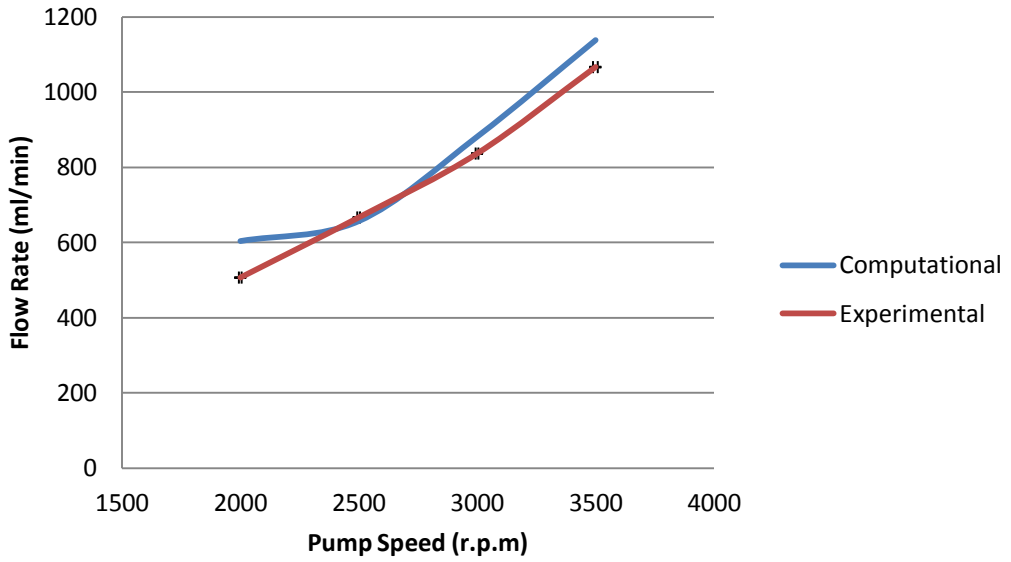


**Figure 114: Graph comparing experimental and computational flow rate vs. impeller rotational velocity for the range of 2000 – 3500 r.p.m. ± 1 Standard Deviation.**

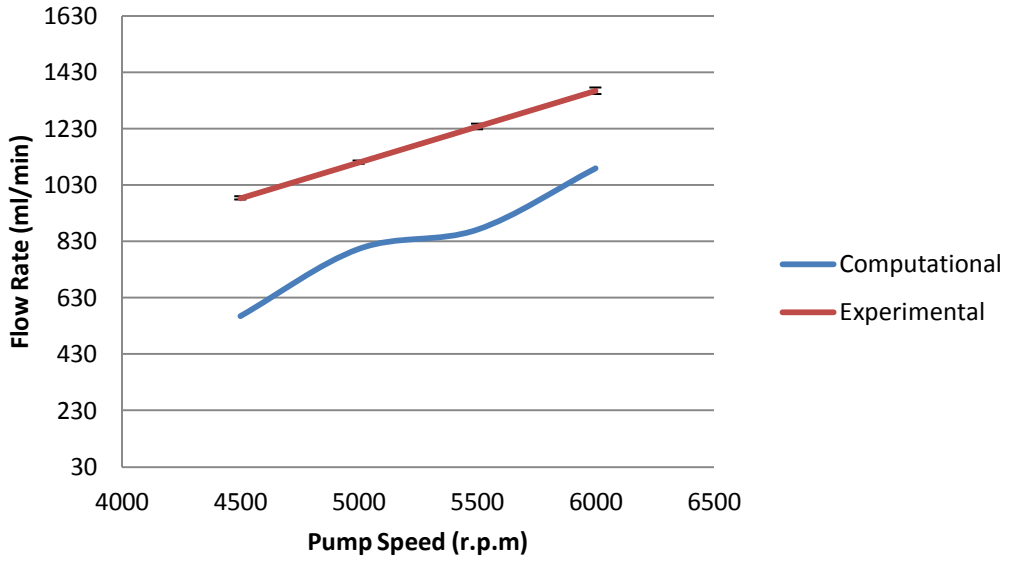


**Figure 115: Graph comparing experimental and computational flow rate vs. impeller rotational velocity for the range of 4500 – 6000 r.p.m. ± 1 Standard Deviation.**

### *Discussion and conclusion*

Comparison of the results shows that the computational model used to simulate the Mark I experiment can be applied successfully to an alternative geometry. The differences between the physical and computational systems can be attributed to imperfections in the physical systems that are impractical to accurately simulate in the CFD analysis. The Mark II model is more accurate when compared to the results of the Mark I model. The improved accuracy can be attributed to improvements in the physical model during the system redesign; hence the physical system is more closely matching the perfect settings of the computational model. The results of this simulation can be used to provide qualitative and quantitative feedback on the pump design. This is particularly useful in indicating the magnitudes and location of the wall shear stresses present. The model can therefore provide an evaluation of the performance of the pump in terms of the haemodynamic requirements of the blood. To help visualize the areas of highest wall shear stress Figure 116 and Figure 117 below show contours of wall shear stress on the impeller and diffuser and on the impeller casing at a rotational speed of 6000 r.p.m respectively.

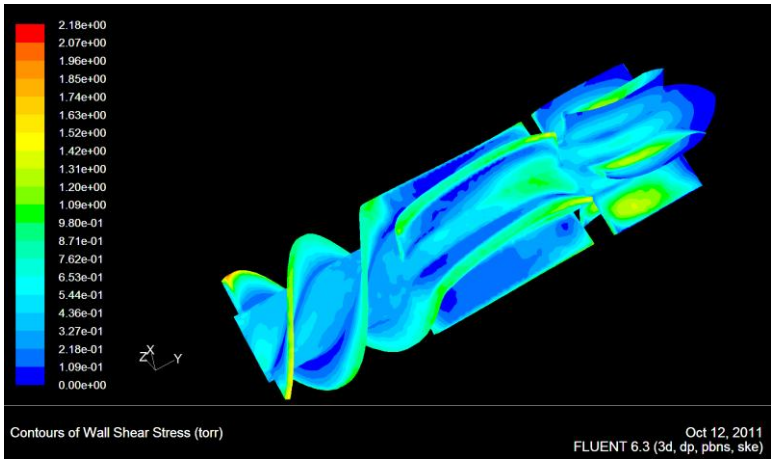


**Figure 116: Contours of wall shear stress on the impeller and diffuser at a pump speed of 6000 r.p.m.**

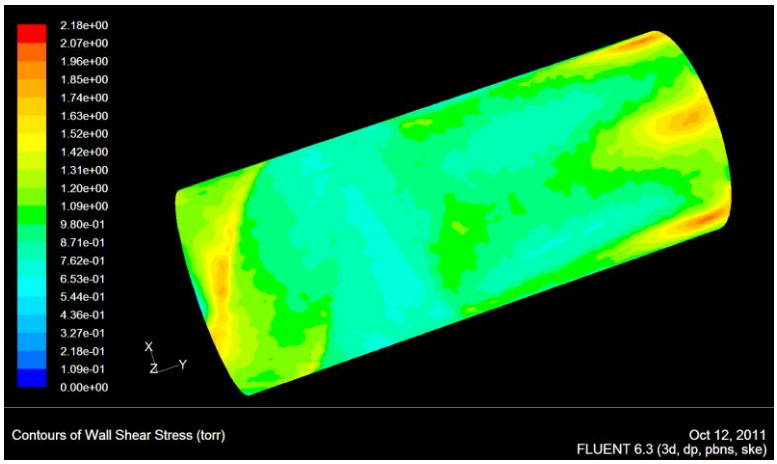


**Figure 117: Contours of wall shear stress on the impeller casing at a pump speed of 6000 r.p.m.**

These shear stress diagrams indicate that at the higher pump speeds this pump is within the thresholds that could potentially to lead to mechanical haemolysis of the blood cells.

### 3.12.5. Conclusions

The Mark II system design has addressed the problems encountered with the Mark I system and as a result the performance is far superior. The redesign of the system has focused on improving two aspects: the experimental configuration and the performance of the pump. In terms of the experimental configuration the new motor and motor controller have made a vast improvement in the control and accuracy of the system. The changes in the pump design have made the system more stable and this was reflected in the comparison between the computational simulation and physical experimentation. Using a transparent tube as the main body of the pump has allowed essential visual feedback of the flow field, which has highlighted specific areas of the design that could be improved. The performance of the pump has improved considerably; however the pump is still unable to provide sufficient performance to satisfy the operational requirements of a live animal experiment. For this reason further critical redesign is required.

## 3.13. Mark III Inducer, Impeller and Diffuser Design

Although the Mark II is a significant improvement over the Mark I design, the results of the physical experiment and computational analysis showed that the design was unable to provide sufficient hydrodynamic or haemodynamic performance. A potential solution to improve the performance is to increase the size of the pump. This will increase the velocity of the fluid at the blade tips, which should increase the potential pressure head that can be generated by the pump. The system should also be able to move greater volumes of fluid; however the increased velocity at the blade tips is likely to increase the wall shear stress on the impeller casing and will also increase the priming volume. To investigate the effect of increased pump volume on hydrodynamic and haemodynamic performance a computational simulation was used.

## 3.14. CFD Analysis to Determine the Effect of Pump Size on Hydrodynamic and Haemodynamic Performance

### 3.14.1. Aims

The aims of this analysis were to use scaled versions of the Mark II pump design to determine the effect of pump size on haemodynamic and hydrodynamic performance.

### 3.14.2. Methods

Six models were generated based upon the design of the Mark II pump increasing in diameter from 22 – 32 mm in 2 mm intervals. Each model was imported into Gambit for meshing. The mesh used was a tetrahedral/hexagonal element hybrid mesh. For consistency both models were meshed in a similar manner to previous analyses. The nodes in each mesh were as follows: 22 mm 261,089 nodes, 24 mm 313,172 nodes, 26

mm 385,073 nodes, 28 mm 424,870 node, 30 mm 496,054 nodes and 32 mm 558,368 nodes. Figure 118 below shows the mesh for the 32 mm Mark II pump design.

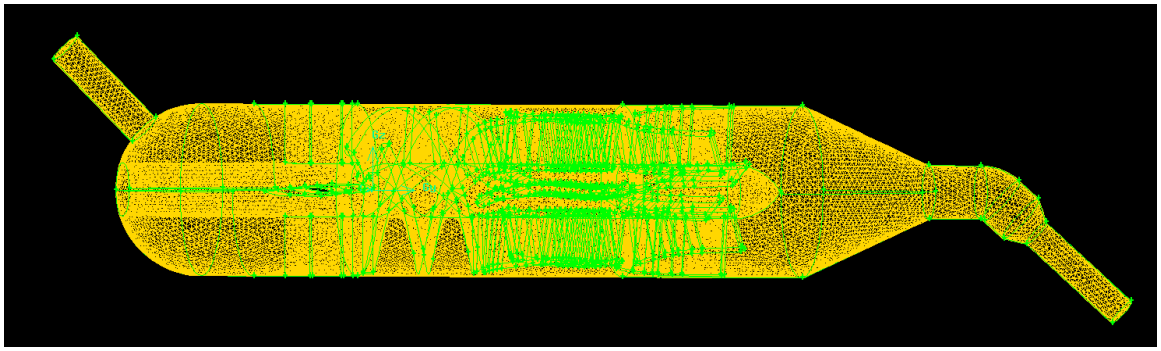

**Figure 118: Gambit mesh of the 32 mm Mark II pump design.**

The CFD analysis was run with the same conditions as used in the previous analyses.

Performance analysis was conducted by running each model at 6000 r.p.m with a flow rate of 500 ml/min using blood modeled as Newtonian with a constant viscosity of 0.0035 (Pa.s) and a density of 1050 ($kg.m^{-3}$).

### 3.14.3. Results

As this analysis was primarily focused on the effect of priming volume on the haemodynamic and hydrodynamic performance of the system the results are shown in terms of the varying pump priming volume. Pressure head and area-weighted average wall shear stress on the impeller casing (as this was recognized to be the area of highest stress) were used as performance characteristics.

Figure 119, Figure 120 and Figure 121 below show pump diameter, pressure head and area weighted average wall shear stress on the impeller casing versus priming volume respectively.

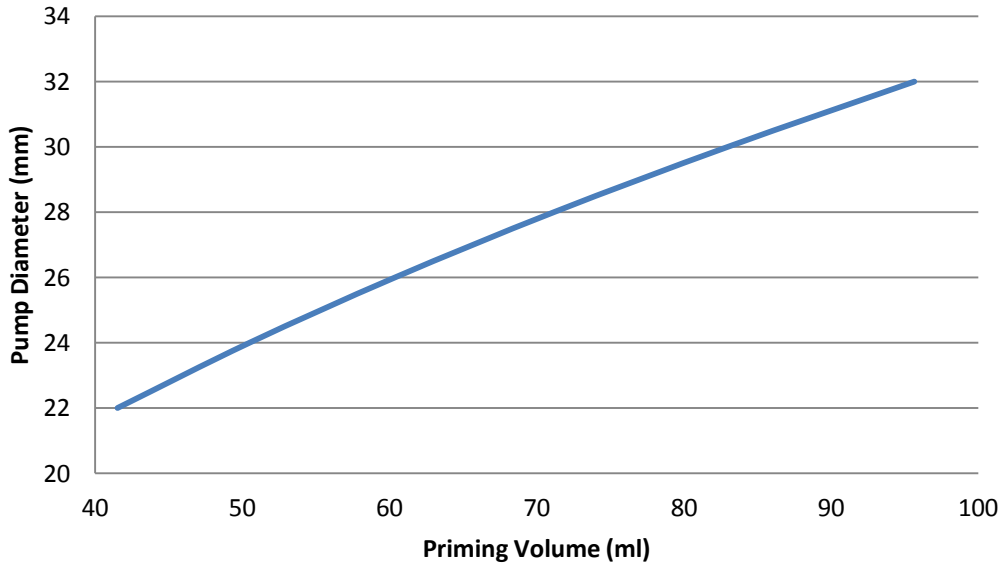


**Figure 119: Pump diameter Vs. Priming volume at a pump speed of 6000 r.p.m and a flow rate of 500 ml/min.**

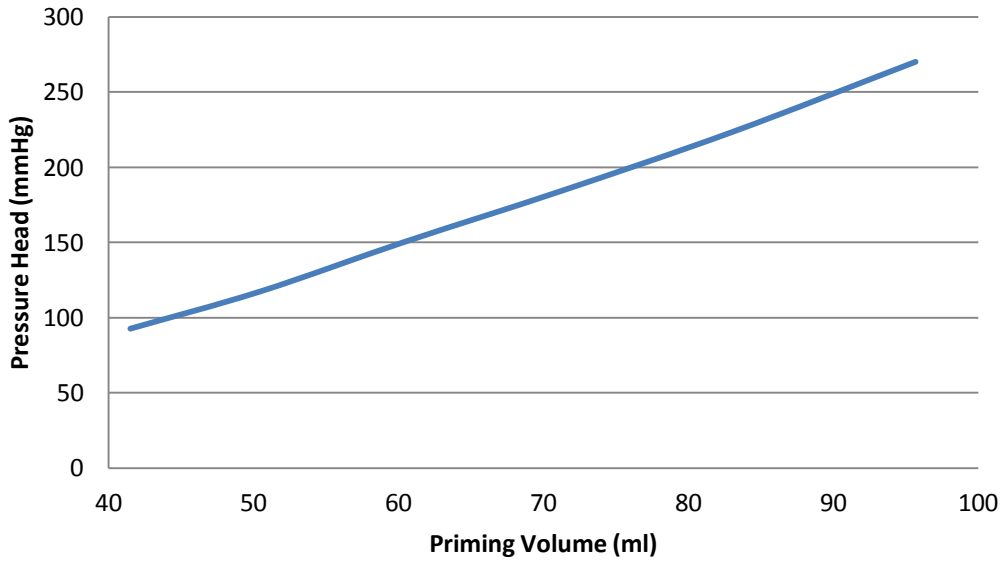


**Figure 120: Pressure head Vs. Priming volume at a pump speed of 6000 r.p.m and a flow rate of 500 ml/min.**

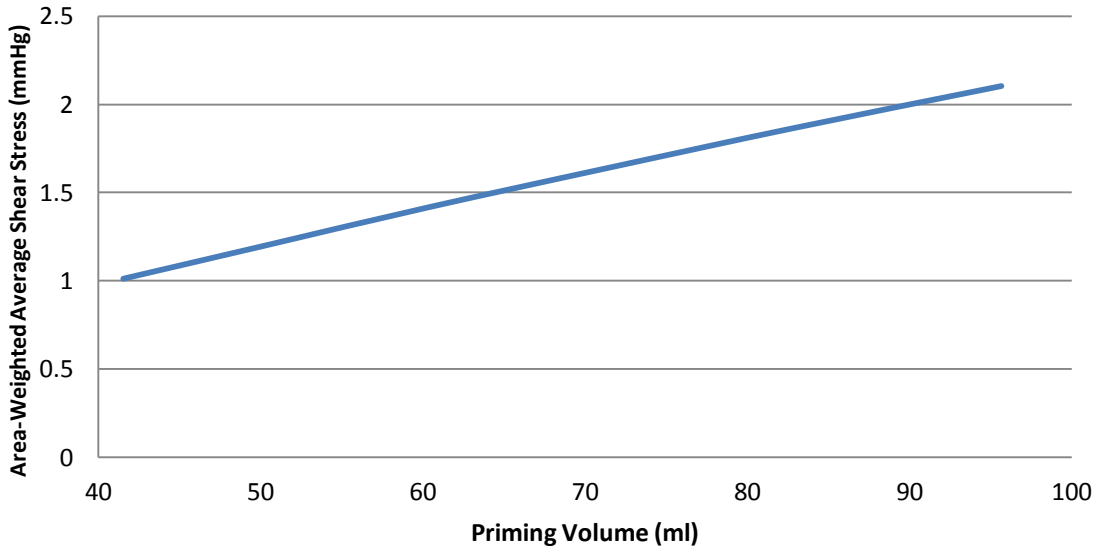


**Figure 121: Area weighted average wall shear stress on the impeller casing Vs. Priming volume at a pump speed of 6000 r.p.m and a flow rate of 500 ml/min.**

### 3.14.4. Discussion and Conclusions

The pump system must be able to overcome approximately 120 mmHg of pressure while providing up to 500 ml/min of flow to meet the performance requirements of the animal experiments. By enlarging the pump diameter the pressure head across the pump increases in a linear manner; however this comes at the cost of a linear increase in wall shear stress and priming volume. From the results the most appropriate pump diameter would appear to be 26 mm. At 6000 r.p.m this achieves a pressure head of 150 mmHg with a flow rate of 500 ml/min with maximum area-weighted average wall shear stress in this model is 1.416 mmHg.

## 3.15. Mark III Inducer/Impeller and Diffuser Pump Design

The results of the CFD analysis suggested that a 26 mm diameter pump was the optimum size to deliver the performance required. The Mark III redesign of the system focused on accommodating the larger diameter impeller and also worked to improve the inlet and the outlet of the device. The inlet of the device was modified such that the rear wall was angled to the same degree as the inlet tube. The intention of this design was to encourage a smoother transition of the flow from the inlet to the flow straightener. Figure 122 and Figure 123 below show cross-sections of the mark II and mark III pump inlets respectively.

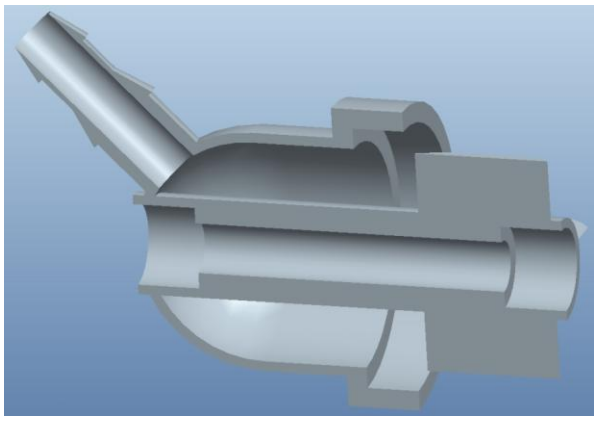

**Figure 122: Cross-section of the Mark II pump inlet design.**

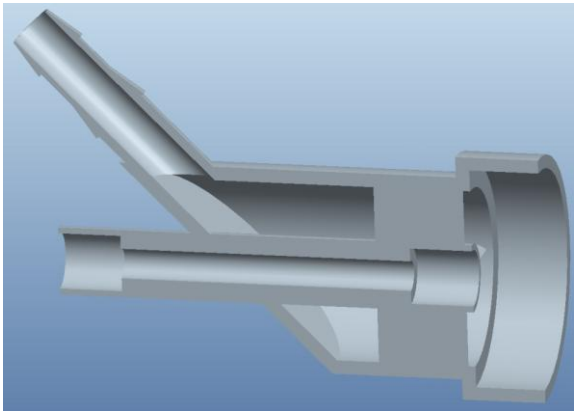

**Figure 123: Cross-section of the Mark III pump inlet design.**

The outlet of the pump was also adapted to remove the sudden right angle featured in the Mark II design. The changes in the outlet design are shown in Figure 124 and Figure 125 below.

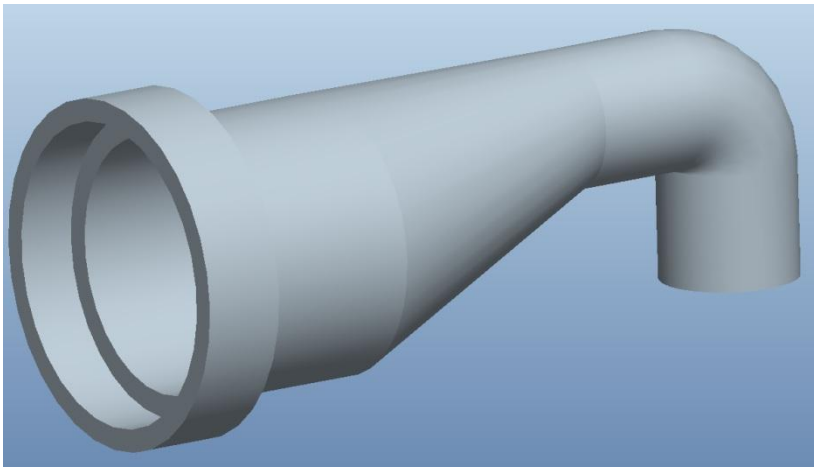

**Figure 124: Mark II pump system outlet design.**

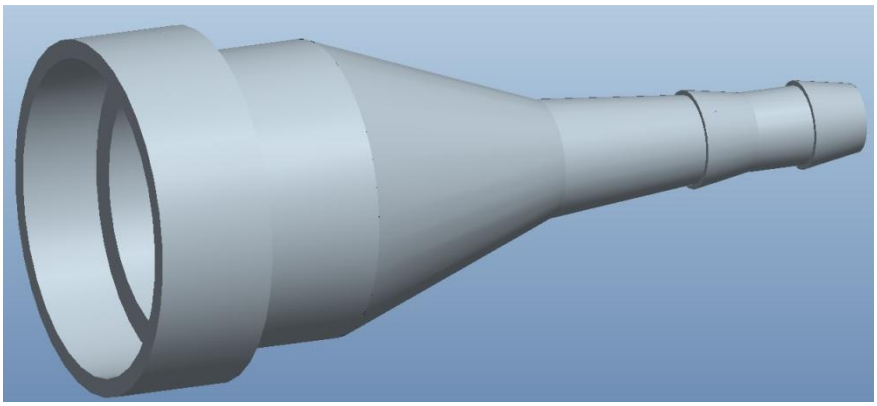

**Figure 125: Mark III pump system outlet design.**

Figure 126 below shows a ProEngineer of the Mark II and Mark III pumps together to help visualize the changes made in the redesign.

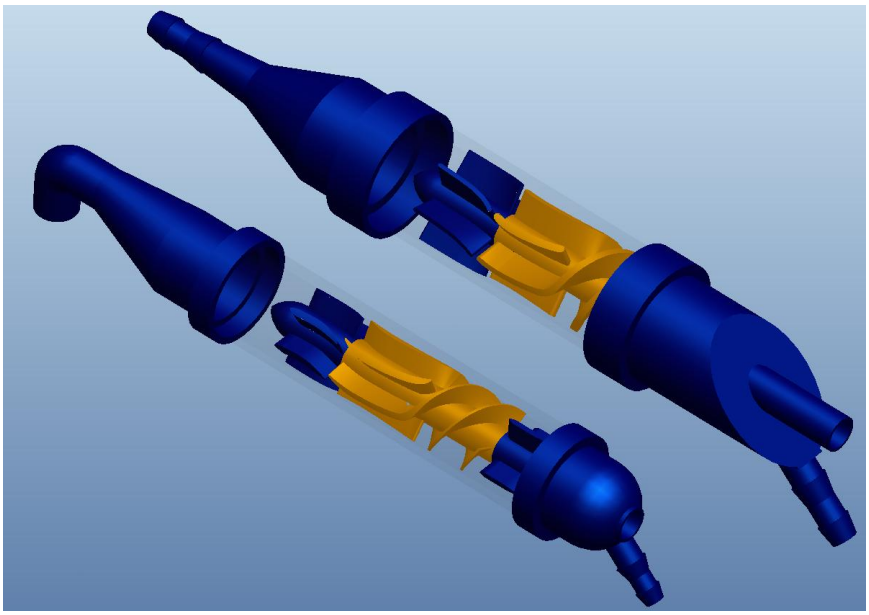

**Figure 126: Proengineer drawing comparing the Mark II and Mark III pump configurations.**

## 3.16. Mark III Inducer/Impeller and Diffuser Testing

### 3.16.1. Aims

The aims of the following experiments were to determine the hydrodynamic performance characteristics of the Mark III inducer/impeller and diffuser pump design.

### 3.16.2. Method and Materials

The principle components used to determine the performance characteristics of each system are shown within Figure 127.

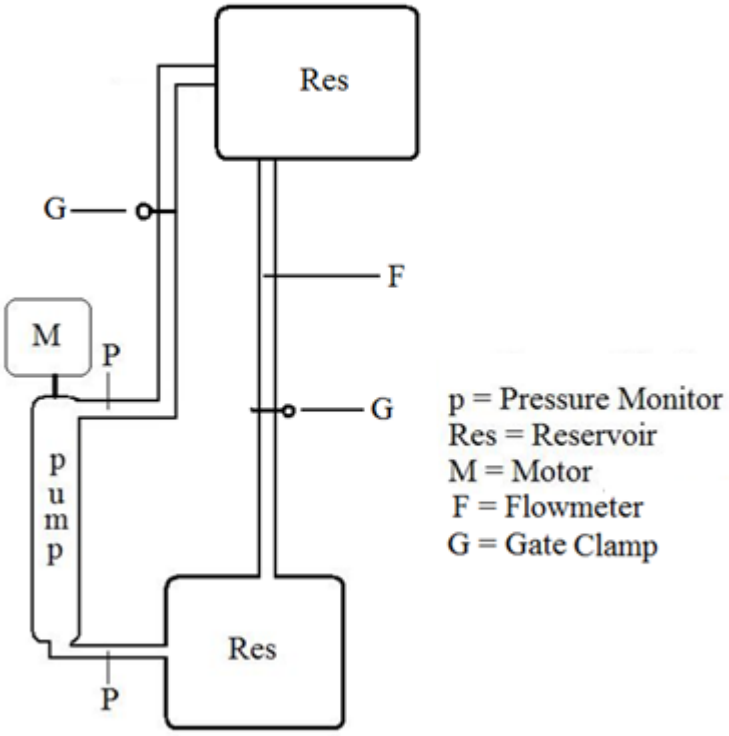


**Figure 127: Diagram of the experimental set-up used to test the Mark III pump system.**

The experiment was conducted using the same equipment as was used in the previous experimental set-up.

The circuit was closed with the pump feeding from a reservoir positioned slightly lower than the inlet pumping fluid to a raised reservoir, which drained by gravity back to the lower reservoir. A gate clamp on the feed to the upper reservoir was used to restrict flow and induce a pressure. A gate clamp was also used on the gravity drain to balance the flow rates to and from each reservoir. Initially the pump speed was set at 4000 r.p.m and the flow was restricted to 100 ml/min using the gate clamp on the feed to the upper reservoir. The clamp was then adjusted to produce flow rates through a range of 100 – 500 ml/min in 50 ml/min intervals with pressure values recorded at each flow rate interval. The experiment was conducted at pump speeds of 4000, 5000 and 6000 r.p.m. The complete experiment was repeated three times.

Figure 128 below show the configuration of the experiment with the main elements numbered and labeled.

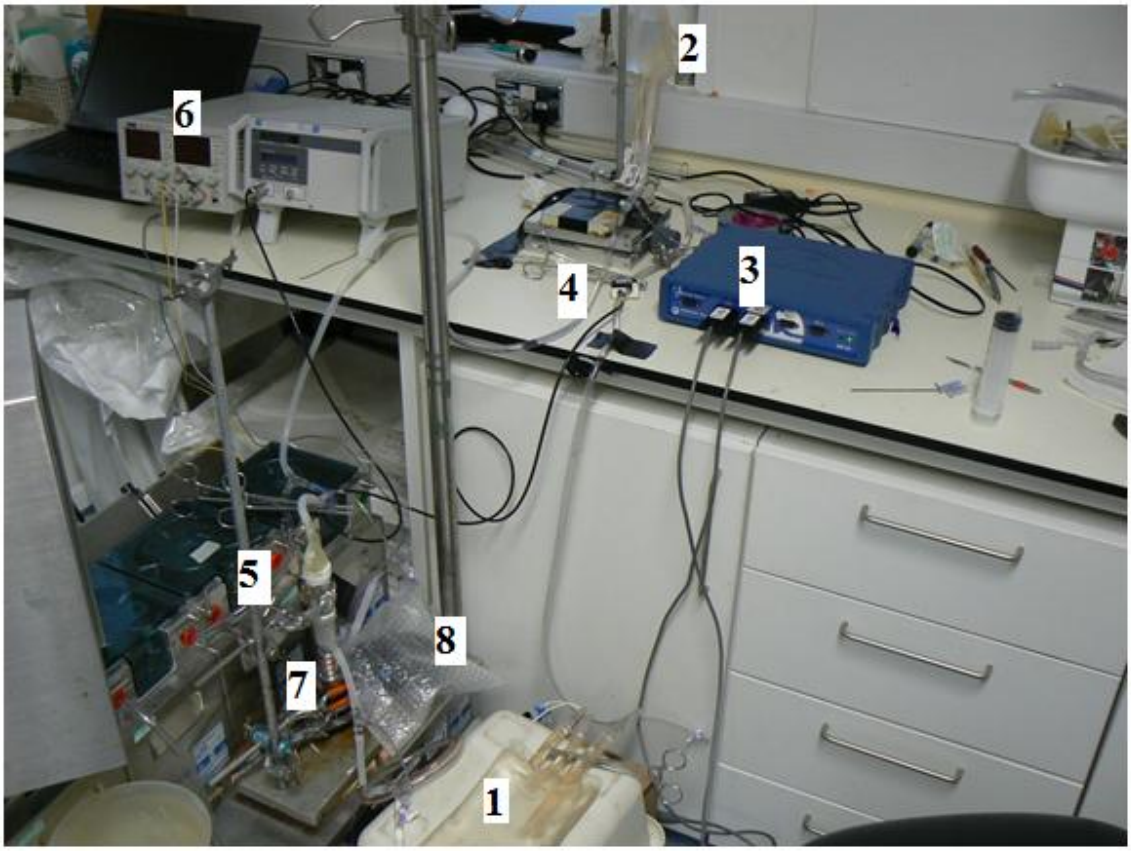


**1 = Lower Reservoir**
**2 = Upper Reservoir**
**3 = Pressure Monitor**
**4 = Flow Meter**
**5 = Pump System**
**6 = Power Supply**
**7 = Motor**
**8 = Motor Controller**

**Figure 128: Experimental configuration used to test the Mark III system with the main elements numbered and labeled.**

### 3.16.3. Results

In this experiment the pump speed was kept constant and the resistance to flow varied in order to produce a flow rate. For this reason the results are given in terms of the pressure head generated against the flow rate achieved at that pressure for each pump rotational velocity. Figure 129 shows the pressure head against flow rate for the pump at 4000, 5000 and 6000 r.p.m.

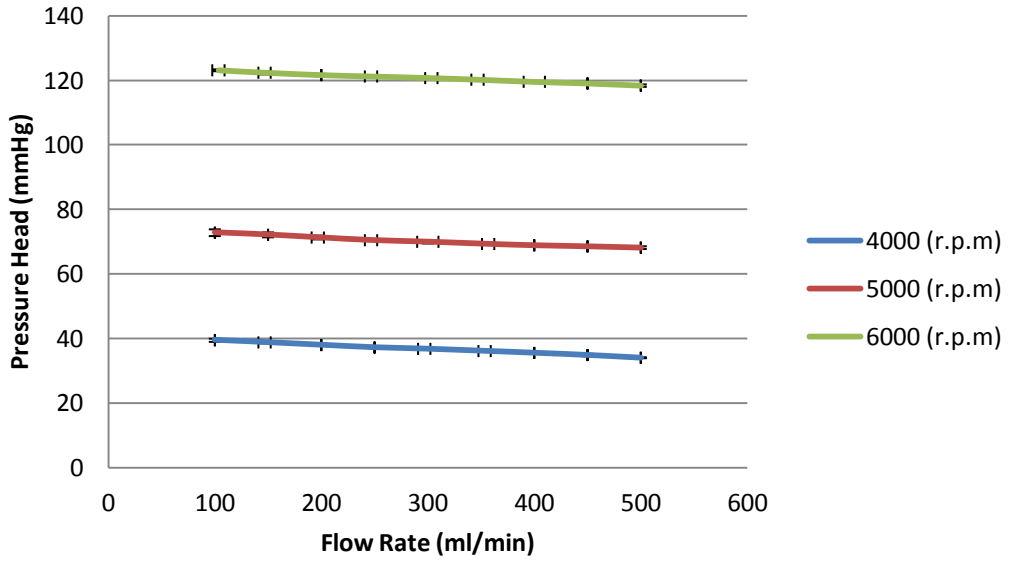


**Figure 129: Graph of pressure head vs. flow rate for the Mark III pump at 4000, 5000 and 6000 r.p.m. ± 1 Standard Deviation.**

### 3.16.4. Discussion

The results of this experiment indicate the performance characteristics of the mark III pump system through the required flow rates. These results show that this pump will require a speed of approximately 6000 r.p.m to produce the performance required of a live animal experiment. Although the hydrodynamic performance requirements have been met the haemodynamic performance of the pump must be evaluated. To allow for

further investigation a CFD analysis was conducted using the parameters observed within the physical experiment as boundary conditions to determine the wall shear stresses present and assess if these are significant enough to result in mechanical haemolysis.

## *CFD analysis of Mark III Pump System Experiment*

### *Aims*

The aims of this experiment were to use the computational method previously developed combined with values from the physical experiment to further investigate the performance of the system. Specifically the wall shear stresses present will be used to evaluate the potential of the system for mechanical haemolysis.

### *Methods*

A model was developed to represent the flow path within the physical prototype developed. The model was imported into Gambit for meshing. The mesh used was a tetrahedral/hexagonal element hybrid mesh of 1,346,555 nodes. Figure 130 below shows the meshed flow path within Gambit.

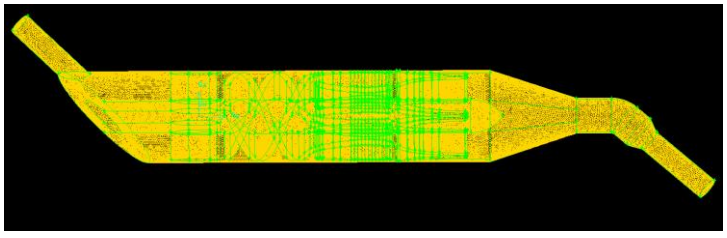

**Figure 130: Gambit mesh of the Mark III 26 mm diameter pump model.**

This simulation followed the protocol used in the previous CFD analysis of the Mark III system with the only difference being that the values used to define the boundary conditions were taken from the Mark III physical experimentation.

### *Results*

The conditions of the experiment were replicated in this simulation and therefore to allow for a direct comparison the results are displayed in the same manner as within the physical experiment. The primary aim of the simulation was to determine the maximum magnitude of the wall shear stresses occurring in the model for this reason the simulation only evaluated the pump at the highest rotational velocity.

Figure 131 and Figure 132 below show graphs comparing the average experimental and computational results for pressure head and area weighted average wall shear stress against flow rate at pump speed of 6000 r.p.m respectively.

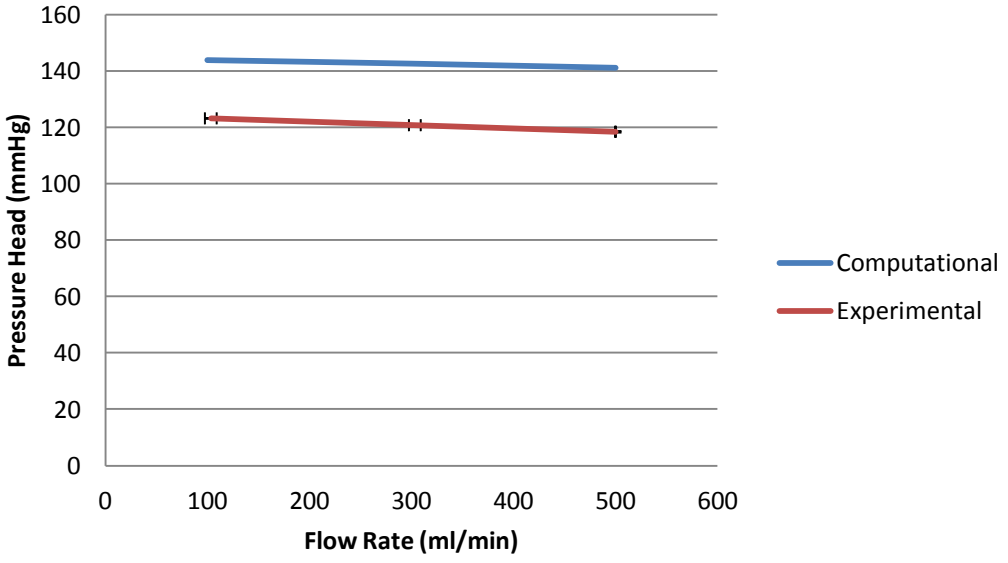


**Figure 131: Comparison of experimental and computational pressure head vs. flow rate for a pump speed of 6000 r.p.m. ± 1 Standard Deviation.**

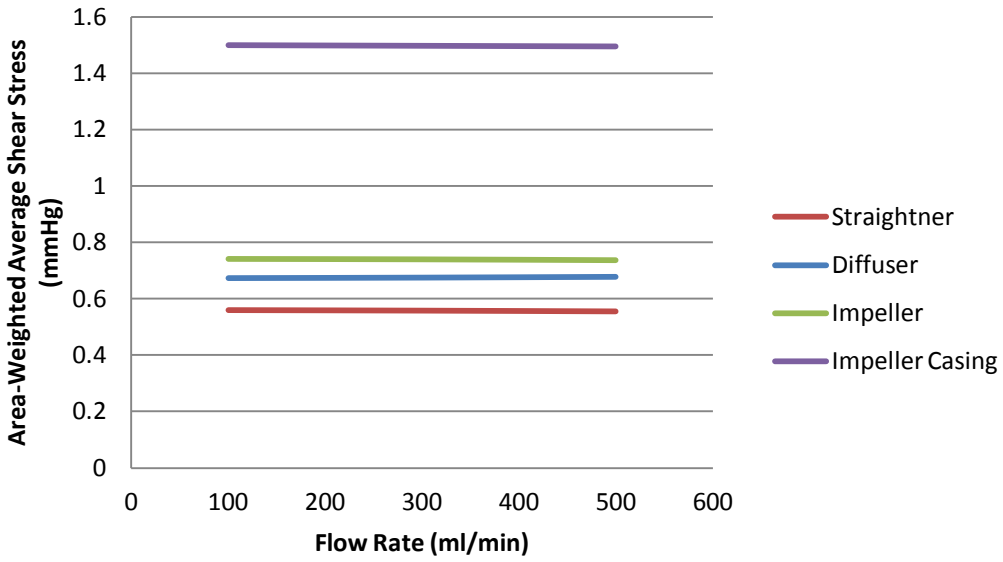


**Figure 132: Graph of area weighted average wall shear stress in the computational model at 6000 r.p.m.**

## *Discussion and conclusion*

Comparison of the results show that the computational model predicts higher performance than obtained in the experimental analysis; however the results are within 20 % and the difference can be attributed to imperfections in the physical experimental configuration. This comparison highlights the evolution of both the computational simulation and physical experimentation as the difference between the two sets is much smaller than for the Mark I and Mark II system indicating a higher accuracy. Furthermore unlike the previous designs this simulation required no adaptation of the computational model to compensate for failings in the physical experiment such as bent inducer blades or an obstructed outlet.

The highest wall shear stresses occur on the impeller casing with a maximum shear stress of approximately 3.49 mmHg and an area-weighted average of approximately 1.5

mmHg. Figure 133 and Figure 134 below show contours of wall shear stress on the impeller casing and on the straightener, impeller and diffuser blades respectively.

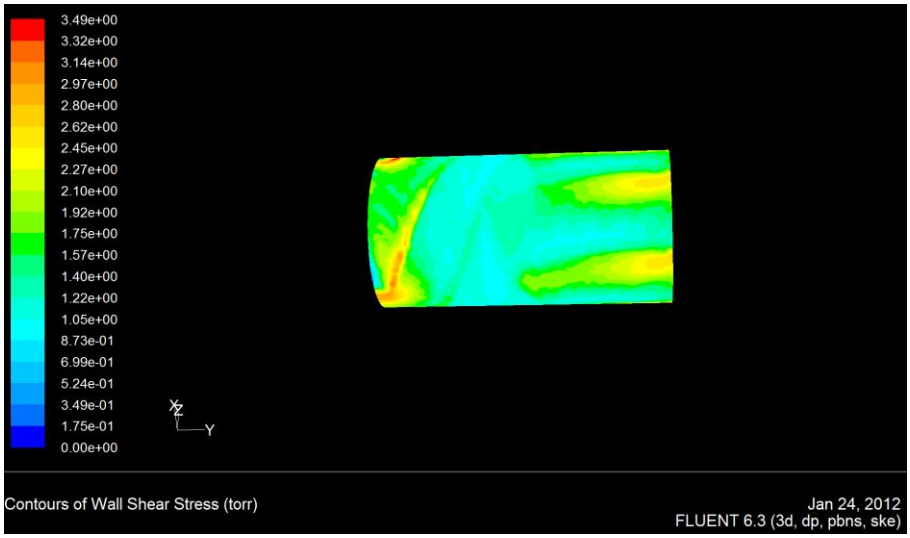


**Figure 133: Contours of wall shear stress on the Mark III impeller casing at 6000 r.p.m.**

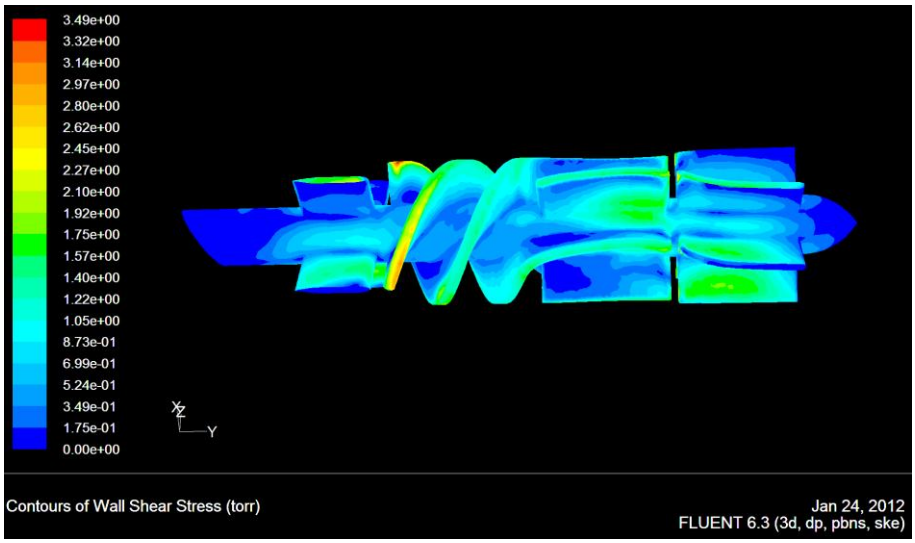


**Figure 134: Contours of wall shear stress on the Mark III straightener, impeller and diffuser blades at 6000 r.p.m.**

These diagrams show that the largest shear stresses occur between the blades of the impeller and the casing, similar to the previous designs. The magnitudes of shear stress

present indicate that mechanical haemolysis is likely; however the amount of haemolysis will depend upon the exposure time of the blood to the stress.

### 3.16.5. Conclusions

The mark III configuration is able to produce the hydrodynamic performance required to meet the initial design requirements. At the pump speeds required to achieve this performance the shear stresses present in the CFD analysis indicate that mechanical haemolysis is likely to occur. Areas of maximum shear stress are localized and so levels of haemolysis should be mild; however physical modeling of the system to determine the actual amount of haemolysis is required before the system can be considered to be suitable for use within a live animal experiment.

## 3.17. Mark III Inducer/Impeller and Diffuser Haemolysis Testing

### 3.17.1. Aims

The aim of the following experiment was to determine the levels of haemolysis generated by the Mark III pump system when operating at the required operational pump speed.

### 3.17.2. Method and Materials

The principle components used to determine the performance characteristics of the system are shown within Figure 135.

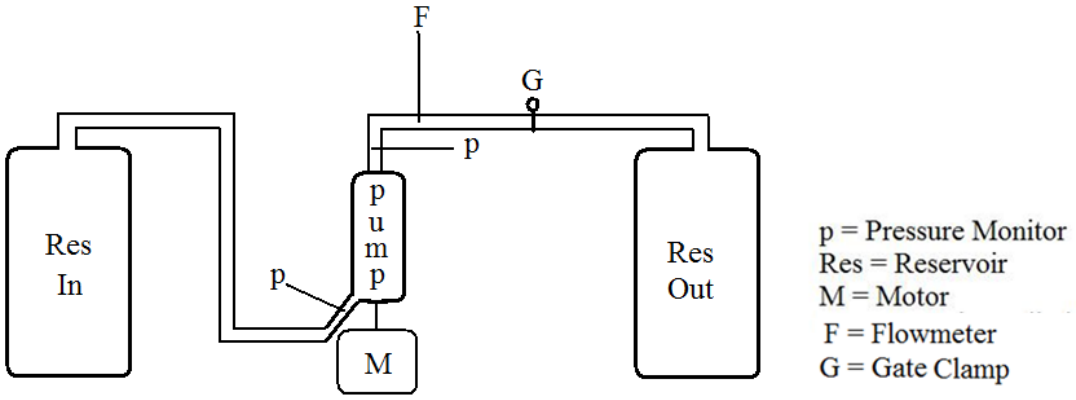


**Figure 135: Diagram of the experimental set-up used to determine the haemolysis characteristics of the Mark III pump system.**

The experiment was conducted using the same components as was used in the previous experimental set-up. The pump system and pressure monitors were primed with 0.9 % saline solution (Baxter, Berkshire, UK) prior to running the motor. Bovine blood treated with 10 ml of 1000 IU/ml Heparin-sodium solution (Wockhardt, Mumbai, Maharashtra, India) with a haematocrit of 42 % was drawn from the inlet reservoir by the pump. The blood was passed through the system to an outlet reservoir. The pump was run at 5000 r.p.m and a gate clamp was used to produce a flow rate of 400 ml/min. The system was allowed to run for 1 minute to ensure flow was properly established then three blood samples were taken from the inlet to and the outlet from the pump spaced over 30 second intervals. A control value was taken from the blood inlet reservoir prior to starting the experiment. Samples were spun for 10 minutes at 5000 r.p.m in a 5415 D centrifuge (Eppendorf, Cambridge, UK) and the plasma was removed.

A spectrophotometric analysis was conducted on the plasma samples using a spectrophotometer (Bibby Scientific Ltd, Staffordshire, UK). The experiment was then repeated at pump speeds of 6000 and 7000 r.p.m. The complete experiment was repeated three times. Figure 136 shows the experimental configuration used to test the haemolytic potential of the Mark III pump system with the major components numbered and labeled.

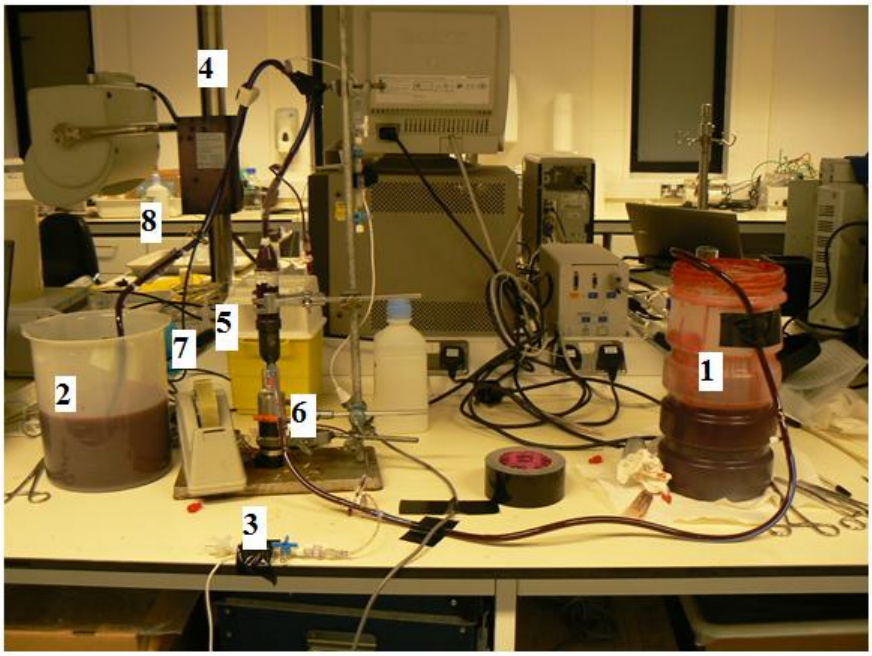


1 = Inlet Reservoir
2 = Outlet Reservoir
3 = Pressure Monitor
4 = Flow Meter
5 = Pump system
6 = Motor
7 = Motor Controller
8 = Gate Clamp

**Figure 136: Experimental configuration used to determine the haemolysis characteristics of the Mark III System with the major components numbered and labeled**

### 3.17.3. Results

Table 5 below shows the results of the spectrophotometric analysis.

| Pump Speed | Plasma free Haemoglobin | | Standard Deviation | |
|---|---|---|---|---|
| | Pre | Post | Pre | Post |
| (R.p.m) | (mg/dL) | (mg/dL) | (mg/dL) | (mg/dL) |
| 5000 | 1.7 | 1.9 | 1.3 | 1.4 |
| 6000 | 1.7 | 2.1 | 1.3 | 1.7 |
| 7000 | 1.7 | 2.3 | 1.3 | 0.9 |

**Table 5: Results of the spectrophotometric analysis.**

### 3.17.4. Discussion

The levels of haemolsysis present increase with increasing pump speed as expected; however they are within acceptable limits. The haemolysis generated through the pump depends upon the shear stresses present and upon the exposure time of the blood to those elements. Although an axial flow pump is not ideally suited to high pressure low flow systems, in this case the pressure requirements of a miniaturized and integrated system are such that the axial flow pump is able to achieve suitable hydrodynamic performance without compromising on haemodynamic performance.

### 3.17.5. Conclusion

This experiment has indicated that the level of haemolysis generate within this pumping system through the pump speed range required to achieve suitable hydrodynamic performance are acceptable. The results therefore suggest that this pump configuration is suitable for further testing in more clinically mimetic conditions.

## 3.18. Endurance Testing of the Mark III Pump System

### 3.18.1. Aims

The aims of the following experiment were to determine the reliability of the pump prototype developed by subjecting the system to conditions that simulate those of a live animal experiment over an extended period of time.

### 3.18.2. Method and Materials

The principal components used to determine the performance characteristics of the system are shown within Figure 137.

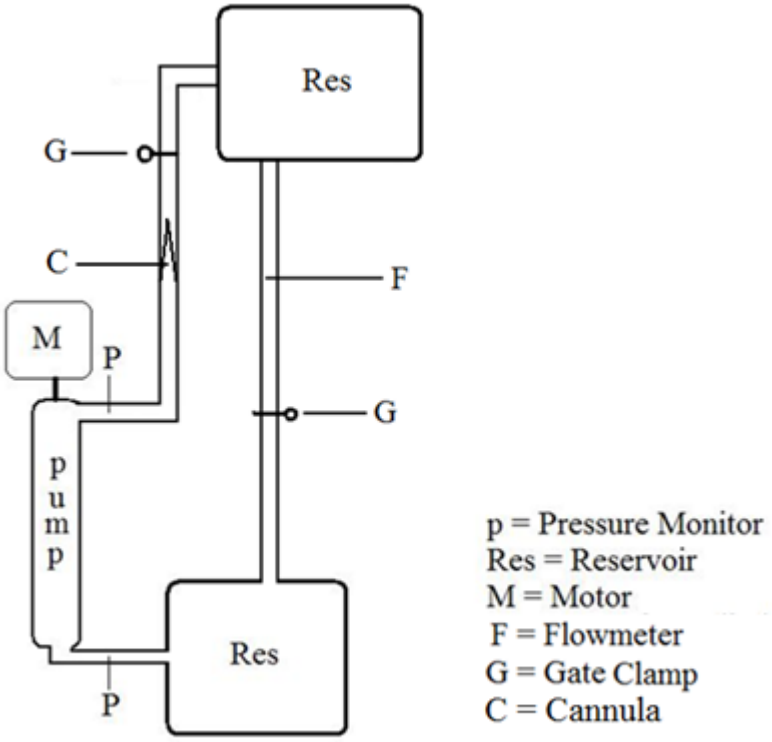


**Figure 137: Diagram of the experimental set-up used to determine the performance characteristics of the Mark III pump system over an extended period of time.**

The experiment was conducted using the same components as was used in the previous experimental set-up. The circuit was closed with the pump feeding from a reservoir positioned slightly lower than the inlet pumping fluid to a raised reservoir, which drain by gravity back to the lower reservoir. An 8 F cannula was placed in the circuit to simulate arterial re-entry conditions. A gate clamp on the feed to the upper reservoir was used to restrict flow and induce a pressure. A gate clamp was also used on the gravity drain to balance the flow rates to and from each reservoir. The pump speed was set at 6000 r.p.m and the gate clamp prior to the upper reservoir was adjusted to achieve approximately 120 mmHg with a flow rate of approximately 400 ml/min. The system was run for 6 hours (this is the time required by the ISO standard for testing of an extracorporeal system) with pressure values at the inlet to and outlet from the pump and flow rate recorded every 5 minutes. The entire experiment was repeated three times.

Figure 138 shows the experimental configuration used in the endurance testing of the Mark III pump with the major elements numbered and labeled.

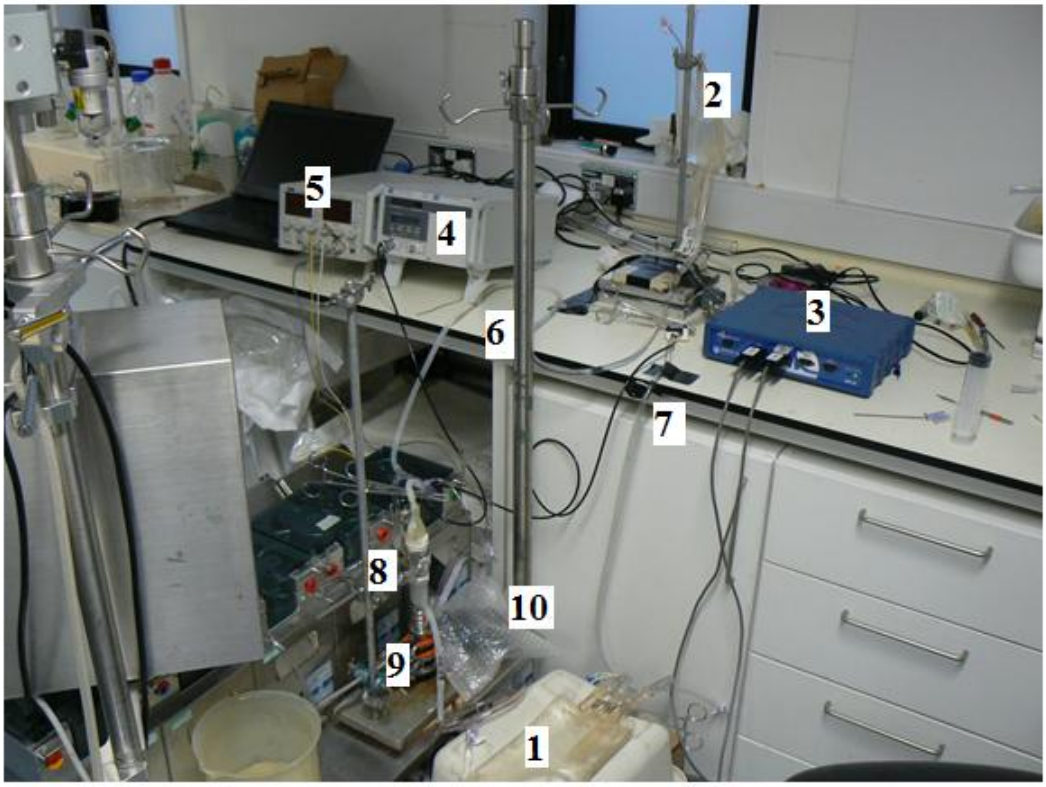


**1 = Lower Reservoir**
**2 = Upper Reservoir**
**3 = Pressure Monitor**
**4 = Flow Meter**
**5 = Power Supply**
**6 = Cannula**
**7 = Gate Clamp**
**8 = Pump System**
**9 = Motor**
**10 = Motor Controller**

**Figure 138: Experimental configuration used to determine the performance characteristics of the Mark III System with the major components of the experiment numbered and labeled.**

### 3.18.3. Results

As this experiment was focused on endurance the typical performance characteristics, pressure head and flow rate, are presented against time. Figure 139 and Figure 140 show pre-load and after-load and flow rate against time for the Mark III pump system.

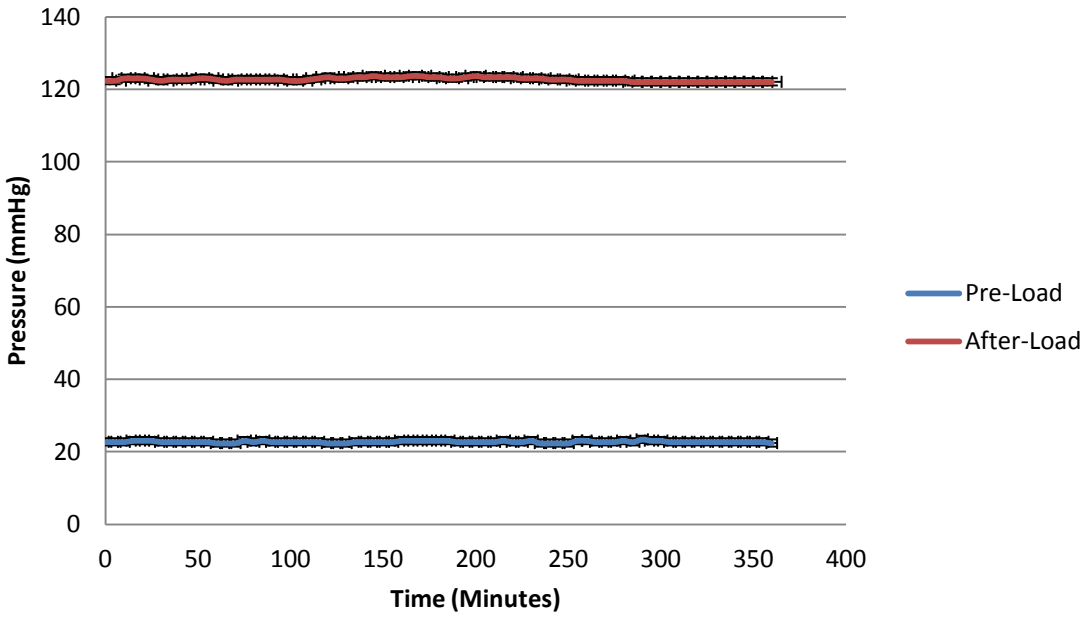


**Figure 139: Pre-load and after-load pressure against time for the Mark III pump system. ± 1 Standard Deviation.**

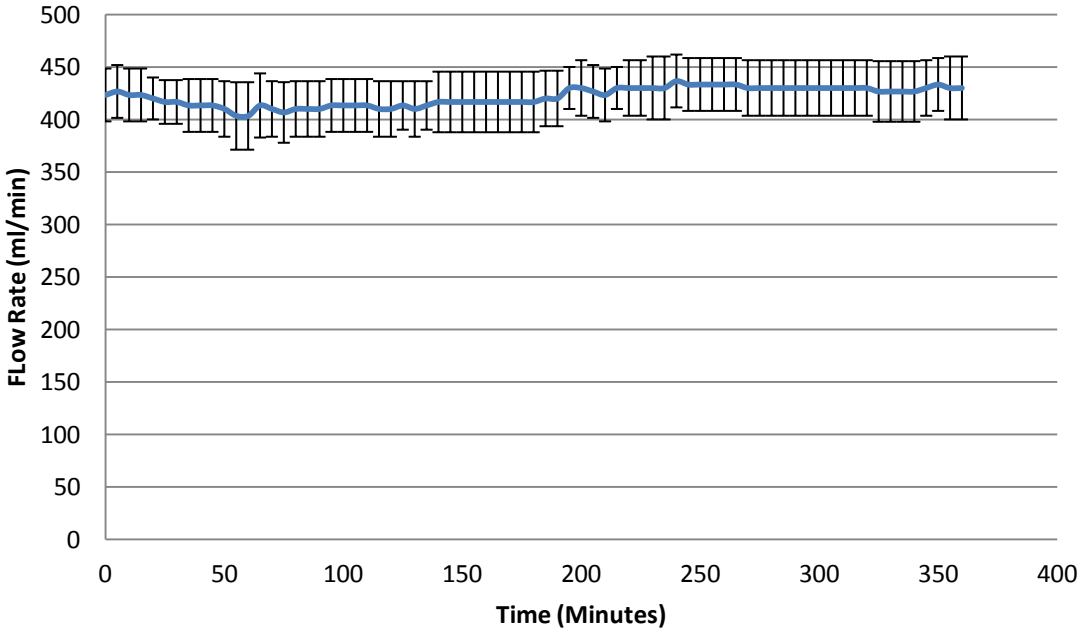


**Figure 140: Flow rate against time for the Mark III pump system. ± 1 Standard Deviation.**

### 3.18.4. Discussion and Conclusions

The results of this experiment have shown that the Mark III prototype is capable of performing adequately and reliably over an extended period of time. The conditions within this experiment were designed to simulate the near clinical conditions in which the pump will be required to function. The experiment has therefore allowed the performance and reliability of the design to be suitably evaluated. The results can be used to justify the design, allowing it to be taken forward and integrated as part of a miniaturised and integrated ECMO system.

## 3.19. Chapter Conclusions

This chapter describes the iterative approach taken to the development of a functional axial flow pump for use within a miniaturised and integrated ECMO system. The development philosophy employed throughout focused on producing concepts and validating them using computational analysis prior to physical prototyping and testing. Using computer simulation as a tool for design optimization saved time and money and reduced the number of physical iterations required.

Physical testing of the prototypes was used to gain further insight into the pump performance characteristics and by direct comparison of the results allowed for validation of the computational simulations. Physical testing also highlighted practical issues with the design in terms of manufacturing and function.

Several design iterations were created; each design evolved from the previous through addressing the problems highlighted by the physical and computational experimentation. Ultimately the work has produced a functioning prototype that satisfactorily meets the design requirements of a miniaturised and integrated ECMO system and also meets the performance requirements of a live animal experiment.

# 4. The Heat Exchanger

## 4.1. Heat Exchange System Development

Homeostasis is the ability to physically regulate the body to maintain stable conditions in response to fluctuations in the outside conditions. Normothermia of a human being is 37 $^{0}$C. Excessive deviations from this temperature can result in death. Maintenance of this key physiological characteristic is an important technical element of the ECMO system. During ECMO patients are generally heavily sedated and experience a slower metabolism; hence their ability to maintain normothermia is compromised. Several steps are taken within the ICU to help prevent a patient's core temperature dropping to unacceptably low levels, including;

a) wrapping the patient in a thermal blanket
b) Maintaining high room temperature
c) keeping the patients skin and bedding dry
d) reducing exposure time and eliminating drafts

The extracorporeal circuit of the ECMO system also contributes to heat loss from patients undergoing ECMO therapy, by losing heat to the environment. The relatively high surface area of the ECMO system can result in considerable heat loss. Despite the other approaches to minimising heat loss, it must be accommodated for by introducing compensatory heat delivery technology within the ECMO system itself, delivering heat to the circulating blood directly. Such devices have come to be known as extracorporeal heat exchangers, and they are common in modern clinical practice. In general heat exchangers function by circulating temperature controlled water on one side of a metallic thermal interface, with blood circulating on the other side of this barrier. In this regard, such devices contribute significantly to the footprint of the ECMO system, with its general complexity and reliance on central services and the priming volume of the overall system. Eliminating this water based device in favour of an alternative approach would be beneficial in reducing the complexity of the end system enabling central service independence, thus enhancing transport capability of the overall system.

## 4.2. Initial Considerations and Design Approach

Heat transfer refers to the transference of thermal energy between systems. Heat transfer typically occurs from a system of higher temperature to a system of lower temperature. Transference of thermal energy results in a change in the internal energies of each system in accordance with the first law of thermodynamics. There are three mechanisms through which heat transfer occurs: conduction, convection and radiation.

### *Heat Transfer by Conduction*

Heat transfer by conduction refers to conduction of heat through a material. It occurs via molecular agitation without movement of the substance as a whole. The exact form of agitation depends upon the state of the material through which the heat is conducting. In solids conduction is generally considered to be transferred by lattice vibrations. The energy is transferred between atoms from the higher energy to the lower. In metals conduction is more efficient due to the "free" electrons, which aid the transfer of energy. In both gases and liquids heat is conducted through collisions between molecules during their random motion and by diffusion. Conduction within a gas is much lower due to the dilution of molecules within the media. Conductance is defined by Fourier's law which for a homogeneous material of one dimensional geometry is defined in Equation 4:

$$\frac{\Delta Q}{\Delta t} = -kA\,\frac{\Delta T}{\Delta x}$$

**Equation 4: Fourier's law of conduction within a homogeneous material of one dimensional geometry.**

Where:

$\frac{\Delta Q}{\Delta t}$ = The amount of heat transferred per unit time (W)
k = Thermal conductivity of material (W/m.K)
A = Area ($m^2$)
$\Delta T$ = Temperature gradient (K)
$\Delta x$ = Distance through which conduction is occurring (m)

Positive heat transfer occurs from the higher temperature to the lower and hence the negative sign within the equation. To reduce the rate of heat transfer by conduction between two points the following must occur:

- Use of a material with lower conductivity (k).
- Decreased cross-sectional area of the material through which the heat transfer is occurring (A).
- Increased distance for conduction to occur ($\Delta x$).
- Decrease the temperature gradient ($\Delta T$).

### *Heat Transfer by Convection*

Heat transfer by convection occurs when a fluid or gas passes over a surface. Convection heat transfer is mostly caused by bulk motion of the fluid particles; however diffusion also plays a part. The total heat transfer rate is defined in Equation 5:

$$q = \bar{h} A_s (\Delta T)$$

**Equation 5: Total heat transfer rate.**

Where:

q = heat transfer (W)

$\bar{h}$ = average convection coefficient (W/m$^2$.K)

$A_s$ = surface area (m$^2$)

$\Delta T$ = Temperature gradient (K)

There are two different forms of convection: natural (free) or forced convection.

In natural convection, bulk fluid motion is created by buoyancy forces. Buoyancy occurs when there is a density gradient and a body force that is proportional to density in a fluid. In the case of heat transfer within an ECMO system the body force is most likely to be gravitational. Figure 141 below shows an ideal gas next to a solid surface of higher temperature.

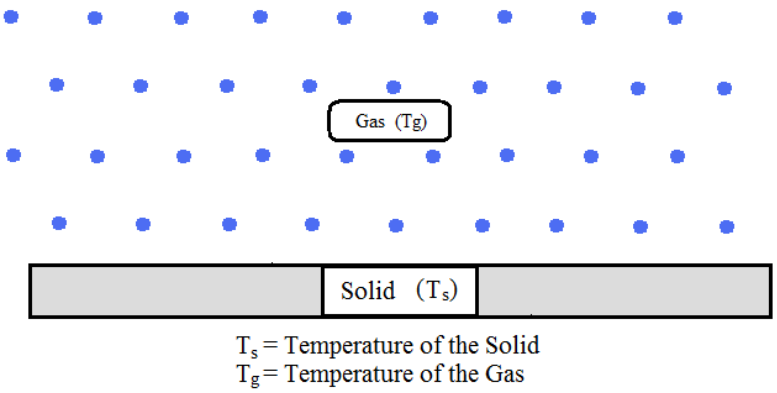


**Figure 141: Diagram of an ideal gas next to a heated solid surface.**

After a certain time (t) the molecules closest to the solid surface will be heated. Following the Ideal Gas Law for an increase in temperature at a constant pressure a decrease in density will occur. The heated molecules will therefore move upwards and the colder molecules downwards as shown within Figure 142.

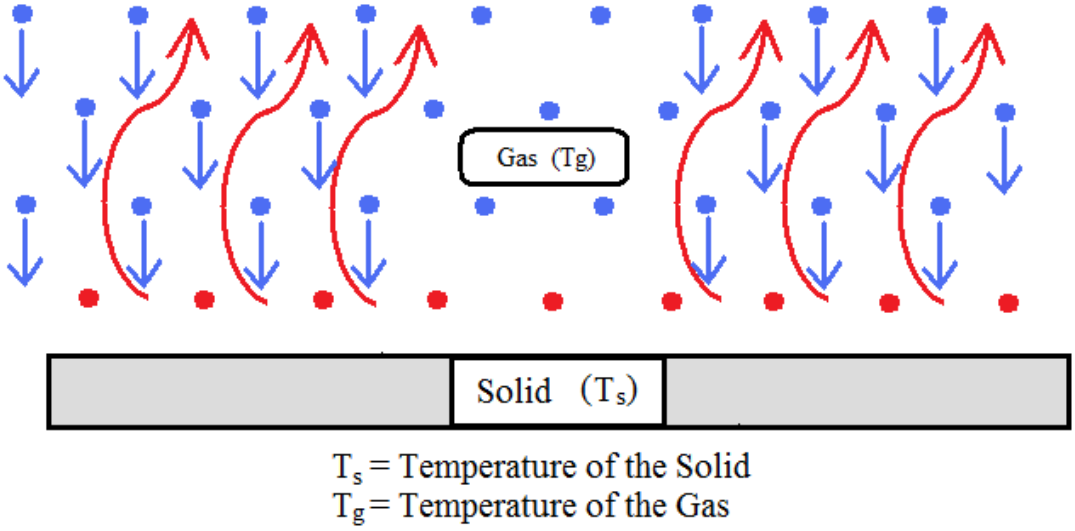


**Figure 142: Diagram showing natural convection currents within the gas close to a heat source.**

Natural convection in liquids occurs in a similar manner. In forced convection the bulk motion of the fluid is induced by an external source such as a fan or a pump. The definition of the average convection coefficient depends upon the type of convection dominant. If there is a combination of natural and forced convection the heat transfer is termed mixed convection. In an ECMO circuit heat loss by convection occurs as the fluid passes through the system with heat being transferred from the warm blood to the cold circuit. Natural and forced convection losses will also occur from the circuit to the surrounding environment. The heat transfer coefficient for natural and forced convection are defined differently and depend upon the circumstance of the convection, the geometries involved and the fluid and material properties.

To reduce heat loss through convection the following must occur:

- Reduce the temperature gradient between the mean fluid temperature and the temperature of the surface over which the fluid is passing.
- Reduce the surface area of material that is exposed to moving fluids.
- Reduce the magnitude of the convection coefficient.

### *Heat Transfer by Radiation*

Heat transfer by radiation occurs due to thermal agitation of atoms and molecules in matter. This movement results in the emission of electromagnetic waves, which transfer energy from the surface of the body of matter. Radiation from a hot body to a cold surrounding is defined by adapting the Stefan-Boltzmann Law which is given in Equation 6:

$$q = \varepsilon\sigma(T_h^4 - T_c^4)A_c$$

**Equation 6: Stefan-Boltzmann law defining heat transfer by radiation.**

Where:

q = heat transfer (W)
$\varepsilon$ = emissivity of the material
$\sigma$ = Stefan-Boltzmann constant ($W/m^2.K^4$)
T = Absolute Temperature (K)
A = Area of emitting body ($m^2$)

To reduce the rate of heat transfer by radiation to the surroundings the following must occur:

- Use a material with low emissivity.
- Reduce the temperature difference between the emitting body and the surroundings.
- Reduce the surface area of the emitting body.

### *The Mechanisms of Heat Loss within an ECMO Circuit*

Fluctuations in temperature during ECMO are likely to occur; however under stable conditions equilibrium between the patient, the system and surrounding environment should be achieved. All of the mechanisms of heat transfer are present, affecting the blood either directly or indirectly. The rate of heat transfer from the patient to the external components of the system is dependent upon the following parameters:

1. Flow rate of the blood through the circuit.
2. Surface area of material that the blood is exposed to.
3. Conductivity of the material that the blood is exposed to.
4. Temperature of the surroundings.
5. External surface area of the system exposed to the surroundings.
6. Emissivity of the material exposed to the surroundings.
7. Conditions in the surroundings (where there are drafts or air conditioning etc.).

The flow rate of the blood supply is set to the required rate for the system and is not a variable for improvement in heat loss. The main factors, which can be influenced in the design of an ECMO system, are the internal and external surface area, volume and properties of the materials used within the system and the conditions within the surrounding environment.

### *Heat Exchanger Design Requirements*

The following is a list of essential requirements for a heat exchanger as part of a miniaturised and integrated ECMO circuit:

- Performance – The system must be able to provide or remove heat at an acceptable rate over a range of potential blood flow rates.

- Haemolysis – The design of the system should be such that haemolysis of blood within the exchanger is kept within clinically acceptable limits.
- Biocompatibility – Platelet activation, adhesion and aggregation, compliment activation and coagulation cascade activation should be minimised.
- Size – To keep priming volume down and to aid in sufficient miniaturisation and integration of the system the size of the device must be kept as small as possible.

## 4.3. Device Performance Requirements

The performance of the heat exchanger is limited by the haemodynamic requirements of the blood. It has been shown that temperatures above $42^0$C can cause haemolysis of the blood components and so this indicates a maximum temperature of the heating elements of the device (Gershfeld and Murayama 1988; Smith and Wagner 2008; Cloherty, Eichenwald et al. 2012). Furthermore thermal shock has also been shown to result in haemolysis of the blood components (Takahashi and J. 1983; Herron, Grabowy et al. 1997). In general clinical practice to avoid haemolysis through thermal shock temperature gradients are limited to a maximum of $12^0$C.

Hypothermia has been suggested as an effective strategy for neuro-protection through lowering the metabolic requirements of the body (Kirkpatrick, Chun et al. 1999; Ichiba, Killer et al. 2003; Guenther, Varelmann et al. 2009). For this reason the ability to effectively cool as well as heat the blood is a performance requirement that the heat exchanger should be capable of.

## 4.4. Chapter Aims

The aims of the work within this chapter are:

- To develop a suitable solid state heat exchange model that meets the requirements of a miniaturised and integrated ECMO system.

- To establish a CFD model that can be used as a tool for design optimization.

- To develop a solid state heat exchanger that can provide sufficient performance at a range of clinically relevant flow rates and that is suitable for use within a live animal experiment.

## 4.5. Solid State Heat Exchanger Development

### 4.4.1. Initial Concept Development

The foundation design for the heat exchanger is based upon concept 3 developed within Chapter 2 – Concept Development. Figure 143 below shows a cross-section of the concept with the heat exchanger geometry highlighted in red.

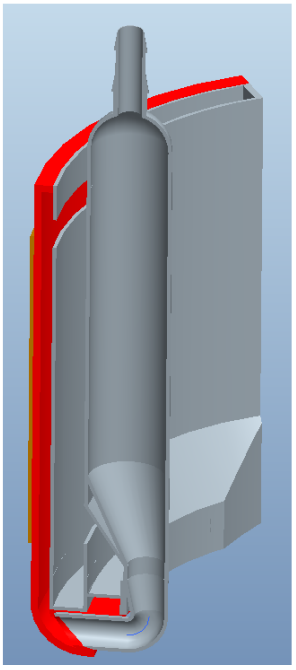

**Figure 143: Concept 3 of Chapter 2 – Concept Development with the heat exchanger highlighted (in red).**

In this design the fluid enters at the base of the heat exchanger from the pump. It then travels up the heat exchanger passing over a thermally conductive surface to which the solid state heat source is attached. Heat is transferred to the blood, which then exits the exchanger to the oxygenator. Figure 144 below shows the basic concept of the heat exchanger design.

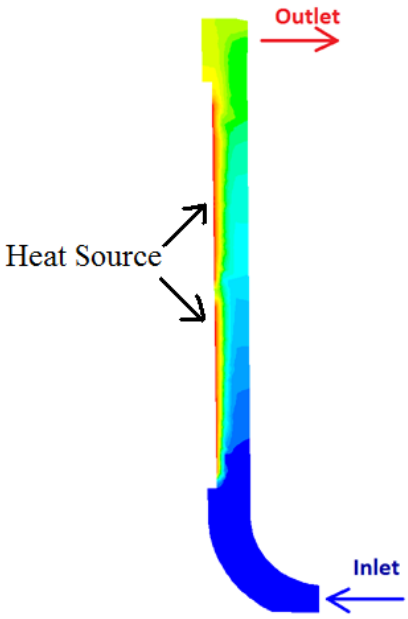


**Figure 144: Diagram of the basic concept behind the heat exchanger design.**

### 4.4.2. Peltier Heater/Coolers

The peltier effect is a thermoelectric phenomenon in which a voltage is applied to a device in order to induce a temperature. The peltier may be made of metals or semi-conductors. When a current is applied to the device, charge carriers try to return to equilibrium by transferring energy from one connector and releasing it at the other. The result is one side of the device becoming hot and the other cool. The direction of heat transfer is controlled by the polarity of the current and hence a peltier device can be used to both heat and cool. A diagram of the peltier effect can be seen within Figure 145 below.

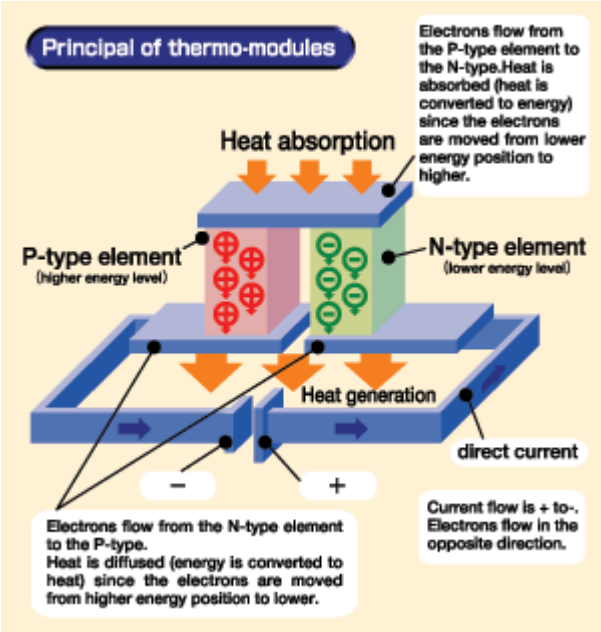


**Figure 145: Diagram showing the peltier effect. (Taken from www.kelk.co.jp)**

Peltiers come in various sizes and offer a range of power outputs depending upon the requirements of the environment they are functioning in. The technology is lightweight, cheap and has relatively low power requirements. Figure 146 below shows a typical peltier element.

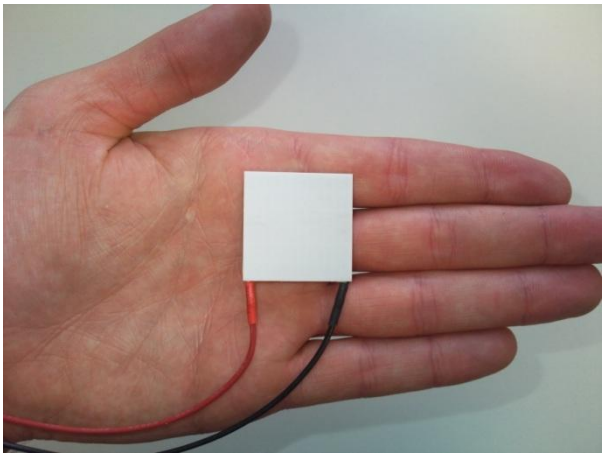

**Figure 146: A typical peltier element.**

## 4.6. Heat Exchanger System Design

To determine the most suitable configuration of the concept 3 geometry two models were initially considered. The first featured a 5 mm fluid gap (Rig A) and the second a 3 mm fluid gap with the additions of fins penetrating the fluid path. These two configurations were selected to determine the overall performance of the design whilst also determining the effect of the fluid gap and fins on performance.

Rig A has a larger fluid gap with no fins. This rig should experience larger diffusion distances but lower fluid velocities and hence higher average exposure time of the bulk fluid to the heating elements. Rig B has a narrower fluid gap and hence should experience higher fluid velocities and lower exposure times; however the fins in the design should help slow the fluid and to create secondary flows to encourage mixing to potentially improve the thermal transfer. Figure 147 below shows a cross-section of each rig side by side for comparison.

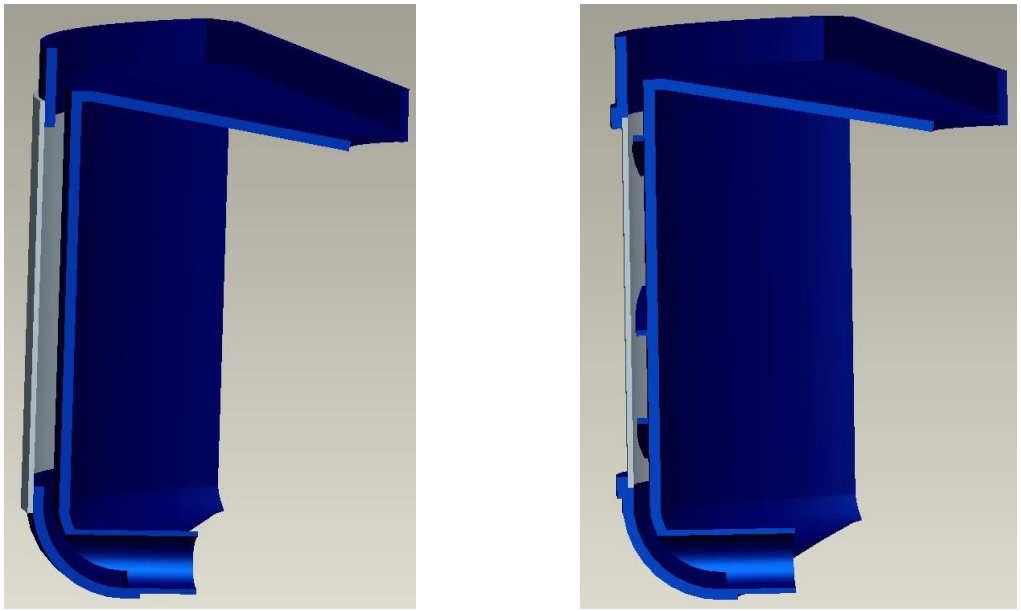

**Figure 147: ProEngineer model comparing the cross-sections of the fluid paths of Rig A and B respectively.**

## 4.7. CFD of the Initial Design

### *Aims*

The aims of this analysis were to investigate the performance of the heat exchanger concept and to determine the most suitable geometry to take forward for further investigation and development.

### *Methods*

Flow paths were developed for each of the rigs and imported into gambit. A mesh analysis was conducted to determine the most suitable mesh. The mesh used was a tetrahedral/hexagonal element hybrid mesh of 5,665,858 nodes (Rig A) and 4,890,678 (RigB). The Gambit mesh of Rig B can be seen within Figure 148 below.

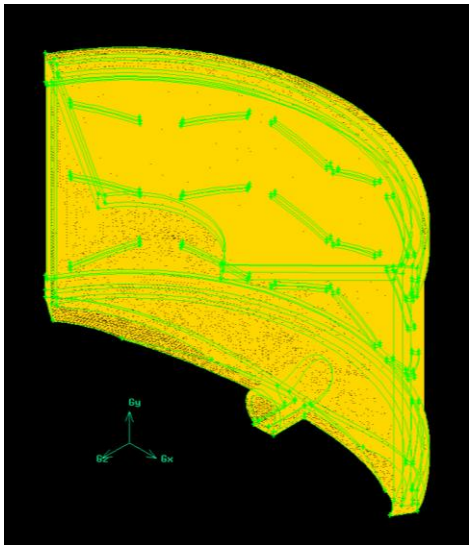

**Figure 148: Gambit tetrahedral/hexagonal hybrid mesh for the geometry of the Rig B Heat Exchanger model.**

CFD analysis was run using Fluent Inc., Fluent version 6.3.26. Boundary conditions were set as a constant velocity at the domain inlet with the outlet set as constant pressure open to the atmosphere. Steady laminar flow was assumed in all cases with liquid water used as the domain fluid with constant viscosity of 0.001003 (Pa.s), specific heat of 4182 (J/kg.K), conductivity of 0.6 (W/m.K) and a density of 998.2 ($kg.m^{-3}$).

The model was run with eight peltier elements on the heating wall surface all with a surface temperature of 42 $^0$C, a water inlet temperature of 30 $^0$C and at a flow rate of 100 ml/min. The experiment was repeated at flow rates of 300 and 500 ml/min for each of the rigs.

***Results***

The most suitable performance characteristic of the heat exchanger rigs was determined to be the area-weighted average temperature at the outlet of the heat exchanger device. The results of the analysis are presented as outlet temperature against fluid flow rate for each of the rigs to determine the effect of flow rate on exchanger efficiency and to allow for a direct comparison between the rig designs. Figure 149 below shows the area weighted average outlet temperature versus flow rate for each rig.

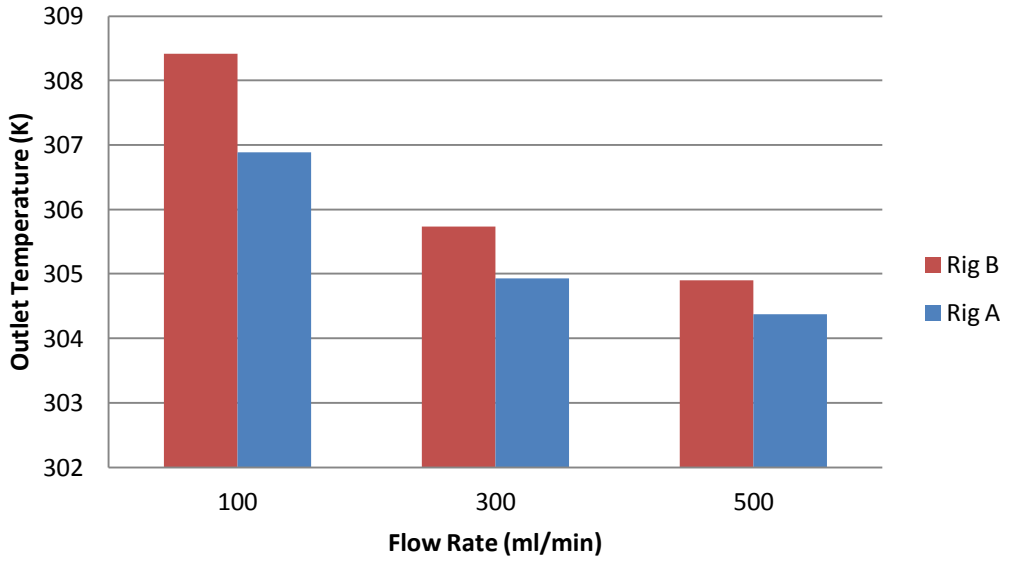


**Figure 149: Graph showing area-weighted outlet temperature versus flow rate for rigs A and B.**

### *Discussion*

In all cases the output temperature decreases with increasing flow rate. As the fluid velocity increases the transit time through the device decreases and hence so does the exposure to the heat elements. To help visualize the effect of flow rate on the temperature distribution, temperature contour diagrams of rig B at flow rates of 100, 300 and 500 ml/min are shown in Figure 150, Figure 151 and Figure 152 respectively.

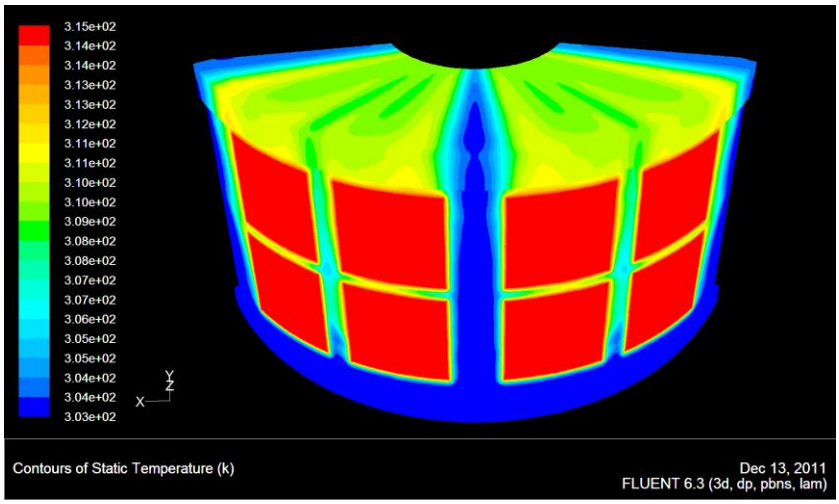


**Figure 150: Temperature contours over Rig B at 100 ml/min.**

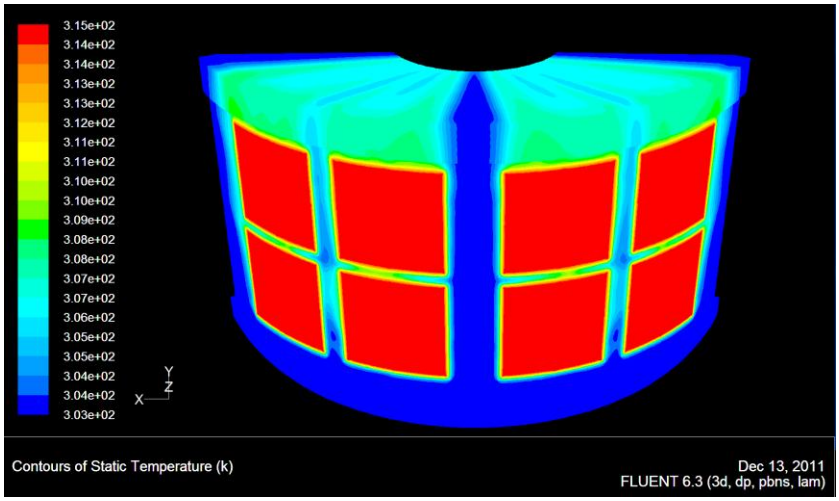


**Figure 151: Temperature contours over Rig B at 300 ml/min.**

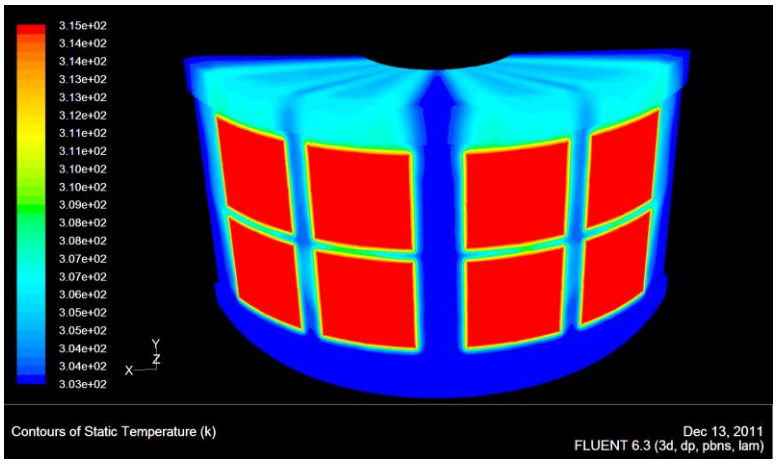


**Figure 152: Temperature contours over Rig B at 500 ml/min**

Determining the distribution of the flow through the device is essential in evaluating the performance and efficiency of the exchangers. Velocity contour diagrams through the middle of rig A and rig B (iso-surfaces y = 0.05) at the highest flow rate of 500 ml/min can be seen within Figure 153 and Figure 154 respectively.

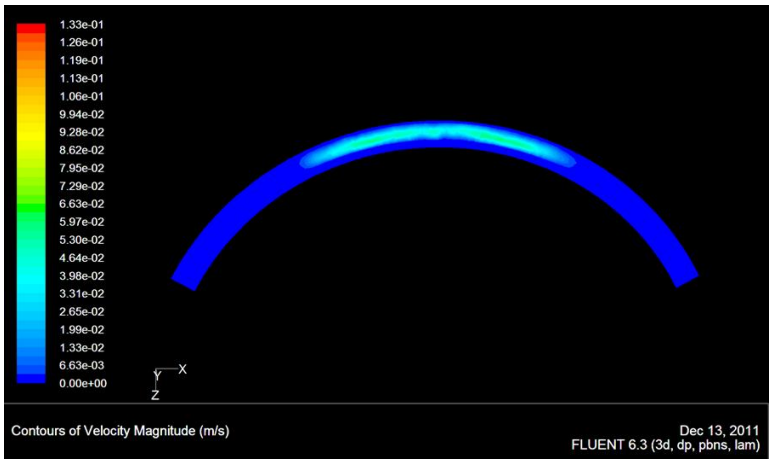


**Figure 153: Velocity contours across the fluid gap of Rig A at 500 ml/min.**

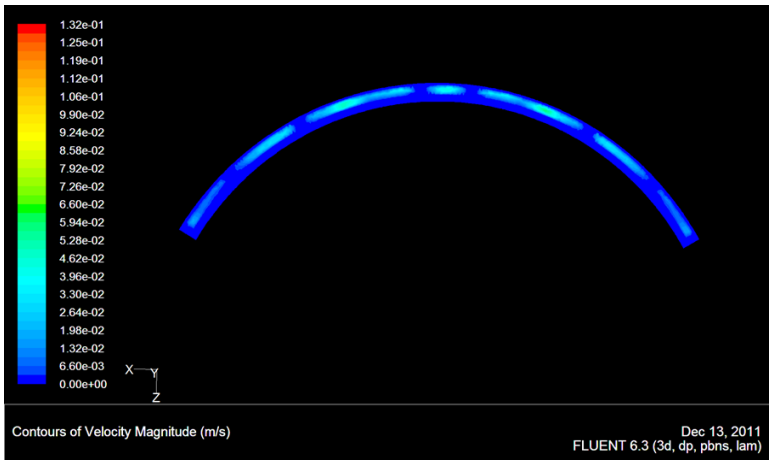


**Figure 154: Velocity contours across the fluid gap of Rig B at 500 ml/min.**

The contour diagrams show that rig A experiences an un-even flow distribution with fast moving flow up the center and slow moving flow at the extremities of the device. Rig B also has an un-even flow field; however the reduced cross-sectional area combined with the presence of the fins on the rear wall has produced an improved flow field compared

to that of rig A. Un-even flow distribution will affect the efficiency of the device. With the configuration of peltier elements used in this design the fastest moving flow is going up the center of the exchanger and is not being exposed to the peltier heat source. The results show that the more evenly distributed flow field of rig B combined with the increased exposure time due to the fins and smaller diffusion distances of the fluid gap result in a more efficient heat exchanger.

### *Conclusion*

This computational simulation has shown that a smaller fluid gap and the presence of fins in the heat exchanger rig results in a more evenly distributed flow path. The even distribution of the flow maximises the potential exposure of the fluid as it passes through the device hence providing a more efficient solution. To validate the computational model used both rigs must be physically prototyped and tested.

## 4.8. Prototype Development

To validate the CFD model and to further investigate the properties of the concept two physical rigs were built based upon the Rig A and Rig B geometries previously discussed. The rigs were 3D modelled and designed to be rapid prototyped by fused deposition modelling. Figure 155 and Figure 156 below show the ProEngineer of the basic model geometry.

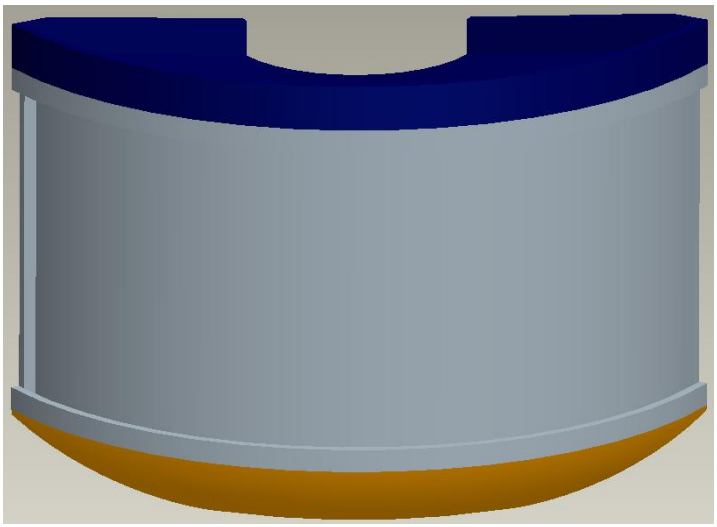

**Figure 155: Front view of ProEngineer Heat Exchanger Rig Model.**

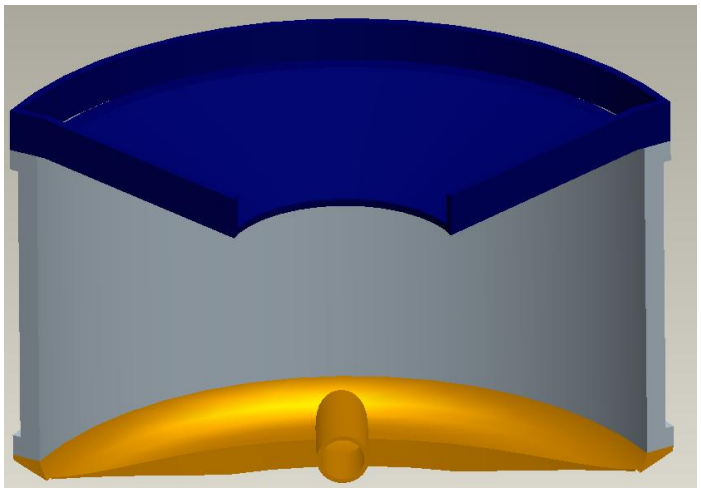

**Figure 156: Rear view of the ProEngineer Heat Exchanger Rig Model.**

In this design a sheet of aluminium was cut and bent to fit the front of the model. For Rig A the sheet was placed over the front lips to produce a 5 mm gap and for Rig B the sheet was placed under the front lips to produce a 3 mm gap at the aluminium interface as highlighted within Figure 157 and Figure 158 respectively.

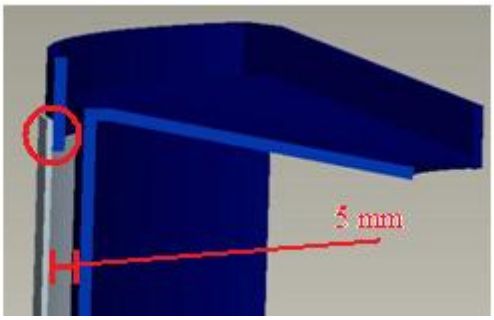


**Figure 157: Model highlighting the positioning of the aluminium sheet in the Rig A prototype.**

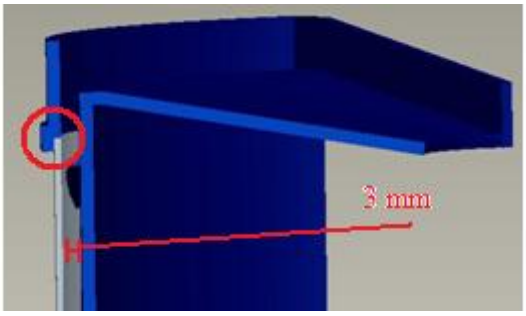


**Figure 158: Model highlighting the positioning of the aluminium sheet in the Rig B prototype.**

The aluminium sheet was bonded to the surface using super glue and a seal was created using Silicon RVT thermal adhesive (Dow Corning Toray co., LTD, Tokyo, Japan). Eight 10 W 30 x 30 mm peltier elements (Greenweld/Permex Ltd, Herts, UK) were bonded to the surface of the aluminium sheet using the same thermal adhesive. K-type thermocouples (RS Components, Northants, UK) were placed under four elements to monitor the array temperature and a TS-67 thermistor was placed under the top right element to provide a feedback signal to the temperature controller used to power the array. Figure 159 below shows the location of the thermocouples and thermistor on the heat exchanger rig.

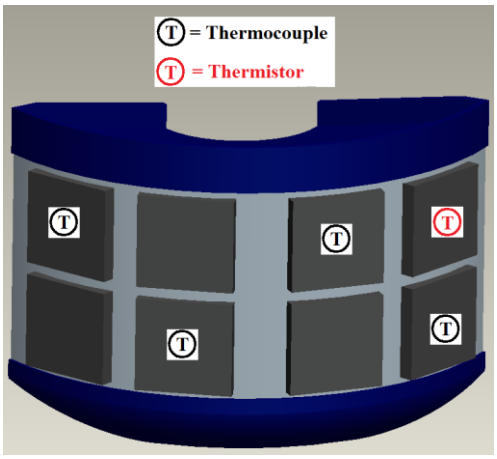


**Figure 159: ProEngineer model showing the location of the thermocouples and thermistor in the peltier array.**

Figure 160 shows the assembled rapid prototype with aluminium sheet, peltiers and thermocouples attached ready for testing within the laboratory.

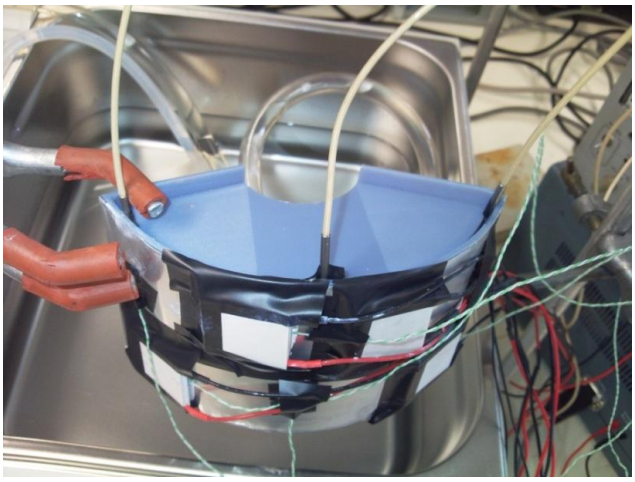

**Figure 160: Picture showing the assembled rig B prototype ready for use in the laboratory.**

Rig A has a priming volume 75.51 ml of and the blood is exposed to a surface area of 36,684 $mm^2$.

Rig B has a priming volume of 51.81 ml and the blood is exposed to a surface area of 35,752 $mm^2$.

## 4.9. Solid State Heat Exchanger Testing

### 4.9.1. Aims

The aims of the following work were to determine the performance characteristics of two experimental heat exchanger rigs, to use the results to validate the CFD model previously created and to determine the most suitable configuration to be used in further testing.

### 4.9.2. Materials and Method

The principle components used to determine the performance characteristics of each rig are shown within Figure 161.

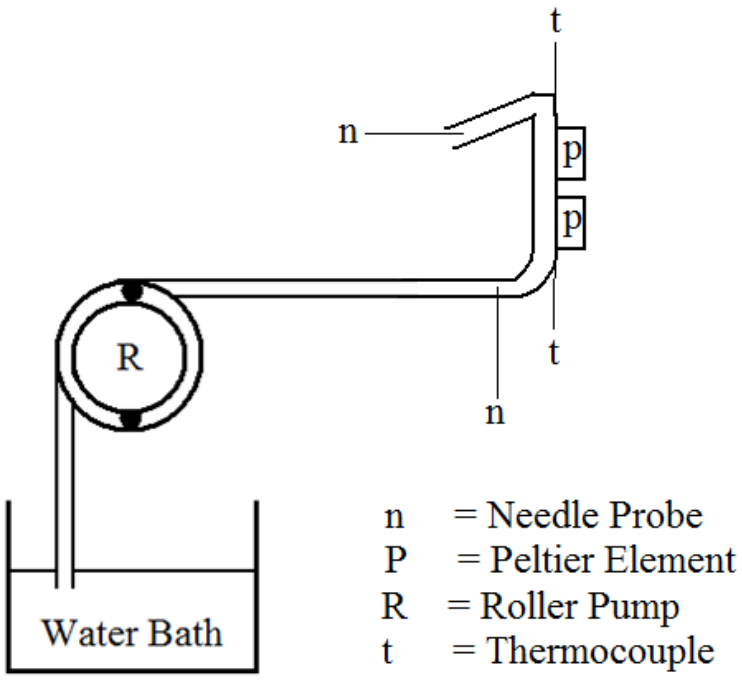


**Figure 161: Diagram of the initial peltier heat exchanger rig physical testing configuration.**

The inlet water reservoir was maintained at 24 $^{0}$C using a water bath (Fisher Scientific, Leicestershire, UK). Flow was achieved using a multiflow roller pump (Stökert, Munich, Germany). Water was pumped from the reservoir through the device and exited from the outlet spout to a basin. The experiment was conducted at flow rates of 100 and 300 ml/min. The entire experiment was repeated three times.

Temperature measurements were taken at the inlet to and at the outlet from the reservoir using MT-29/1 T type hypodermic needle microprobes (Physitemp Instruments Inc., Clifton, NJ, USA) and from the peltier array using the previously placed thermocouples. Measurements were recorded at a rate of 1 per second for 500 seconds using a TC-08 USB data logger (Pico Technology, Cambridgeshire, UK).

Control values were taken for the system at 100 and 300 ml/min with the peltier array unpowered. The peltier array temperature was then adjusted in 1 $^{0}$C increments through a range of 26 – 42 $^{0}$C with the array temperature controlled by a TC-36-25 RS232 temperature controller (TE Technology, Michigan, USA).

Figure 162 below shows the experimental configuration with the main elements of the experiment numbered and labeled.

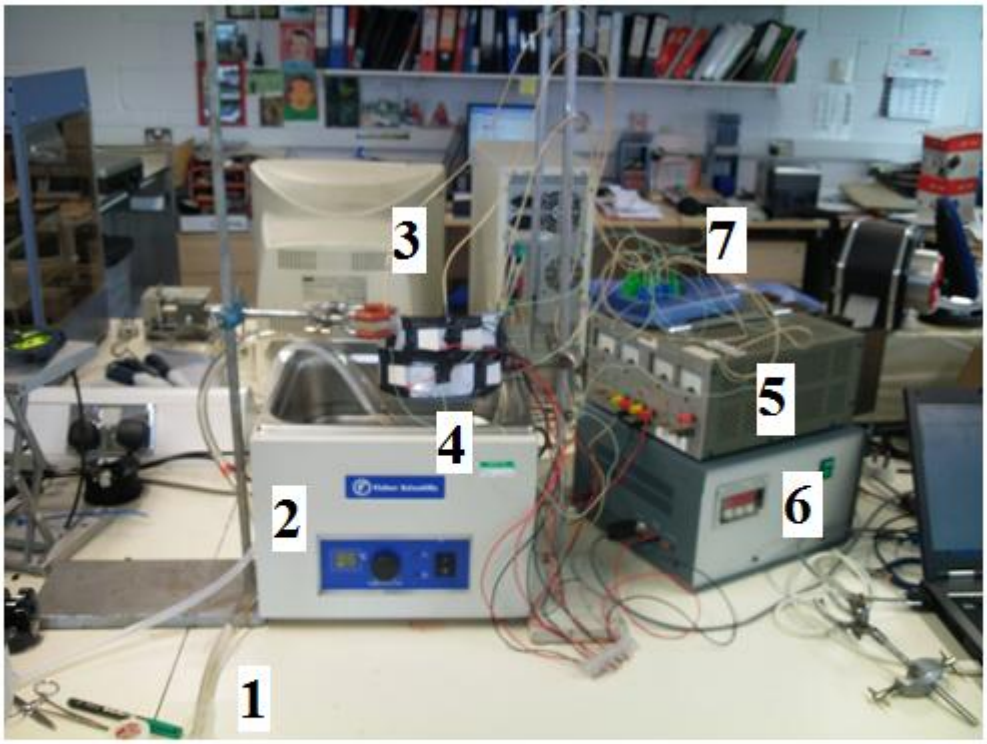


**Figure 162: Experimental set-up used in the initial rig testing with the main elements numbered and labeled.**

### 4.9.3. Results

To determine the effect of the peltier array temperature on performance the results are presented in terms of the water inlet, outlet and control water outlet temperatures against peltier temperature. The effect of flow rate on performance is also established by showing results for the system at 100 and 300 ml/min. Figure 163, Figure 164, Figure 165 and Figure 166 show the control water outlet, water outlet and water inlet temperatures against peltier array temperature for rig A at 100 and 300 (ml/min) and rig B at 100 and 300 (ml/min) respectively.

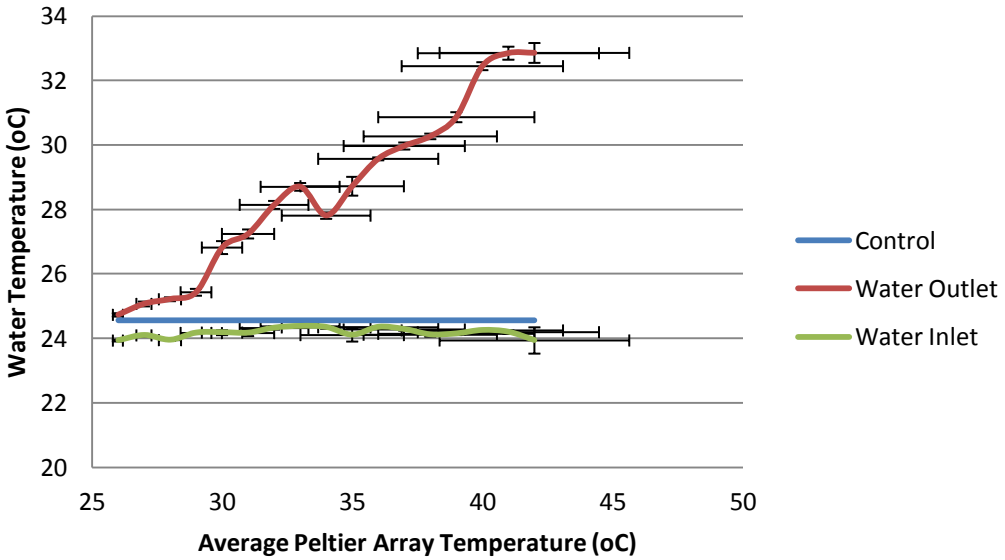


**Figure 163: Water inlet and outlet and control outlet temperature versus peltier array average temperature for heat exchanger rig A at a water flow rate of 100 ml/min. ± 1 Standard Deviation.**

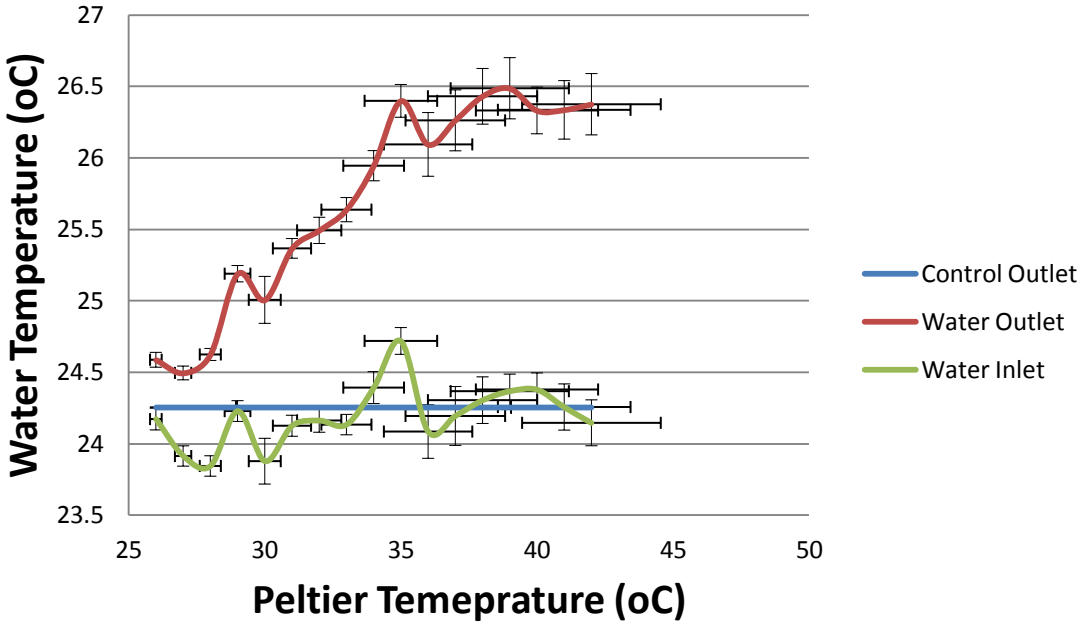


**Figure 164: Water inlet and outlet and control outlet temperature versus peltier array average temperature for heat exchanger rig A at a water flow rate of 300 ml/min. ± 1 Standard Deviation.**

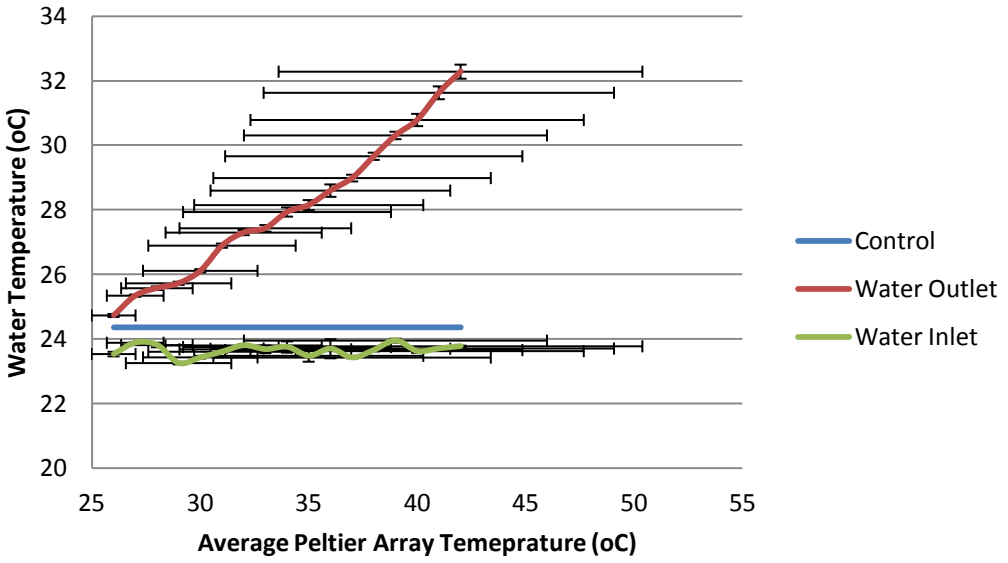


**Figure 165: Water inlet and outlet and control outlet temperature versus peltier array average temperature for heat exchanger rig B at a water flow rate of 100 ml/min. ± 1 Standard Deviation.**

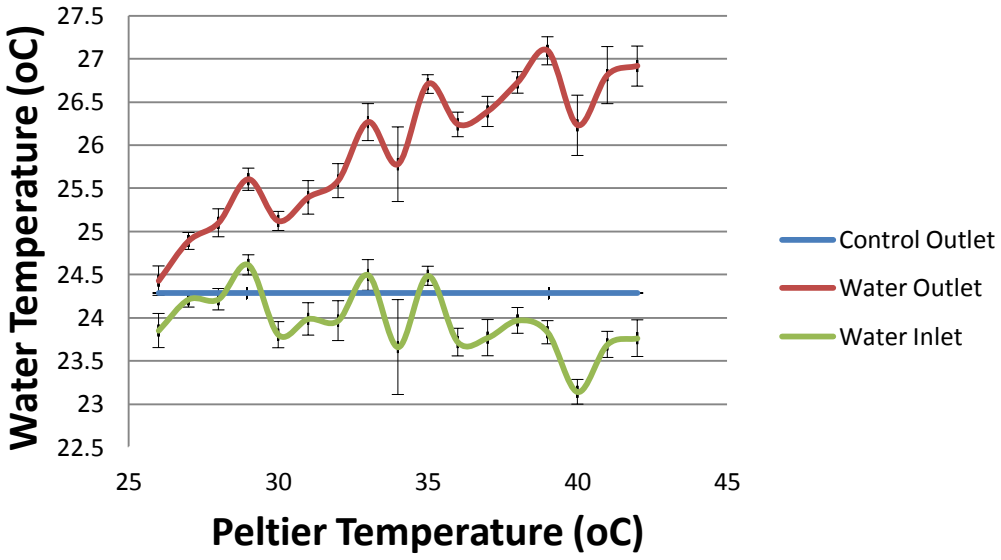


**Figure 166: Water inlet and outlet and control outlet temperature versus peltier array average temperature for heat exchanger rig B at a water flow rate of 300 ml/min. ± 1 Standard Deviation.**

### 4.9.4. Discussion

The results show that both rigs are able to successfully provide positive heat transfer to fluid. The amount of heat addition falls considerably as the flow rate increases most likely due to the reduce exposure time of the fluid to the heating elements. Both rigs could not be tested at 500 ml/min as the maximum power output of the peltier elements was reached before the peltier elements could heat through the desired range.

Figure 167 and Figure 168 below compare the results of each rig at 100 ml/min and 300 ml/min respectively.

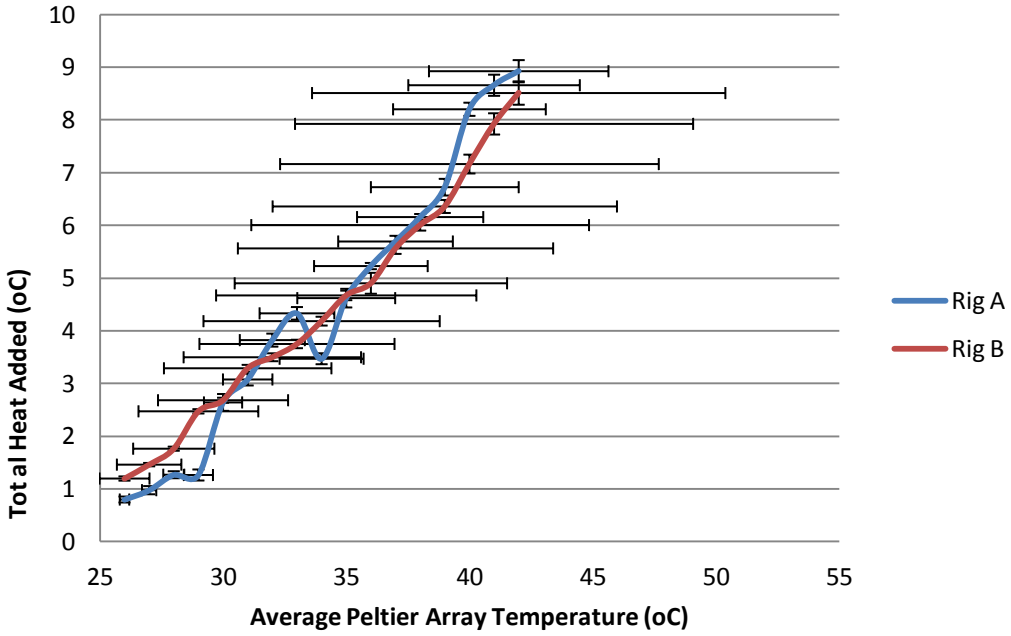


**Figure 167: Total heat added vs. Average pletier Array Temperature for Rig A and B at 100 ml/min. ± 1 Standard Deviation.**

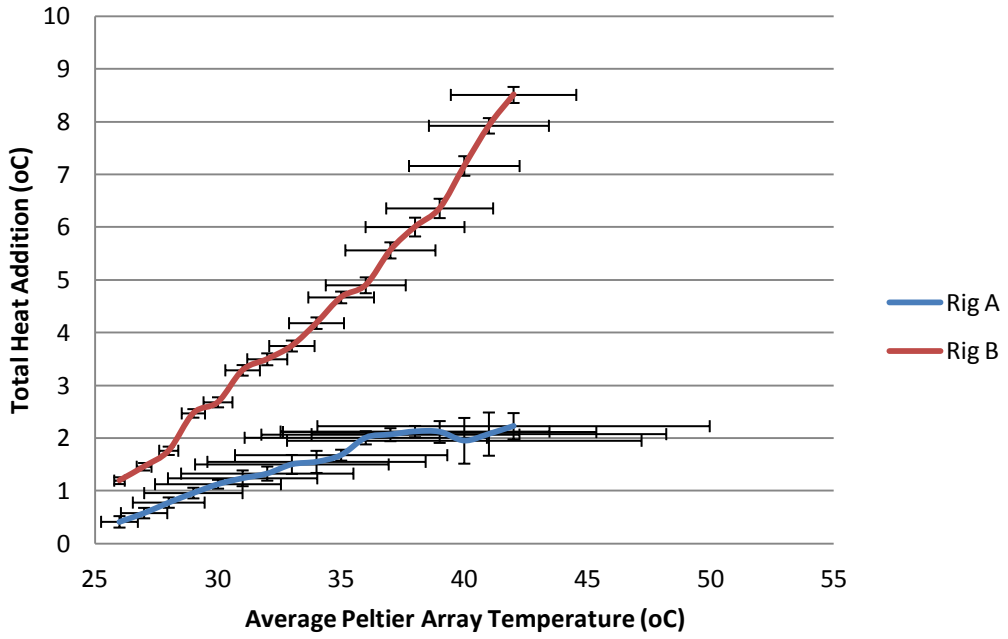


**Figure 168: Total heat added vs. Average peltier Array Temperature for Rig A and B at 300 ml/min. ± 1 Standard Deviation.**

At the lower flow rate both of the systems perform similarly; however at 300 ml/min Rig B achieves approximately 50 % higher output than Rig A. Compared to Rig B, Rig A has a larger cross-sectional area through which the fluid is flowing and so fluid velocity will be less, increasing the duration of the fluid within the exchanger; however the improvement in performance of Rig B can be attributed to reduced diffusion distances within the fluid path and from the finned surface, which should act to restrict the flow and to produce secondary flow that encourages mixing and hence improved heat transfer throughout the fluid volume. In general the quality of performance from both rigs was less than that predicted by the CFD analysis previously conducted. The poor performance can be attributed to the following:

- Un-even temperature distribution between the peltier elements.

The temperature measurements taken throughout the experiment show an uneven temperature distribution though the peltier array. The maximum temperature difference

between peltiers was 21.29 $^0$C at 100 ml/min and 19.08 $^0$C at 300 ml/min for Rig A and 18.86 $^0$C at 100 ml/min and 16.02 $^0$C at 300 ml/min for Rig B. The temperature measurements indicate that the bottom row of the peltier elements experience the highest loading. The loading on the outer elements was also less than that of the inner elements. The extreme change in cross-sectional area at the inlet of the design is encouraging an uneven velocity distribution with faster moving flow up the center of the device. As a result the inner elements are exposed to higher fluid velocities and therefore higher loading.

As the fluid moves through the exchanger it initially encounters the lower row of elements. The fluid is heated by these elements and so is partially heated prior to exposure to second row of elements. The reduced temperature gradient between the fluid and the peltiers results in a lower loading. The uneven loading of the peltier elements has resulted in an uneven distribution of temperature throughout the device. The peltier elements were not powerful and the recorded temperatures reflected the peltier location. The peltiers on the inside of the first row producing temperatures considerably lower than the control set temperature and the peltiers on the outside of the upper row producing considerably higher temperatures. This temperature distribution will affect the efficiency and performance of the heat exchanger and temperatures higher than 42 $^0$C may lead to spot heating of the blood and potential haemolysis. At maximum power output the array provided 80 W total; this was clearly insufficient.

- Poor thermal contact between the elements and the aluminium wall.

The peltier elements were 30 mm by 30 mm squares, which did not sit flush with the curved aluminium wall of the exchanger. Thermally conductive adhesive was used to bond the peltiers to the wall and to fill the air gaps at the sides; however this process was particularly difficult, especially with the elements that had thermocouples placed between them and the heat exchange wall.

- Bowing of the rapid prototype plastic

The material used to rapid prototype the rigs was FullCure 720 polypropylene-like polymer (Objet Inc., Massachusetts, USA). This material has a heat deflection temperature of 40-45 $^{0}$C at a pressure of 0.45 mPa. In several cases, due to the uneven temperature distribution, the temperature and pressure that the polymer was subjected to were higher than the HDT and therefore deformation occurred as shown within Figure 169 and Figure 170 below.

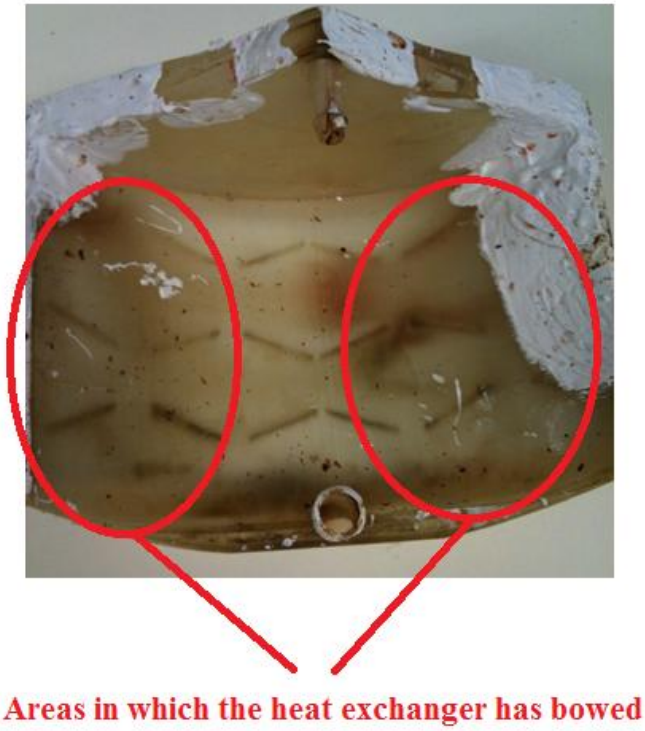


**Figure 169: Top view of a heat exchanger rig that has bowed under pressure and temperature.**


**Figure 170: Top view of a heat exchanger rig that has bowed under pressure and temperature.**

To further investigate the system and to verify the CFD previously used to model the system an analysis was conducted using values from the physical experiment as boundary conditions of the computational analysis.

## *CFD analysis of Heat Exchanger Rig Experiment*

### *Aims*

The aims of this experiment were to validate the process used to simulate the heat exchange system by using values obtained from the physical experiment. The analysis should allow for comparison between the physical and computational systems and

validation of the CFD model. The model will then be used to further investigate the results of the physical experiment and as a tool for optimization in future designs.

## *Methods*

The same method used in the initial CFD analysis was applied. The boundary conditions were modified in the following way in order to replicate the experimental configuration:

- Water flow rate, inlet temperature and peltier element temperatures from the experiment were used in each analysis.

- The thermal conductivity of the aluminium plate was reduced to 1 W/m.K to replicate the poor thermal contact between the peltiers and the aluminium sheet.

- The outer surfaces of the rigs were given a surface heat flux to model the cooling effect of air by natural convection.

The model was run at average peltier element array temperature of 26, 30, 34, 38 and 42 $^{0}$C at 100 and 300 ml/min for each rig.

## *Results*

To allow for a direct comparison between the experimental and computational systems the results were displayed in terms of the total heat addition across the heat exchanger (water outlet minus water inlet temperature) versus the average peltier array temperature.

Figure 171, Figure 172, Figure 173 and Figure 174 below show graphs comparing the average experimental and CFD results for total heat addition between inlet and outlet vs. average peltier array temperature for Rig A and B at 100 and 300 ml/min respectively.

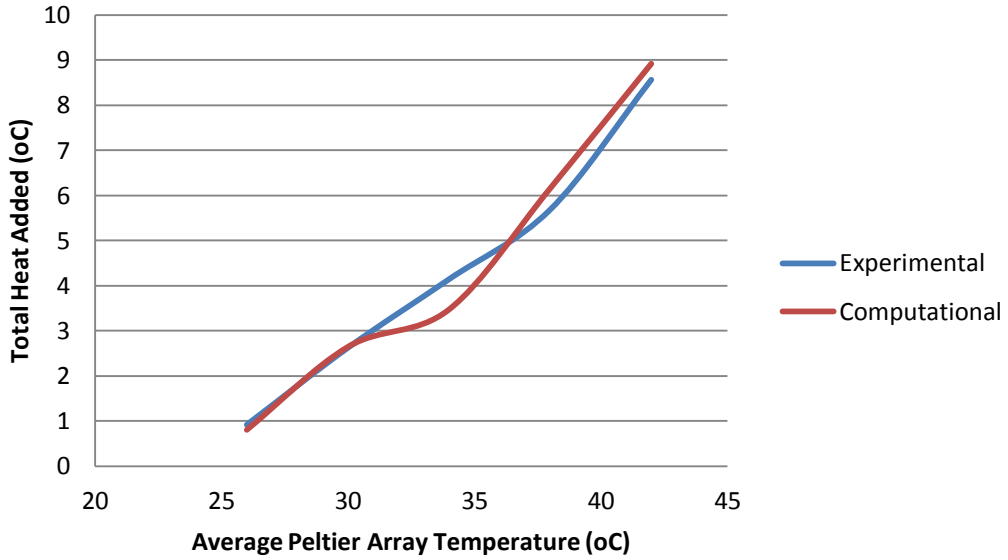


**Figure 171: Graph showing total heat addition vs. average peltier array temperature for Rig A at 100 ml/min.**

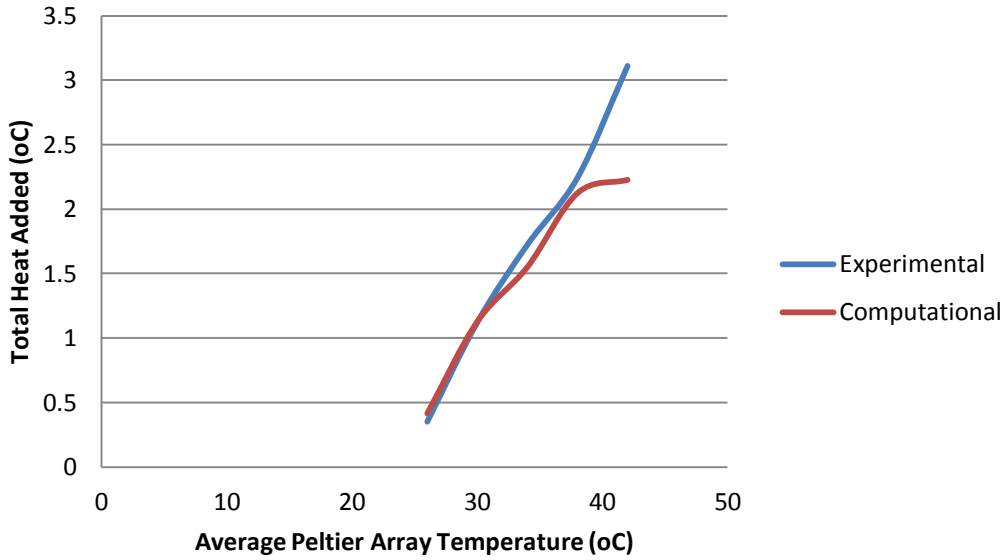


**Figure 172: Graph showing total heat addition vs. average peltier array temperature for Rig A at 300 ml/min.**

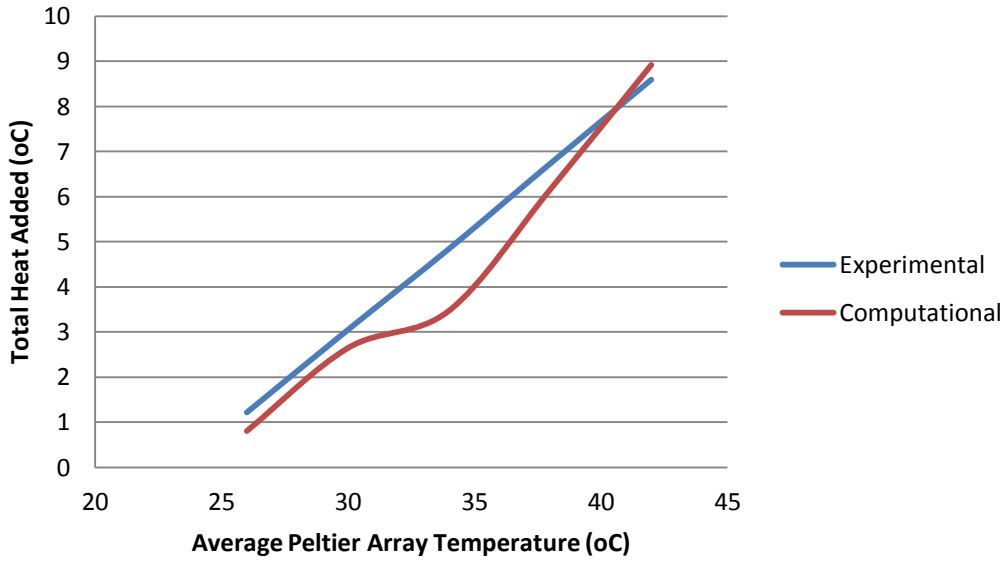


**Figure 173 Graph showing total heat addition vs. average peltier array temperature for Rig B at 100 ml/min.**

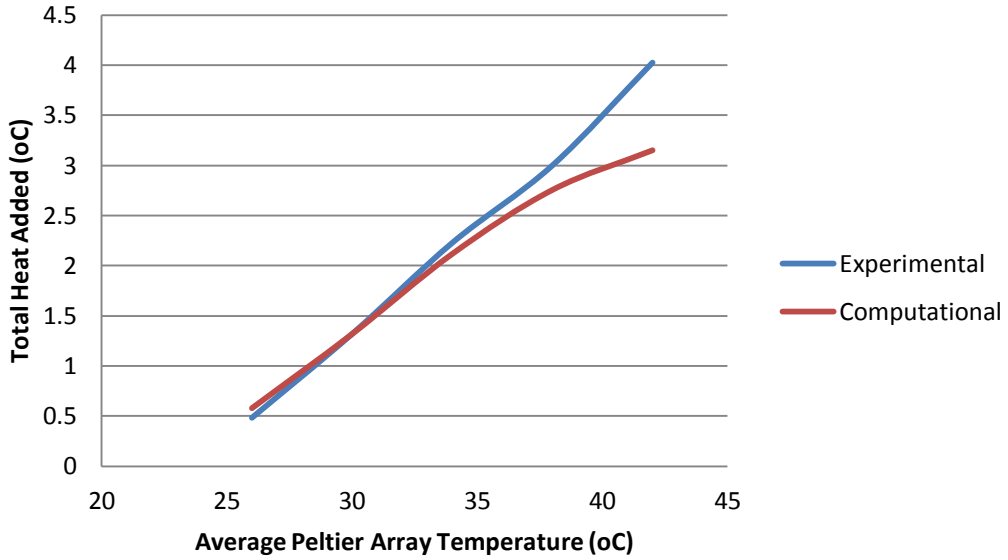


**Figure 174: Graph showing total heat addition vs. average peltier array temperature for Rig B at 300 ml/min.**

### *Discussion and Conclusions*

The results show that with the modified boundary conditions the CFD analysis provides an accurate representation of the physical system. The model can now be used to provide both qualitative and quantitative input into the design process allowing iterations of the design to be evaluated on the computer rather than being physically prototyped and tested, which should potentially result in reduce time and cost.

The magnitude of reduction in the conductivity of the aluminium plate required to model the imperfect thermal connection between the peltiers and the exchanger highlights the severity of the problem. This poor conduction results in a significant reduction in the efficiency of the exchanger. To highlight the effect of the thermal connection between the peltier elements and the aluminium conduction plate Figure 175 and Figure 176 show contours of temperature for an imperfect and perfect thermal connection respectively.

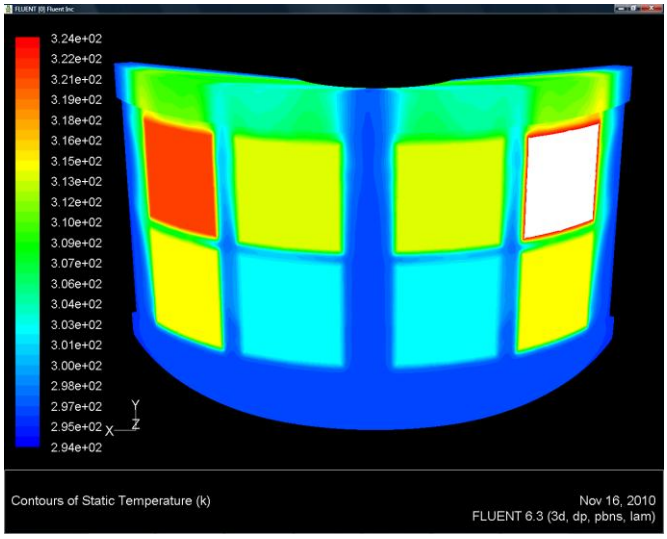


**Figure 175: Contours of temperature for imperfect thermal connections of Rig B at 100 ml/min.**

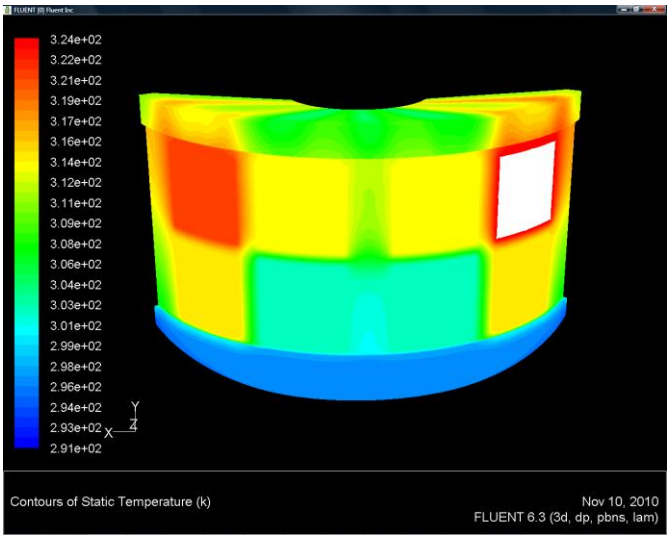


**Figure 176: Contours of temperature for perfect thermal connections of Rig B at 100 ml/min.**

The analysis shows that an area weighted average water outlet temperature of 37 $^{0}$C would be achieved with a perfect thermal connection compared to the 32.29 $^{0}$C achieved by the actual experimental set-up.

The figures above highlight the uneven temperature distribution that was observed in the experiment previously described.

### 4.9.5. Conclusions

The experimentation conducted has successfully validated the computer model used to simulate the system. This model can therefore be used to optimize the design process and potentially reduce the cost and time associated with iterative physical prototyping. The results have shown that the smaller blood gap and the presence of fins within the flow field of Rig B has improved efficiency, performance, priming volume and the surface area that the blood is exposed to; however in general the results suggest that this design is not practical and will be incapable of satisfying the requirements of a miniaturized and integrated ECMO system for use in an animal model.

The computational model has allowed for a more detailed investigation of the heat exchanger units and the results have highlighted several problems with the design that have ultimately hindered performance. Re-design of the rig is necessary with design requirements focused on satisfying the following:

- Improved thermal contact between the peltier array and the heat exchange surface.

The curved nature of the heat exchanger made establishing effective thermal contact very difficult. This poor contact significantly impacted the performance of the heat exchanger.

- Improved velocity distribution throughout the module.

The dramatic change in cross-section from the pump outlet to the curve at the base of the heat exchanger resulted in a non-uniform velocity distribution, which lead to non-uniform loading of the peltier array and hence an un-even temperature distribution throughout the exchanger.

- Improved temperature distribution of the peltier array.

The peltier elements used could not cope with the loading applied. Powering the elements as an array resulted in each element pulling current related to the thermal load and hence elements with the highest loading were significantly under the set-temperature value and those with the lowest loading were significantly higher than the set-temperature value.

- Improved material properties.

The HDT of the polymer used to rapid prototype each rig was inappropriate for the requirements of the experiment. A material with more appropriate properties is required.

## 4.10. Heat Exchanger Re-Design

The foundation design for the heat exchanger was based upon the miniaturized and integrated system concept 3 developed in Chapter 2 – Concept Development. The design requirements of this concept focused upon maximizing miniaturization and integration of the system components. The aim of using this concept as a foundation for each of the components was to make the final integration a much simpler task and to ensure that the design was dedicated to achieving the fundamental requirements defined at the start of the project; however investigation of the design has revealed that the geometry hinders the potential performance and complicates the manufacturing process.

To achieve suitable performance redesign must focus on addressing the problems previously raised. To do this effectively compromise of the initial concept is required. The implications of this are that the integration of the final components may be more complicated resulting in the need for further component redesign; however at this stage of the project his is considered to be an acceptable compromise.

## 4.11. Mark II Heat Exchanger Concept Development

In the previous design the curved geometry created many of the problems encountered. The redesigned concept was based upon a solid state version of a traditional shell and

tube heat exchanger. Figure 177 below shows the initial ProEngineer model of the system.

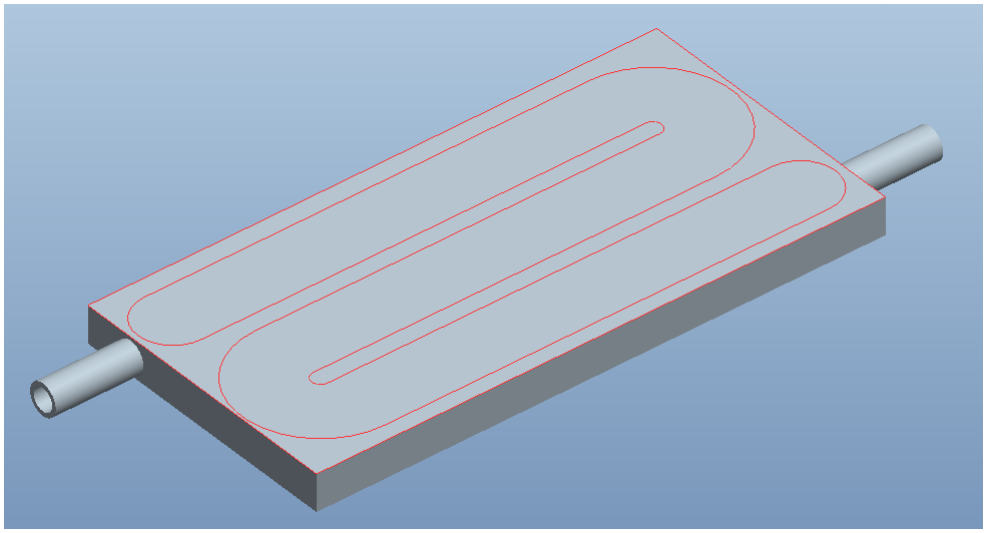

**Figure 177: ProEngineer model indicating the general configuration of the Mark II heat exchanger.**

In this design blood enters the module and moves through the device along the channel. The Peltier elements will be placed upon the top of the device and heat the blood as it passes through. This design addresses each of the problems of the Mark I design in the following ways:

1. The curved geometry has been eliminated.

The curve of the initial design made it difficult to establish an efficient thermal connection between the peltier elements and the exchanger surface. The dramatic change in cross-section from the circular outlet of the pump to the wide arc at the base of the exchanger also resulted in a non-uniform velocity distribution, which exaggerated the un-even loading of the peltier array and resulted in a non-uniform temperature distribution. In this design the peltiers can sit flat on the surface, which should make mounting considerably easier and allow for greater quality control during the assembly process.

2. Improved material properties.

The design is very simple and should therefore allow it to be machined from steel or aluminium. This will remove the limitations set by the previous polymer but may introduce some insulation issues.

3. Improved thermal distribution.

Although the design will reduce the loading on the peltier elements the temperature distribution problem has been addressed by changing the eight peltier array to two 270 W, 62 x 62 mm peltier array. These peltier elements can provide 460 W higher power output and should therefore be able to handle the loads that they will be subjected to. A new control system was also constructed that allows each of the elements to be powered and controlled individually rather than in an array. Thermocouples below each peltier element provide a feedback signal, which is compared to the programmed set temperature. The system then provides each element with adequate power to allow it to meet the set temperature. Figure 178 below shows a screen shot of the programs user interface.

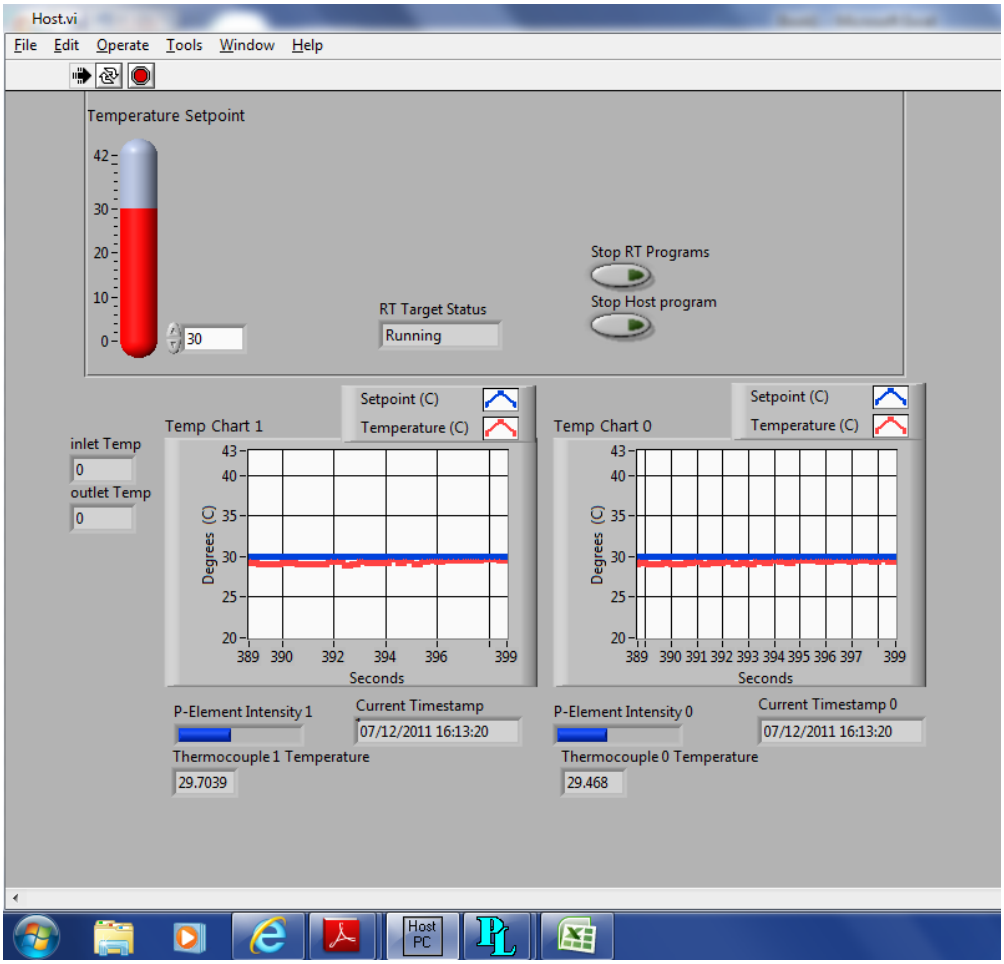


**Figure 178: Temperature control program user interface.**

The design has a priming volume of 25.24 ml and blood is exposed to a total surface area of 22154 $mm^2$.

## 4.12. CFD of the Mark II Design

### *Aims*

The aims of this analysis are to investigate the performance of the Mark II heat exchanger design and to highlight any potential problems that need to be addressed prior to prototyping.

### *Methods*

The ProEngineer model used to develop the initial Mark II concept was adapted to make the CFD model. It was imported into gambit and a mesh analysis was conducted. The most suitable mesh was found to be a tetrahedral/hexagonal element hybrid mesh of 1,880,120 nodes. The Gambit model and mesh can be seen within Figure 179 below.

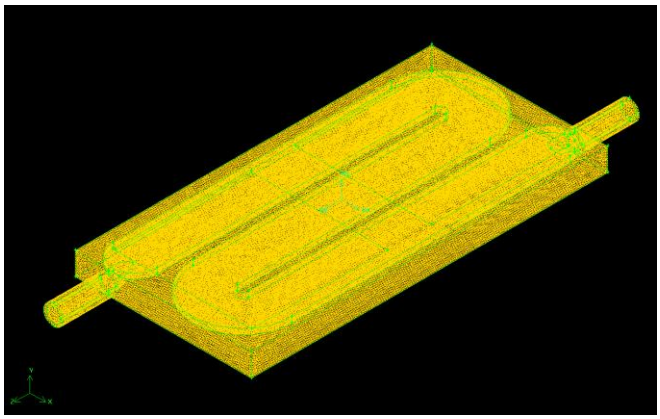

**Figure 179: Gambit mesh of Mark II Heat Exchanger model.**

The CFD analysis was run using the same conditions as used in the previous analysis.

The model was run with both peltier elements at a surface temperature of 42 $^{0}$C, with a water inlet temperature of 30 $^{0}$C and at a flow rate of 100, 300 and 500 ml/min.

### *Results*

To allow a direct comparison with the results of the initial CFD analysis run for the Mark I heat exchanger the results have been displayed in terms of outlet temperature against flow rate through the device.

Figure 180 below compares the area weighted average outlet temperature for the Mark I and Mark II heat exchangers.

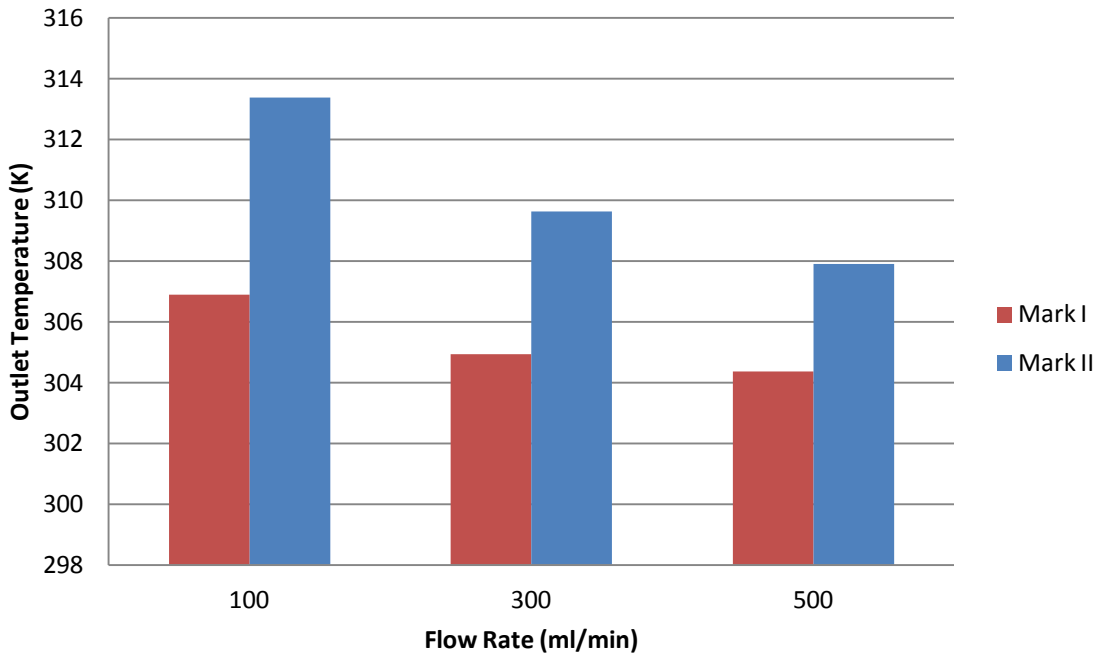


**Figure 180: Graph showing area-weighted outlet temperature versus flow rate for the Mark I and Mark II heat exchangers.**

### *Discussion*

The Mark II system shows a significant improvement in area weighted average outlet temperature over the Mark I system. In this system the fluid has a uniform fluid path and the aluminium is acting as a heat sink to the peltier elements and as a heat source to the fluid flow. The result is a flow path that is heated at all exposed surfaces. To highlight the temperature, velocity and area-weighted average wall shear stress distribution through the device contour diagrams are shown within Figure 181, Figure 182, Figure 183 and Figure 184.

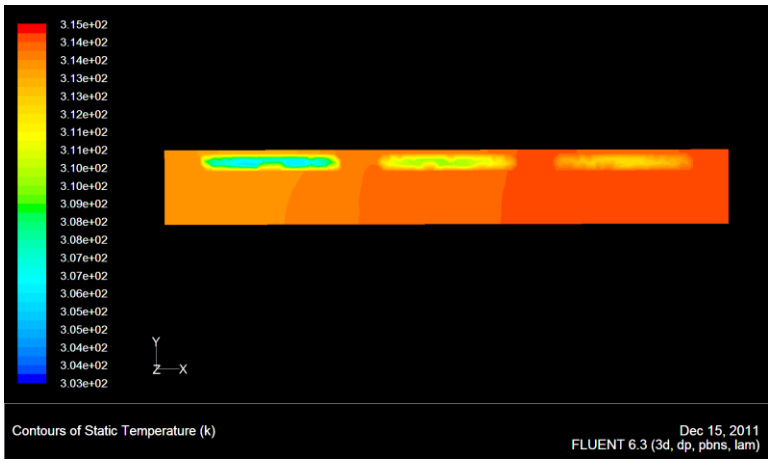


**Figure 181: Temperature contours across an iso-surface in the x axis for Mark II at 100 ml/min.**

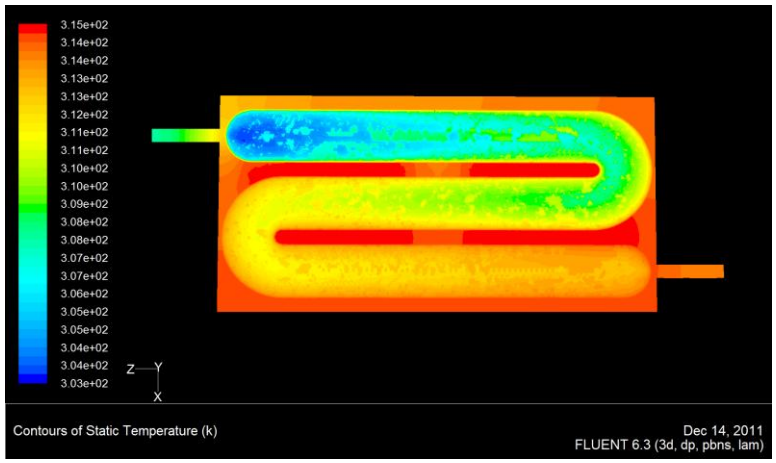


**Figure 182: Temperature contours across an iso-surface in the y axis for Mark II at 100 ml/min.**

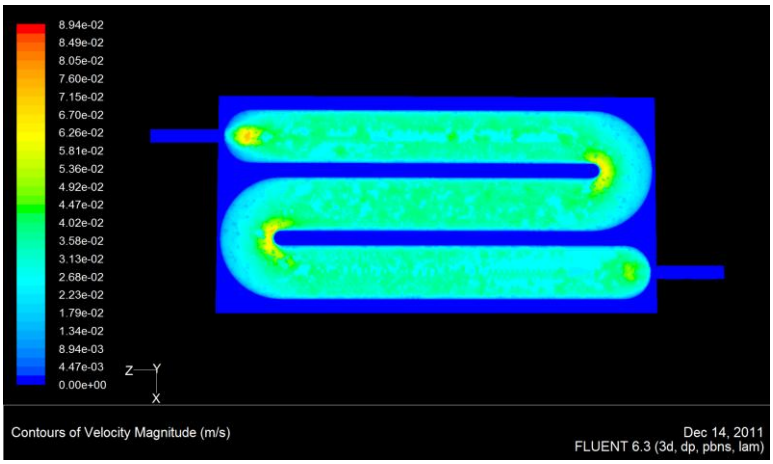


**Figure 183: Velocity contours across an iso-surface in the y axis for Mark II at 100 ml/min.**

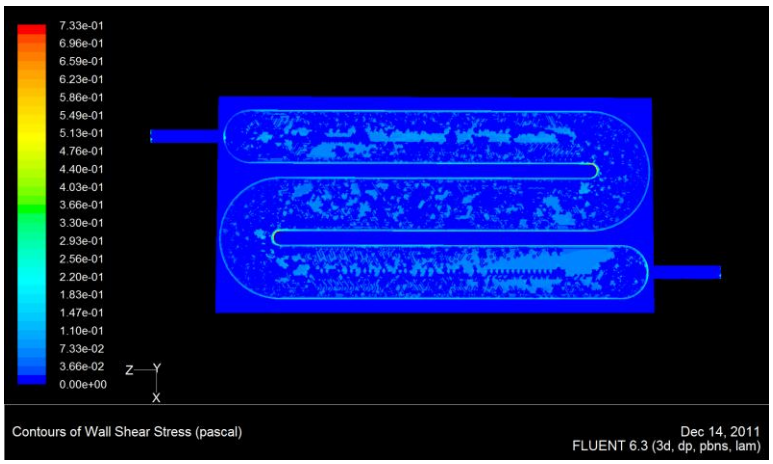


**Figure 184: Wall Shear stress contours across an iso-surface in the y axis for Mark II at 100 ml/min.**

These results show highly efficient heat exchange, uniformly distributed velocity and minimal shear stress.

## *Conclusions*

Using the validated CFD modelling approach previously developed the analysis on the Mark II redesigned heat exchanger has successfully shown that the performance characteristics observed are far superior to the previous design. The flow field is

uniform, the gradual curves of the channels do not induce excessive shear and the aluminium of the model acts to heat the entire fluid path. This model can therefore be used to justify physical prototyping of this configuration to allow for further validation of the CFD model and investigation of the design.

## 4.13. Mark II Prototype Development

The design was cut in once piece from aluminium as shown within Figure 185 below.

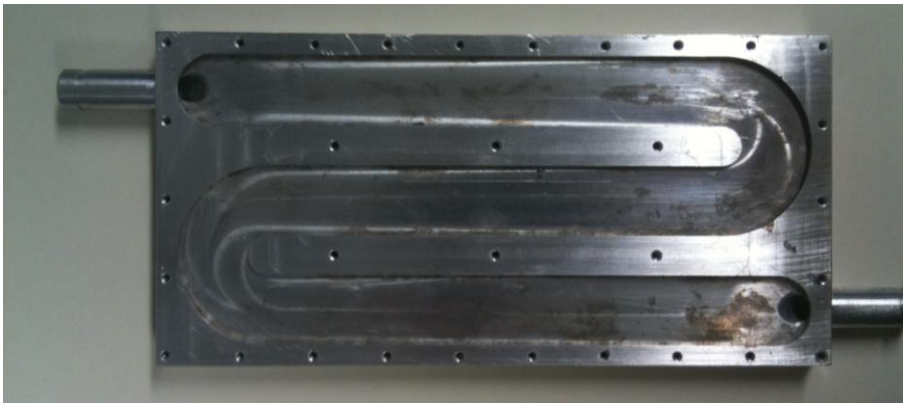

**Figure 185: Mark II Heat exchanger cut in aluminium.**

The conducting plate was cut to size from 0.5 mm thick aluminium sheet. Twenty two screws were used to fix the sheet to the exchanger base with gasket seal (Halfords, UK) used to seal the device. The two peltier elements were bonded to the surface of the device using thermally conductive adhesive (Dow Corning Toray co., LTD, Tokyo, Japan) with two K-type thermocouples (RS Components, Northants, UK) bonded in place beneath. Figure 186 below shows the completely assembled prototype ready for use within the laboratory.

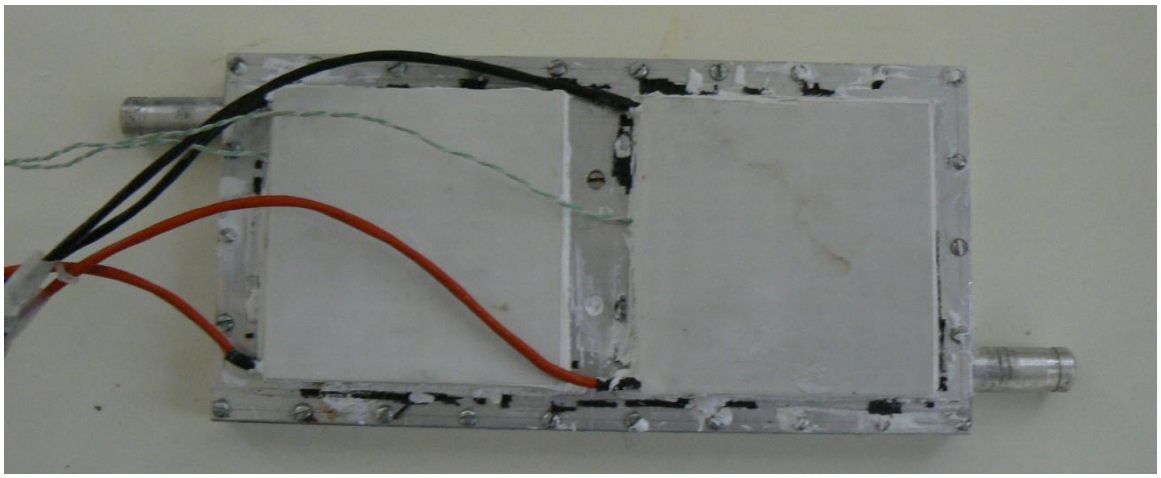

**Figure 186: Assembled Mark II prototype ready for use within the laboratory.**

## 4.14. Mark II Heat Exchanger Testing

### 4.14.1. Aims

The aim of this experiment was to determine the performance characteristics of the Mark II heat exchanger.

### 4.14.2. Methods and Materials

The principle components used to determine the performance characteristics of the Mark II exchanger are shown within Figure 187.

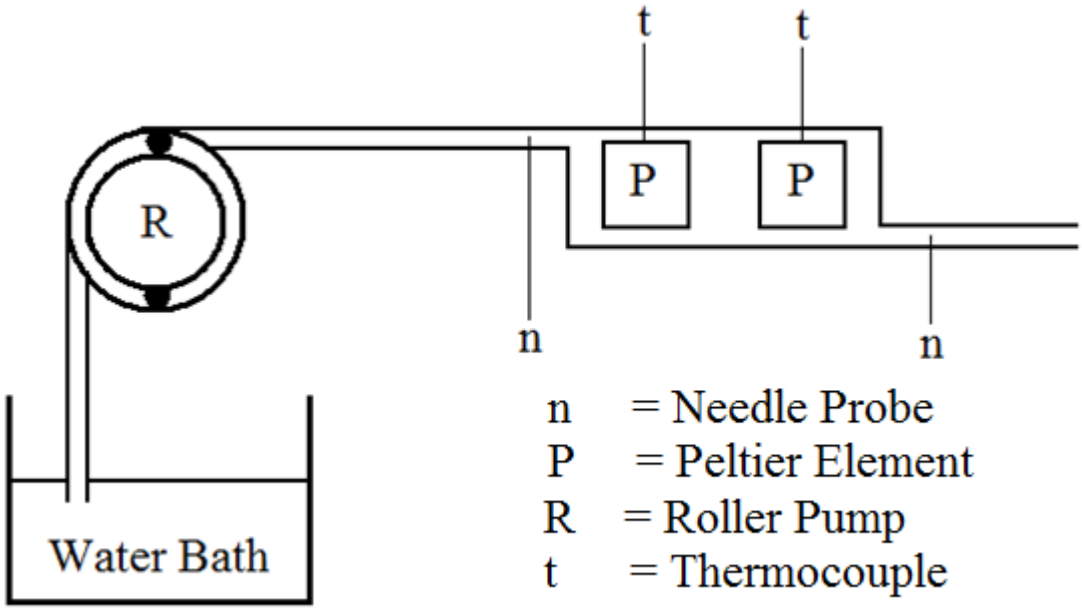


**Figure 187: Diagram of the set-up of the Mark II peltier heat exchange rig physical testing.**

The inlet water reservoir was maintained at 30 $^{0}$C using a water bath (Fisher Scientific, Leicestershire, UK). Flow was achieved using a multiflow roller pump (Stökert, Germany). Water was pumped from the reservoir through the device. The experiment was conducted at flow rates of 100, 300 and 500 ml/min. The entire experiment was repeated three times.

Temperature measurements were taken at the inlet to and at the outlet from the reservoir using MT-29/1 T type hypodermic needle microprobes (Physitemp Instruments Inc., Clifton, NJ, USA) and from the peltier array using the previously placed thermocouples. Measurements were recorded at a rate of 1 per second for 60 seconds using a TC-08 USB data logger (Pico Technology, Cambridgeshire, UK).

Control values were taken for the system at each flow rate with the peltier array unpowered. The peltier array temperature was then adjusted in 2 $^{0}$C increments through a range of 34 – 42 $^{0}$C with the array temperature controlled using a NI control system (National Instruments, Austin, Texas, USA) and a custom made temperature controller.

Figure 188 below shows the experimental configuration with the main elements of the numbered and labeled.

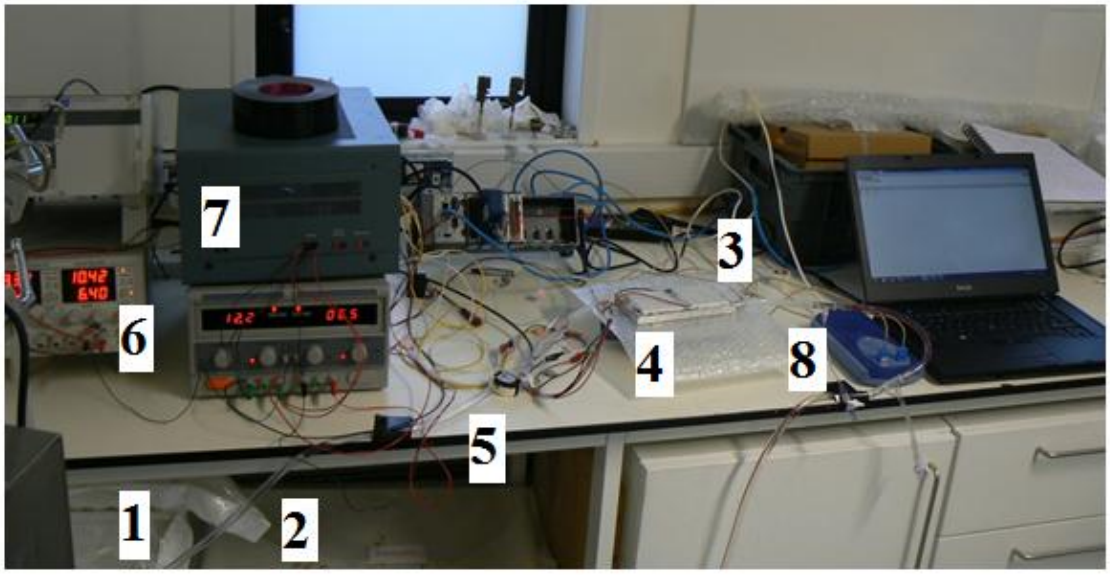


1 = Roller Pump
2 = Water Bath
3 = Needle Probes
4 = Heat Exchanger
5 = Flow Meter
6 = Power Supply
7 = Temperature Controller
8 = Data Logger

**Figure 188: Experimental configuration used for the Mark II rig testing with the main elements numbered and labeled.**

### 4.14.3. Results

Similar to the physical experimentation undertaken for the Mark I design the results are reported in terms of the water inlet and outlet temperatures and control outlet temperature against average peltier array temperature for each flow rate at which the rig was tested.

Figure 189, Figure 190 and Figure 191 below show control, water inlet and water outlet temperatures at 100, 300 and 500 ml/min respectively.

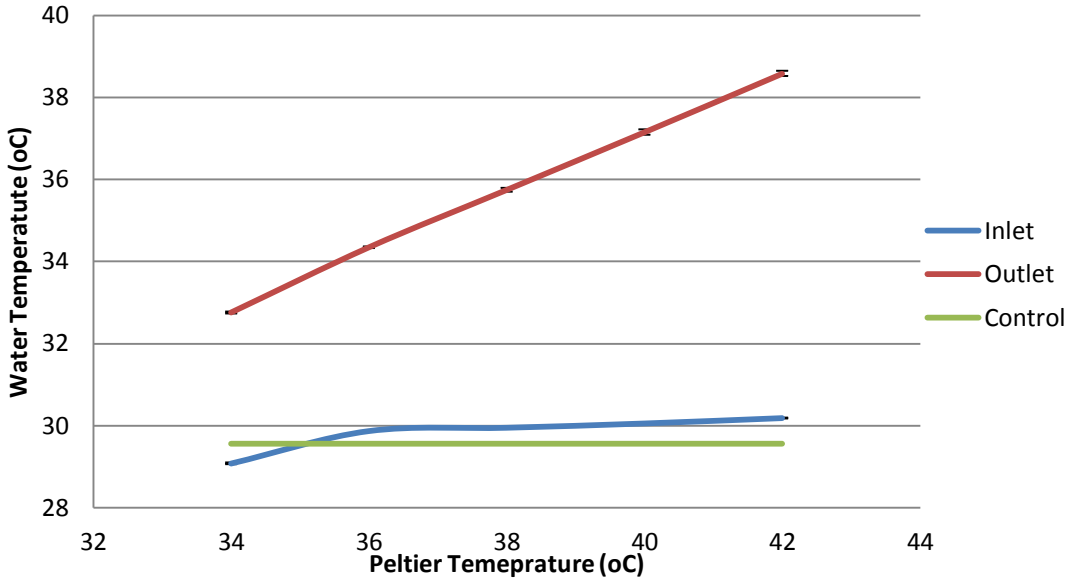


**Figure 189: Control, Water Inlet and Water Outlet values for the Mark II heat exchanger at 100 ml/min. ± 1 Standard Deviation.**

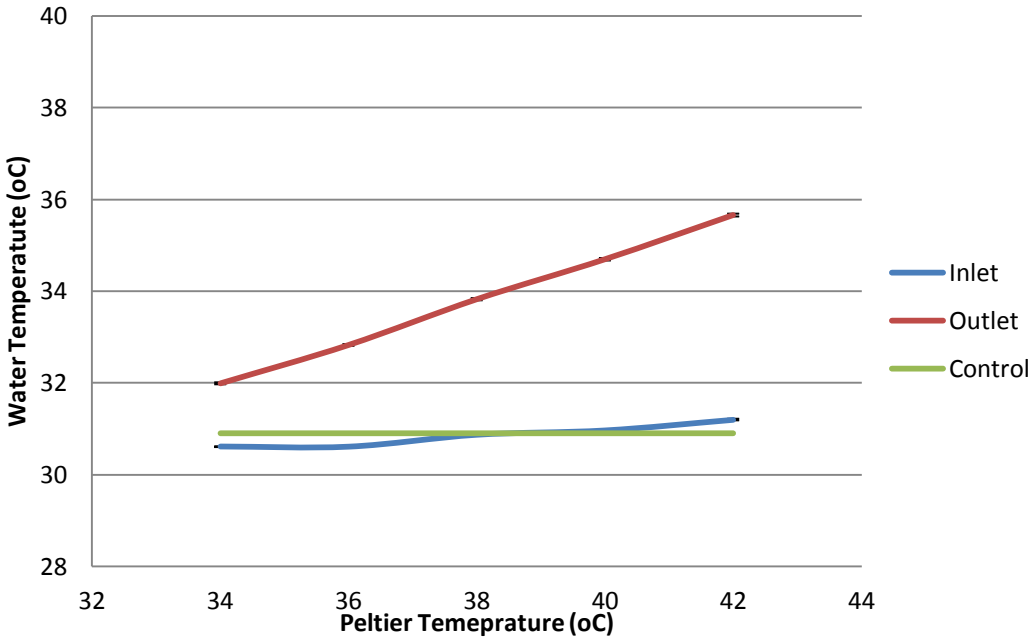


**Figure 190: Control, Water Inlet and Water Outlet values for the Mark II heat exchanger at 300 ml/min. ± 1 Standard Deviation.**

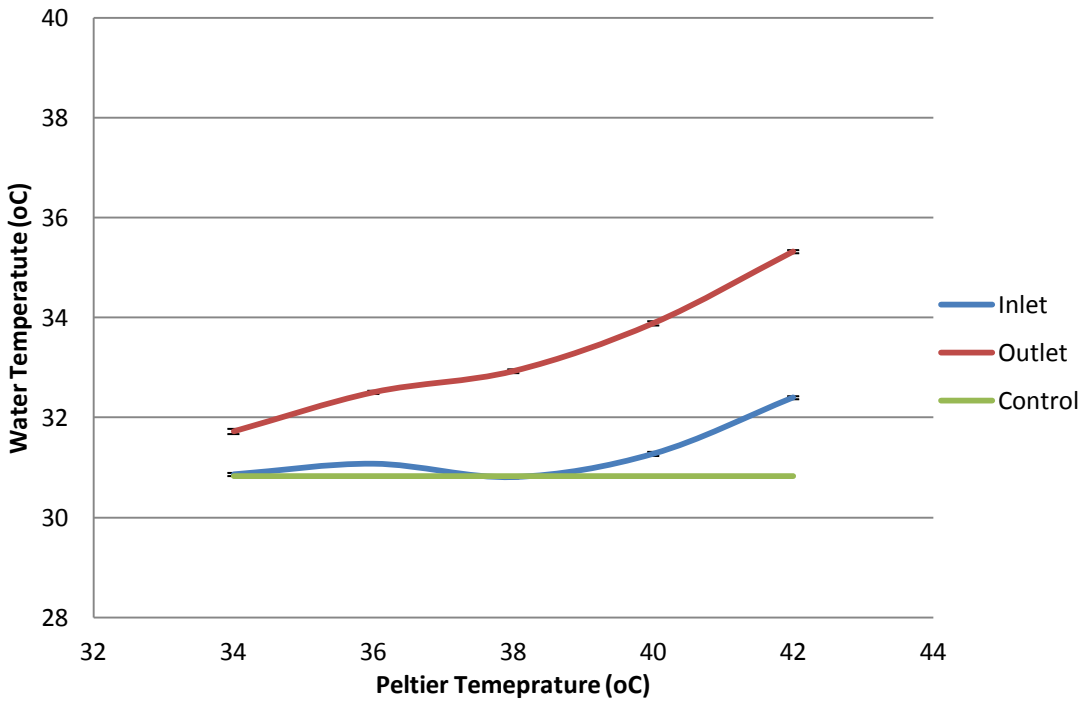


**Figure 191: Control, Water Inlet and Water Outlet values for the Mark II heat exchanger at 500 ml/min. ± 1 Standard Deviation.**

### 4.14.4. Discussion

Due to the more powerful peltier elements this heat exchanger was able to reach temperatures that the Mark I heat exchanger was unable to reach. At 100 ml/min the outlet temperature had increased by over 8 degrees. The drop in temperature between flow rates was approximately 30 % less for the Mark II when compared with the Mark I design. The rig was much easier to assemble and to set-up within the lab environment. It was also considerably more robust, never having to undergo the constant repairs required with the Mark I prototype.

To further investigate the system and to verify the CFD previously used to model the system an analysis was conducted using values from the physical experiment as boundary conditions of the computational simulation.

# *CFD analysis of the Mark II Heat Exchanger Rig Experiment*

## *Aims*

The aim of this experiment was to produce a computational model using the boundary conditions of the physical experiment to allow for a more detailed investigation of the system.

## *Methods*

The same rigs and testing method used within the initial CFD analysis were applied. The boundary conditions were modified in the following way in order to replicate the experimental set-up:

- Water flow rate, inlet temperature and peltier element temperatures from the experiment were used in each analysis.

- The outer surfaces of the rigs were given a surface heat flux to model the cooling effect of air by natural convection.

The model was run at average peltier element array temperature of 34, 36, 38, 40 and 42 $^{0}$C at 100, 300 and 500 ml/min.

### *Results*

Similar to the CFD analysis previously conducted for the Mark I design to allow a direct comparison between the experimental and computational systems the results are presented in terms of the total heat addition across the exchanger with varying average peltier array temperature.

Figure 192, Figure 193 and Figure 194 below show graphs comparing the average experimental and CFD results for total heat addition across the heat exchanger vs. peltier array temperature at 100, 300 and 500 ml/min respectively.

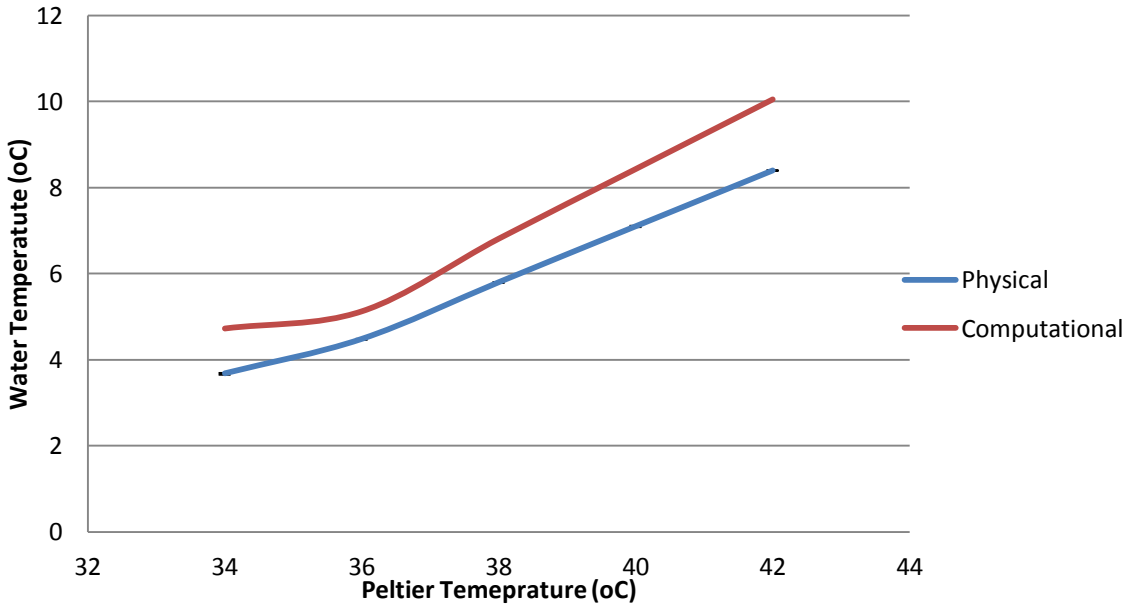


**Figure 192: Graph comparing experimental and computational total heat addition vs. average peltier array temperature for the Mark II exchanger at 100 ml/min.**

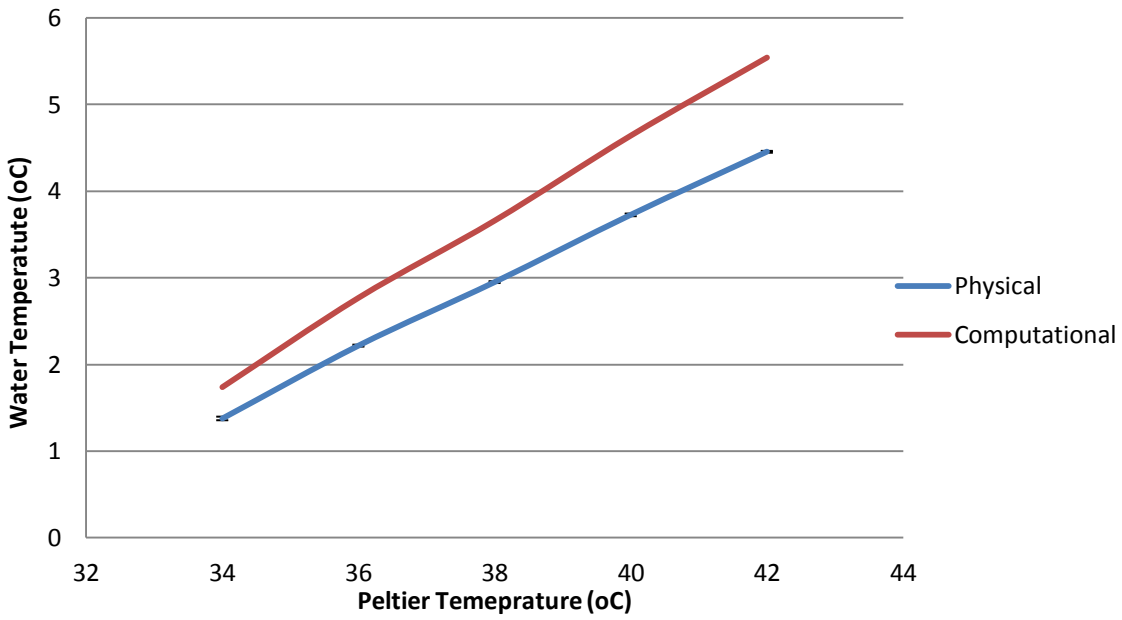


**Figure 193: Graph comparing experimental and computational total heat addition vs. average peltier array temperature for the Mark II exchanger at 300 ml/min.**

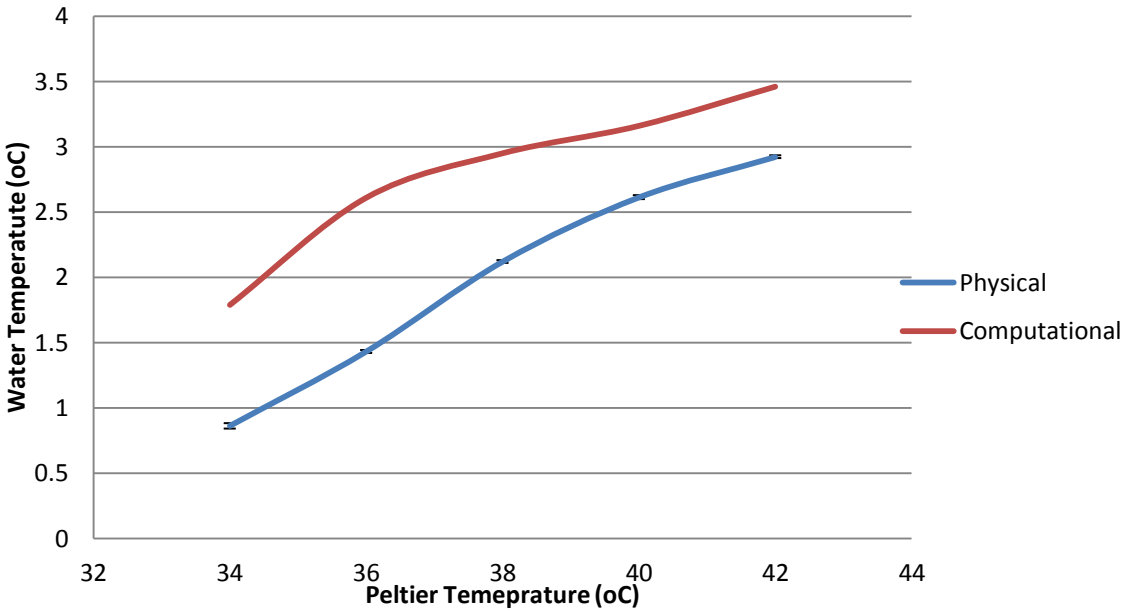


**Figure 194: Graph comparing experimental and computational total heat addition vs. average peltier array temperature for the Mark II exchanger at 500 ml/min.**

In all cases the computational model has over predicted the total heat addition in the system. This is due to the fact that the aluminium conductivity was kept at 202 (W/m.K) modeling an ideal system rather than adjusting for poor thermal contact. When compared with the Mark I system, which required an approximately 200 % reduction in the conductivity to compensate for poor thermal conduction it can be seen that this configuration is much more efficient.

### 4.14.5. Conclusions

The results of this experiment and computational analysis show that by addressing the short comings of the Mark I system the Mark II heat exchanger has shown considerable improvement in performance.

The system is easier to manufacture, more robust and easier to control. Compared to the Mark I system the Mark II has a 51 % lower priming volume and has 38 % reduction in the surface area that the blood is exposed to.

## 4.15. Mark II Heat Exchanger Endurance Testing

### 4.15.1. Aims

Having established that the Mark II heat exchanger configuration was associated with acceptable thermal transfer characteristics, the question of whether it is capable of performing over a clinically mimetic timeframe had to be resolved if it were to be considered as a genuine option for a device for clinical deployment. The aims of this series of experiments was to test the Mark II exchanger under more clinically relevant conditions and to determine if this design will meet the requirements of a miniaturized and integrated system to be used for animal testing.

### 4.15.2. Methods and materials

The principle components used to determine the performance characteristics of each rig are shown within Figure 195.

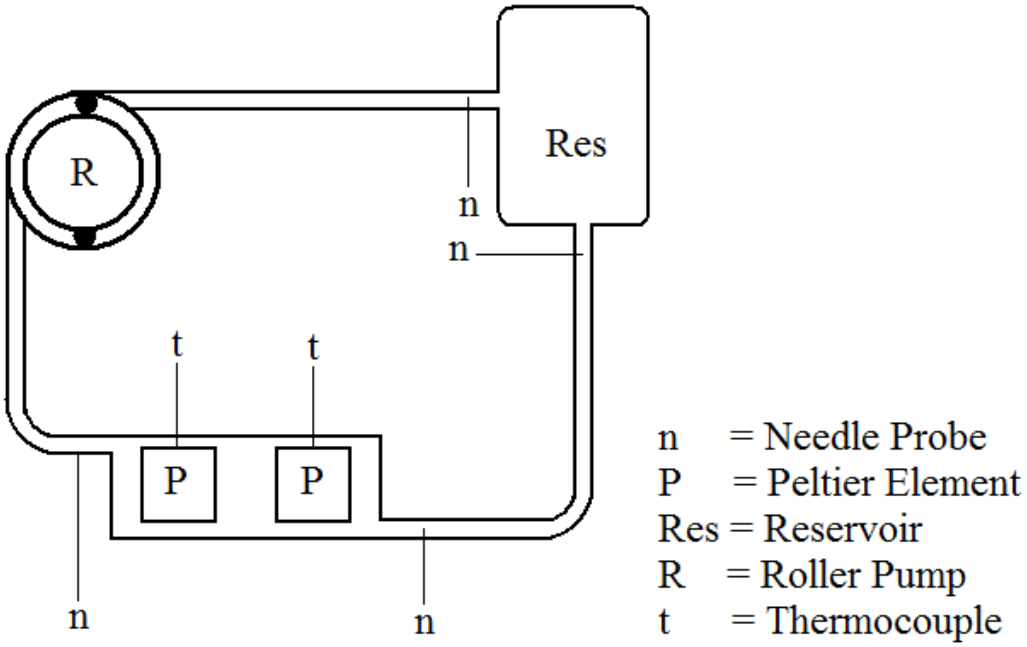


**Figure 195: Diagram of the set-up of the Mark II peltier heat exchange rig physical testing.**

The system was filled with water at 30 $^{0}$C and closed. Flow was achieved using a multiflow roller pump (Stökert, Germany). Water was pumped from the reservoir through the device at a flow rate of 400 ml/min for the duration of the experiment.

Temperature measurements were taken at the inlet to and at the outlet from the reservoir and heat exchanger using MT-29/1 T type hypodermic needle microprobes (Physitemp Instruments Inc., Clifton, NJ, USA) and from the peltier array using the previously placed thermocouples. Measurements were recorded at a rate of 1 per minute for 360 minutes using a TC-08 USB data logger (Pico Technology, Cambridgeshire, UK).

Control values were taken for the system at each flow rate with the peltier array unpowered. The peltier array temperature was set to 42 $^{0}$C with the array temperature controlled using a NI control system (National Instruments, Austin, Texas, USA) and a custom made temperature controller. The entire experiment was repeated three times. Figure 196 below shows the experimental configuration with the main elements numbered and labeled.

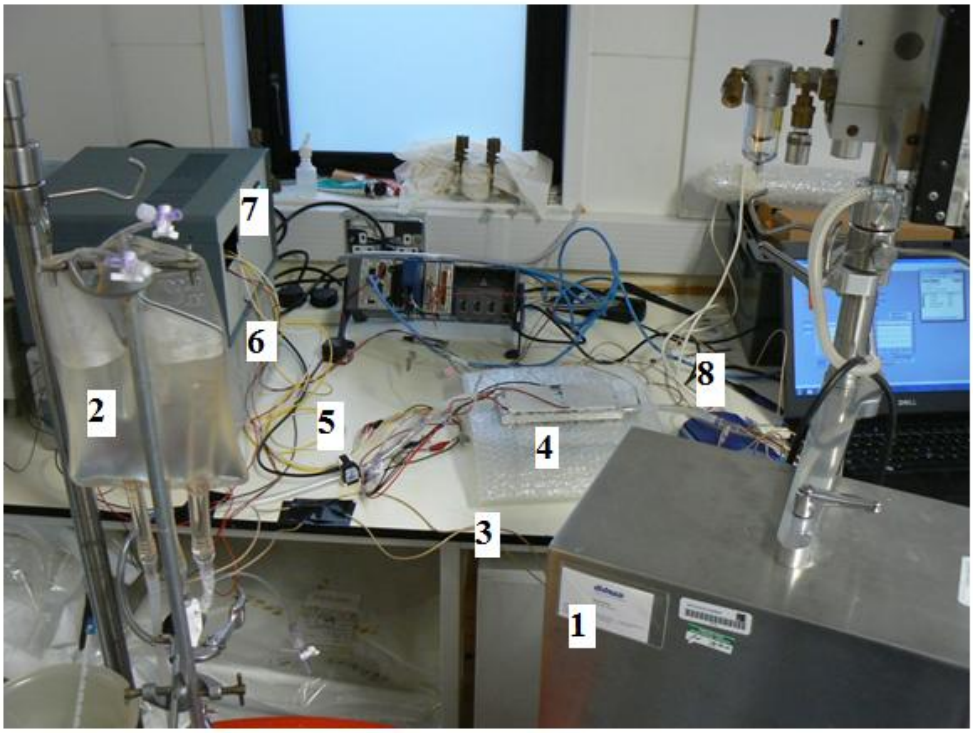


**1 = Roller Pump**
**2 = Reservoir**
**3 = Needle Probe**
**4 = Heat Exchanger**
**5 = Flow Meter**
**6 = Power Supply**
**7 = Temperature Controller**
**8 = Data Logger**

**Figure 196: Experimental configuration used for the endurance testing of the Mark II rig with the main elements numbered and labeled.**

The experiment was repeated for 50 minutes using the Mark I heat exchanger to allow the systems to be compared.

### 4.15.3. Results

The results are displayed in terms of the inlet and outlet temperatures as they vary with time. Figure 197 and Figure 198 below show reservoir outlet and heat exchanger outlet temperature versus time for Mark II rig over 6 hours and reservoir outlet temperature for the Mark I and Mark II rigs over 50 minutes respectively.

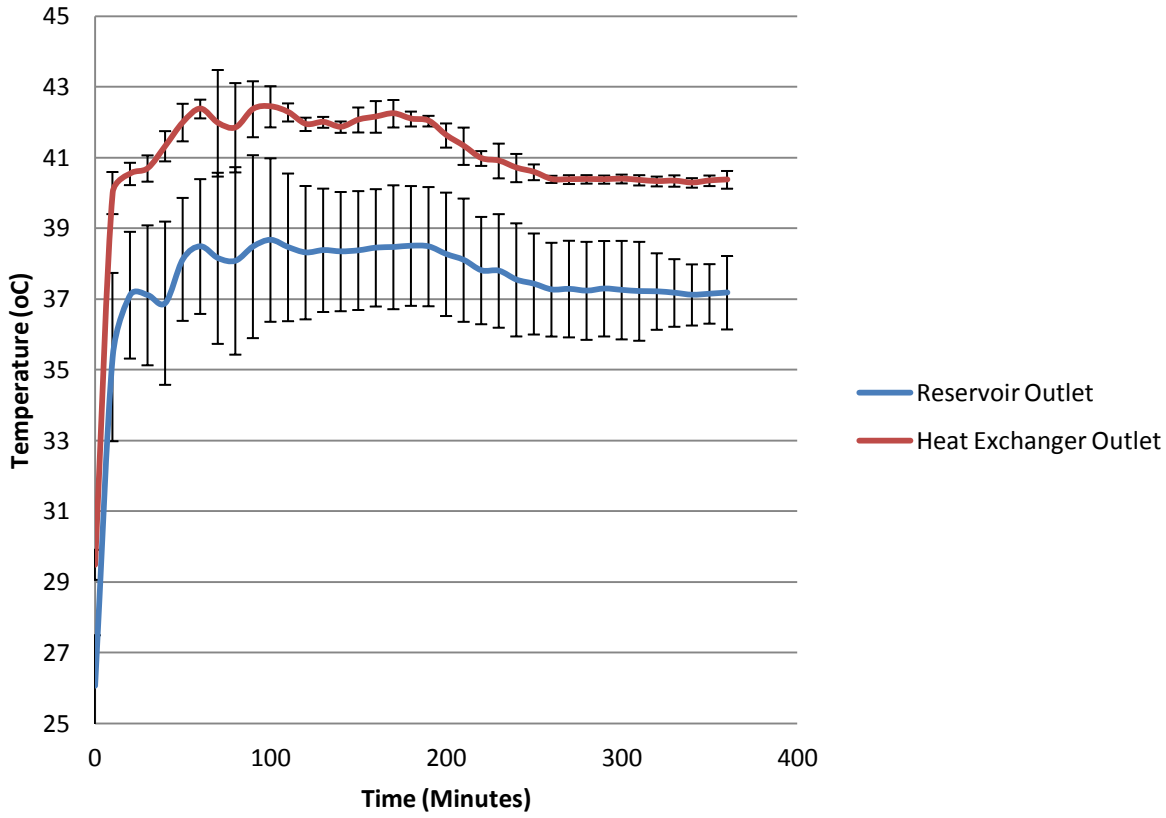


**Figure 197: Reservoir and heat exchanger outlet temperature versus time for the Mark II rig. ± 1 Standard Deviation.**

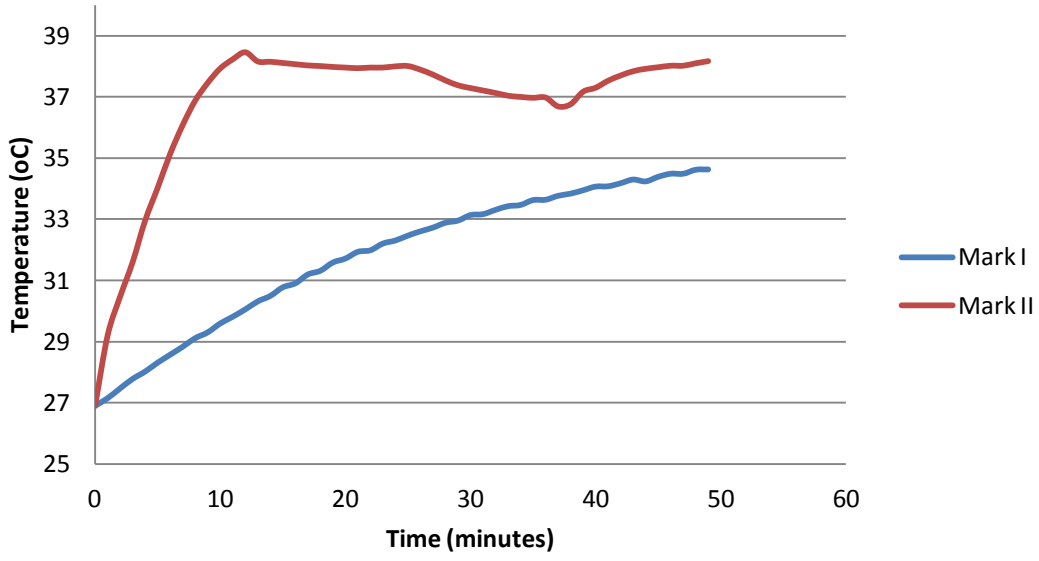


**Figure 198: Reservoir outlet temperature versus time for the Mark I and Mark II heat exchangers.**

### 4.15.4. Discussion

These results show that the Mark II heat exchanger is able to perform under clinically relevant conditions over an extended period of time. Within approximately 10 minutes the exchanger was able to raise the outlet temperature of the reservoir to over 38 $^{0}$C and maintain that consistently throughout the 6 hour duration. Slight fluctuation in the temperature occurred as conditions within the room changed, such as people entering and exiting creating a draft; however the control the system automatically adjusts to temperature fluctuations and worked to raise temperature back to the set value. Comparing the Mark I and Mark II data it can be seen that the Mark I system fails to provide sufficient heat addition to overcome the losses within the circuit over the 50 minute time frame. The benefit of the design changes and more powerful peltier elements can be clearly seen.

### 4.15.5. Conclusions

The Mark II system is capable of performing satisfactorily under clinically relevant conditions. The results can be used to validate this design as a suitable heat exchanger to be used as part of a prototype miniaturized and integrated extracorporeal membrane oxygenation system with the aim of testing the system under near clinical conditions using an animal model.

## 4.16. Chapter Conclusions

Current ECMO system use water based heat exchangers. This system requires an additional pump, water heat exchanger and tubing circuit to supply the temperature regulated water supply to the blood heat exchanger. This water based system was identified as a significant contributor to the size and complexity of current ECMO systems and for this reason the work within this chapter aimed at producing a solid state heat exchanger.

The design approach used focused on producing a computer model, verified by physical experimentation that could be used as a tool for design optimization. This method allowed configurations to be tested on the computer prior to physical prototyping and remove several iterations of physical modeling that would have been necessary in a system that did not utilize CAD.

A solid state heat exchanger has been produced that is robust, reliable, and efficient and can perform under clinically relevant conditions over an extended period of time. The device is easy to manufacture and to operate. For these reasons the device developed can be said to satisfy the second and third of the chapter aims completely; however the first aim has only been partially satisfied due to the fact that the foundation design was compromised for the sake of system performance. Although necessary, this compromise has led to a design that has not been developed based upon an integrated system. The device may therefore require redesign to help it integrate with other components. This work will have to be conducted once the configurations of the other components have been established and the system is ready for integration.

# 5. The Oxygenation System

## 5.1. Introduction

The human respiratory system is a group of organs consisting of airways, lungs and linked blood vessels and muscles used to aid breathing. Air enters through the mouth or nasal cavity where it is moistened and warmed. It then passes through the larynx and trachea before entering the lungs. During transportation to the lungs germs and foreign particles are removed via cilia which line the airways. Within each lung there is a large network of bronchi and bronchioles which terminate in alveolar sacs, which in turn contain multiple alveoli. Gas exchange occurs at the alveolar sac with oxygen from the inhaled air diffused through the membrane into and carbon dioxide removed from the blood. The human lung is ideally designed for gas exchange. There are approximately 150 million alveoli in each adult lung surrounded by an extensive network of capillaries. Gas exchange occurs via diffusion due to pressure gradients across the respiratory membrane, which can, in parts, be as thin as 0.1 µm. The large surface area, through the abundance of alveoli, combined with the extremely fast diffusion rates, due to the ultra-thin respiratory membrane, results in a highly efficient system. A diagram of the human respiratory system can be seen within Figure 199 below.

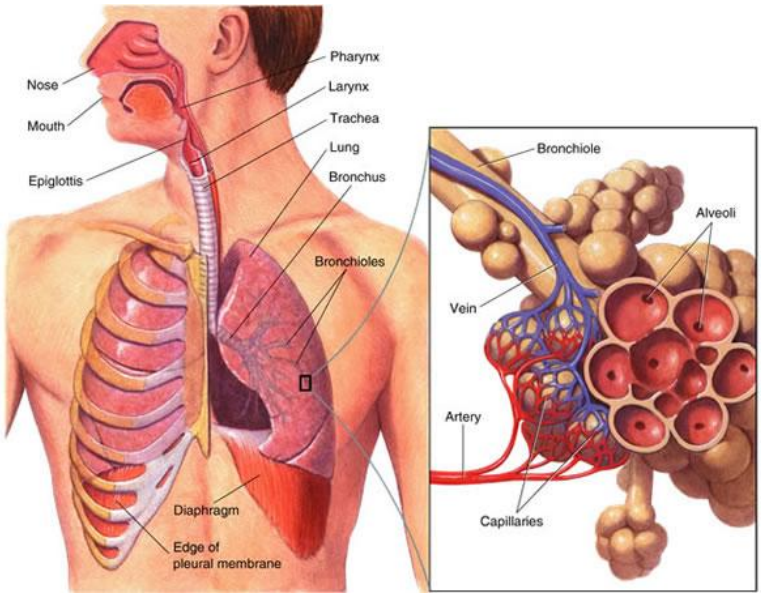


**Figure 199: Diagram of the human respiratory system (Taken from www.goldieroom.org).**

ECMO is used to treat patients with reversible damage to their lungs. The treatment allows the organs to recover by temporarily replacing the lung function with an artificial lung or oxygenator.

## 5.2. Initial Considerations

As discussed within section 1.6.4 of the literature review (Hollow Fiber Membranes – Development of the Modern Oxygenator) the most efficient design of oxygenator currently is the hollow fibre membrane oxygenator with a counter-current extra-luminal blood flow configuration. In this design blood flows over a matt of hollow membrane fibres, through which gas is passed. A diagram of an extra-luminal configuration and a typical commercial oxygenator, the Medos membrane oxygenator are shown within Figure 38 and Figure 42 respectively. Within the oxygenator gas exchange occurs through diffusion driven by pressure gradients between the blood and the gas. Gas transfer rates are dependent upon a number of different variables: Gas and blood flow rates, gas $pO_2$ and blood $pCO_2$, temperature, pH, haemoglobin and oxyhaemoglobin saturation (Gaylor, Hickey et al. 1994). The configuration of the gas diffusion structure, the fibre, plays an important part in the exchanger process. The rate at which diffusion occurs through a material depends upon the diffusivity of the material and the concentration gradient and is defined by Fick's law (Equation 7).

$$J = -D.\frac{d\emptyset}{dx}$$

**Equation 7: Fick's law of diffusion.**

Where:

J = diffusive flux ($mol/m^2.s$)

D = material diffusivity ($m^2/s$)

$\phi$ = concentration ($mol/m^3$)

x = position (m)

From this equation it can be seen that the diffusive flux can be improved by either increasing the partial pressure of gas, reducing the distance through which diffusion occurs or increasing diffusivity of the material used.

Clinical and experimental work suggests that increasing the surface area available for diffusion and hence surface area to which the blood is exposed will result in higher inflammatory reaction through exposure to a foreign surface and higher overall priming volume of the device (Gourlay, Stefanou et al. 2001). Reducing the distance through which the diffusion can occur by tightly packing fibres and encouraging blood filming results in high pressure drop across the module. For fully developed, laminar, incompressible fluid flow through a cylinder, wall shear stress is related to the pressure drop across the vessel as defined by Equation 8:

$$\tau_w = \frac{\Delta P r}{2L}$$

**Equation 8: Relationship between wall shear stress and pressure drop for fluid moving through a cylindrical tube.**

Where:

$\tau_w$ = Wall shear stress (mmHg)

$\Delta P$ = Pressure Drop (mmHg)

r = vessel radius (m)

L = vessel length (m)

This equation shows that wall shear stress increases with increasing pressure drop and hence the potential for mechanically induced haemolysis increases. Effective oxygenator design must therefore focus on balancing and tuning the above parameters to produce an optimised configuration both in terms of performance and safety. Modern oxygenators generally use cross-woven mats to encourage disruption of the concentration boundary layer with high fibre packing ratios. This configuration ensures

maximum exposure of the fibre surface area whilst producing blood filming over the fibres and mixing of the blood flow.

### 5.2.1. The Path of Least Resistance

In a modern oxygenator the percentage of membrane hollow fibres to the total module volume is known as the packing fraction. Typically a fraction of 70 – 80 % is required to achieve suitable oxygenation without producing excessive resistance to flow. The configuration forces blood to spread out through the bundle, moving through the tiny channels between the fibres. This ensures short diffusion distances and maximum use of the surface area of fibre in the bundle. Blood flowing through a channel will experience a resistance to flow. The magnitude of resistance is determined by the following factors:

1. The viscosity of the fluid.
2. The density of the fluid.
3. The mean velocity of the fluid through the channel.
4. The friction of the surface over which the fluid is passing.
5. The cross-sectional area of the channel.

As a result of the resistance to flow, a pressure differential will occur. For fully developed, incompressible, laminar flow through a channel of circular cross-section the pressure differential generated is defined by Equation 9:

$$\Delta P = f \frac{\rho u_m^2}{2D}(x_2 - x_1)$$

**Equation 9: Pressure differential for fully developed, incompressible, laminar fluid flow through a cylinder.**

Where:

$\Delta P$ = Pressure Differential (Pa)
f = Moody Friction Factor
$\rho$ = Density ($kg.m^{-3}$)
$u_m$ = mean fluid velocity ($m.s^{-1}$)
D = Tube Diameter (m)
$(x_2 - x_1)$ = axial position (m)

In high resistance and pressure systems uniform distribution of the fibres is essential. If there is a lack of uniformity and larger channels exist the flow will take the path of least resistance. When blood flows through a void in an oxygenator rather than through the fibre mat, it is known as shunting of the flow and this can significantly affect the efficiency of the oxygenator. The larger cross-sectional area of shunts results in the flow through the core of the shunt passing through the oxygenator without intimate contact with the oxygenation fibre surface. Avoidance or control of shunting is therefore a key element in the design of efficient oxygenation devices. To illustrate this and aid in our design process a CFD model was created to highlight the effects of flow shunting. Firstly a model was created in which flow was forced to move through nine channels of equal cross-sectional area. As expected the flow was evenly distributed with each channel taking approximately one ninth of the flow. Figure 200 and Figure 201 below show velocity contour diagrams of the flow path in the middle of the shunt model in the y and x axis respectively.

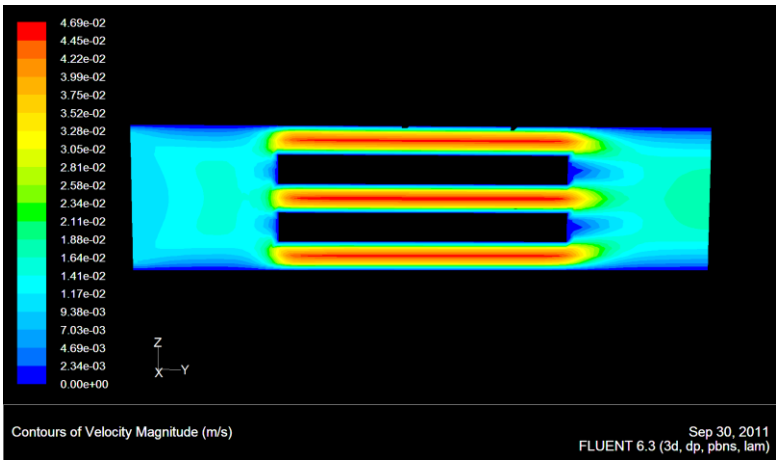


**Figure 200: Velocity contour diagram showing an x axis cross section of the evenly distributed model.**

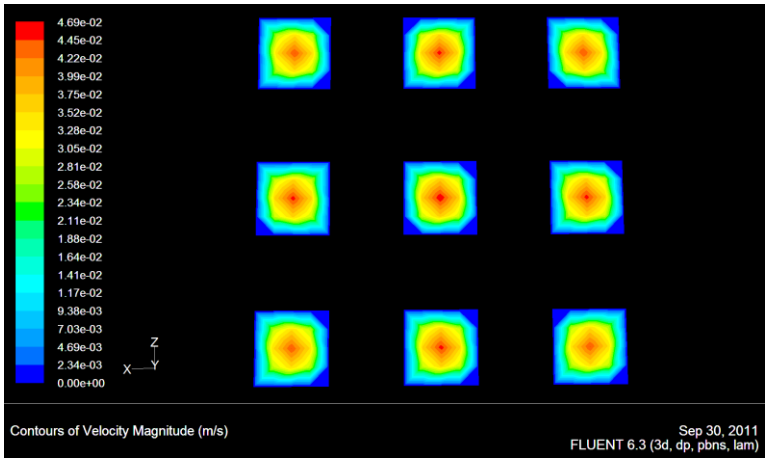


**Figure 201: Velocity contour diagram showing a cross section of the evenly distributed model in the y axis in the middle of the channels.**

The model was then adjusted by reducing the cross-sectional area of eight of the outer channels by 10 % and adding this to the cross-sectional area of the centre channel. The model was then re-run at the same mass-flow rate. This resulted in uneven distribution as can be seen in Figure 202 and Figure 203 which show the velocity contour diagrams in the same locations as for the previous model under these new conditions.

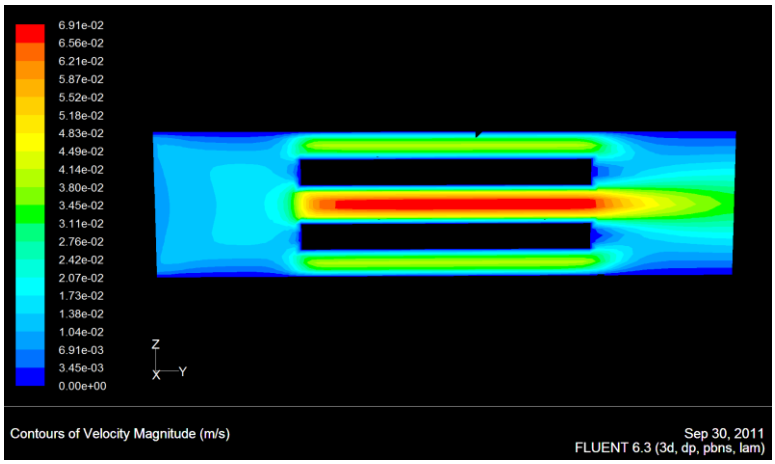


**Figure 202: Velocity contour diagram showing an x axis cross section of the unevenly distributed model.**

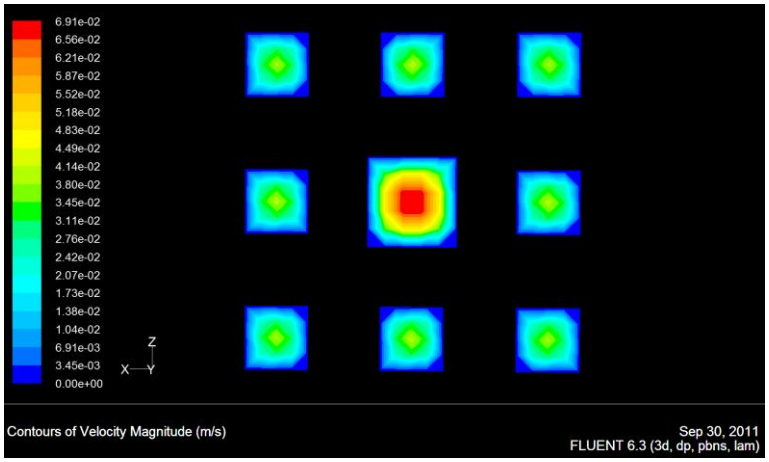


**Figure 203: Velocity contour diagram showing a cross section of the evenly distributed model in the y axis in the middle of the channels.**

The results show that each of the eight outer channels experienced a 21.6 % reduction in flow rate and the centre channel experiencing an increased flow of 173.2 %. This example confirms that very slight changes in the uniformity of the vessel geometry can have a dramatic effect on the distribution of flow.

## 5.3. Device Performance Requirements

To determine the performance requirements of the oxygenation system a currently available commercial oxygenator was chosen as a performance baseline. The Medos Hilite 800 LT was chosen as the most suitable oxygenator. At a flow rate of 500 ml/min in vitro testing of the oxygenator using pig blood showed an oxygen transfer rate of approximately 65 ($mlO_2$/LBlood) with a corresponding pressure drop of approximately 30 (mmHg). The data sheet for the Medos Hilite 800 LT is provided in the Appendix.

## 5.4. Chapter Aims

The aims of this chapter are as follows:

- To produce a manufacturing method capable of consistently producing functioning oxygenators.

- To produce an oxygenator bundle that provides acceptable levels of oxygenation and carbon dioxide removal at a range of clinically relevant blood and gas flow rates, which is tested under conditions that are as close to AAMI/ISO standards as possible within our laboratory setting.

- To develop a CFD model to be used to optimize the performance of the oxygenator model and reduce the time and cost involved in iterative prototyping.

## 5.5. Oxygenator Development

As with the previous development chapters the foundation design is based upon Concept 3, which was established within the concept development process (Chapter 2 – Concept Development). The basic geometry of the oxygenation module of concept 3 can be seen highlighted in blue in Figure 204 below.

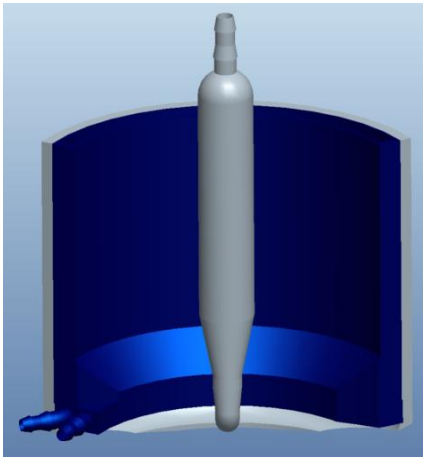

**Figure 204: ProEngineer Model highlighting the position of the oxygenator (in blue) in the concept 3 design developed within Chapter 2 – Concept Development.**

As previously discussed the most efficient oxygenator configuration has already been established in the form of a counter current, extra-luminal blood flow oxygenator utilising membrane hollow fibres. And so unlike the previous development chapters there is little flexibility in the design envelope available for achieving the required performance characteristic. In terms of the oxygenator design the factors, which can be influenced are the oxygenator geometry, the fluid flow path and the orientation and packing fraction of the fibres within the module. Acceptable performance of the hollow fibres being employed is assumed insofar as they represent state-of-the-art in this application, and so design success can be based upon maximising oxygenation through manipulation of the fluid path and optimisation of fibre orientation and packing fraction without compromising on the pressure drop across the module.

The development work in this chapter will follow the same design strategy previously adopted. The first step in this strategy is developing a suitable computational model to allow the evaluation of the performance of the initial concept prior to physical prototyping. The model used to simulate the conditions within the oxygenator will be based upon approximating the fluid flow through the bundle using a porous media model. This method of modelling has been shown to be successful in previous studies (Matsuda 1999; Gage 2002).

A commercially available paediatric oxygenator, Medos Hilite 800 LT, was selected as a standard comparative device upon which to base performance outcomes of the concept devices. As a porous media approximation of the bundle is being used in the computer simulation, accurate definition of the permeability coefficients of this media is essential. To obtain these coefficients a CFD simulation is required to replicate the fluid path through the Medos Hilite 800 LT. The results of this simulation can be compared with physical experimental data and the boundary conditions iterated until a suitable configuration is achieved. Figure 205 below shows pressure drop versus flow rate for the physical testing of the Medos Hilite 800 LT device taken from www.Medos-ag.com.

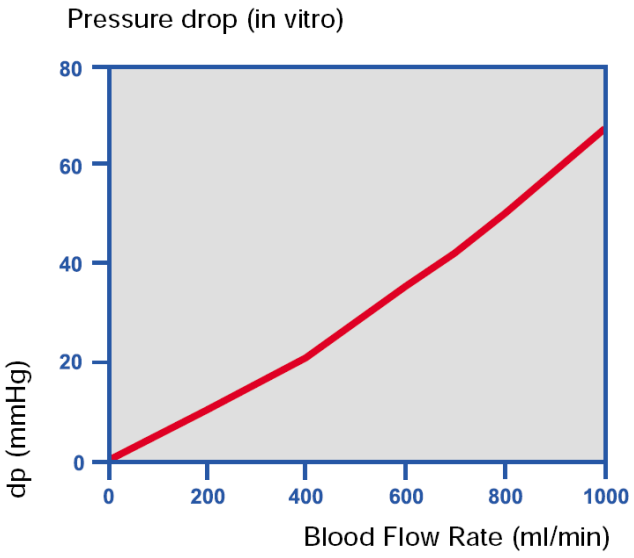


**Figure 205: Pressure drop versus flow rate for the physical testing of the Medos Hilite 800 LT pediatric oxygenator (taken from www.medos-ag.com.**

## 5.6. CFD Modelling of an Oxygenator

### *Aims*

The aims of this analysis were to investigate the design of a current commercial oxygenator and to use physical data to determine a suitable porous media model to be used as a tool for optimization in future design work.

### *Methods*

A model of the fluid path of a Medos HiLite 800 LT paediatric oxygenator was created. To allow the fibre bundle to be defined as a porous media the model was split into three volumes: fluid inlet, porous media and fluid outlet. The developed fluid path can be seen within Figure 206 below.

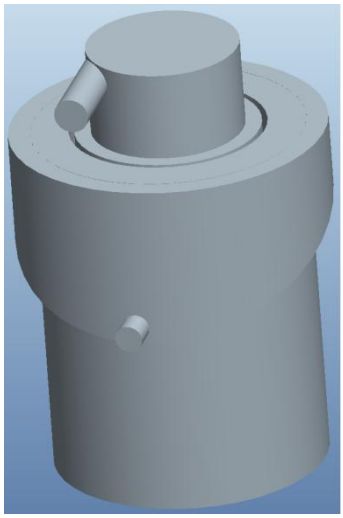

**Figure 206: A proEngineer model of a fluid path based upon the dimensions of a Medos Hilite 800LT pediatric oxygenator.**

The most suitable mesh of the complete model was found to be a tetrahedral/hexagonal element hybrid mesh of 584,908 nodes and can be seen within Figure 207 below.

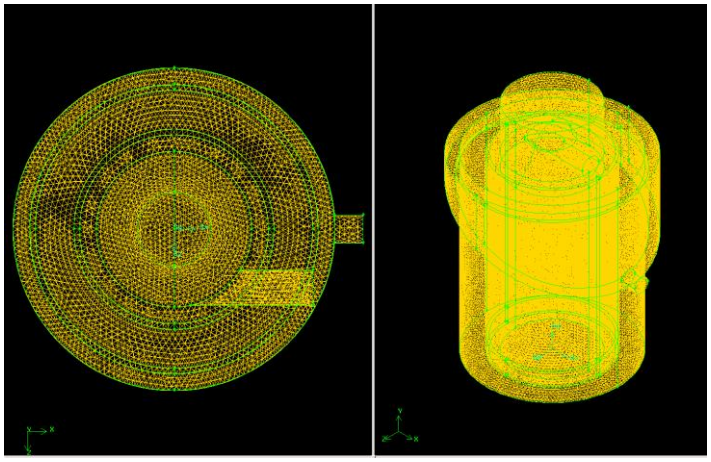

**Figure 207: Diagram showing the tetrahedral/hybrid mesh generated for the medos fluid path generated within Gambit.**

CFD analysis was run using Fluent Inc., Fluent version 6.3.26.

Boundary conditions were set as a constant velocity at the domain inlet with the outlet set as constant pressure. Steady laminar flow was assumed in all cases with blood modelled as Newtonian with a constant viscosity of 0.0035 (Pa.s) and a density of 1050 ($kg.m^{-3}$). The porous media was modelled with the momentum losses approximated using Darcy's law which is defined by Equation 10:

$$\Delta P = -\frac{\mu}{\alpha} v$$

**Equation 10: Darcy's Law defining the pressure drop generated as a fluid passes through a porous media.**

Where:

$\Delta P$ = Pressure Drop (Pa)

$\mu$ = viscosity (Pa.s)

$\alpha$ = porous media permeability ($m^2$)
v = superficial velocity ($m.s^{-1}$)

The porous media permeability was determined by comparing the hagen-poiseuille equation and Darcy's law equation, assuming laminar, viscous and incompressible flow. Equation 11 shows the relationship between the permeability coefficient, the vessel diameter and the void fraction of the porous media.

$$\alpha = \frac{d^2\varepsilon^3}{32(1-\varepsilon)^2}$$

**Equation 11: Relationship between permeability coefficient, vessel diameter and void fraction of the porous media, obtain through comparing the hagen-poiseuille equation and Darcy's Law.**

Where:
$\alpha$ = porous media permeability ($m^2$)
d = Outer diameter of the hollow fibre (m)
$\varepsilon$ = Void fraction of fibres in casing

The asymmetry of the fibre bundle was modelled under the assumption of equal magnitude porous media in the x and z dimensions and a ratio of $\alpha_{x.z} = 4.5\ \alpha_y$ in the y dimension. Values were calculated using the relationship defined within Equation 12:

$$\alpha = \sqrt{\frac{\alpha_{x,y}^2 - \alpha_z^2}{2}}$$

**Equation 12: Relationship determining permeability coefficients**

The inertial resistance coefficient was assumed to be negligible in the laminar flow domain.

To determine the most suitable permeability coefficients the model was run with the porous media defined with varying void fractions from 20 % - 35 % in 5 % increments and at a flow rate of 200 ml/min representing the mid-range of flow rate for our concept device. The result of this analysis was compared with the pressure value at 200 ml/min obtained in the physical testing of the device to determine the most suitable void fraction and corresponding permeability coefficient. These values were then used in a model, which was tested through a range of flow rates from 200 – 1000 ml/min in 200 ml/min increments to allow for a more detailed comparison with the physical testing results.

### *Results*

To determine the most suitable void fraction and corresponding porous media coefficients for the porous media the pressure drop across the module was plotted against increasing void fraction as shown in Figure 208 below.

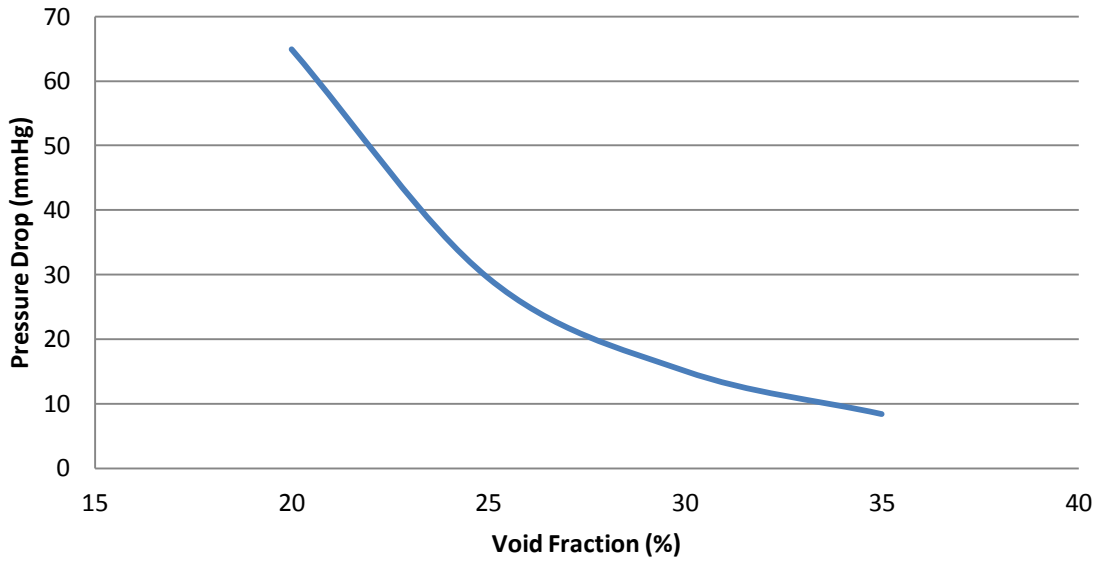


**Figure 208: Graph showing the effect of varying the void fraction of the porous media model in terms of the pressure drop across the module at a flow rate of 200 ml/min.**

At 200 ml/min the pressure value from the physical testing was approximately 10 mmHg. From the figure above this corresponds to a void fraction of approximately 34 %. Figure 209 below shows a comparison between the physical testing of the Medos oxygenator and the values obtained in the CFD analysis of the model ran with permeability coefficients that represent a porous media with a 34 % void fraction.

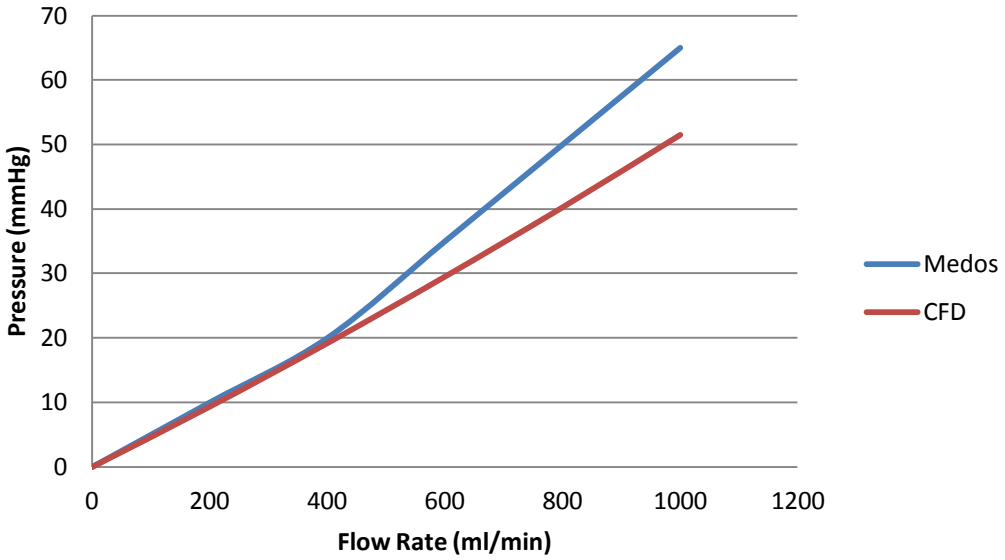


**Figure 209: Graph comparing pressure drop versus flow rate for the Medos HiLite 800 LT and the CFD model with permeability coefficients that represent a porous media with a 34 % void fraction.**

### *Discussion*

The results show that the model created is very accurate at lower flow rates; however the model becomes less accurate at the higher flow rates. The change in pressure in the physical model can be attributed to secondary flows, which are not being represented in the laminar CFD model.

The oxygen modules being developed within this chapter are required to operate in a range of 0 – 500 ml/min and therefore the results of this analysis show that in this flow

rate range the computational model can provide accurate simulation of the system. Using this model, assuming that at the flow rates there was no influence of an inertial component , the viscous coefficients for the porous media were calculated to be $k_{x,z}$ = 5,660,872,542 $m^{-2}$ and $k_y$ = 1,257,971,676 $m^{-2}$.

***Conclusions***

This CFD analysis has produced permeability coefficients for a porous media model based on a current commercial oxygenator. These coefficients can be used to define the porous media in future simulations providing an accurate and realistic model.

## 5.7. Oxygenator Manufacture

Modern hollow fibre membrane oxygenators are designed to produce gas exchange solely through diffusion across the membrane wall. In this design the blood and gas paths must be completely separated. Separation of the paths is achieved using a special adhesive that neither expands nor contracts upon setting. The potting compound used in this case was a two part compound – Texaflex 5397 A and 5396 B (Texachem International, Novara, Italy).

In oxygenator manufacture sealed hollow fibres are placed within the blood chamber of the device. The adhesive is then injected into the device and the oxygenator is spun in a centrifuge or by using a vacuum process. The centrifugal force moves the adhesive to the outer boundaries of the blood chamber and after time the layer of adhesive sets. Figure 210 shows the potting compound in a feeding tube and highlights the path taken by the compound as the module is spun.

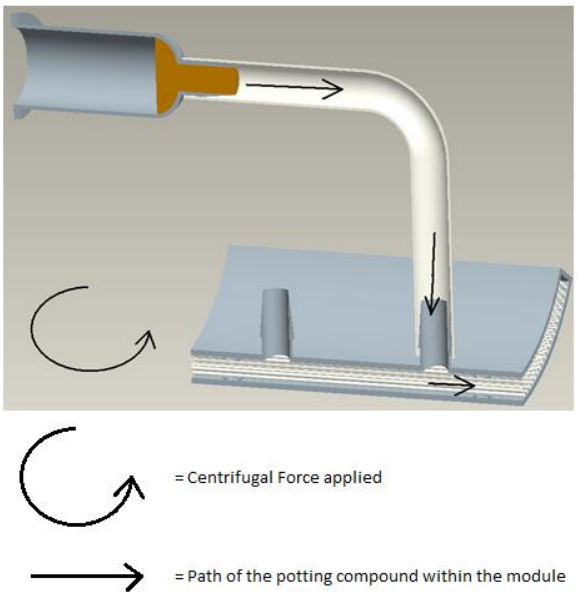


**Figure 210: Diagram showing the potting compound being inserted into a feeding tube and highlighting the path taken by the compound as the module is spun in a centrifuge.**

Under the centrifugal force the compound moves through the module. Once it reaches the outer boundary the centrifugal force is maintained while the compound sets. This ensures an even layer of compound is achieved and reduces resin wetting of the outer fiber surfaces due to capillary creep. Figure 211 shows a diagram of the final position of the potting compound.

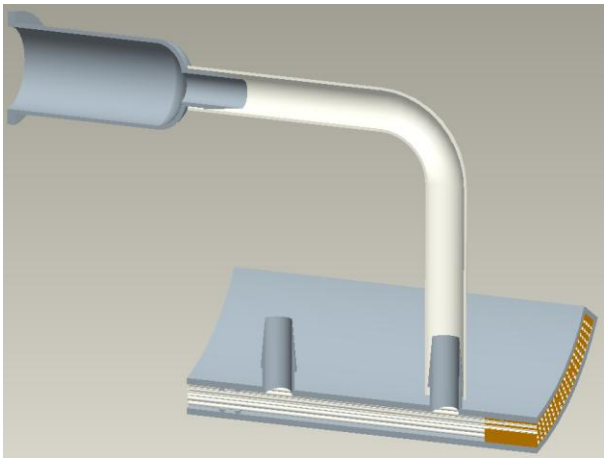

**Figure 211: Diagram showing a cross-section of an oxygenator module after the module has been spun in a centrifuge with the potting compound set in place at the extremity of the module.**

This process is then repeated for the opposite end of the device. The set adhesive surrounds the hollow fibres and acts as a cork separating the blood from the gas. This process is known as “potting”. After potting has occurred a fine layer of the adhesive is cut from the upper surface of the compound, opening up the end-sealed hollow fibres. Figure 212 shows a potted module that has yet to have the top layer of potting compound removed.

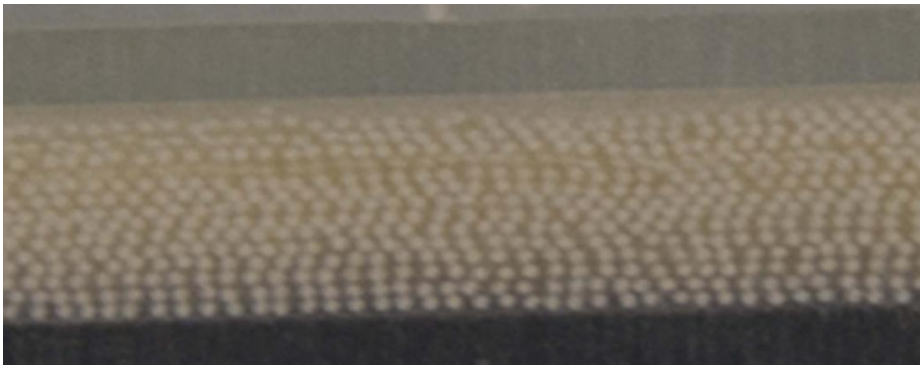

**Figure 212: Picture showing fibers within a rapid prototyped oxygenator module, prior to the fibers being opened.**

Figure 213 shows the same module after the layer of potting compound has been removed. In this figure the donut shape of the open hollow fibers can clearly be seen.

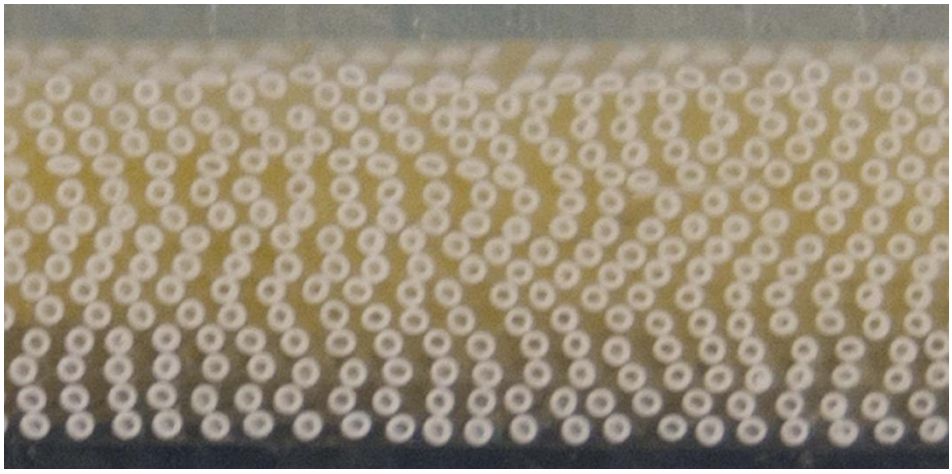

**Figure 213: Picture showing fibers within a rapid prototyped oxygenator module with opened fibers.**

The manufacturing process involved in creating a functioning oxygenator is a complicated and sensitive process. In industry each step is heavily automated to maximise efficiency and to ensure quality. Automation of the process is not feasible under the resource constraints of this project. For this reason manufacturing of the oxygenator initially concentrated on developing a reliable manufacturing method before optimizing the module geometry.

## 5.8. Development of the Oxygenator Manufacturing Method

A simplified prototype module was created solely for developing the mechanics of the manufacturing method. The design featured a simple chamber with feeding tubes for the potting compound. The model was designed in ProEngineer and then rapid prototyped for laboratory testing. A cross section of the ProEngineer model and the rapid prototype can be seen within Figure 214 and Figure 215 respectively.

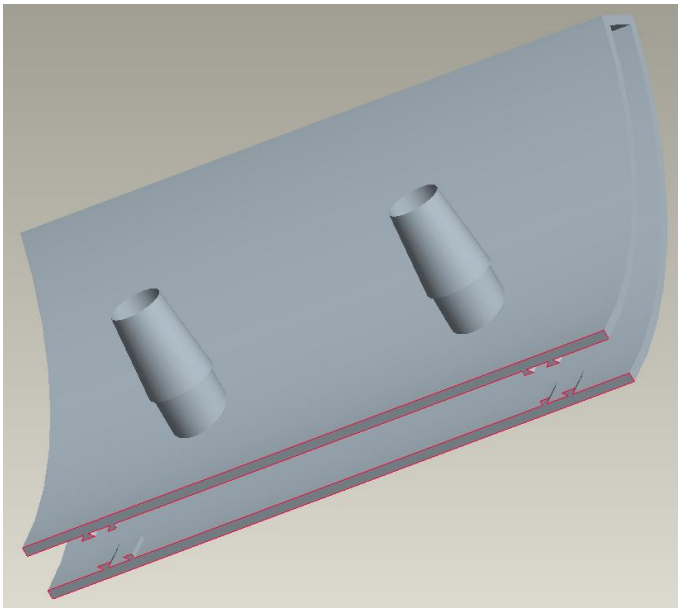

**Figure 214: ProEngineer model of the basic oxygenator module designed to aid in the development of a suitable manufacturing method.**

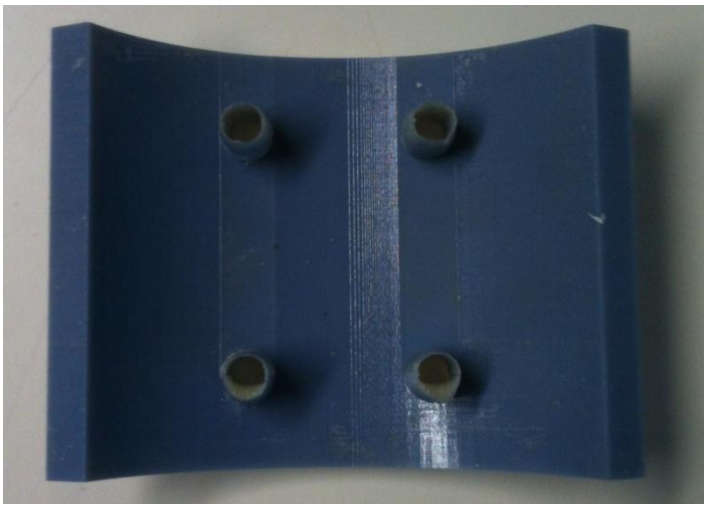

**Figure 215: Rapid prototype of the basic oxygenator module designed to aid in the development of a suitable manufacturing method.**

The prototype was designed with connectors for ½ inch tubing for insertion of the potting compound under gravity. Small rungs were set along the top of the device to give the potting compound extra grip on the surface of the module.

A centrifuge was constructed using a modified Whirlpool top loading washer/dryer. The main drum was removed from the device and replaced with a metal disc which was fitted with the necessary restraints to hold the oxygenator columns and potting compound in place during rotation. The washer was able to achieve a spin rate of 600 rpm. The modified washer drier can be seen within Figure 216.

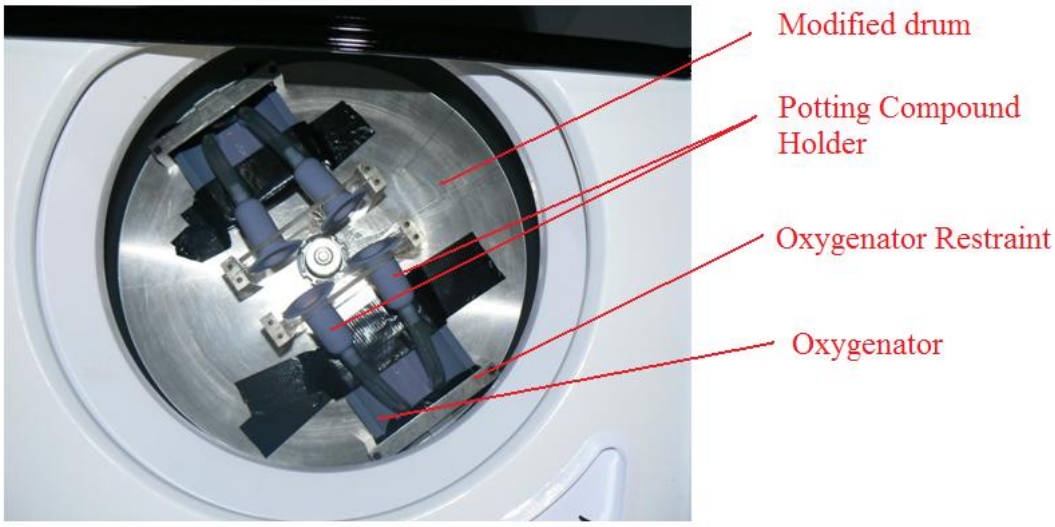


**Figure 216: Whirlpool washer/dryer modified into a centrifuge with the main aspects highlighted.**

The manufacturing method used to create the oxygenator module was as follows:

- Holes were drilled at the top of the front face and the bottom of the rear face to act as the inlet and outlet to the blood compartment of the rapid prototyped module.

- The fibres were cut to the size of the column using a pizza cutter. This method ensured the hollow fibres were closed at both ends prior to potting.

To maintain consistency with the CFD simulation previously conducted the hollow fibres used were the same as used within the Medos Hilite 800 LT – Membrana Oxyplus plasma tight hollow fibre. Initially the number of hollow fibres within the unit was set to equal the surface area achieved within the Medos Hilite 800LT of 0.32 $m^2$, which employs a similar fibre. The hollow fibres were in mat form with approximately 18 fibres per cm. The length of mat required was calculated as follows:

Circumference of fibre = $\pi$.D = 0.001131 (m)
Length of fibre = 0.09 (m)
Surface area per fibre = 0.001131 x 0.09 = 0.000102 ($m^2$)
Number of fibres in 0.32 $m^2$ = 0.32 / 0.000102 = 3143.8 (fibres)
Length of fibre mat required = 3144/18 = 174.667 (cm)

- The fibres were placed within the module and poly film was used to cover the end of the column. To prevent leakage of potting compound during the spin cycle a potting cap with silicon lube was also positioned on the end of the module over the poly film. The cap was secured using adhesive tape.

- Both of the potting compound elements were heated to 48 $^0$C to lower viscosity prior to use. The compounds were measured out and mixed together at the required ratio using a metal spatula to gently fold the mixture without introducing bubbles.

The volume of potting compound required was calculated as follows:

Inner radius of module = 0.072 (m)
Outer radius of module = 0.08 (m)
Total area of 120 degree arc = $\pi$.(($0.08^2$)-($0.072^2$)).120/360 = 0.001273 ($m^2$)
Length of section = 0.02 (m)
Volume of Section = 0.001273 x 0.02 = 2.54678 e -05 ($m^3$)
Radius of fibre = 0.00018 (m)
Area of fibre = $\pi$.($0.00018^2$) = 1.01788 e -07 ($m^2$)
Area of 3144 fibres = 1.01788 e -07 x 3144 = 0.00032002 ($m^2$)
Length of fibre in potting compound = 0.02 (m)
Volume of fibre in potting compound = 0.00032002 x 0.02 = 6.4004 e -06 ($m^3$)
Volume of potting compound = 2.54678 e -05 – 6.4004 e -06 = 1.90674 e -05 ($m^3$)
= 19.067 (ml)

The volume was rounded to 20 (ml) and split into the required mixing ratio of 42:58 resulting in 8.4 (ml) of compound 5397 and 11.6 ml of compound 5396 B per end of the oxygenator.

- The modules were secured in place in the modified centrifuge using Velcro ties and adhesive tape.

- The compound was injected into the feeding tubes by syringe and allowed to enter the modules via gravity.

- The centrifuge was then set on a 4 minute spin cycle at 600 r.p.m. The modules were spun for approximately 20 minutes (5 cycles) before being removed and allowed to cure overnight.

- The process was then repeated for the other side of the oxygenator after setting.

- After potting was completed the inlet nozzles were removed and sealed using aluminium patches.

- A 2 mm section was removed from the top and bottom of the module using a band saw. This was done to compensate for uneven fibre lengths at the module extremities.

- A thin layer of potting compound was removed, using a scalpel, to open up the fibres. Both the top and bottom surfaces were then checked using a microscope to ensure that all of the fibres were open and that there were no holes within the potting compound.

- A male to male leur connection was inserted into the previously drilled holes to act as inlet and outlet to the blood compartment.

- A gas inlet was designed to fit over one end of the oxygenator with the other end left open to atmosphere. A ProEngineer of the inlet design can be seen within Figure 217 below with the gas inlet attached and highlighted in blue.

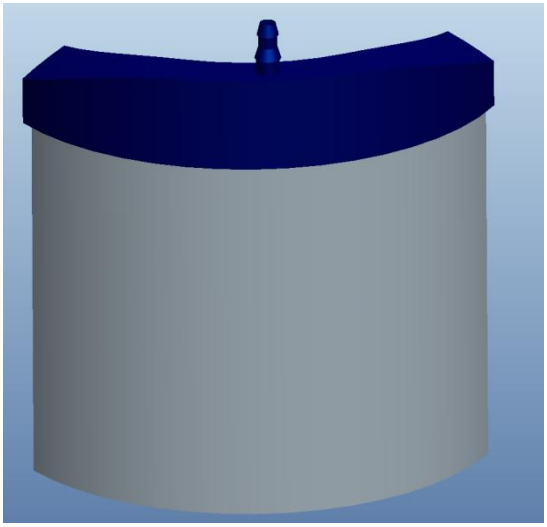

**Figure 217: Pro-Engineer model showing the oxygenator module designed for testing the manufacturing method with the gas inlet attached highlighted in blue.**

This work has shown that it is possible to manufacture a sealed oxygenator in the laboratory environment. Developing the method of manufacture prior to designing the working module should improve the quality of the prototypes and highlight manufacturing requirements that may need to be factored into the module design.

## *5.9.* Oxygenator Device Development

With the manufacturing method established the next step in the design strategy was to focus on the performance of the oxygenator module prototype. As previously discussed the foundation design upon which this work will be based is the geometry of Concept 3 developed within Chapter 2 – Concept Development. To determine the suitability of this design a computational simulation is required.

### 5.7.1. CFD Analysis of Oxygenator Design

#### *Aims*

The aims of this analysis were to determine the inlet velocity profiles, fluid distribution and pressure drop across the module using the previously established porous media approximation.

#### *Methods*

An oxygenator module was designed for simulation based upon Concept 3 of Chapter 2 – Concept Development. To accurately model the inlet conditions of the concept the heat exchanger was included on the rear wall of the module. Blood passes through the heat exchanger prior to entering the oxygenator. It moves down and across the fiber bundle and exits to a small reservoir that focuses the flow to a single exit point.

The porous media model developed in the previous analysis was applied to the geometry of the miniaturized and integrated oxygenation concept. The flow path was designed

based upon the oxygenator geometry of Concept 3 developed within Chapter 2 – Concept Development and can be seen within Figure 218 below.

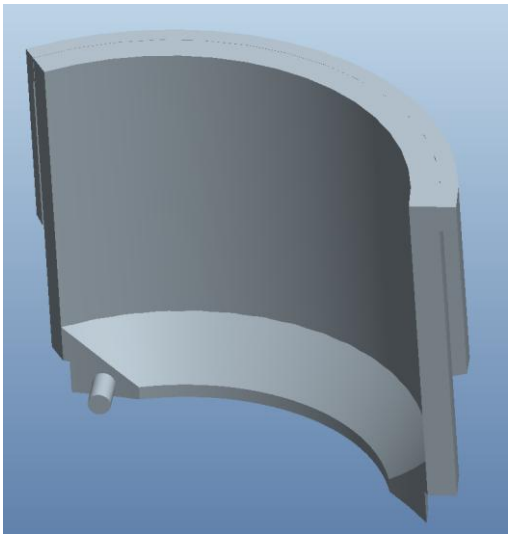

**Figure 218: ProEngineer model showing the fluid path developed for the CFD analysis based upon the oxygenator geometry of Concept 3 developed within Chapter 2 – Concept Development.**

The model was imported into gambit and meshed as three connected volumes to allow the porous media to be characterized individually. The most suitable mesh of the complete model was found to be a tetrahedral/hexagonal element hybrid mesh of 1,147,530 nodes and can be seen within Figure 219 below.

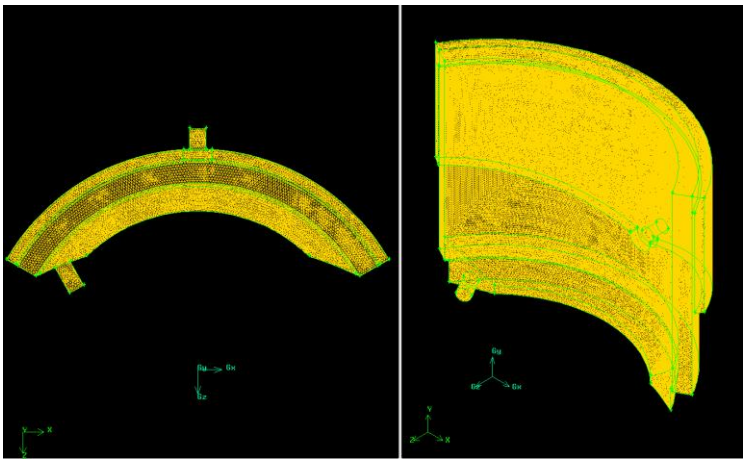

**Figure 219: Tetrahedral/hexagonal hybrid mesh of the Concept 3 oxygenator flow path.**

CFD analysis was run using Fluent Inc., Fluent version 6.3.26. Boundary conditions were set as a constant velocity at the domain inlet with the outlet set as constant pressure. The oxygenator volume was modelled as a porous media with a 66 % packing fraction with previously established viscous coefficients of $k_{x,z}$ = 5,660,872,542 $m^{-2}$ and $k_y$ = 1,257,971,676 $m^{-2}$ again assuming a zero inertial coefficient. Steady laminar flow was assumed in all cases with blood modelled as Newtonian with a constant viscosity of 0.0035 (Pa.s) and a density of 1050 ($kg.m^{-3}$). The fluid flow rate was increased from 100 – 500 ml/min in 100 ml/min intervals.

### *Results*

The most suitable performance characteristic to allow for accurate evaluation of the simulation was determined to be the pressure drop across the module. As the porous media model was based upon the permeability parameters previously established the pressure drop should be directly related to the configuration and geometry of the module design created. Figure 220 below shows pressure drop across the module versus flow rate.

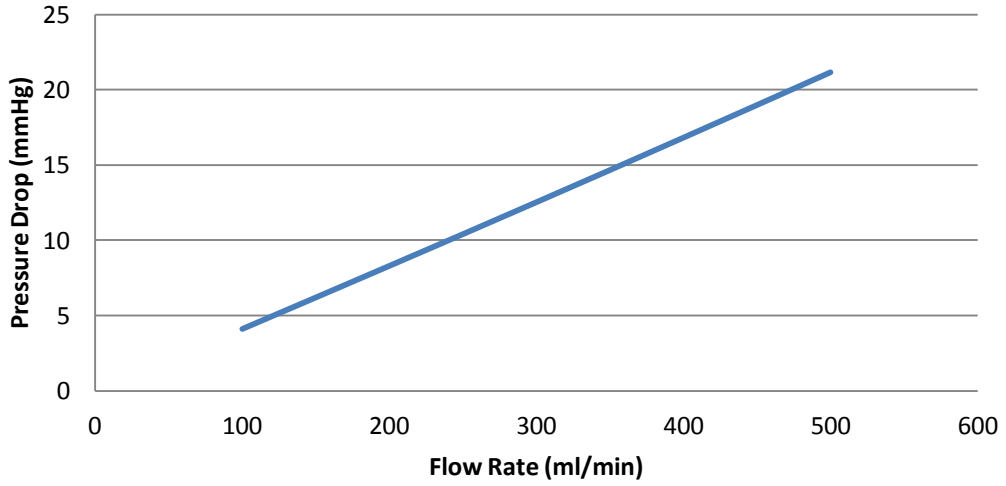


**Figure 220: Graph showing Pressure drop Vs. Flow rate for the Oxygenator flow path**

### *Discussion and Conclusions*

The results of this analysis give an indication of the pressure drop likely to occur over this module with a packing fraction of 65 % of fiber. When compared to the Medos hilite 800 LT the results show that the oxygenator concept geometry developed produces a reduced pressure drop of approximately 17 %. Figure 221, Figure 222 and Figure 223 below show contours of velocity at cross sections in the y axis at iso-surfaces of y = 0.04, y = 0.08 and x = 0 respectively at a flow rate of 500 ml/min.

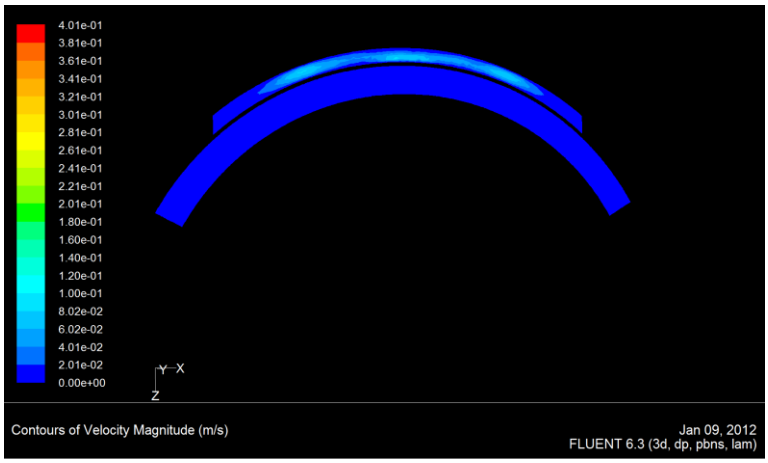


**Figure 221: Velocity contours across the module at an iso-surface of y = 0.04.**

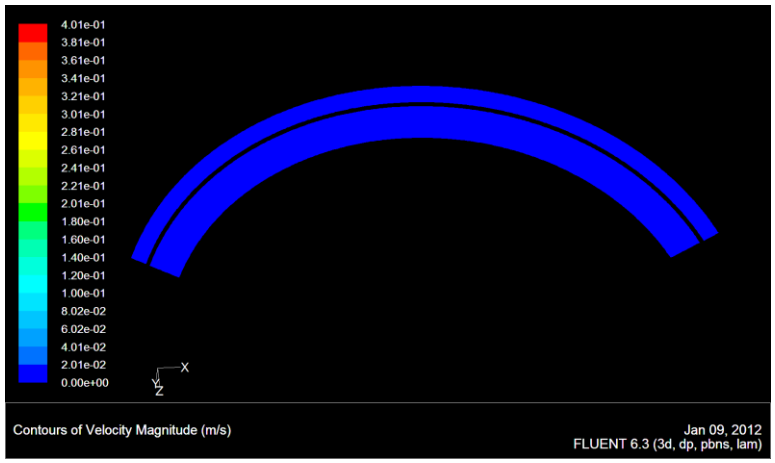


**Figure 222: Velocity contours across the module at an iso-surface of y = 0.08.**

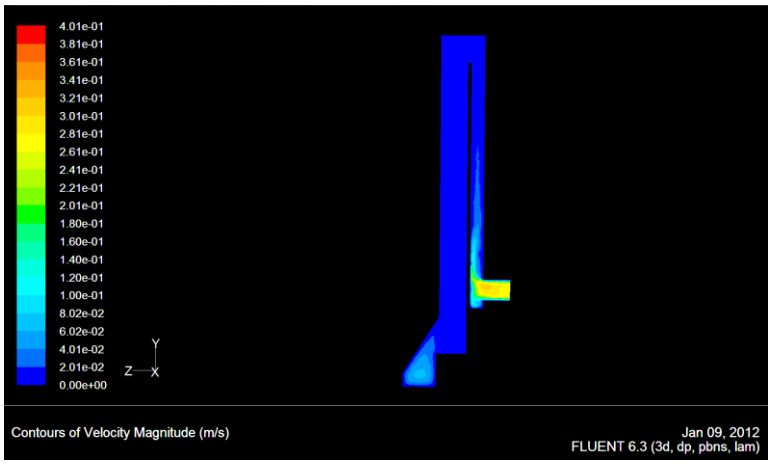


**Figure 223: Velocity contours across the module at an iso-surface of x = 0.**

The sharp change in cross-sectional area in moving from the inlet through the arc of the heat exchanger results in an un-even distribution of the flow as highlighted in Figure 221. Although this is the case in the initial stages of the exchanger the high resistance to flow, due to the porous media, acts to reduce fluid velocity and hence an even flow distribution is achieved prior to entry to the oxygenator module as shown within Figure 222 and Figure 223.

The fully integrated design of concept 3 positions the heat exchanger prior to the oxygenation module. To function efficiently the heat exchanger requires blood to be exposed over a certain cross-sectional area. As a result the radius of the arc of the oxygenator module is large and the concept geometry has almost twice the priming volume of the Medos Hilite 800 LT of 79 ml. This high priming volume could be reduced by limiting the thickness of the arc of the module; however at this stage in the design the manufacturing process is likely to be made considerably easier using a larger volume and so the higher priming volume was deemed an acceptable shot-term compromise. Overall the results of this CFD analysis were promising and suggest that the design chosen is suitable for physical prototyping to allow for further investigation.

## 5.10. Oxygenator Module Design

A physical prototype was developed based upon the geometry used in the CFD simulation previously conducted. The complicated geometry of the oxygenator module makes the design impractical for manufacture by conventional tooling methods. The most suitable method for manufacturing was therefore determined to be through rapid prototyping. Although this method allowed the complicated geometries to be successful produced, modifications to the design were required. As explained previously the rapid prototyping process used to manufacture the parts involves the use of a soft support material, which must be removed upon completion of the printing process. The use of this manufacturing process places some configuration restrictions on the design. In this case the main casing had to feature holes to facilitate the removal of support material from the internal structure, which in turn required plugs to ensure the module was sealed effectively.

The system was designed to be manufactured in six parts.

- The main body - including inlet, outlet and potting ports (Figure 224).


**Figure 224: ProEngineer model of the oxygenator main body.**

- Two plugs used to seal holes required to remove the support material used in the rapid prototyping process.

The holes and corresponding plugs can be seen within Figure 225 and Figure 226.

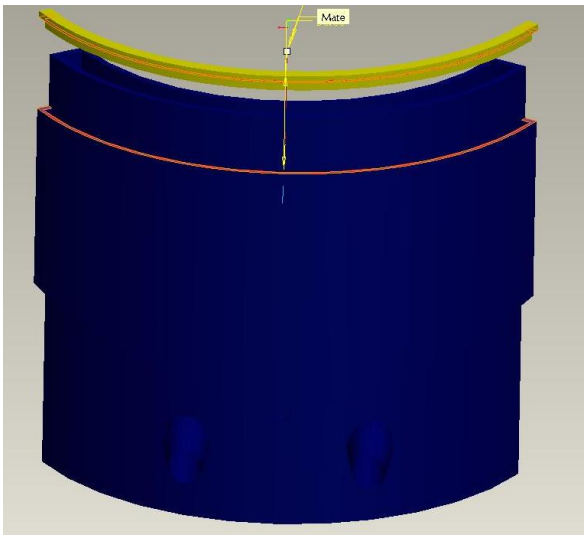


**Figure 225: ProEngineer model of the plug used to fill the support material removal hole at the inlet of the oxygenator module.**

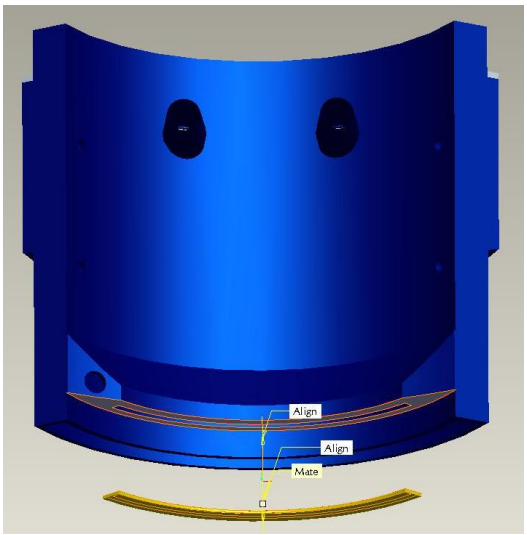


**Figure 226: ProEngineer model of the plug used to fill the support material removal hole at the outlet of the oxygenator module.**

- Two potting caps to cover the ends of the oxygenator during the potting process (Figure 227).

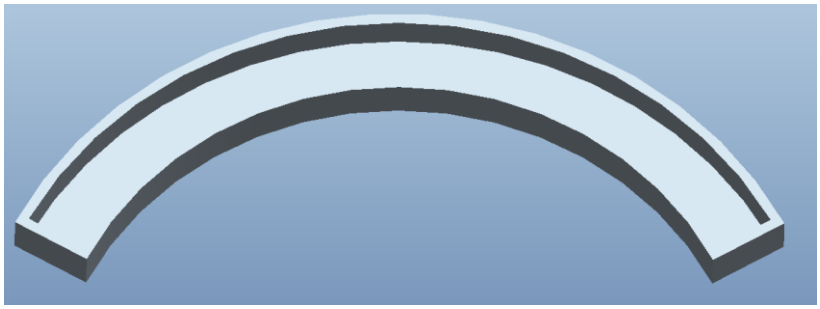

**Figure 227: ProEngineer model of the potting cap used to prevent leakage of compound during the potting process.**

- A gas cap to allow gas to enter the module (Figure 228).

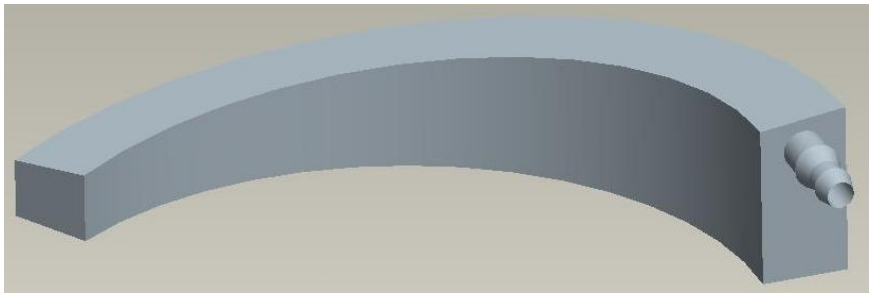

**Figure 228: ProEngineer model of the gas cap used on the module.**

The gas cap was designed with a slope from inlet to the far end of the oxygenator chamber. This cap encouraged gas to flow across the entire cross-section of the module resulting in an even gas flow distribution. Figure 229 shows an exploded view of all of the parts used in the operational oxygenator module.

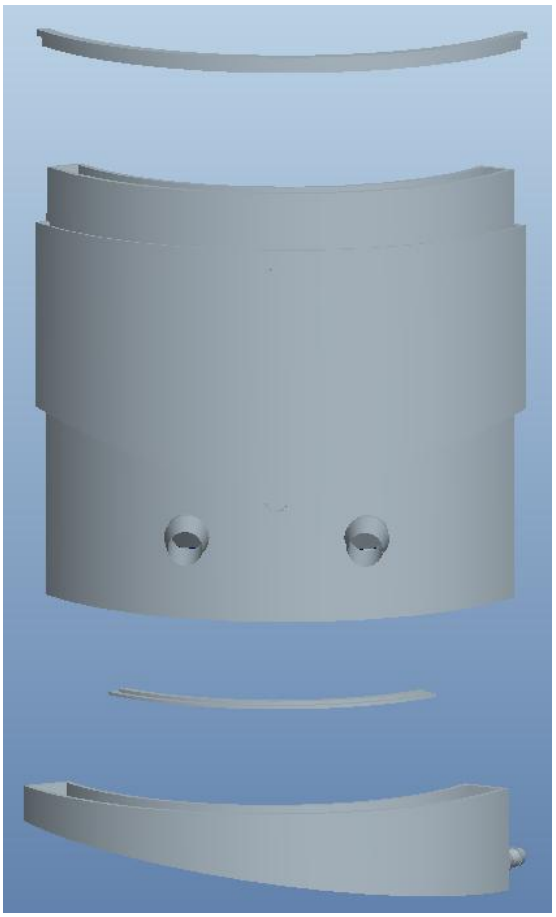

**Figure 229: ProEngineer model showing an exploded view of the operational oxygenator module.**

## 5.11. Mark I Oxygenator Device Manufacturing Process

The mark I oxygenator was manufactured using the following steps:

- Fiber mat was measured and cut into individual sections and placed within the module main body achieving a packing fraction of approximately 30 - 40 %.

- Both of the support material holes were sealed using the printed plugs. The plugs were sealed using Silicone adhesive (Dow Corning Toray Co., Ltd, Tokyo, Japan).

- The potting caps were lubricated and polyfilm was placed over each end of the oxygenator module. Caps were then put into place and secured using adhesive tape.

- Both of the modules were placed inside the modified washing machine centrifuge. A lower viscosity potting compound mixture – Texaflex 5396B (Texachem International, Novara, Italy). – was put into the potting compound holders and gravity fed into the oxygenator modules.

- The modules were then spun for 1 hour (15 cycles) using the prototype potting apparatus, after which they were removed and allowed to cure for 24 hours.

- The process was then repeated for the opposite end of the module.

- After both ends were potted and had cured the potting ports were removed and sealed using aluminium sheet and silicone adhesive.

- The potting caps and a 2 mm section of the modules were removed by band saw.

- The modules were then cut using a scalpel to open up the fibers.

- The gas cap was then placed on the module and sealed using silicone adhesive.

- Finally a hole was drilled in the upper section of the device and a male to male leur was placed in to allow for a purge tap to be fitted.

Although the lower viscosity potting compound successfully penetrated the fiber bundle, the rotational velocity of the washing machine did not result in a sufficient centrifugal force and a parabolic profile of potting compound was formed. As a temporary solution to this problem the modules were potted a second time to help produce a more even layer of potting compound. A further problem encountered was that the fiber mats moved during the spin cycle resulting in uneven distribution of the mats and larger areas for potential flow shunting. To solve this, holes were drilled into the casing and potting compound was injected to fill the cavities. Figure 230 below shows a picture of a completed module ready for testing in the laboratory.

**Figure 230: Rapid prototyped oxygenator potted and sealed ready for use in the lab.**

## 5.12. Mark I Oxygenator Performance Testing

### 5.10.1. Aims

The aim of this experiment was to determine the performance characteristics of the physical prototype developed.

### 5.10.2. Methods and materials

The principle components used to determine the performance characteristics of the system are shown within Figure 231.

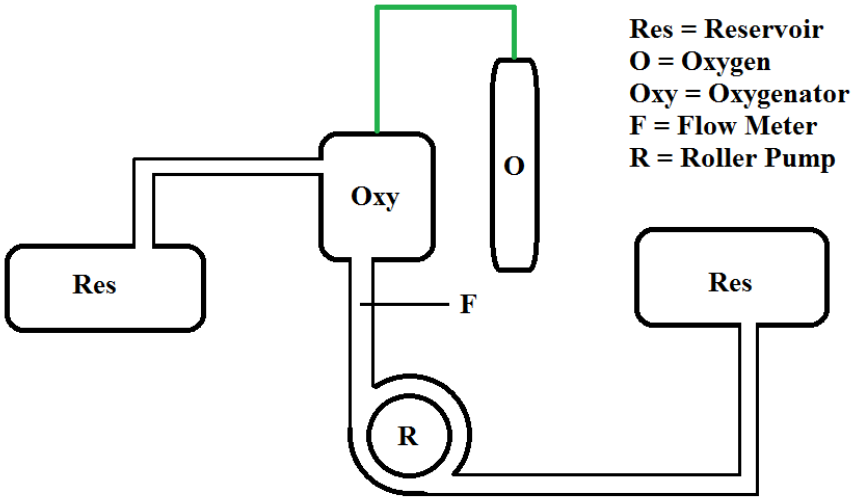


**Figure 231: Diagram of the principle components used in the performance testing of the oxygenator prototype.**

Bovine blood treated with 10 ml of 1000 IU/ml Heparin-sodium solution (Wockhardt, Mumbai, Maharashtra, India) was diluted with 0.9 % saline solution (Baxter, Berkshire, UK) to a haematocrit of 36 % and warmed to 37 $^{0}$C. To ensure the oxygenator was sealed properly the blood path was tested by running saline through the device and the gas path was tested by submersing the module in a water tank.

The module was held between two clamp stands over a drip tray. Oxygen was provided via pressurised cylinder and the flow rate was regulated using a Sechrist gas blender (SECHRIST Industries Inc., California, USA). A roller pump (Stöckert Instruments, Munich, Germany) was used to pump the blood through the system. Blood samples were taken and analysed in a Rapidlab 865 blood gas analyser (Novartis Vaccine and Diagnostics, California, USA).

An initial control value was taken from the blood reservoir. Blood was then pumped through the system at a flow rate of 100 ml/min. After the system was successfully primed three blood samples were taken at a rate of one per minute. This was repeated at a flow rate of 300 and 500 ml/min. The entire experiment was repeated six times. Figure 232 below shows an oxygenator column being tested within the lab.

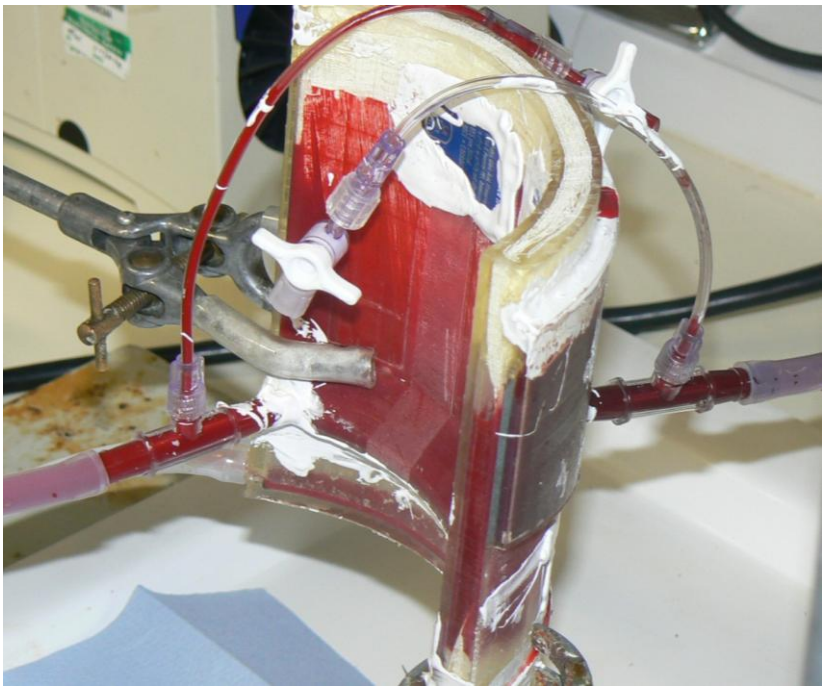

**Figure 232: Picture of the initial rapid-prototype oxygenator design being tested in the lab.**

### 5.10.3. Results

The most suitable characteristic to evaluate the performance of the oxygenators was determined to be the partial pressure of oxygen and carbon dioxide in the blood. These values give an indication of the oxygenation and carbon dioxide removal that occurs as the blood passes through the module. Figure 233 and Figure 234 below show oxygen partial pressure and carbon dioxide partial pressure against blood flow rate for each of the oxygenation modules tested (n=6).

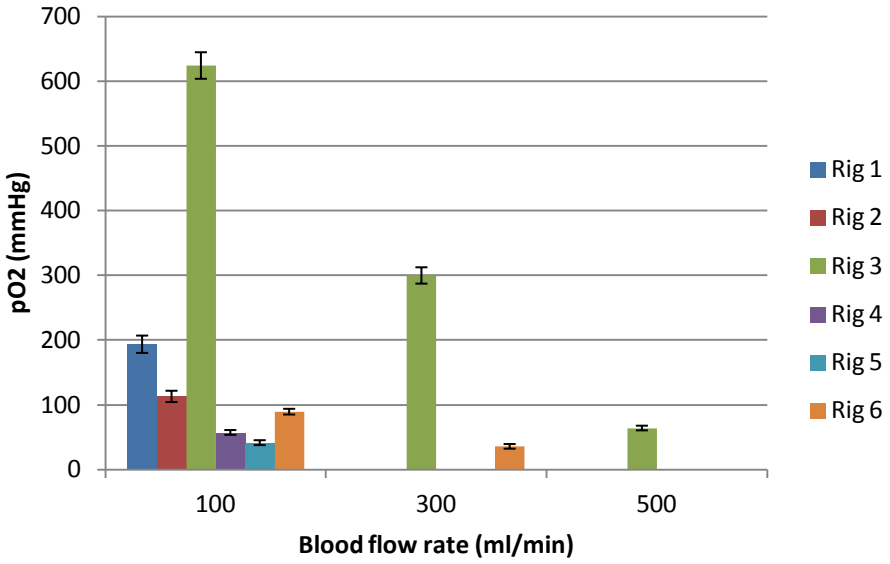


**Figure 233: Oxygen partial pressure against blood flow rate for six of the Concept 3 geometry oxygenators. ± 1 Standard Deviation.**

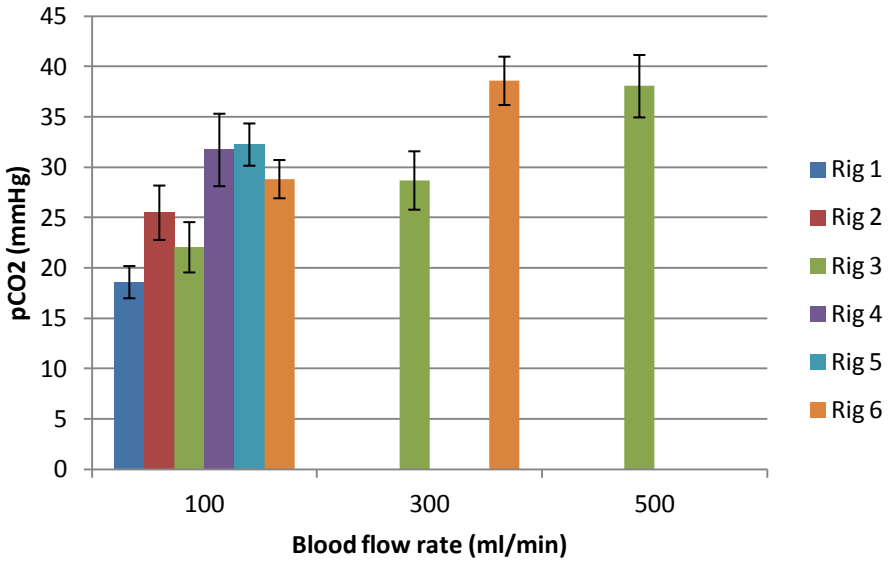


**Figure 234: Carbon dioxide partial pressure against blood flow rate for six of the Concept 3 geometry oxygenators. ± 1 Standard Deviation.**

Modules 1, 2, 4, 5 and 6 do not have full data sets as experiments were terminated after poor performance.

### 5.10.4. Discussion

The results of this experiment show that consistent, adequate performance could not be achieved using this configuration with only one in six oxygenators able to produce reasonable and consistent results. In the majority of cases the poor performance could be attributed to insufficient packing fraction and uneven fiber distribution and as a result shunting within the device. Figure 235 and Figure 236 below show areas of bright oxygenated and dark un-oxygenated blood in the main casing and in the outlet of the oxygenator respectively confirming that shunting of the flow was indeed occurring within the modules.


**Figure 235: A picture of bright oxygenated blood next to dark un-oxygenated blood in the main casing confirming the presence of flow shunting in the oxygenator module.**

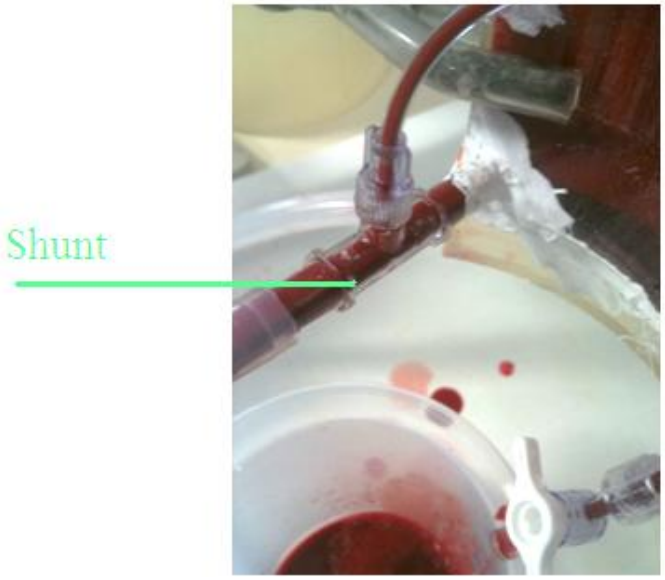


**Figure 236: A picture of bright oxygenated blood next to dark un-oxygenated blood at the outlet confirming the presence of flow shunting in the oxygenator module.**

The curved geometry of the concept made effective packing of the fibers particularly difficult. As a result a poor packing fraction was achieved with the fibers unevenly

distributed in the module. As the module was potted the uneven distribution of fibers offered varying resistance to the flow of the potting compound. The modified washing machine used as a centrifuge was only capable of a maximum 600 r.p.m. The combination of varying resistance within the module, the high viscosity of the potting compound and the limited centrifugal force provided resulted in an overall poor quality of potting. In several cases a second potting run was required to produce a more even distribution of compound. The lack of quality control in the manufacturing process combined with the low packing fraction of fibers resulted in oxygenator modules that were particularly susceptible to shunting. To investigate the potential effect of shunting of the flow on module performance a CFD analysis was run using the previously established porous media model.

## *CFD Evaluation of the Mark I Oxygenator*

### *Aims*

The aims of this analysis were to determine effect of shunting on the performance of the concept oxygenator module and to evaluate the sensitivity of the geometry to shunting.

### *Methods*

The porous media model previously established was modified by splitting the porous volume into three. The shunt was placed at the center of the arc, where the poorest fiber packing and distribution was observed in the physical prototypes. Figure 237 below shows an assembly of the three volumes with the shunt highlighted in yellow.

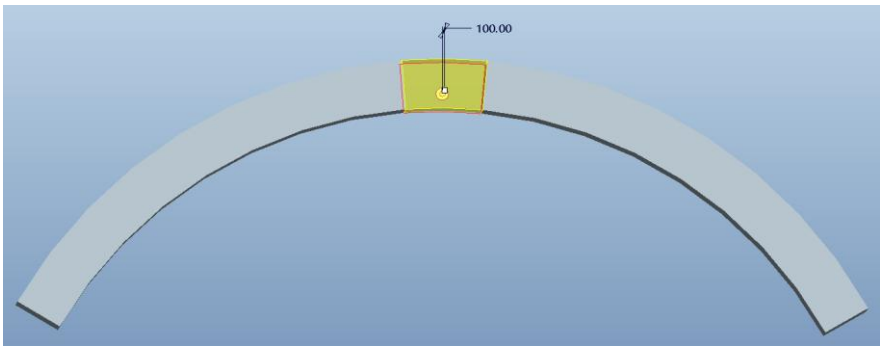


**Figure 237: ProEngineer model highlighting the position of the shunt (in yellow) in the oxygenator porous media volume.**

The middle volume was defined as non-porous to act as a void zone to encourage shunting of the flow. Several models were constructed with void zones of 0.5, 1, 2.5, 5 and 10 % of the total porous volume. Each model was imported into gambit and meshed as an assembly of several volumes to allow the porous media to be characterized individually. The most suitable mesh of the complete model was found to be a tetrahedral/hexagonal element hybrid mesh of 1,147,530 nodes.

CFD analysis was run using Fluent Inc., Fluent version 6.3.26. Boundary conditions were set as a constant velocity providing a flow of 100 ml/min at the domain inlet with the outlet set as constant pressure. The same porous media model as used in the previous analysis was adopted here. Steady laminar flow was assumed in all cases with blood modelled as Newtonian with a constant viscosity of 0.0035 (Pa.s) and a density of 1050 ($kg.m^{-3}$). The simulation was repeated to at flow rates of 300 and 500 ml/min.

### *Results*

The most important performance characteristics in this analysis were determined to be the percentage of total flow that passed through the shunt and the corresponding pressure drop across the module. The percentage of flow passing through the shut represents the

volume of un-oxygenated blood due to shunting. The corresponding reduction in pressure drop can also be used to indicate the severity of shunting within the module. Figure 238 and Figure 239 below show percentage flow rate through the shunt and pressure drop versus percentage of shunt volume to total volume respectively.

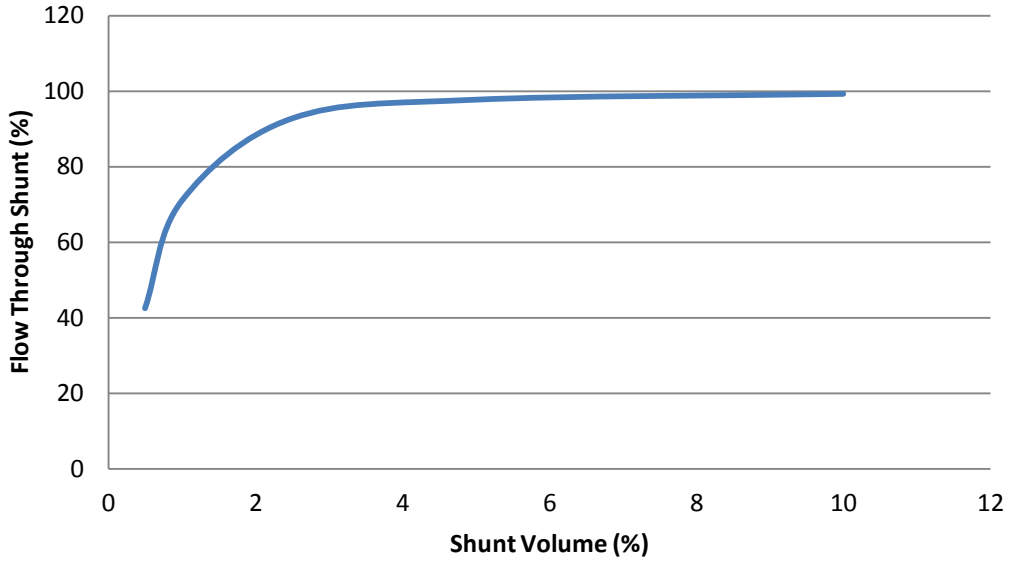


**Figure 238: Graph showing percentage flow rate through the shunt versus percentage of shunt volume to total volume.**

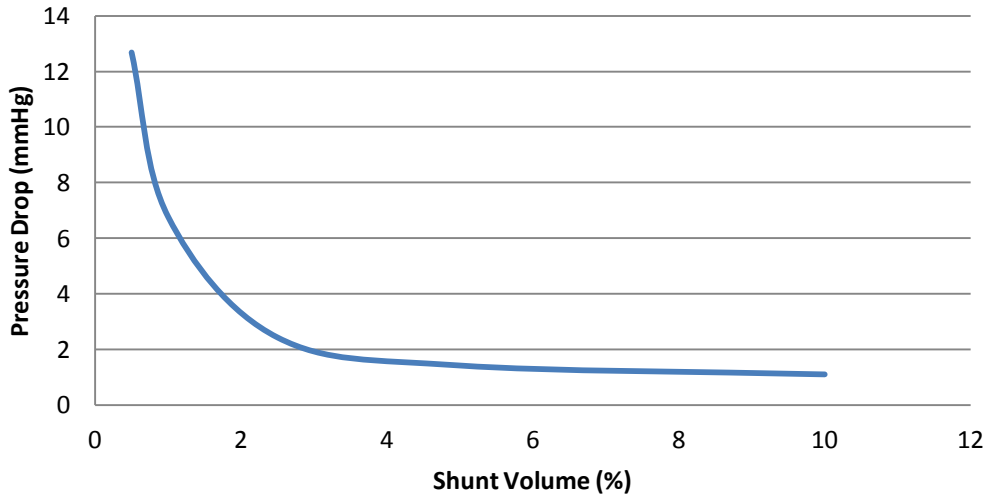


**Figure 239: Graph showing pressure drop versus percentage of shunt volume to total volume.**

## *Discussion and Conclusions*

Shunting is a common problem in oxygenator production. The severity of the problem depends upon several factors:

- Shunt volume
- Shunt orientation
- Shunt location
- Oxygenator geometry
- Fluid flow path through the oxygenator
- Pressure drop across the oxygenator.

This CFD simulation has shown that for this specific geometry with the shunt at the center of the arc the oxygenator is particularly sensitive to flow shunting. Very slight shunts can have a dramatic effect on the oxygenator performance.

Increasing flow rate results in an increasing pressure drop across the module. A higher pressure drop makes the system more susceptible to shunting as a higher percentage of the flow will be diverted through the shunt. This effect was observed in the physical experiment with the most substantial oxygenation and carbon dioxide removal observed at the lower flow rate of 100 ml/min.

Fluid exiting the pump system enters the heat exchanger at the center of the device. The fluid then undergoes a dramatic change in cross-sectional area. This configuration is such that jetting of the flow is encouraged up the center of the arc; however in the presence of an evenly distributed fiber mat with uniform resistance to flow jetting of the fluid is eliminated. In the case of a non-uniformly distributed fiber mat, particularly one with shunt volumes at the center of the arc, the geometry of the oxygenator is likely to encourage flow up the center hence making the oxygenator more sensitive to shunting.

### 5.10.5. Conclusions

The initial CFD analysis conducted on the oxygenator suggested that with an effective packing fraction and distributed fiber mat an even flow field throughout the column would be achieved; however the manufacturing process used proved to be particularly difficult and the results of the physical experimentation showed that despite measures taken to mitigate the problems encountered the majority of the oxygenators failed through shunting of the flow. To produce an efficient and effective oxygenator suitable packing fraction and distribution of fibers within the module is essential. The limitations of the laboratory environment used to produce the oxygenators were such that a manual manufacturing process was required. The curved geometry of the concept design has been shown to be impractical, further complicating an already challenging manufacturing process.

A complete redesign of the oxygenator module is required. The results of this experiment suggest that by addressing the packing fraction and fiber distribution in the modules the performance of the oxygenators can be considerably improved. To do this the oxygenator redesigned must be such that it more realistically addresses the limitations of a manual manufacturing process in order to produce a higher level of quality and consistency.

## 5.13. Mark II Oxygenator Device Redesign

The foundation design upon which the mark I oxygenator was based was one that focused upon integration of the oxygenator with other miniaturized components to aid the post development integration stage. However it was clear from the testing conducted that a radical redesign was required. The previous configuration was complicated to manufacture and failed to meet acceptable performance standards. For these reasons the redesign of the oxygenator will move away from the foundation concept towards a more conventional design.

The design requirements for the mark II oxygenator device are as follows:

1. Redesign the oxygenator geometry in order to enhance performance by improving the fluid flow path through the device. A more even fluid distribution is required to enhance the exposure of the blood to the hollow fibers and to reduce the sensitivity of the device to shunting.

2. Design for improved manufacturing with a focus on increasing the packing fraction and to improve on the distribution of the potting compound by having the compound fed into the module under pressure rather than through gravity.

Figure 240 below shows a ProEngineer drawing of the proposed mark II oxygenator redesign.

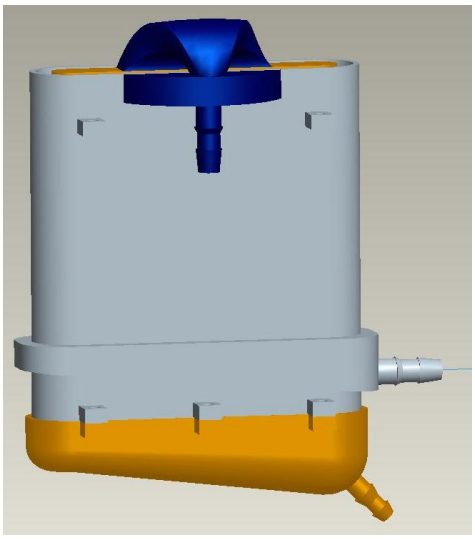

**Figure 240: ProEngineer model of the assembled components of the mark II oxygenator device design.**

The redesign focused on producing a more conventional configuration based upon Concept 2 of Chapter 2 – concept development. The main body of this design features a rounded rectangular shape, which is ideal for mounting the other aspects of the system.

A sparger was used in this design to improve on the fluid distribution throughout the module, encouraging more thorough penetration of the fiber bundle, increasing the opportunity for diffusion. The sparger also provides an internal structure about which the hollow fiber mat can be wound. This should simplify the manufacturing process and allow for increased packing fraction with improved fiber distribution. To overcome the increased resistance to flow due to the higher packing fraction the potting feeding tubes were resized to fit the outlet of a syringe and placed on both sides of the oxygenator. This allowed pressure to be applied to the compound to improve on the volume and distribution of potting compound in the module.

## 5.14. Mark II Oxygenator Device Manufacturing Process

The oxygenator was designed in five parts:

- Oxygenator main casing (Figure 241)

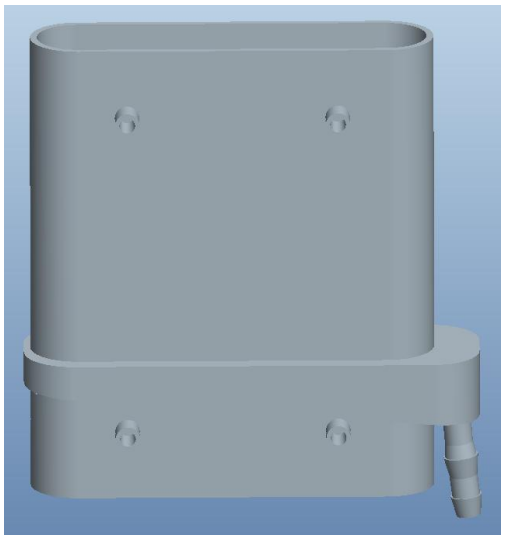

**Figure 241: Mark II oxygenator main casing.**

- Sparger with potting cap connected (Figure 242)

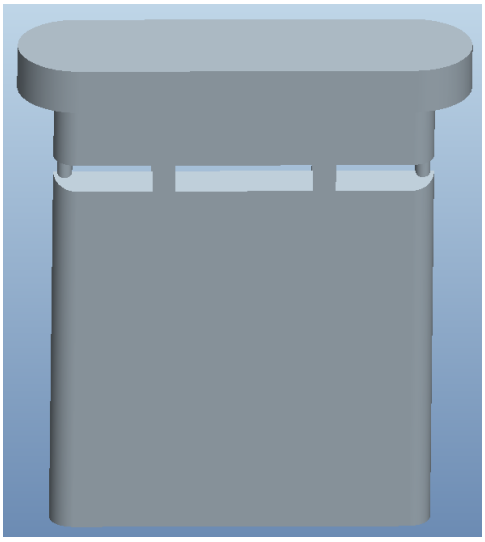

**Figure 242: Mark II sparger with potting cap.**

- Potting cap (Figure 243)

**Figure 243: Mark II potting cap**

- Gas cap (Figure 244)

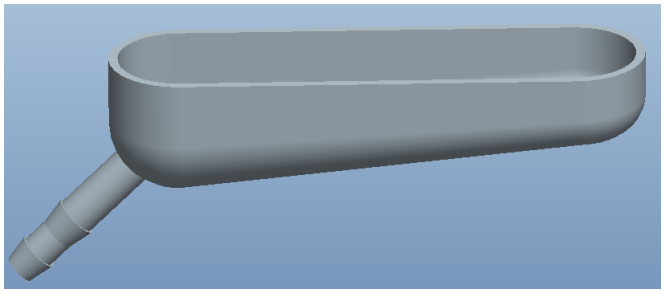

**Figure 244: Mark II gas cap.**

- Inlet port to sparger.

This part was specifically designed for testing of the rig. It features a ¼ inch tubing connection and has an interface section that fits into the sparger, to encourage a tight fit and allow the module to be easily sealed. The design can be seen within Figure 245 below.

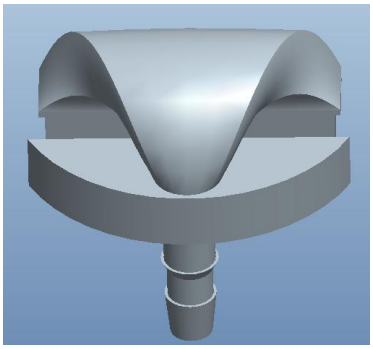

**Figure 245: Mark II inlet port to the sparger.**

The manufacturing process used to construct this module was as follows:

- The fiber mat was measured and cut to size in one continuous length. One end of the mat was taped to the sparger and then was wrapped around it. The mat was kept as taught as possible during wrapping to maximize packing fraction. The mat and sparger were then inserted into the module. Figure 246, Figure 247 and Figure 248 below show the rapid prototyped sparger, the sparger with fibers wrapped around it and the sparger with fibers in the main casing respectively.

**Figure 246: Rapid prototyped Mark II sparger.**

**Figure 247: Mark II sparger with hollow fiber membrane mat wrapped around it.**

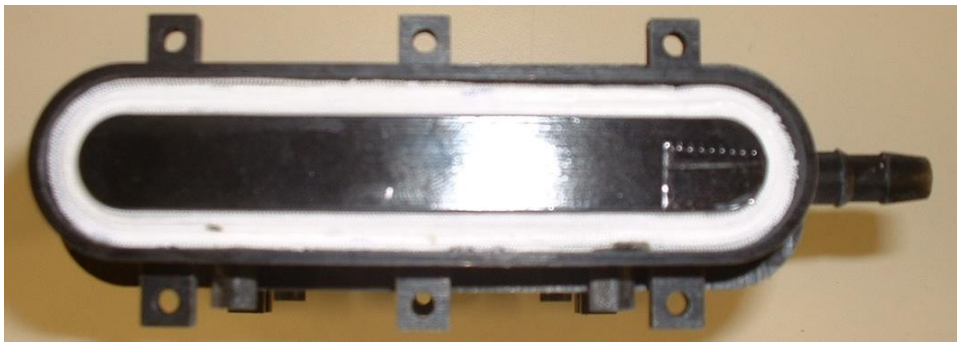

**Figure 248: Sparger and fiber mat in place within the Mark II main casing.**

- The other potting cap was glued into place using silicon adhesive (Dow Corning Toray co., LTD, Tokyo, Japan) and the modules were placed within the modified centrifuge.

- The potting compound used was TEXAFLEX 5394 A and 5396 B (Texachem International, Novara, Italy), which was the lowest viscosity mixture that Texachem offer. As the sparger was hollow, to prevent potting compound entering it during the potting stage the compound it was inserted in four parts.

Firstly 2.5 ml was inserted into left and right ports on the front of the module then the module was spun for 4 minutes. It was then flipped and the same volume of compound was inserted in the ports on the rear face of the module. This process was repeated again on each side to make a total of 20 ml of compound.

- The modules were spun for 1 hour (15 cycles) and then removed and allowed to cure for 24 hours.

- The potting process was then repeated for the opposite end of the module.

- Approximately 3 mm of material was then removed from each end of the module using a band saw and the sides of the potting caps ground away. This left the sparger open and free of potting compound. Figure 249 shows a cross-section of the oxygenator module with the top of the sparger removed, leaving the middle of the sparger "floating" in the module supported by the potting compound.

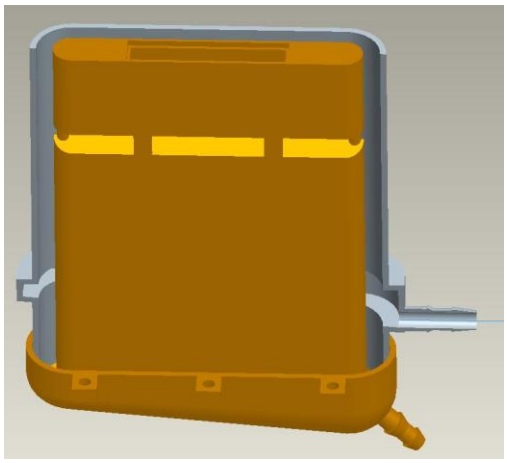

**Figure 249: ProEngineer of the sparger within the main casing after the top has been removed to leave the sparger "floating" in the main casing supported by potting compound.**

- A thin layer of potting compound was then removed from each end of the module using a scalpel to open up the fibers.

- Silicon adhesive was placed around the inlet-sparger intersection and the inlet was inserted in place. More adhesive was added around the top of the inlet to ensure that the part was sufficiently sealed.

- The gas cap was put on to the bottom of the module and sealed using silicon adhesive.

Figure 250 and Figure 251 below show a cross-section of the complete Mark II oxygenator configuration in ProEngineer and the assembled rapid prototyped system ready for use in the laboratory respectively.

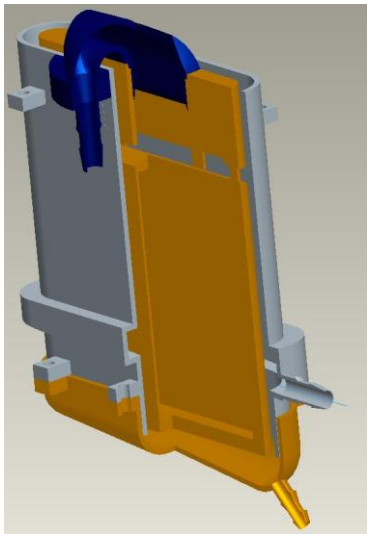

**Figure 250: ProEngineer model of the sparger suspended within the module.**

**Figure 251: Complete rapid prototyped model constructed and ready for use in the laboratory.**

## 5.15. CFD of the Mark II Design

### *Aims*

The aims of this analysis were to determine the performance characteristics of the redesigned oxygenator, the influence of sparger volume on performance and the sensitivity of the design to flow shunting.

### *Methods*

Two flow paths were created based upon the redesigned concept geometry; one with a 3 mm sparger and one with an 8 mm sparger. To determine the effect of shunting each model was remade with the porous media split into two volumes with a shunt of 0.5, 1,

2.5, 5 and 10 % of the total porous media volume created. Figure 252 below shows the 8 mm sparger with 10 % total volume shunt.

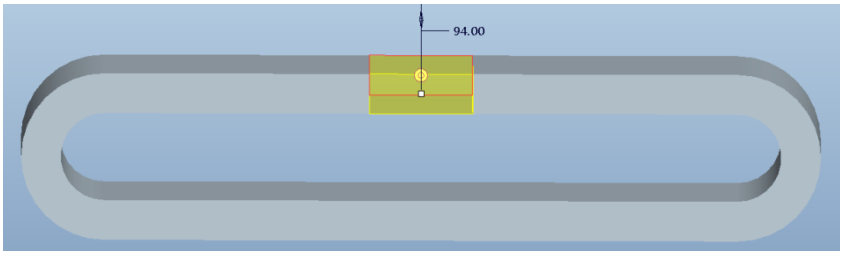


**Figure 252: ProEngineer model showing the location of the shunt volume used to determine the effect of shunting on the Mark II geometry, in this case the 8 mm sparger model.**

Both models were imported into Gambit and meshed. The most suitable mesh was found to be a tetrahedral/hexagonal element hybrid mesh of 913,843 nodes for the 3 mm sparger and 993,179 nodes for the 8 mm sparger. Figure 253 below shows the mesh for the 3 mm sparger.

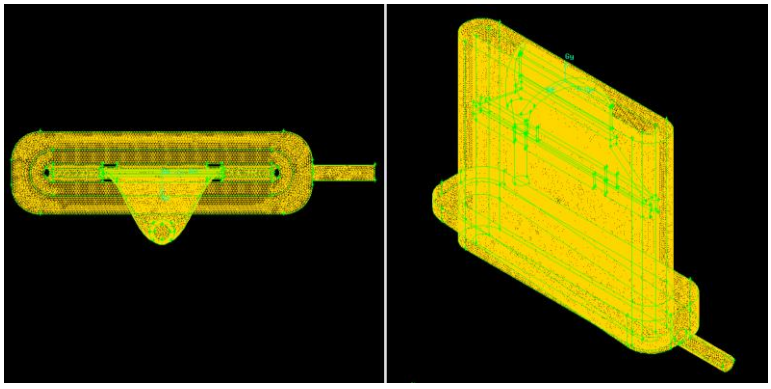

**Figure 253: Gambit mesh of the Mark II oxygenator geometry, in this case the 3 mm sparger flow path.**

CFD analysis was run using Fluent Inc., Fluent version 6.3.26.

Boundary conditions were set as a constant velocity at the domain inlet with the outlet set as constant pressure. Steady laminar flow was assumed in all cases with blood modelled as Newtonian with a constant viscosity of 0.0035 (Pa.s) and a density of 1050

(kg.m$^{-3}$). The porous media model used was the same as that for the previous CFD analyses run with a packing fraction of 66 % fibre. The analysis was run at 100, 300 and 500 ml/min for both models without shunt and at 500 ml/min for each of the designs with a shunt.

### *Results*

To allow for a comparison with the previous CFD simulation conducted on the Medos Hilite 800 LT pressure drop against increasing flow rate for each model is given within Figure 254 below.

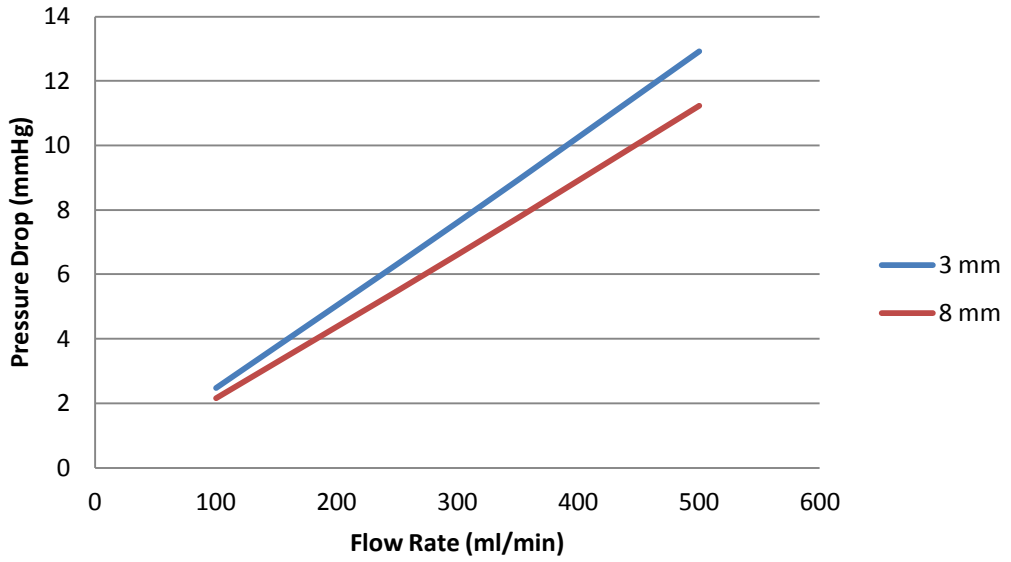


**Figure 254: Graph showing Pressure drop Vs. Flow rate for the Mark II oxygenator flow path in 3 mm and 8 mm configurations.**

Percentage flow rate through and pressure drop across the oxygenator module versus percentage of shunt volume to total volume for the Mark I and the 3 mm and 8 mm Mark II oxygenators is given within
Figure 255 and Figure 256 respectively.

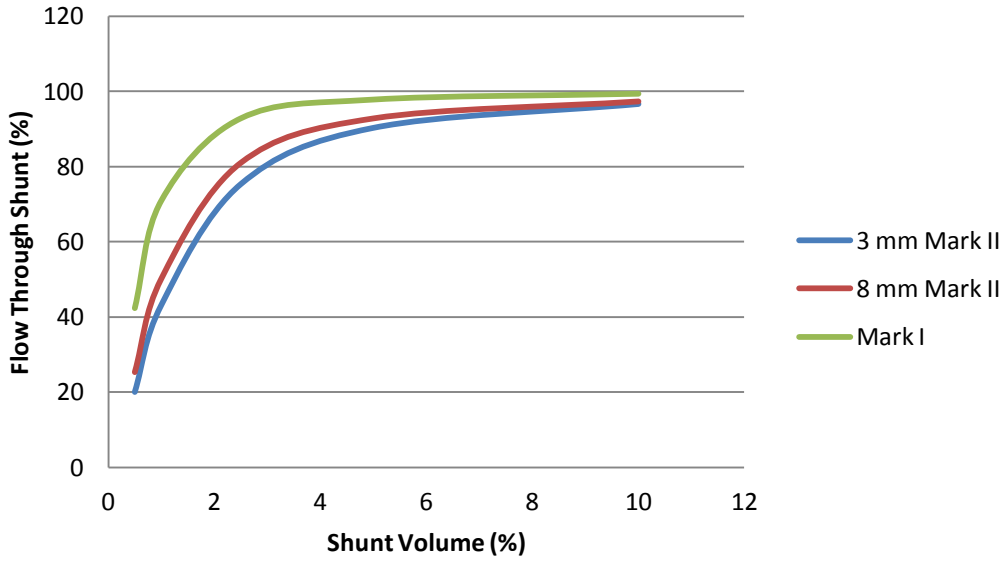


**Figure 255: Graph of percentage flow rate through the shunt vs. percentage shunt volume of total volume for the Mark I and the 3 mm and 8 mm Mark II oxygenators.**

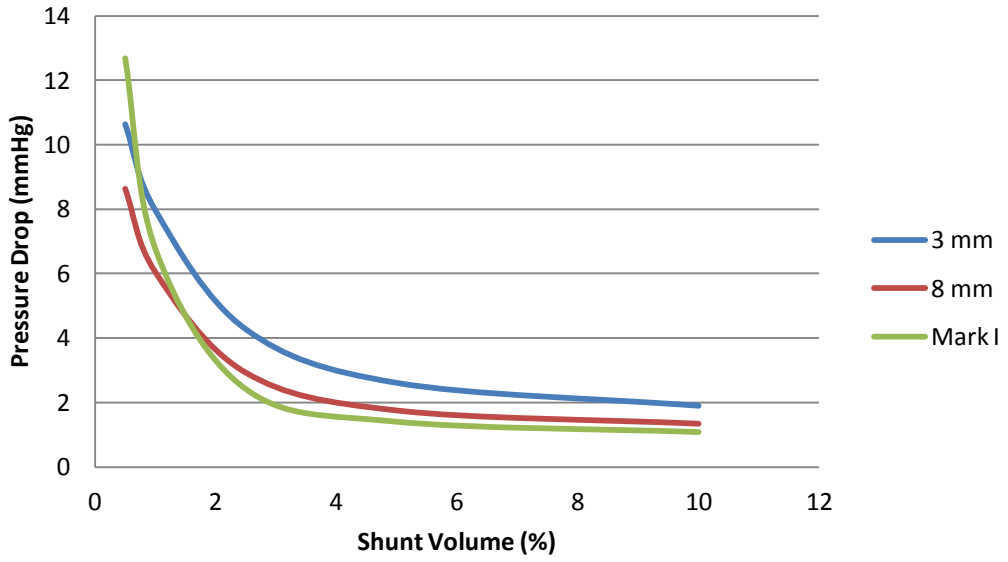


**Figure 256: Graph of pressure drop vs. percentage shunt volume of total volume for the Mark I and the 3 mm and 8 mm mark II oxygenators.**

### *Discussion and Conclusions*

The results of this analysis show that compared to the Mark I design there is a reduced pressure drop for both the 3 mm and 8 mm sparger designs. The 3 mm sparger, due to the reduced cross-section at the oxygenator inlet has a slightly higher pressure drop than the 8 mm. Figure 257, Figure 258, Figure 259, Figure 260, Figure 261 and Figure 262 below show velocity contours at iso surfaces of x = 0, y =-0.034 and y = -0.05 for the 3 mm and 8 mm modules respectively.

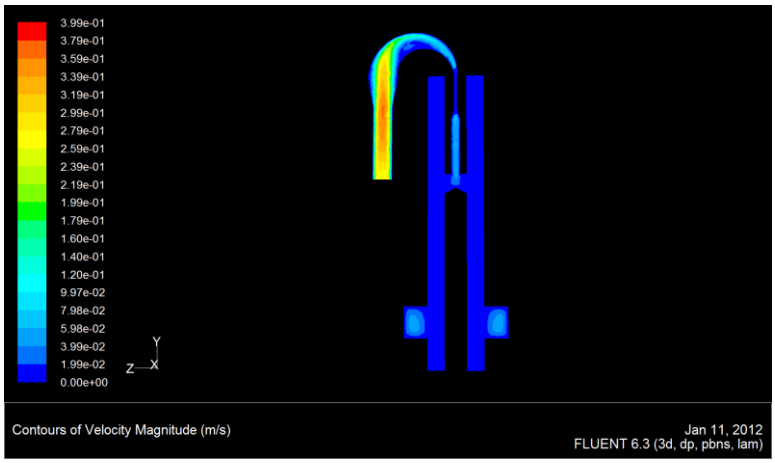


**Figure 257: Velocity contours at iso-surface x = 0 for the 3 mm mark II oxygenator.**

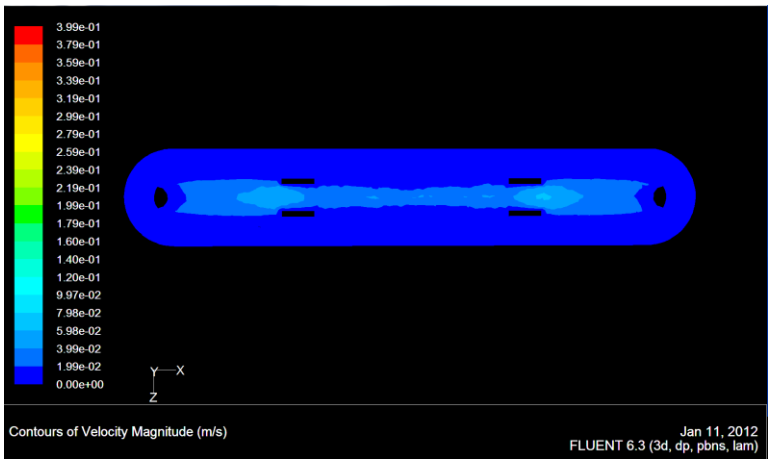


**Figure 258: Velocity contours at iso-surface y= - 0.034 for the 3 mm mark II oxygenator.**

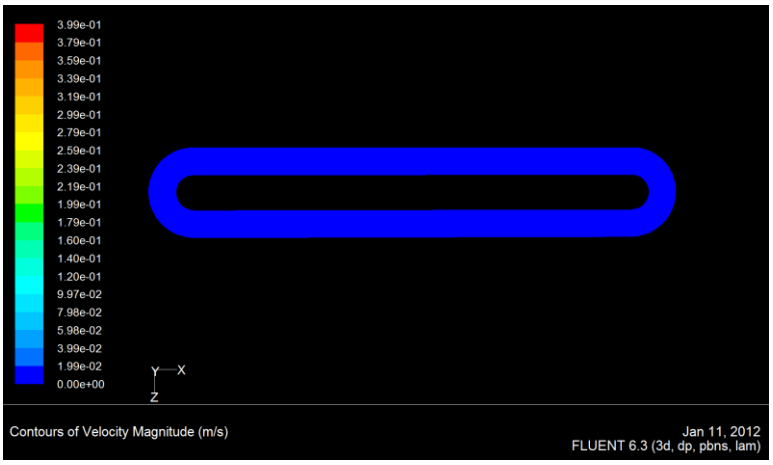


**Figure 259: Velocity contours at iso-surface y= - 0.05 for the 3 mm mark II oxygenator.**

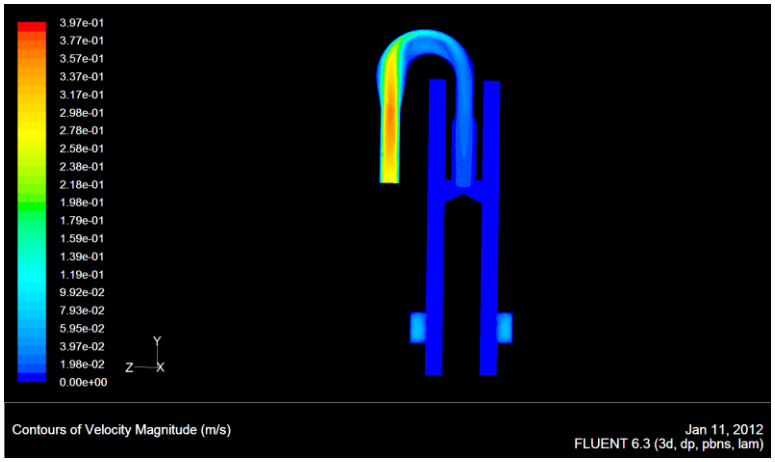


**Figure 260: Velocity contours at iso-surface x = 0 for the 8 mm mark II oxygenator.**

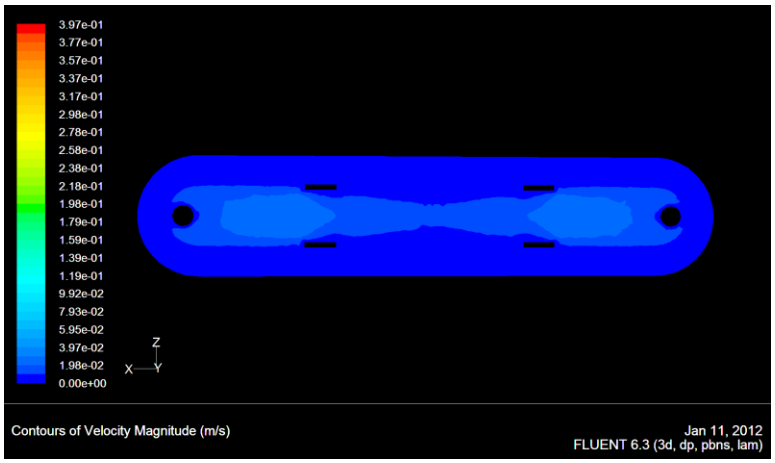


**Figure 261: Velocity contours at iso-surface y= - 0.034 for the 8 mm mark II oxygenator.**

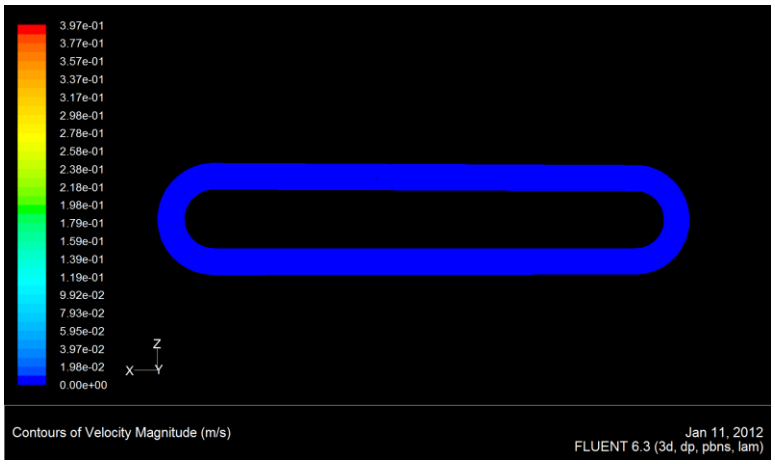


**Figure 262: Velocity contours at iso-surface y = -0.05 for the 8 mm mark II oxygenator.**

These contour diagrams show that uniform velocity distribution is achieved in both modules at the inlet to and throughout the porous media. The uniform flow field of the Mark II oxygenators makes the design less sensitive to flow shunting when compared to the Mark I design as highlighted within Figure 255.

This analysis therefore suggests that the Mark II design should be capable of producing a higher consistency and level of quality when compared with the Mark I design.

## 5.16. Oxygenator Mark II Testing

### 5.14.1. Aims

The aims of this experiment were to determine the performance characteristics of the Mark II oxygenator, and the most suitable inlet configuration and packing fraction of fibres.

### 5.14.2. Methods and materials

Nine modules were tested within this experiment. The first two modules (oxygenator 1 - 3) featured a 3 mm width sparger, with 3.1 m of fibre mat within the column giving a packing fraction of 70.1 %. The next three (oxygenator 4 - 6) modules featured spargers of 8 mm width with 4 m of fibre mat and the final three (oxygenator 7 – 9) with 4.6 m of mat giving packing fractions of 75.4 and 79.8 % respectively.

Bovine blood treated with 10 ml of 1000 IU/ml Heparin-sodium solution (Wockhardt, Mumbai, Maharashtra, India) used was diluted with 0.9 % saline solution (Baxter, Berkshire, UK) to a haematocrit of 36 % and warmed to 37 $^{0}$C by submersing the container within a water bath (Fisher Scientific, Essex, UK). To ensure the oxygenator was sealed properly the blood path was tested by running saline through the device and the gas path was tested by submersing the module in a water tank.

In common with previous tests the module was held between two clamp stands over a drip tray. Oxygen was provided via pressurised cylinder and the flow rate was measured by a gas flow meter (SECHRIST Industries Inc., California, USA). A Caps roller pump (Stöckert Instruments, Munich, Germany) was used to pump the blood through the system. Blood samples were taken and analysed in a Rapidlab 865 blood gas analyser (Novartis Vaccine and Diagnostics, California, USA). An arterial filter was placed in

the system pre-oxygenator. Pressure monitors were placed pre and post oxygenator with pressure constantly monitored throughout the experiment.

Initially a control value was taken from the blood supply. Blood was then pumped through the system at a flow rate of 100 ml/min. After the system was successfully primed three blood samples were taken at a rate of one per minute. This was repeated at a flow rate of 300 and 500 ml/min. Figure 263 below shows the set-up of the experiment within the lab. Blood samples for haemolysis testing were taken pre and post oxygenator for each flow rate during the testing of the fifth oxygenator.

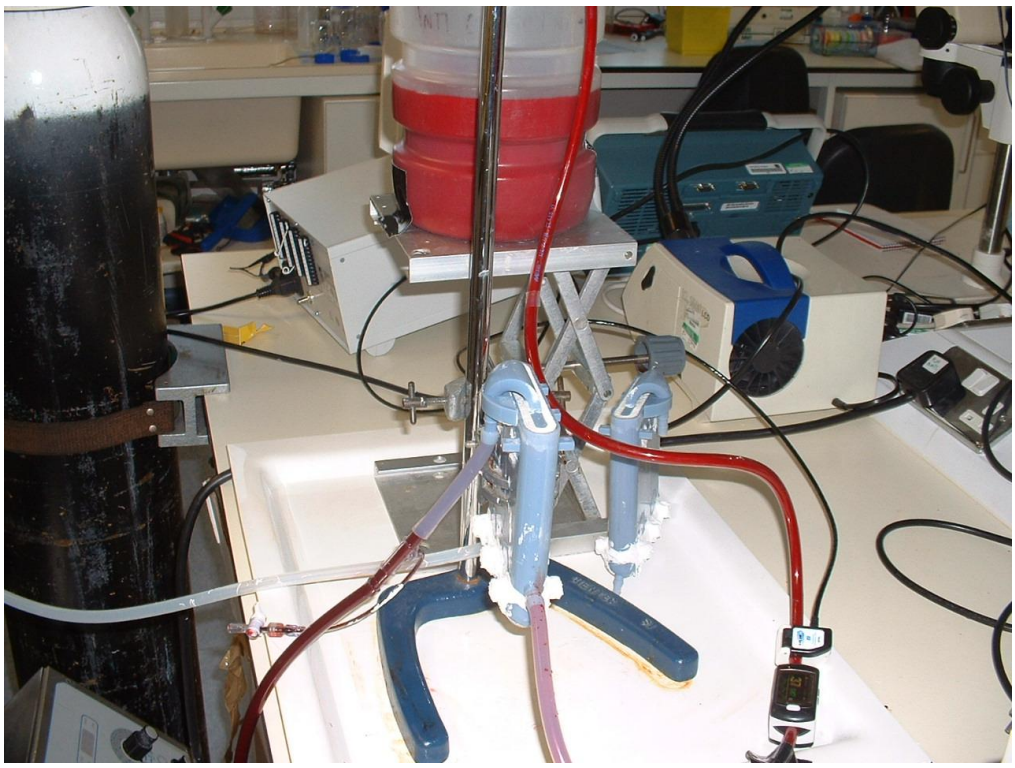

**Figure 263: Picture of the initial rapid-prototype oxygenation column testing within the lab.**

To allow comparison with a commercial oxygenator the oxygen gas transfer rates were calculated using Equation 13.

$$Oxygen\ Transfer\ Rate = Q(C_aO_2 - C_vO_2)\ (\text{mlO}_2\text{/L Blood})$$

**Equation 13: Gas transfer equation used to calculate the oxygen transfer rates occurring throughout the oxygenator experiments.**

Where:

Q = Blood flow rate
$C_aO_2$ = blood $O_2$ content calculated at the outlet (ml.$O_2$/L.Blood)
$C_vO_2$ = blood $O_2$ content calculated at the inlet (ml.$O_2$/L.Blood)

Outlet and inlet blood $O_2$ content are defined by Equation 14 and Equation 15 respectively (assuming total haemoglobin concentration of 12 g/dL):

$$C_aO_2\left(\frac{mlO_2}{LBlood}\right) = \left(1.2\left(\frac{gHb}{100mlBlood}\right) * 1.34\left(\frac{\frac{mlO_2}{gHb}}{\frac{1000mlBlood}{LBlood}}\right) * O_2Sat_a(\%)\right) + (PO_{2a}(mmHg) * 0.00314\left(\frac{mlO_2}{LBlood}\right))$$

**Equation 14: Blood $O_2$ content calculated at the outlet. *Taken from FDA guidelines (501k) for oxygen gas transfer in a membrane oxygenator.**

$$C_vO_2\left(\frac{mlO_2}{LBlood}\right) = \left(1.2\left(\frac{gHb}{100mlBlood}\right) * 1.34\left(\frac{\frac{mlO_2}{gHb}}{\frac{1000mlBlood}{LBlood}}\right) * O_2Sat_v(\%)\right) + (PO_{2v}(mmHg) * 0.00314\left(\frac{mlO_2}{LBlood}\right))$$

**Equation 15: Blood $O_2$ content calculated at the inlet. *Taken from FDA guidelines for oxygen gas transfer in a membrane oxygenator.**

### 5.14.3. Results

Figure 264, Figure 265, Figure 266 and Figure 267 below show oxygen partial pressure, carbon dioxide partial pressure, oxygen saturation and pressure drop for each of the modules tested.

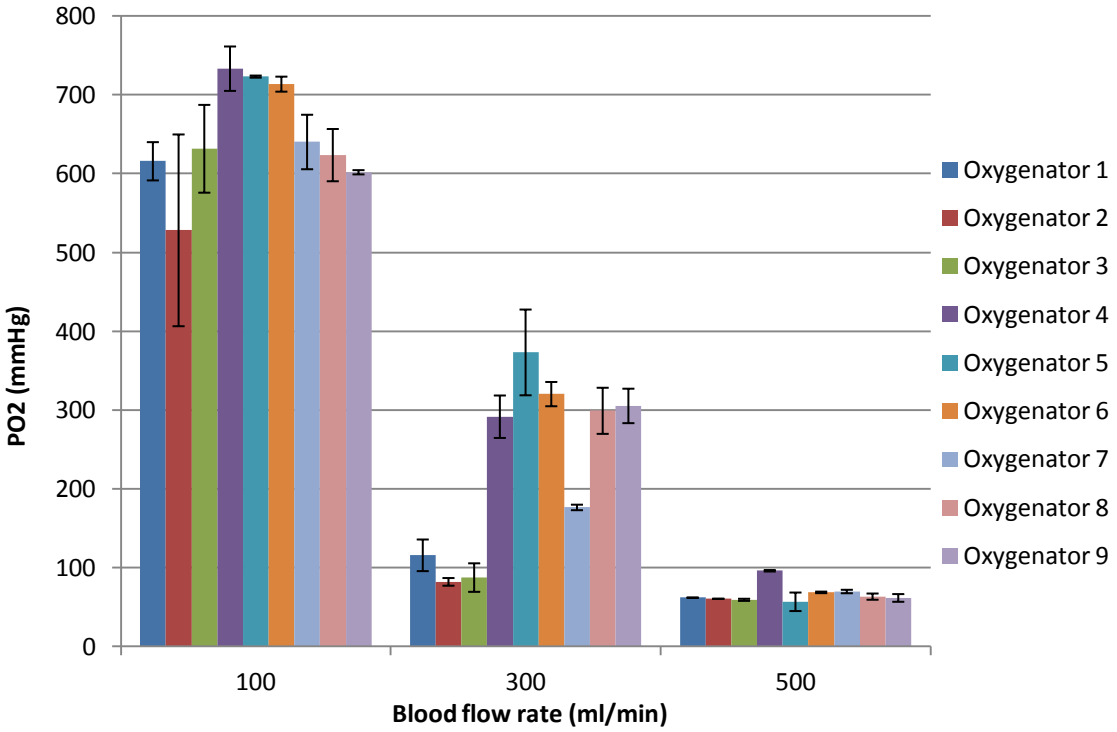


**Figure 264: Oxygen partial pressure vs. blood flow rate for each of the modules tested. ± 1 Standard Deviation.**

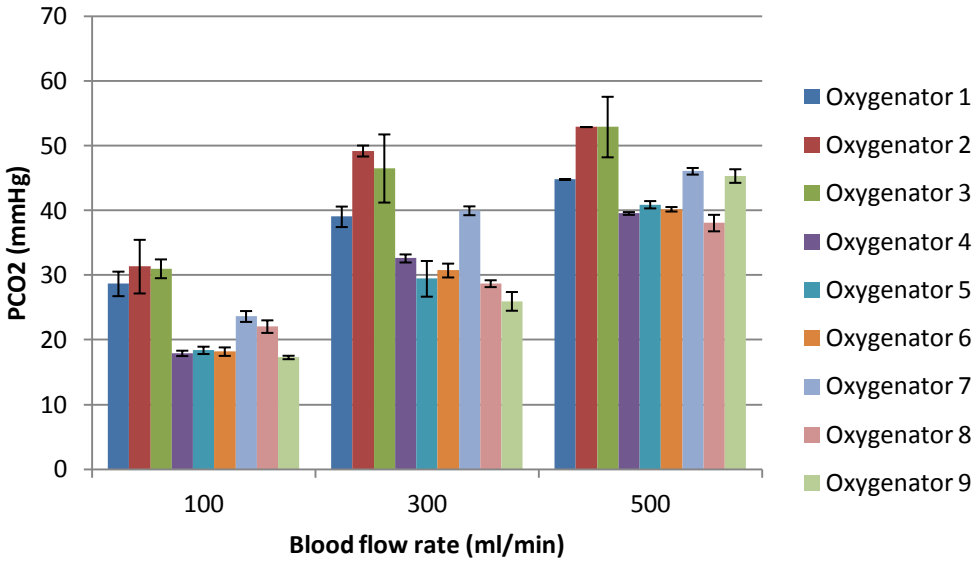


**Figure 265: Carbon Dioxide partial pressure vs. blood flow rate for each of the modules tested. ± 1 Standard Deviation.**

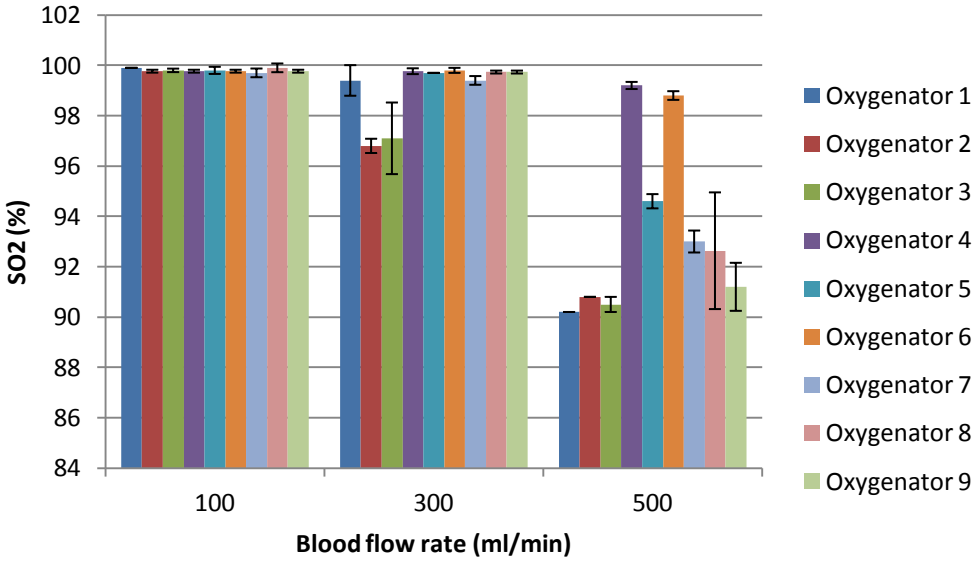


**Figure 266: Oxygen saturation vs. blood flow rate for each of the modules tested. ± 1 Standard Deviation.**

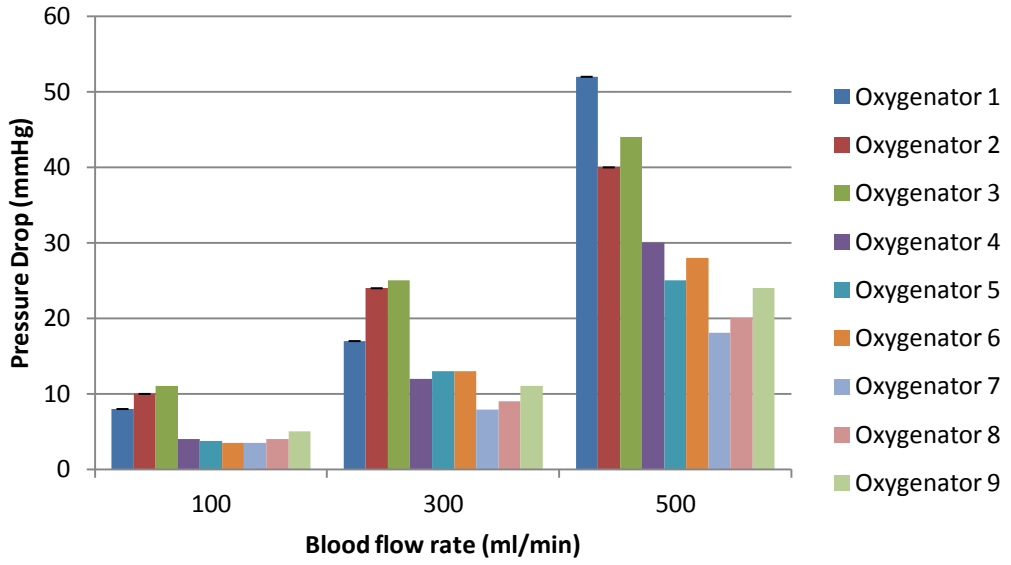


**Figure 267: Pressure drop across the module vs. blood flow rate for each of the modules tested.**

Oxygen transfer rates using the average values for oxygenators (1 – 3), oxygenators (4 – 6) and oxygenators (7 – 9) against flow rate are given in Figure 268 below.

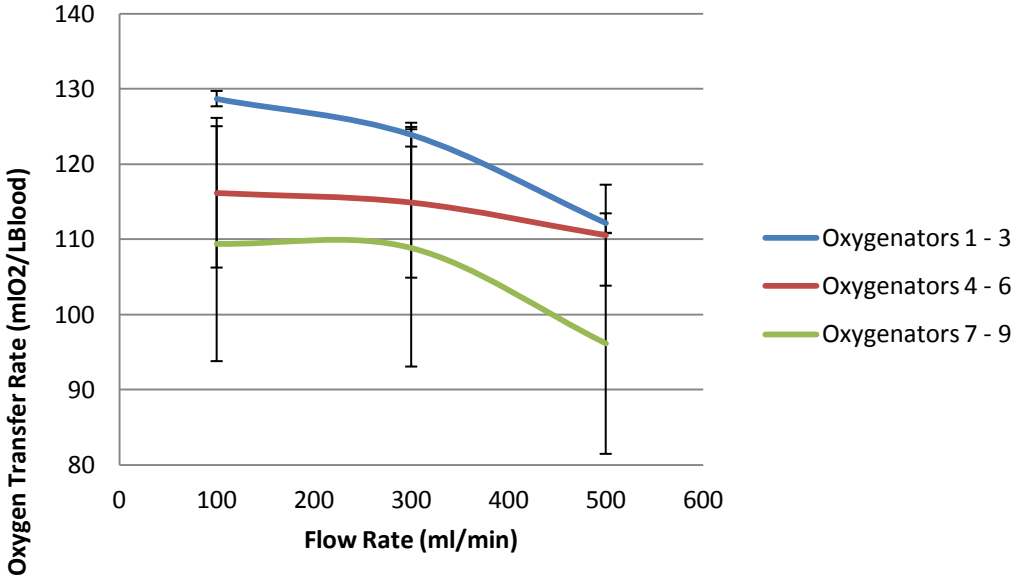


**Figure 268: Oxygen transfer rates using the average values for the oxygenator groupings by % packing fraction against flow rate. ± 1 Standard Deviation.**

### 5.14.4. Discussion

Each of the oxygenators tested were able to oxygenate the blood supply to some degree at each flow rate. The highest performance in all cases was seen at the lowest flow rate.

The drop in performance at the higher flow rates can be attributed to the following:

- Diffusion within the module is time dependent and hence faster moving flow will experience less oxygenation and carbon dioxide removal.

- At the higher flow rates the pressure within the modules is higher. This will increase the drive of the fluid to the path of least resistance resulting in a higher percentage of flow passing through shunts in the module without being exposed to the hollow fiber membranes. At high pressures and flow rates the fluid could also potentially move the fibers increasing the volume of void spaces.

- The hardness deflection temperature of the material used to rapid prototype each module was such that at the temperature and pressures present bowing of the module occurred. Figure 269 below compares a module pre and post experiment with the profile highlighted in red.

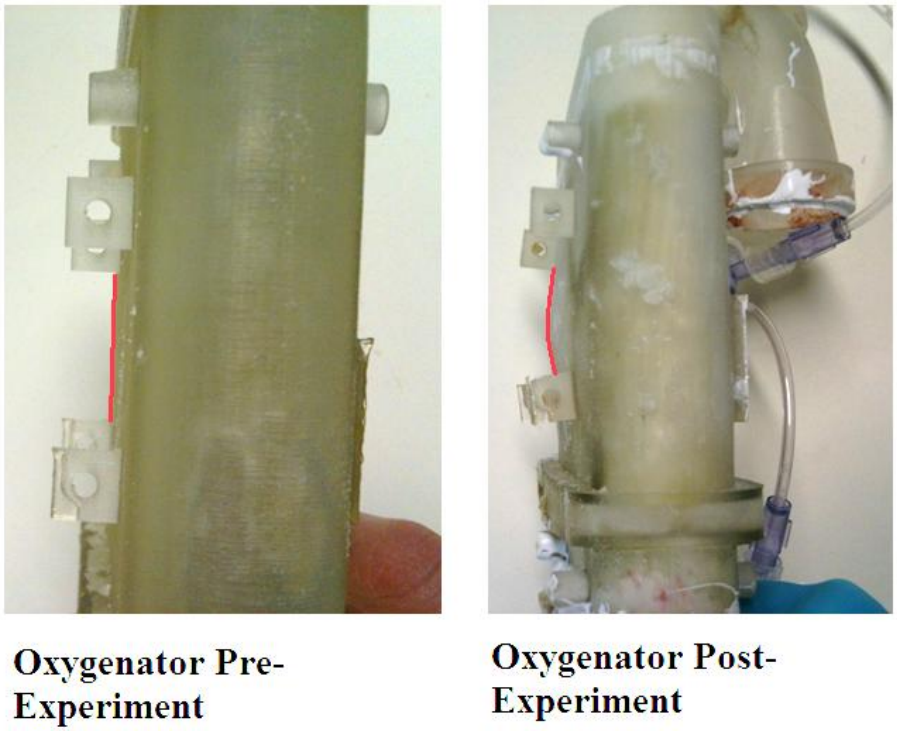


**Figure 269: Comparison of an oxygenator module pre and post experiment with the profile highlighted in red to show the bowing that occurred under the temperature and pressure applied.**

In each case the performance achieved was considerably better than within the Mark I design. This improvement can be attributed to the following:

- Improved manufacturability

The mark II design allows for a much simpler manufacturing process when compared to the Mark I design, which specifically allows for a higher packing fraction and better distribution of fibers in the bundle. This reduces the potential for shunting and increases the surface area of fiber available for diffusion. By designing the module for a more simple manufacturing process the level of quality achievable was increased and was attained more consistently.

- Improved fluid flow path.

This design is based on a more conventional configuration with blood having 360 $^{0}$ access to the fiber bundle. The outlet of the sparger provides a greater cross-sectional area and hence the pressure drop across the module is reduced. The configuration provides a more uniform flow path when compared with the Mark I geometry. As a direct result of this the design is less susceptible to shunting.

This module has a slightly higher priming volume of approximately 81 ml when compared with the Mark I oxygenator; however a large percentage of the oxygenator fiber bundle is dead space. This space does not contribute to the performance of the module but increases the priming volume. Figure 270 below shows a cross section of the Mark II flow path with the dead space highlighted in red.

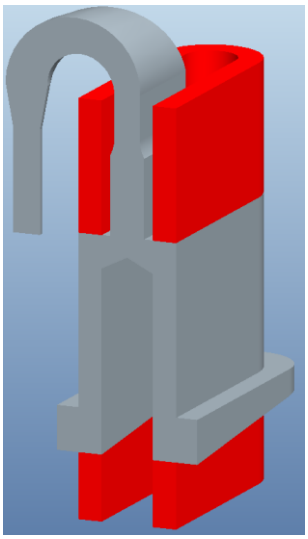

**Figure 270: ProEngineer drawing showing a cross-section of the Mark II oxygenator fluid flow path, highlighting the areas of dead space (in red), which contribute to priming volume but not performance.**

In the manufacturing process some distance is required between the top of the oxygenator and the inlet to the sparger and from the bottom to the outlet reservoir. If this space is too small during the potting phase compound could enter and clog the

sparger or outlet. As the manufacturing process was limited in its quality and reliability this space was made quite large to prevent this from occurring. This compromise was considered acceptable at this stage in the project with the knowledge that this could be remedied in future work on the oxygenator design. To investigate the results more fully a CFD analysis was conducted using values from the physical experiments as boundary conditions in the simulation.

## *CFD Evaluation of the Mark II Oxygenator*

### *Aims*

The aims of this analysis were to use values from the physical experimentation in the computational simulation to allow for further investigation of the results.

### *Methods*

The same flow paths and Gambit meshes for the 3 mm and 8 mm mark II oxygenator created in the previous analysis were used. CFD analysis was run using Fluent Inc., Fluent version 6.3.26.

Boundary conditions were set as a constant velocity at the domain inlet with the outlet set as open to atmosphere. Steady laminar flow was assumed in all cases with blood modelled as Newtonian with a constant viscosity of 0.0035 (Pa.s) and a density of 1050 ($kg.m^{-3}$). The porous media model viscous resistance coefficient was modified to

represent the packing fractions of each of the three groups of oxygenators tested. Each model was run at 100, 300 and 500 ml/min flow rates.

### *Results*

Figure 271, Figure 272 and Figure 273 below compare the average pressure drops obtained within the physical experiment and the computational analysis versus flow rate for each of the three packing fraction oxygenator module groups respectively.

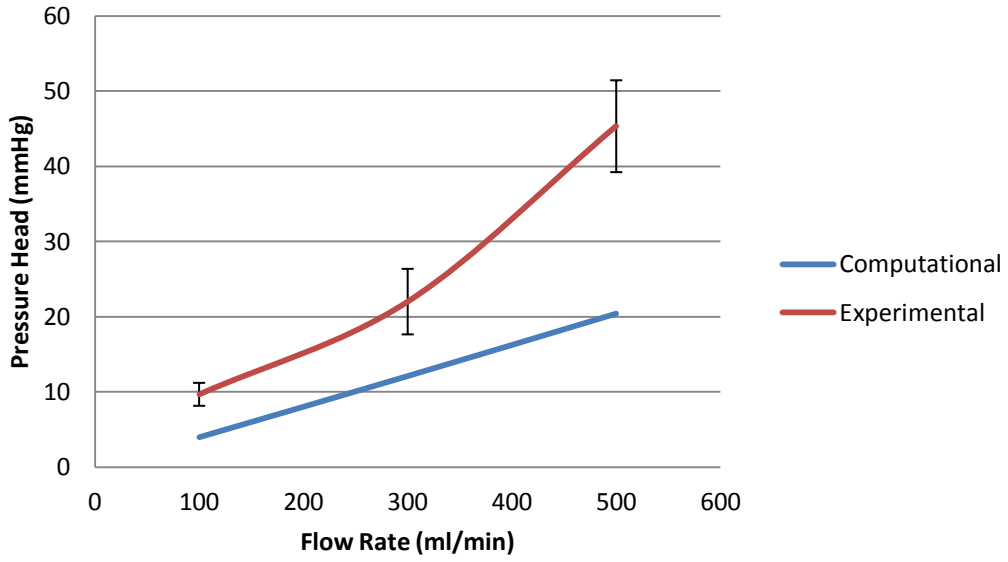


**Figure 271: Graph comparing the computational and experimental pressure drop vs. flow rate for (oxygenators 1 - 3). ± 1 Standard Deviation.**

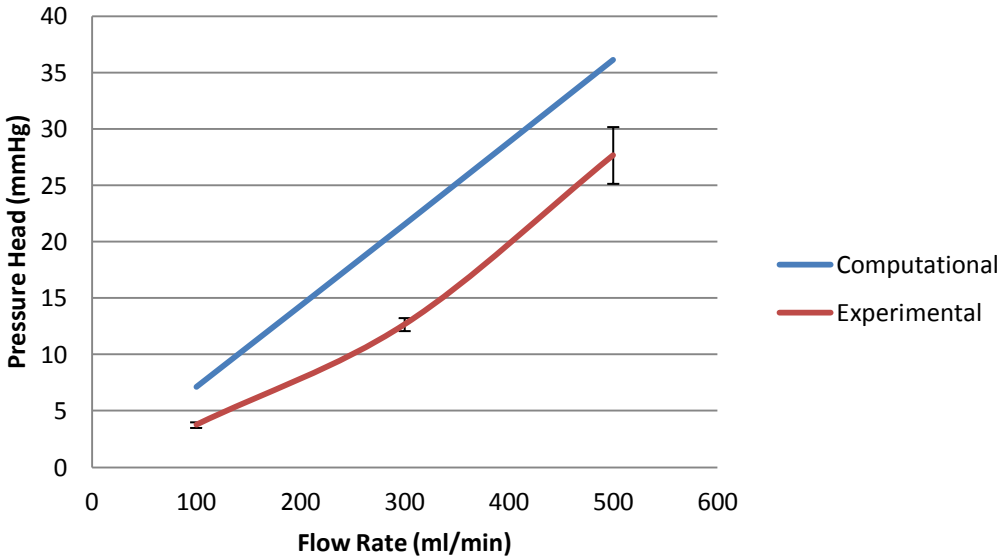


**Figure 272: Graph comparing the computational and experimental pressure drop vs. flow rate for (oxygenators 4 - 6). ± 1 Standard Deviation.**

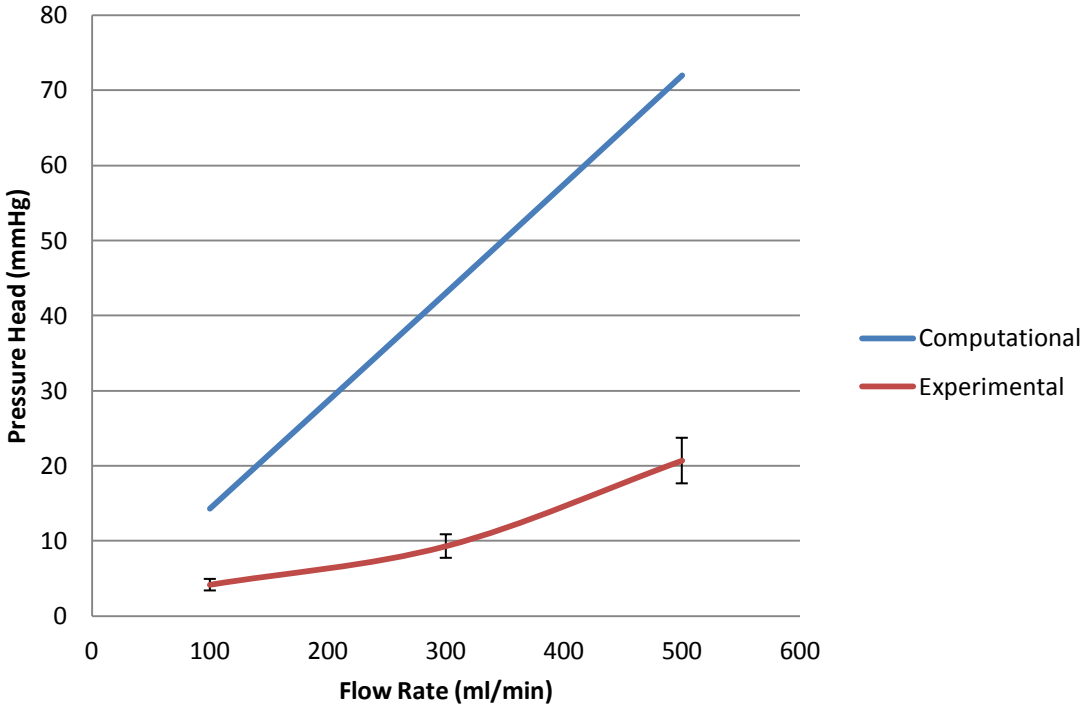


**Figure 273: Graph comparing the computational and experimental pressure drop vs. flow rate for (oxygenators 7 - 9). ± 1 Standard Deviation.**

## *Discussion and Conclusion*

The manual manufacturing methods used to construct the oxygenator modules is a difficult process and imperfections are almost guaranteed to occur, which will affect module performance, most likely through shunting.

The oxygenators (1 – 3) with the 3 mm sparger and narrower column experience the highest oxygen transfer rates at each flow rate; however carbon dioxide removal and oxygen saturation levels fall considerably at the higher flow rates. The module also has the highest pressure drops, which again increase significantly at the higher flow rates. Post experiment examination of the modules indicated that in each case the 3 mm sparger had warped under the temperature and pressure of the blood flow. The warped sparger tended to fold into itself impeding the blood flow path and hence the higher pressures were observed. These results are reflected in the CFD analysis, which indicate that the pressures observed in the physical experimentation are considerably higher than predicted by the computational analysis.

The larger cross-sectional area of the 8 mm sparger module designs prevented bowing becoming critical factor. The modules with the lower packing fraction of 75.4 % had only slightly lower pressure drop than the CFD analysis indicating that the modules were particularly well constructed. This was reflected in the performance characteristics displayed by each module.

Oxygenators 7, 8 and 9 with the higher packing fraction showed a considerably lower pressure drop in the experimental results compared to the computational simulation suggesting that shunting was occurring to a degree that significantly reduced performance. At the higher packing fraction the modules were more susceptible to the effects of shunting as the resistance to flow through the module is greater. This is

reflected in the performance characteristics obtained in the experimental analysis, which although low are still considerably better than those achieved by the Mark I design.

### 5.14.5. Conclusions

The CFD and experimental analysis has shown that the Mark II design is capable of producing a considerably higher standard of performance when compared to the Mark I design. The redesign has resulted in a more efficient manufacturing process, which has in turn improved the performance and reliability of the module design. The flow path produces a more even flow field making the module less susceptible to shunting by distributing the flow more effectively. Although greater transfer rates were achieved in the smaller modules (1 – 3) the material used in the rapid prototyping process had an inappropriate hardness deflection temperature and as a result the material was warped. This phenomenon was not observed in the larger 8 mm sparger designs; however the level and consistency of the performance was slightly lower. At this stage in the project the slight drop in performance is considered an acceptable compromise to ensure reliability of the system and to minimize the number of physical iterations required. The oxygenator design with the larger sparger and lower packing fraction (oxygenators 4 – 6) is therefore the most suitable configuration to take forward for further testing.

## 5.17. Oxygenator Mark II Endurance Testing

### 5.15.1. Aims

The aims of this experiment were to determine if the Mark II oxygenator could perform consistently over an extended period of time under conditions that reflect those to which the module will be exposed in a live animal experiment.

### 5.15.2. Methods and materials

The principle components used to determine the performance characteristics of the system are shown within Figure 274.

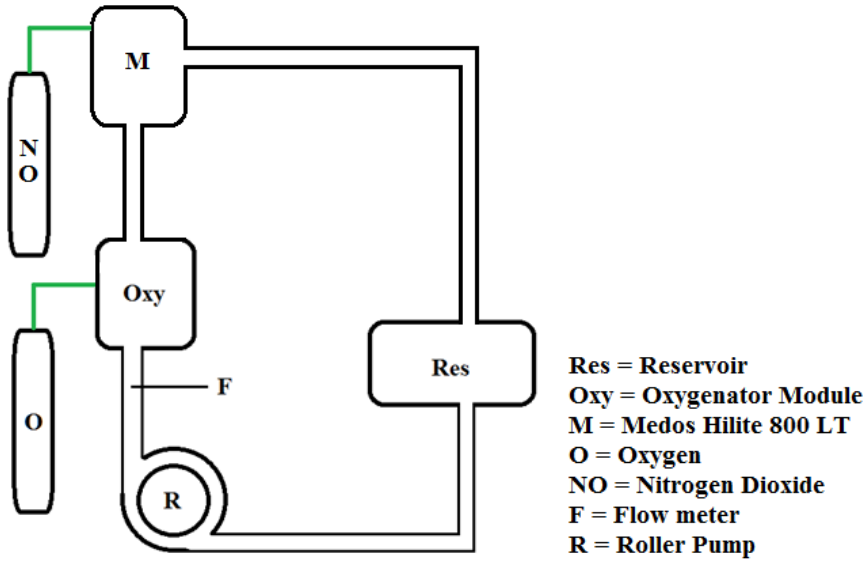


**Figure 274: Diagram showing the principle components used in the endurance testing of the Mark II oxygenator module.**

Bovine blood treated with 10 ml of 1000 IU/ml Heparin-sodium solution (Wockhardt, Mumbai, Maharashtra, India) used was diluted with 0.9 % saline solution (Baxter, Berkshire, UK) to a haematocrit of 35 %. Activated clotting time was recorded as 496 seconds using an automated ACT measuring system (hemochron, ITC, Edison, NJ, USA). To ensure the oxygenator was sealed properly the blood path was tested by running saline through the device and the gas path was tested by submersing the module in a water tank.

The system was set-up as a closed loop. Blood from a reservoir was passed through the oxygenation module. A Medos Hilite 800 LT oxygenator was placed into the loop after the oxygenator module to act as a de-oxygenator. Oxygen and nitrogen dioxide were provided via pressurised cylinder to the oxygenator and de-oxygenator respectively with

flow rates measured by a gas flow meter (SECHRIST Industries Inc., California, USA). Upon exiting the de-oxygenator the blood was pumped back to the reservoir. A Caps roller pump (Stöckert Instruments, Munich, Germany) was used to pump the blood through the system. Blood samples were taken and analysed in a Rapidlab 865 blood gas analyser (Novartis Vaccine and Diagnostics, California, USA). An arterial filter was placed in the system pre-oxygenator. Initially a control value was taken from the blood supply. Blood was then pumped through the system at a flow rate of 300 ml/min. After the system was successfully primed three blood samples were taken at the inlet to and outlet from the oxygenator and at the outlet of the de-oxygenator a rate of one per fifteen minute. This experiment was run for six hours. The entire experiment was repeated three times. Figure 275 below shows the set-up of the experiment within the lab.

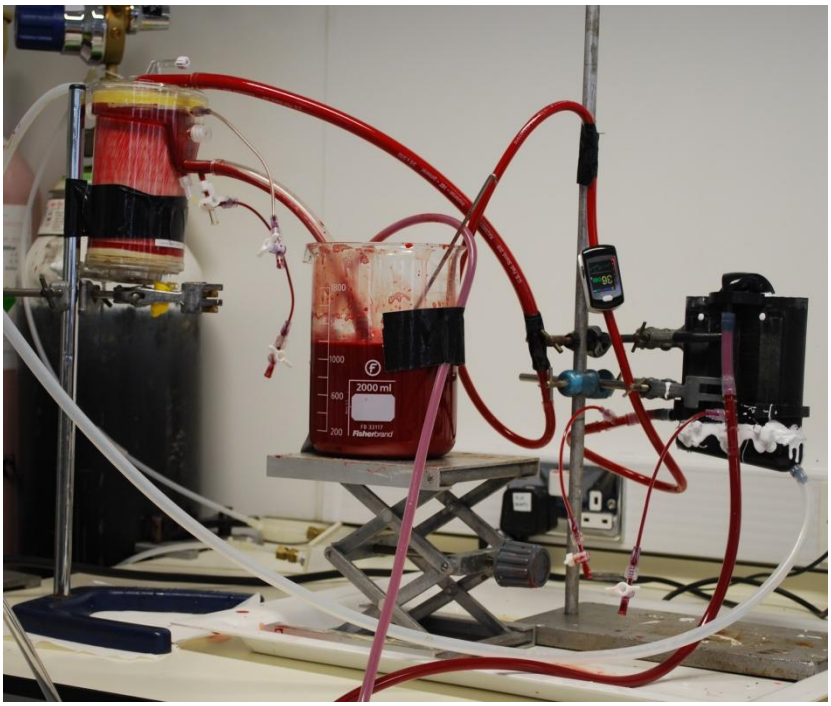


**Figure 275: Picture showing the experimental set-up used in the endurance testing of the Mark II oxygenator.**

### 5.15.3. Results

As this experiment was focused upon the endurance capabilities of the oxygenator system and so the results are displayed in terms of the most essential performance characteristics (blood oxygen partial pressure and saturation) against time. Figure 276 and Figure 277 below show blood oxygen partial pressure and saturation against time respectively.

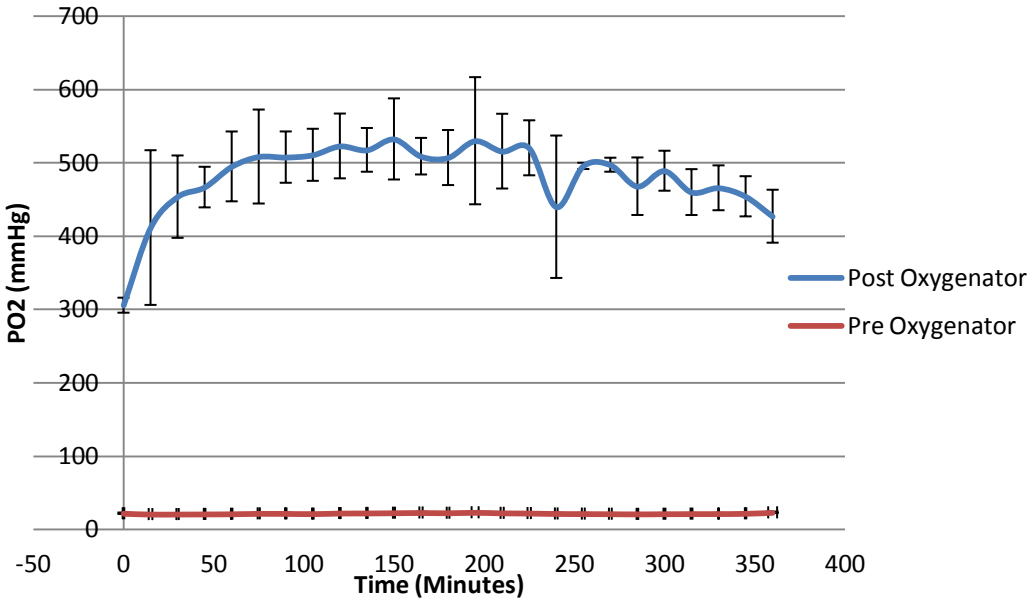


**Figure 276: Graph showing the blood partial oxygen pressure pre and post oxygenator against time. ± 1 Standard Deviation.**

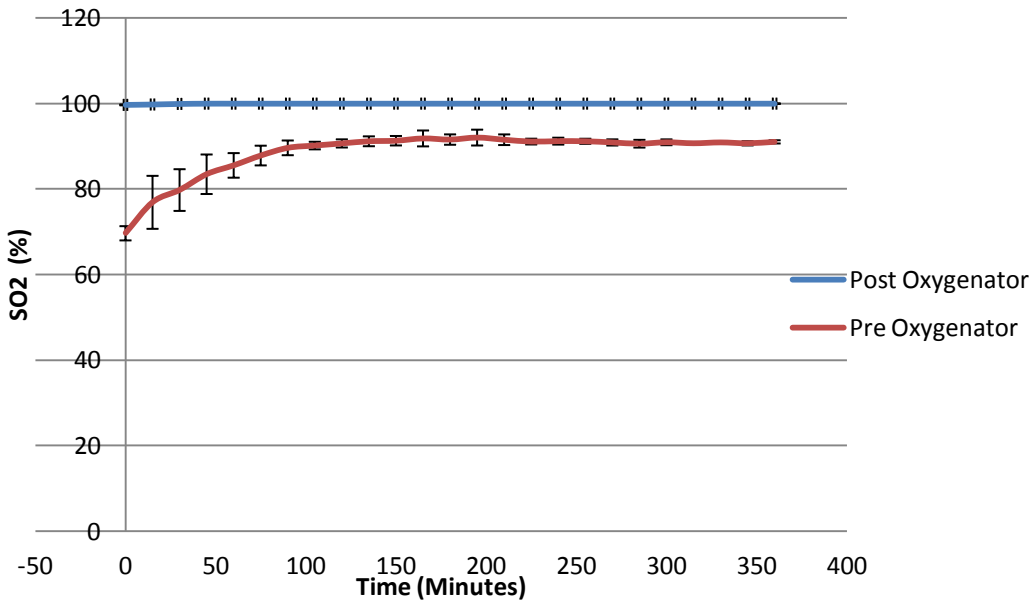


**Figure 277: Graph showing the blood oxygen saturation pre and post oxygenator against time. ± 1 Standard Deviation.**

### 5.15.4. Discussion

The results of this experiment show that the oxygenation module developed is able to perform over an extended period of time. The module achieved satisfactory performance throughout the duration of the experiment.

Carbon dioxide is not displayed with the other results. The reason for this is that the circuit used in the experiment did not provide a source of carbon dioxide. Therefore the $CO_2$ in the blood was removed as the blood passed through the oxygenator early in the experiment. With limited carbon dioxide present the production of carbonic acid in the blood was limited and as a result a rise in blood pH was observed. The effect of pH on haemoglobin is defined by the Bohr Effect; an increase in pH causes the haemoglobin molecules to release their oxygen supplies less readily, hence an increase in the oxygen saturation was observed at the inlet to the oxygenator throughout the experiment.

### 5.15.5. Conclusion

This experiment has shown that the oxygenation module developed is capable of performing consistently and satisfactorily over an extended period of time. The conditions used to test this system were similar to the conditions of a live animal experiment and therefore these results can justify this design as suitable to be taken forward and used as part of a miniaturized and integrated ECMO system.

## 5.18. Chapter Conclusions

In many ways the development of the oxygenator column was the most challenging of all of the fundamental components that make up the miniaturized and integrated ECMO system. Unlike the heat exchanger and the pump systems, the performance of this device depended entirely upon the manipulation of a previously established technology - the hollow fiber membrane. This provided an additional constraint to the development process in that the manufacturing method used to produce the oxygenators became a critical factor in the success or failure of the design and there was little room for creative development. For this reason the CFD analyses were used as a tool to evaluate the performance of the physical prototypes rather than to provide qualitative data to inform and optimize the design process.

A significant part of the oxygenator component of the system development was focused on perfecting the manufacturing method used; specifically in the placement of the hollow fiber membranes in the oxygenator module. A flawed method resulted in poor fiber distribution and failure of the module through shunting of the flow. The modules were required to be produced in the laboratory setting hence the resources available limited the potential solutions. Despite this, we were able to produce a device which both met the performance demands of a clinical device, but lent itself both to manufacture and ultimately to integration. The final device can be considered to be suitable for deployment in the near clinical animal setting, and with appropriate material selection for clinical use.

# 6. System Integration

## 6.1. Introduction

The aim of system integration is, in essence, to form a single system from its disparate parts. This must be done in such a way as to ensure that the system functions as a whole. In a miniaturised and integrated extracorporeal membrane oxygenation system integration involves combining the blood pump, oxygenator, heat exchanger and, if possible, some of the monitoring and control devices together. This integration must take into consideration safety, performance and convenience.

## 6.2. Initial Considerations

The integration strategy used will focus on the chain of devices shown within Figure 278 below.

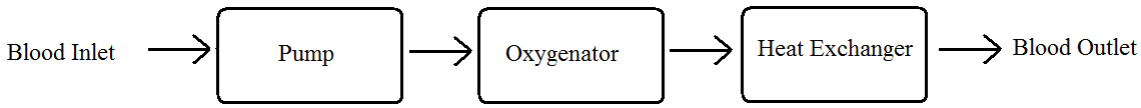


**Figure 278: Flow chart showing the desired Miniaturized and Integrated ECMO system device train configuration.**

In this configuration the AFP is the first element in the system. Positioning the pump as the first component of the integrated system ensues that only a positive pressure is present at the oxygenator bundle, minimising the risk of negative phase gas transfer across the fibres into the blood flow path. In addition positioning the pump in direct contact with the patient venous interface enhances the responsiveness of the pump to changing haemodynamic conditions which affect venous inlet flow. The heat exchanger is placed at the outlet of the device to ensure minimum heat loss between the system and the patient, simplifying thermal control at the patient interface.

In terms of perfusion safety, it is essential that the passage of air through the system is eliminated. Air within an oxygenation system could be potentially fatal to a patient, leading to gaseous emboli. To protect against this, bubble traps are used in extracorporeal circuits, eliminating air as it passes through the system. Bubble traps operate by providing raised volumes above low velocity zones in the fluid path. Air at these zones will separate from the fluid path and rise through buoyancy into the bubble trap, where it will remain until vented. Bubble traps must be considered in the integration of an ECMO system to ensure patient safety. In addition the integration must consider access to the fluid path for blood sampling and transfusion of volume expanding fluids. Although fully recognising the need and advantages of integrating monitoring devices into the system, this process is largely beyond the scope of the present work and external devices will be employed to fulfil these functions. Integration of these control systems is considered to be a key element of future development work.

## 6.3. Chapter Aims

The aims of this chapter are:

- To develop a strategy for the integration of the miniaturised components previously developed.

- To build a computer model to determine the performance characteristics of the integrated design and to highlight potential problems with the integration strategy.

- To produce a working prototype and develop a suitable experimental testing method to determine the performance characteristics of the miniaturised and integrated system.

## 6.4. Integration Strategy Development

To determine the most efficient integration strategy the finalised designs of each of the components was reassessed. Figure 279, Figure 280 and Figure 281 below show the ProEngineer drawings of the final configuration of blood pump, heat exchanger and oxygenator respectively.

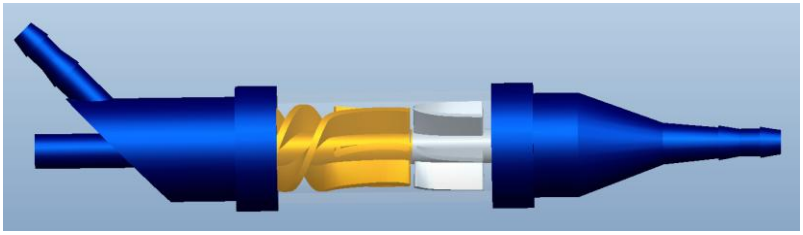

**Figure 279: Proengineer model of the final blood pump configuration prior to integration.**

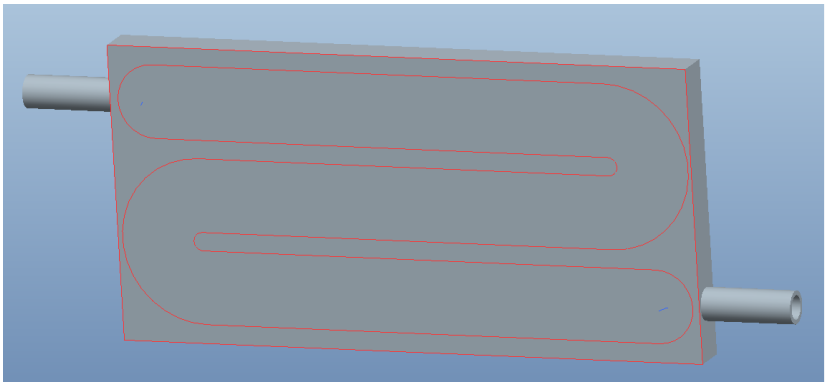

**Figure 280: Proengineer model of the final heat exchanger configuration prior to integration.**

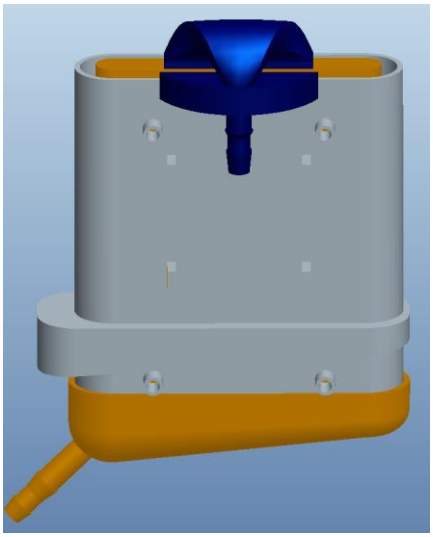

**Figure 281: Proengineer model of the final oxygenator configuration prior to integration.**

Figure 282 below is an assembly of all of the final configurations of the fundamental components developed previously. This figure suggests a possible configuration of the components based upon satisfying the device train requirements previously discussed.

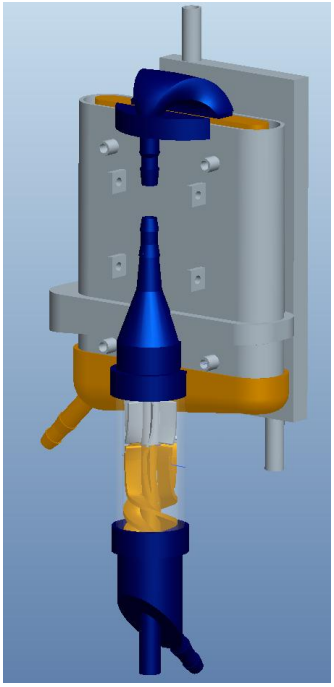

**Figure 282: ProEngineer assembly model of the pre-integration components suggesting a possible configuration for integration.**

The assembly of the final components shows a configuration similar to that of Concept 2 developed within Chapter 2 – Concept Development shown within Figure 283 below.

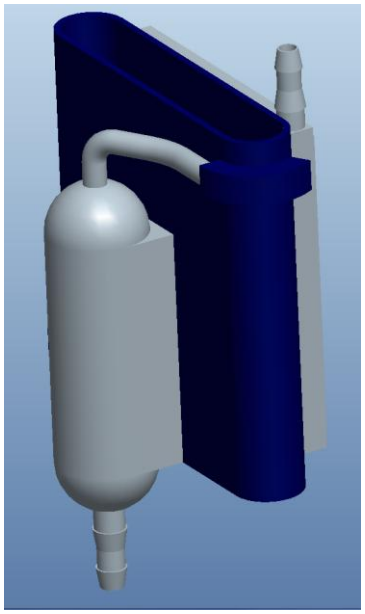

**Figure 283: ProEngineer model of Concept 2 from Chapter 2 – Concept Development.**

### 6.4.1. Pump and Oxygenator Integration

To address the needs of the EMCO setting, the integration of the pump and oxygenator must be such that the outlet of the pump and the inlet to the oxygenator are combined. We found that this could be achieved through the adaptation of the inlet to the oxygenator that was designed to be used in the testing of the device within Chapter 5 – Oxygenation System. Using this modified design would require the pump to be positioned in the center of the oxygenation module. Figure 284 below shows the pump and oxygenator integrated using the modified oxygenator inlet.

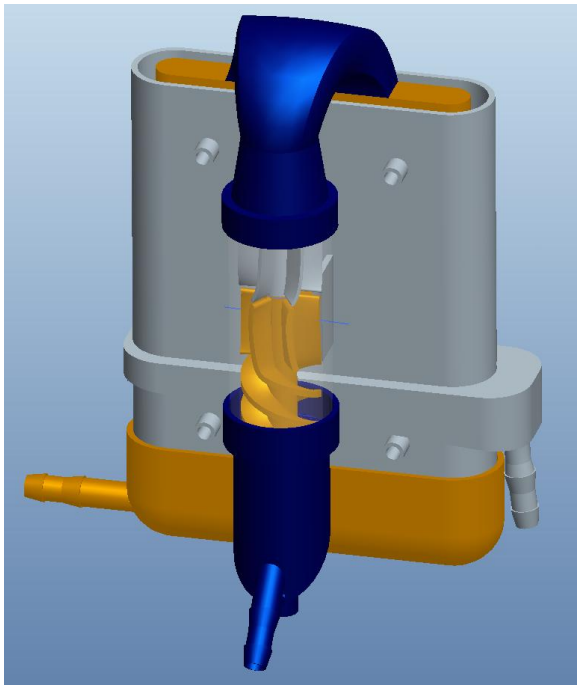

**Figure 284: ProEngineer model highlighting the integration of the pump and the oxygenator components.**

This conduit, between the pump and the oxygenator represents an ideal position for a bubble trap as it would mark the highest point in the system and is an area of low flow due to the diffuser of the pump and high resistance of the oxygenator. Figure 285 below shows the integrated design including a bubble trap positioned at the pump/oxygenator interface.

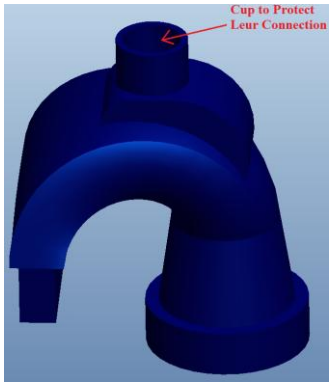


**Figure 285: ProEngineer model showing the integration connection between the pump and oxygenator including a bubble trap with a leur connection protection cup which is highlighted.**

To add an additional margin for safety it was decided to position a second bubble trap at the outlet of the oxygenator. This configuration, incorporating two independent bubble traps represents the best solution to the bubble protection without resorting to secondary devices. Figure 286 below shows the oxygenator casing with bubble trap.

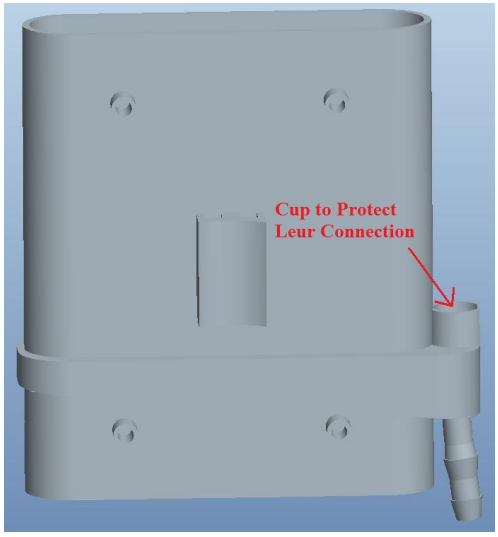


**Figure 286: ProEngineer model showing the location of the bubble trap on the oxygenator casing with a leur connection protection cup which is highlighted.**

### 6.4.2. Oxygenator and Heat Exchanger Integration

During the development of the oxygenator and heat exchanger the foundation designs were compromised for the sake of performance. The resulting components are therefore not designed specifically for integration. The flow path through the oxygenator is such that flow is encouraged to move through the whole of the fiber bundle, maximizing the diffusion within the module. This flow path requires a small reservoir at the outlet in order to refocus the flow to a single flow path. This small reservoir also functions as a bubble trap. The heat exchanger is designed for single pass efficiency and the inlet and outlet are diametrically positioned, an additional safety feature. These component configurations were derived to maximize performance and safety. The easiest way to integrate would be through simple connection between the outlet of the oxygenator and

the inlet to the heat exchanger using conventional circuit tubing. However, it is likely that this connection will be more fully integrated in future devices. This single "soft" connection also aided assembly of the prototype devices under laboratory conditions. Figure 287 below shows the integrated connection between the oxygenator and the heat exchanger.

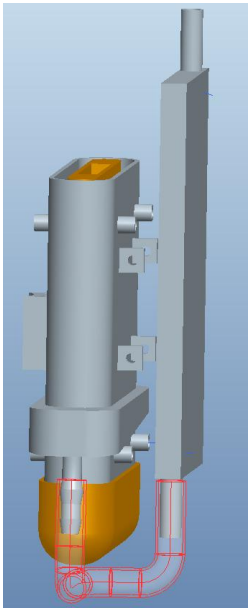

**Figure 287: ProEngineer model highlighting the integration connection between the oxygenator and the heat exchanger.**

### 6.4.3. Complete Integrated configuration

Figure 288 and Figure 289 show the components of the ECMO system assembled together and integrated in an isometric and exploded view respectively.

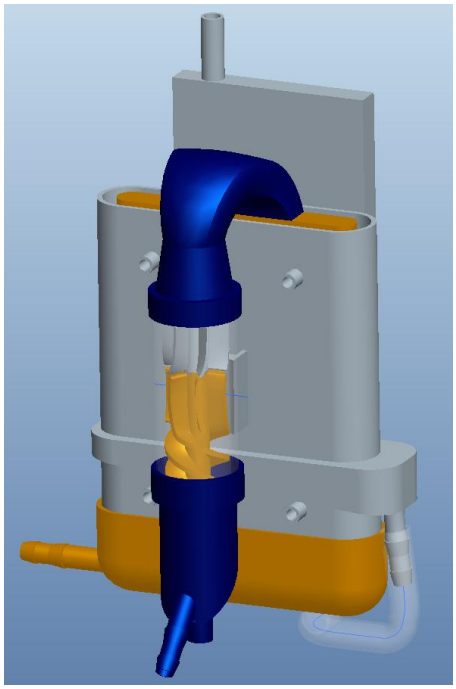

**Figure 288: ProEngineer drawing showing the assembled and integrated components of the miniaturized and integrated device in an isometric view.**

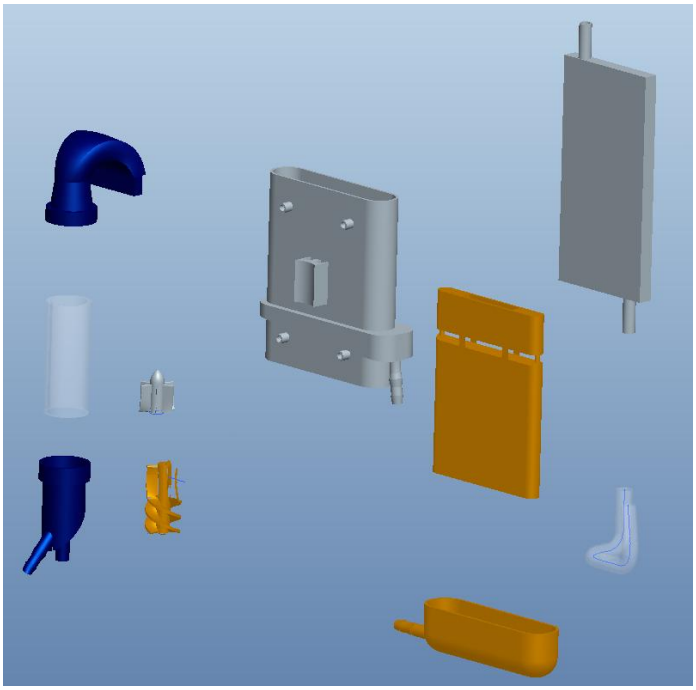

**Figure 289: ProEngineer drawing showing the assembled and integrated components of the miniaturized and integrated device in an exploded view.**

## 6.5. CFD analysis of the integrated design

### 6.5.1. Aims

The aims of this procedure were to produce a computational model based upon the methods used in the previous component development chapters. These models were integrated to determine the performance characteristics of the integration strategy and to demonstrate if the configuration was suitable to proceed to physical modeling. As outlined in Chapter 2 – Concept Development if it were shown that the model was incompatible in some aspect or has some identified performance insufficiency redesign can be carried out without resorting to multiple physical modeling exercises.

### 6.5.2. Methods

The integrated design was based upon eight volumes:

- Pump Inlet – Static fluid volume
- Impeller – Rotating fluid volume
- Pump Outlet with oxygenator Inlet - Static fluid volume
- Oxygenator Bundle – Porous media fluid volume
- Oxygenator Outlet with connection to Heat Exchanger - Static fluid volume
- Heat Exchanger Fluid path - Static fluid volume
- Heat Exchanger Aluminium Casing – Static solid volume

- Heat Exchanger Conduction plate with Peltiers – Static solid volume

The inlet and outlet to the device were modified to represent a 10 French and 8 French cannula respectively, sizes typically employed in neonatal ECMO practice. Each volume was imported into Gambit and assembled. A tetrahedral/hexagonal element hybrid mesh of 2,247,352 nodes was used. Figure 290 below shows the meshed model within Gambit.

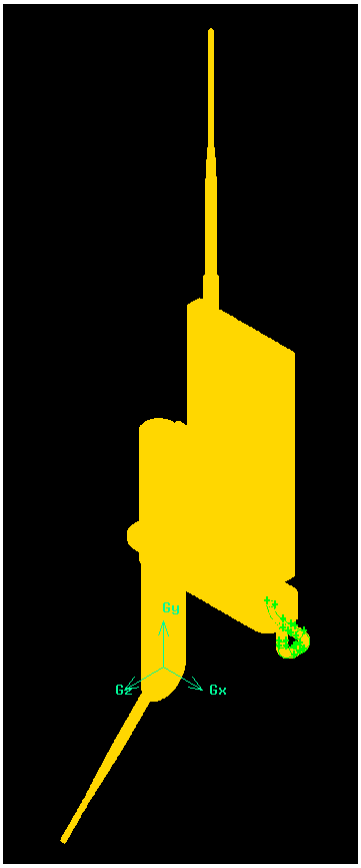


**Figure 290: Gambit mesh of the integrated system.**

CFD analysis was run using Fluent Inc., Fluent version 6.3.26. The analysis was performed as a turbulent flow with the Reynolds averaged Navier Stokes equations solved for turbulent incompressible flow with a two equation k-epsilon model with

enhanced wall treatment for turbulence closure. Turbulence was defined by providing a turbulence intensity and hydraulic diameter at the inlet to and outlet from the pump. The porous media was defined using the properties previously established for an oxygenator with a 66 % packing fraction, giving viscous coefficients of $k_{x,z}$ = 5,660,872,542 $m^{-2}$ and $k_y$ = 1,257,971,676 $m^{-2}$. Peltier temperatures were set to the maximum temperature of 42 $^0$C.

In each analysis Fluent material properties for water and aluminium were used to define the fluid and solid materials present. This produced a model which in terms of material characteristics was as close to the deliverable technology as possible, recognizing that there is performance differences associated with different material combinations. Inlet boundary conditions were set to simulate flow rates of 100, 300 and 500 ml/min with temperatures set at 34 $^0$C and a pump speed of 6000 r.p.m. Outlet boundary condition was set as a pressure outlet open to atmosphere.

### 6.5.3. Results

Performance of the model is evaluated in terms of pressure and temperature across the device and of the maximum area-weighted wall shear stress, which were found to occur at the impeller casing, on the impeller, on the diffuser and on the flow straightener. The performance characteristics are plotted against the varying flow rates at which the model was tested to determine the impact of flow rate on performance.

Figure 291, Figure 292 and Figure 293 show pressure head, temperature and area-weighted average wall shear stress against flow rate respectively.

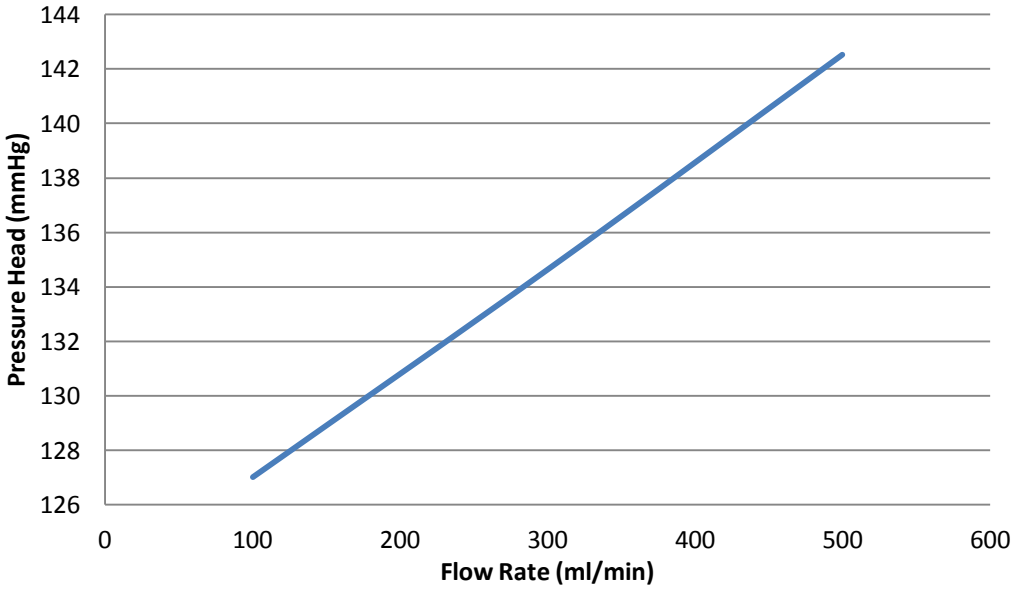


**Figure 291: Graph of pressure head Vs. flow rate for the integrated system.**

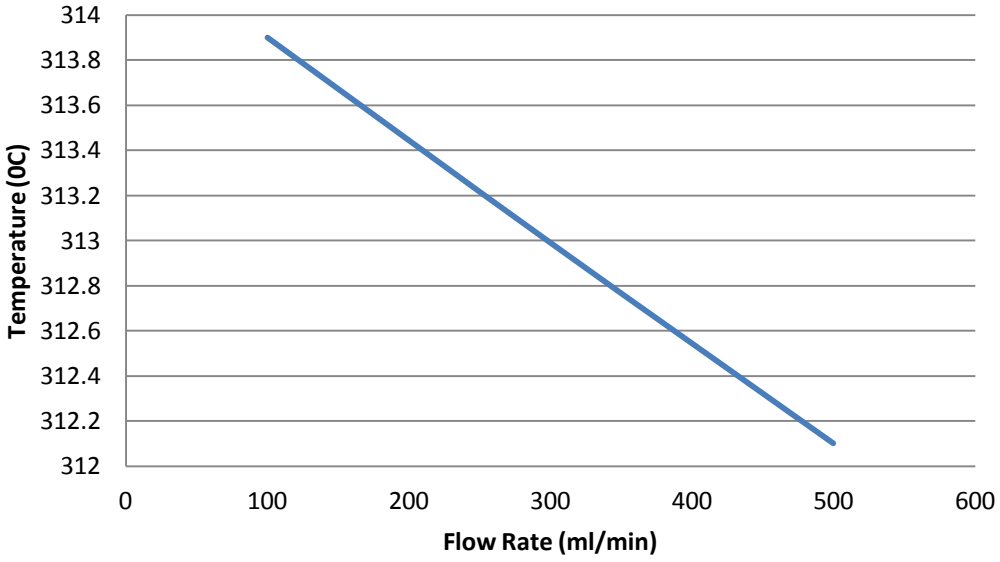


**Figure 292: Graph of temperature Vs. flow rate for the integrated system.**

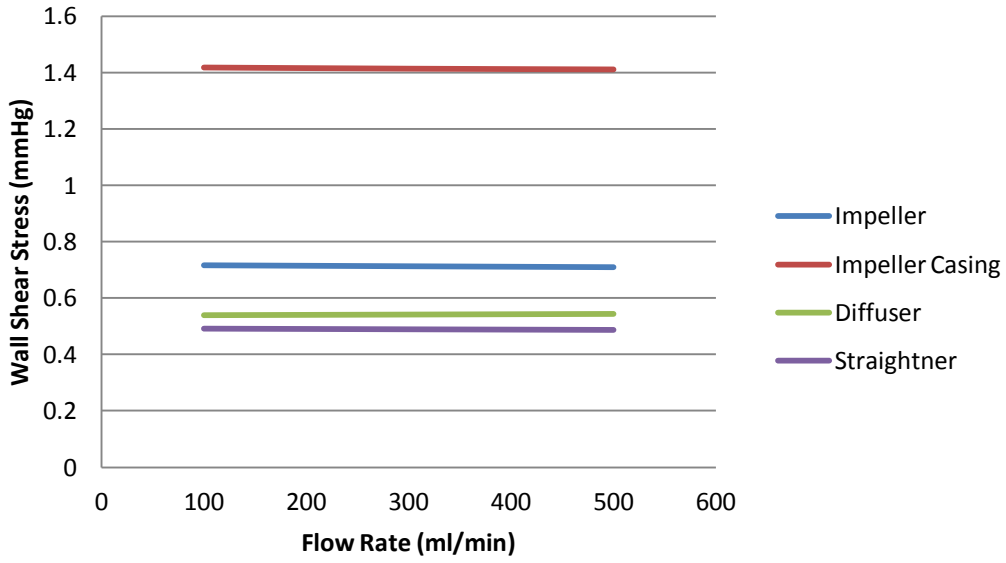


**Figure 293: Graph of wall shear stress Vs. flow rate for the model at 500 ml/min.**

Post processing of the model was conducted at the highest flow rate as this represented the extreme of the performance requirement range. The most convenient way to display the performance characteristics was deemed to be through filled contour diagrams. Pressure, velocity and temperature contour diagrams through the middle of the system (iso-surface x =0) can be seen within Figure 294, Figure 295 and Figure 296. To offer a more detailed evaluation of the temperature distribution within the heat exchanger an additional temperature contour diagram on a surface cut through the centre of the heat exchanger (iso-surface z = -0.069) can be seen within Figure 297.

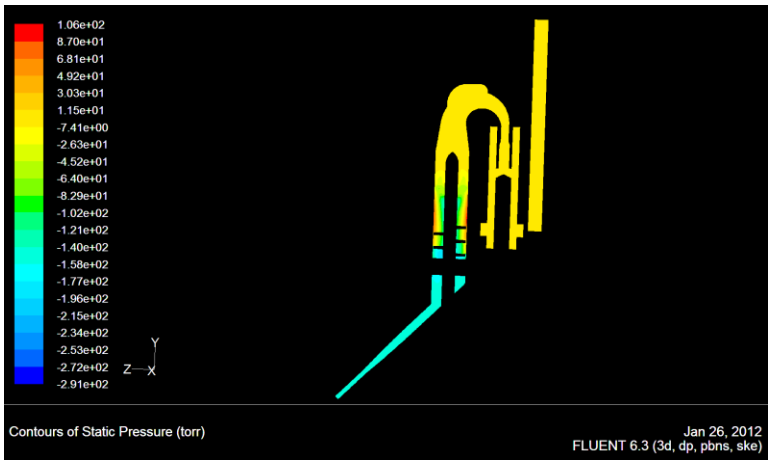


**Figure 294: Pressure contours at an iso-surface of x = 0 for the fully integrated model.**

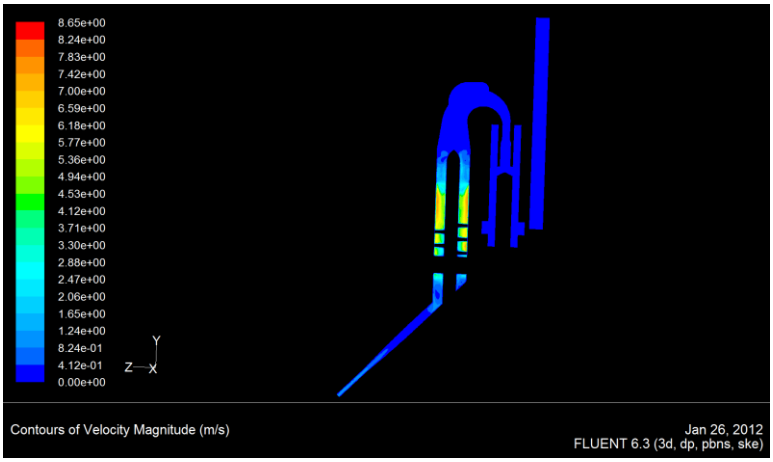


**Figure 295: Velocity contours at an iso-surface of x = 0 for the fully integrated model.**

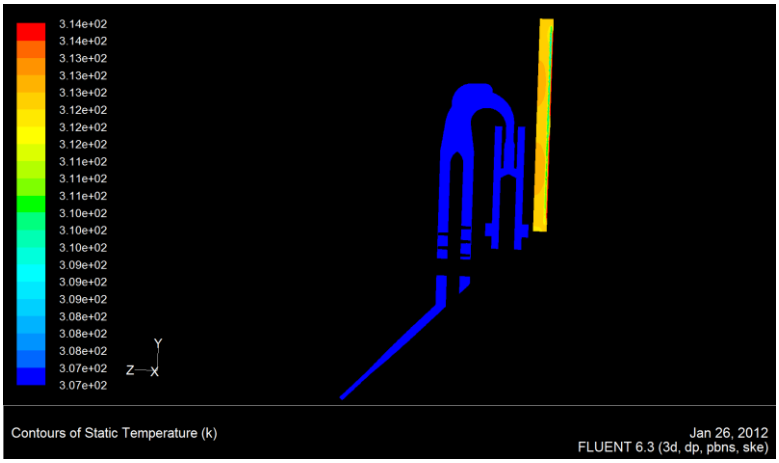


**Figure 296: Temperature contours at an iso-surface of x = 0 for the fully integrated model.**

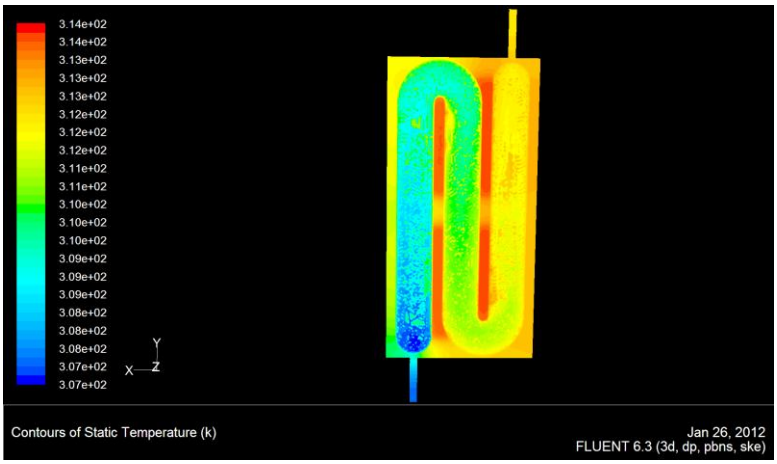


**Figure 297: Temperature contours at an iso-surface of z = -0.069 for the fully integrated model.**

Contours of wall shear stress on a surface through the middle of the model (iso-surface x = 0), including the impeller blades to enhance visuals can be seen within Figure 298. To allow for a more detailed evaluation of the areas of highest wall shear stress, contour diagrams of the impeller casing and of the straightener, impeller and diffuser walls are given within Figure 299 and Figure 300 respectively.

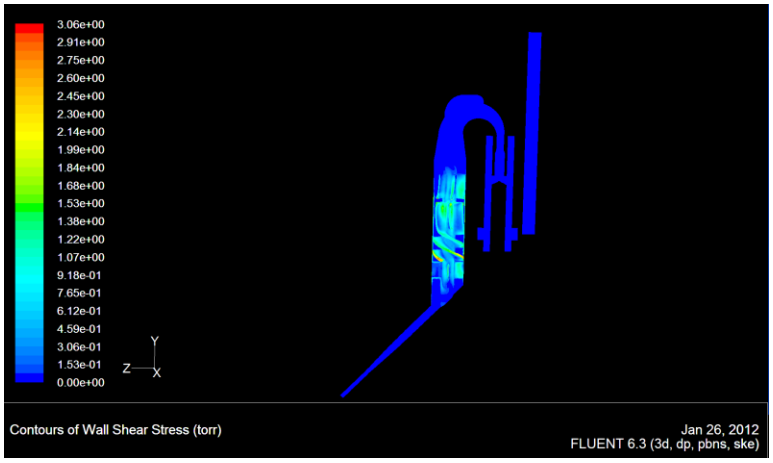


**Figure 298: Contours of wall shear stress at an iso surface of x = 0 for the model at 500 ml/min.**

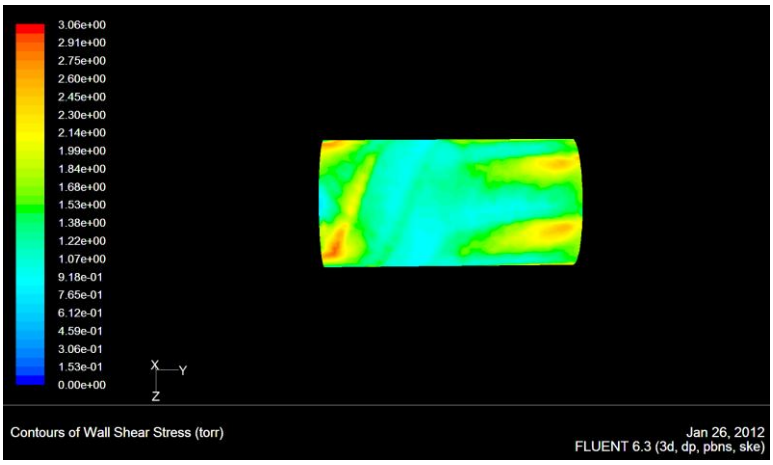


**Figure 299: Contours of wall shear stress on the impeller casing for the model at 500 ml/min.**

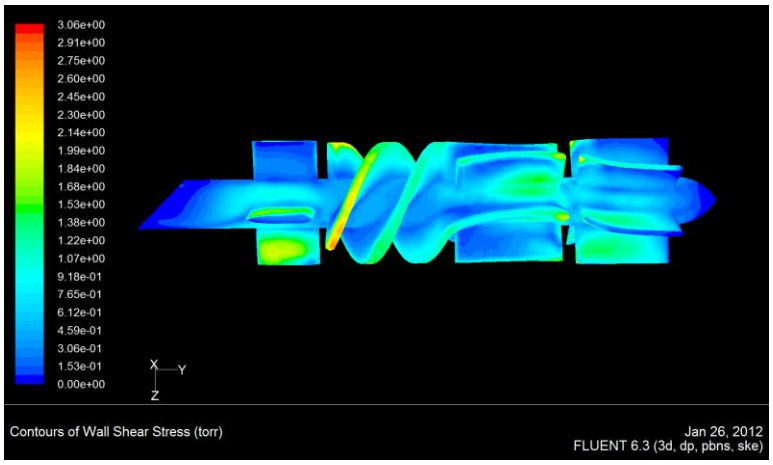


**Figure 300: Contours of wall shear stress on the straightener, impeller and diffuser for the model at 500 ml/min.**

### 6.5.4. Discussion

This model provided a realistic simulation of the physical challenges that must be addressed in the integration of the individual components of the miniaturised ECMO system. By using the previously defined computer models, combined with the additional elements and in the configuration defined in the integration strategy, this model was able to provide a realistic simulation. The performance of the integrated device could be compared to that of each of the individual components therefore highlighting the effectiveness of the strategy used. It also provided a more realistic

approximation of the conditions of a live animal experiment by including the inlet and outlet cannulae, components known to influence flow during clinical ECMO.

The pressure head across the device suggests that 6000 r.p.m was a suitable pump speed for this configuration to generate clinically appropriate blood flows. With the peltiers running at maximum temperature of 42 $^0$C the system was capable of increasing the bulk fluid temperature by over 5 degrees from a conservative inlet condition of 34 $^0$C to 39.1 $^0$C in a single pass at the highest flow rate. Maximum wall shear stresses were limited to the AFP where the highest fluid velocities occurred, specifically at the impeller casing. The magnitudes were similar to those encountered in the pump development chapter. This consistency is, once again, most encouraging. Following this integration strategy the system, excluding inlet and outlet cannula had a priming volume of 186.63 ml and has a surface area to which the blood is exposed of 0.1053 m$^2$.

### 6.5.5. Conclusion

The analysis suggests that this configuration of the complete integrated system is able to meet the hydrodynamic and haemodynamic requirements of a miniaturized and integrated system. The performance as a whole was very similar to that derived from the study of its individual components confirming that the integration strategy used had a minimal impact on overall system performance. Each of the computational models developed for the fundamental components was validated in the respective development chapters and the accuracy of these models is assumed to hold in this integrated configuration. The results are encouraging and suggest that this integration strategy is good enough to merit physical prototyping to allow for further investigation and development.

## 6.6. Development of the Miniaturized and Integrated ECMO Prototype Device – The Final Configuration

With the integration of the components complete a casing was designed. The requirements of the casing were to protect and support the components of the system and to make testing of the system in the laboratory environment safer and easier. The form was also designed to enhance the aesthetics of the integrated device.

The casing configuration was based around the form of the fundamental components and the additional elements defined by the integration strategy. To allow for easy assembly the casing was split into two halves. This allowed the assembled integrated system to be placed in one half of the casing and then the other half slid into place. The casing was designed to be held together using magnetic couplings so that it could be easily assembled and disassembled allowing it to be used multiple times. Ultimately, the entire device, including the casing shroud will be uniformly disposable. However the current shroud design represents a cost effective protective component for the overall integrated system and gives users the opportunity at this early stage to see the device as a "near finished" technology. Figure 301, Figure 302 and Figure 303 show a model of the complete casing, the location of some of the mounting holes for the magnet couplings and a rapid prototype of the casing, which is being coated with a white acrylic paint.

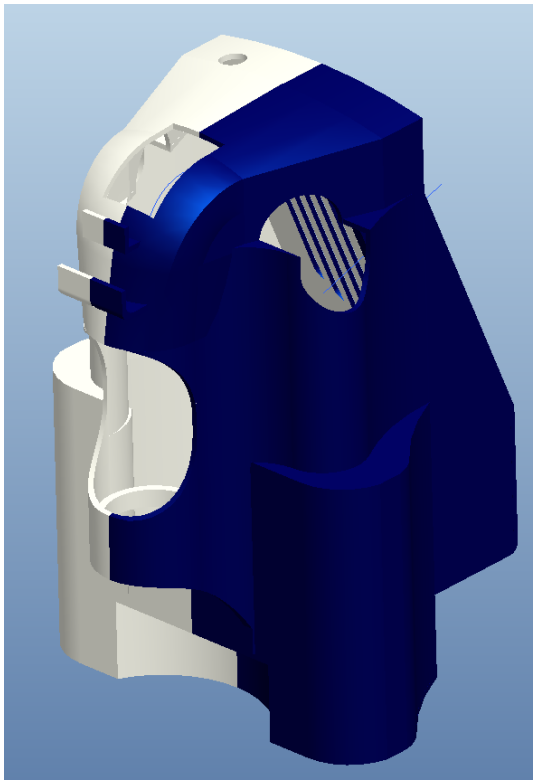

**Figure 301: Proengineer model of the complete casing.**

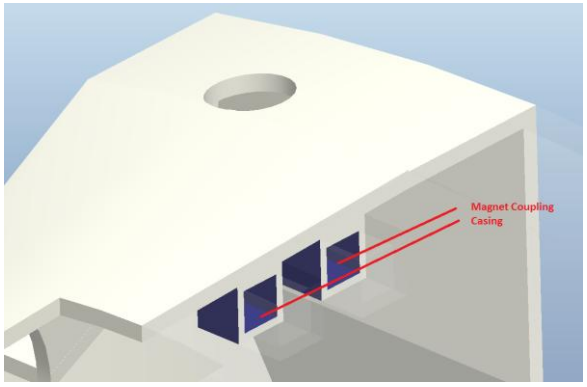


**Figure 302: Model highlighting the location of some of the magnetic couplings used to hold the casing together.**

**Figure 303: Picture of the rapid prototyped casing being sprayed in the paint bay.**

Figure 304 below shows an assembly of all of the components of the integrated system complete with casing. To allow the internal structure to be seen, one half of the casing has been made transparent.

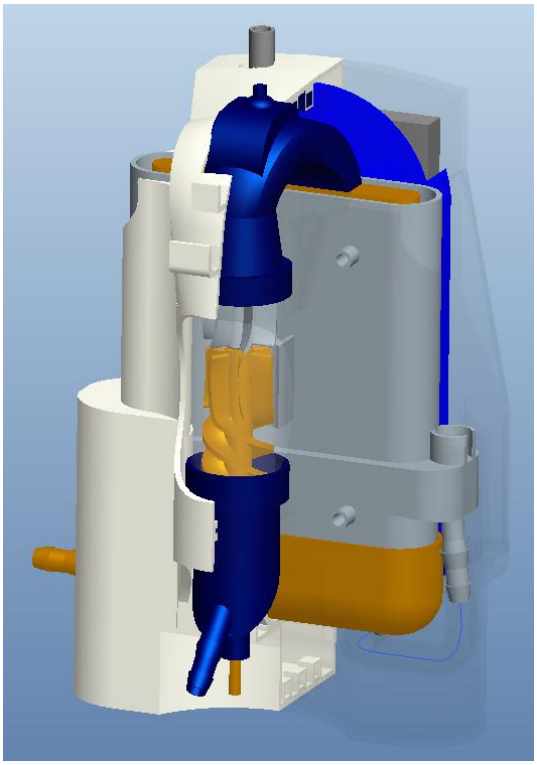

**Figure 304: ProEngineer assembly of the miniaturized and integrated ECMO prototype.**

The complete integrated prototype is comprised of the following parts:

- Pump inlet – Rapid prototyped
- Pump impeller – Rapid prototyped
- Pump diffuser – Rapid prototyped
- Impeller drive shaft – 4 mm stainless steel rod
- Pump bearings and oil seals
- Impeller casing – 26 mm ID, 32 mm OD transparent acrylic tube.
- Pump outlet/oxygenator inlet – Rapid prototyped
- Oxygenator sparger – Rapid prototyped
- Oxygenator fiber bundle – 4 m of Membrana Oxyplus fiber mat.
- Oxygenator casing – Rapid prototyped
- Oxygenator/heat exchanger Casing – ¼ inch Silicone tubing
- Oxygenator gas inlet – Rapid prototyped
- Heat exchanger mount – Rapid prototyped
- Heat exchanger – Custom made aluminium exchanger
- Heat exchanger conduction plate – 0.5 mm aluminium plate
- Peltier heating elements –
- Casing – Rapid prototyped

An exploded view of all of the components can be seen within Figure 305 below.

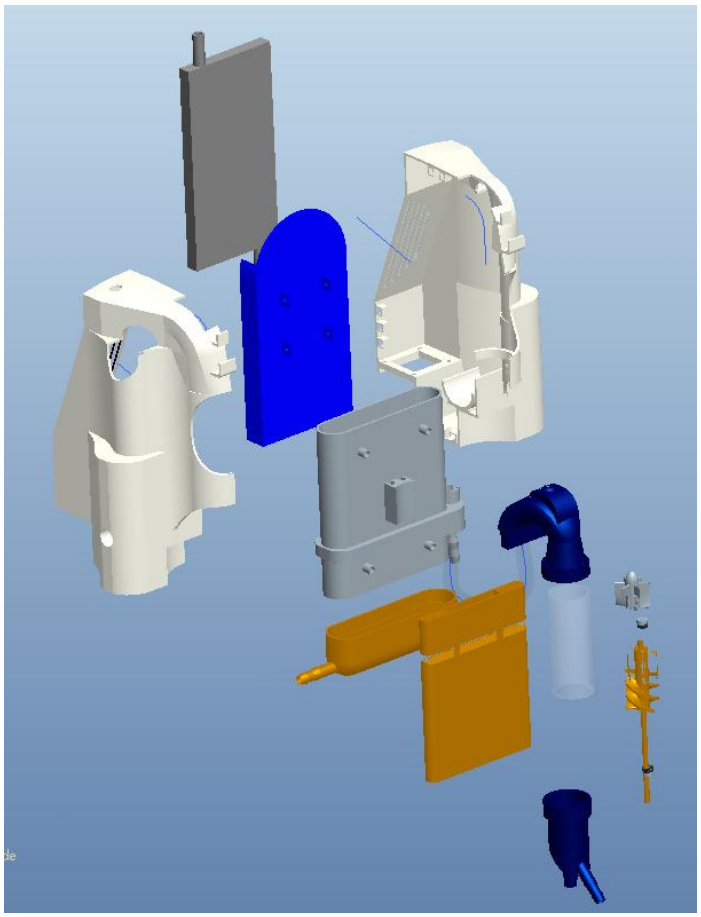

**Figure 305: ProEngineer model showing an exploded view of all of the parts that assemble to make the complete integrated design.**

The system is assembled in the following way:

- The stainless steel rod was cut to size with the impeller bonded on to it using araldite.
- Bearings and oil seals were bonded to the pump inlet and to the diffuser.
- The impeller was mounted into the pump inlet.
- The impeller casing (transparent acrylic tubing) was then placed over the impeller and bonded to the pump inlet using araldite.
- The diffuser was placed into the casing and onto the drive shaft. The diffuser was bonded to the impeller casing by running superglue down the blade edges.

- The pump outlet was then bonded to the impeller casing using silicon adhesive.
- The oxygenator was potted and prepared for used as described within section 5.12 of chapter 5.
- The pump was bonded to the oxygenator sparger inlet using silicon adhesive. The oxygenator casing was designed with a rounded support for the pump. The impeller casing was bonded to the oxygenator at this mount using silicon adhesive.
- The heat exchanger had double sided tape put on to its lowest side and was placed within its mount.
- The mount was bolted to the oxygenator.
- The heat exchanger and oxygenator were connected using silicon tubing.
- The device was inserted into the right hand side of the casing.
- The left hand side of the casing was then slid into place.

Figure 306 below shows the rapid prototyped system, which has been assembled ready for use in the lab. The set-up shown includes the direct drive motor system which is highlighted.

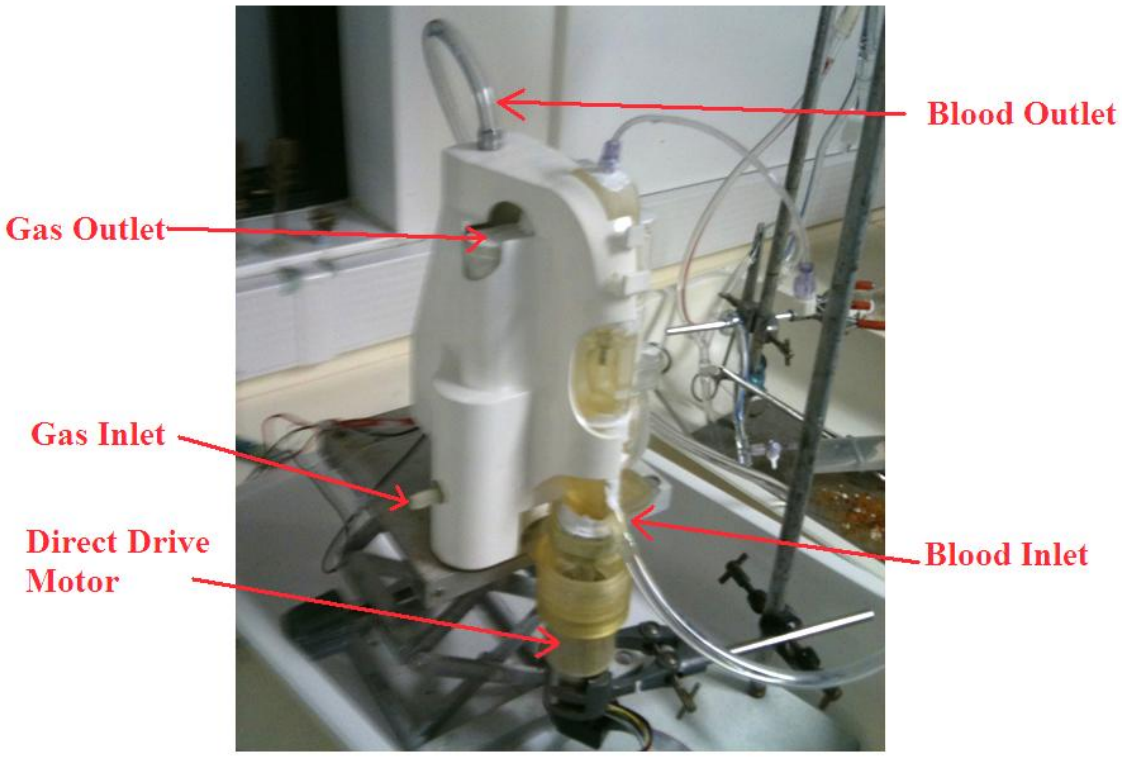


**Figure 306: Complete integrated prototype ready for use in the lab with blood and gas inlet and outlet highlighted along with the direct drive motor.**

## 6.7. Miniaturized and Integrated ECMO – Complete Prototype Testing

### 6.7.1. Aims

The aims of the following experiment were to determine performance and reliability of the integrated prototype prior to its use in animal experiments. The computer simulations suggested that this configuration of components will be suitable for clinical deployment however in order that some reassurance can be gained with regard to device performance before this step, recognition to international performance standards were applied. There exists a set of standards for blood pumps, oxygenators and heat

exchangers. These ISO standards set out the basic performance envelopes for such devices, and importantly the test conditions which should be applied in their development. Although we recognize these standards fully in the laboratory we were not equipped to meet them in entirety. In performing our device testing we employed modified ISO protocols, within the limitations of our laboratory facilities. Indeed, in some instances the test conditions were more taxing than ISO standards.

### 6.7.2. Method and Materials

The principle components used to determine the performance characteristics of the system are shown within Figure 307.

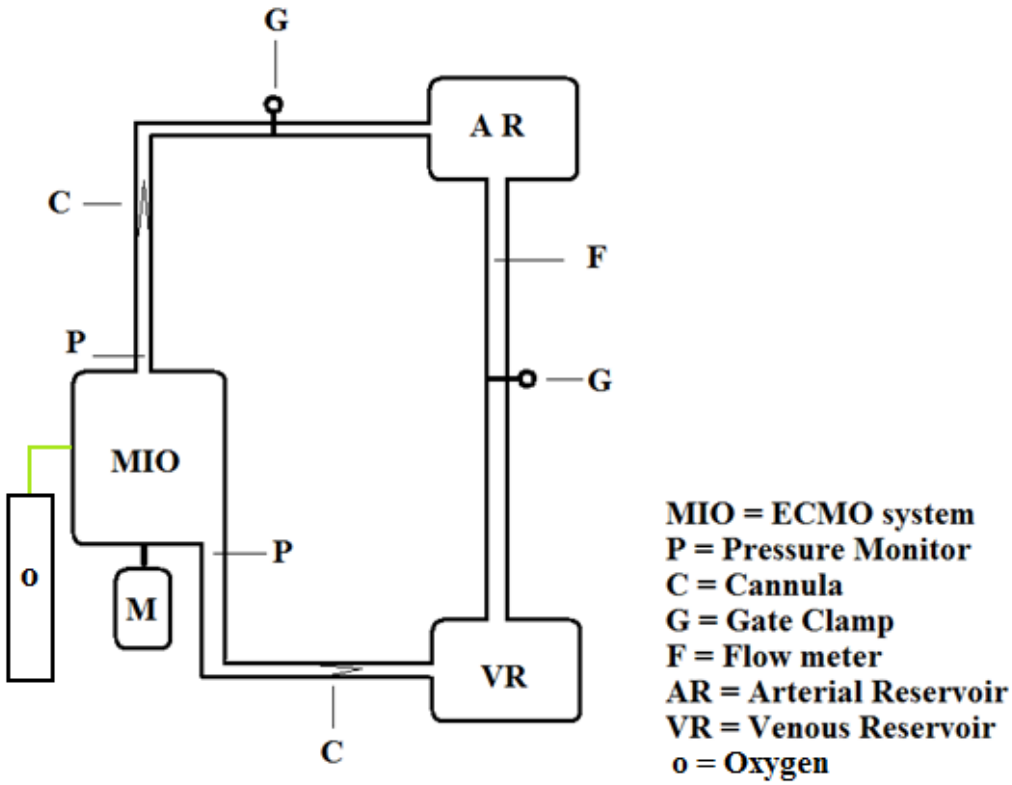


**Figure 307: Diagram of the experimental set-up used to test the miniaturized and integrated prototype system.**

Figure 308 shows the experimental set-up within the lab with each of the elements of the experimental set-up highlighted.

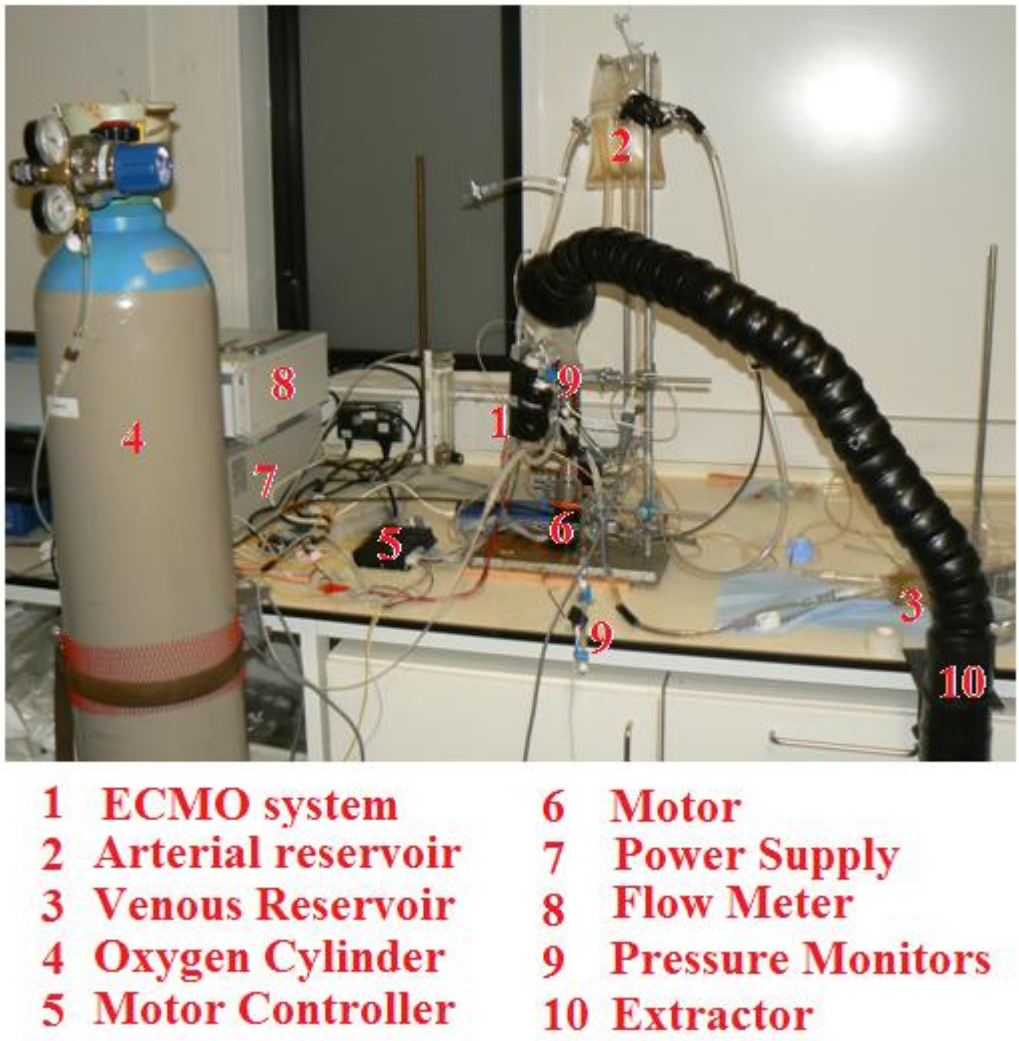


**Figure 308: Experimental set-up used to determine the performance characteristics of the integrated system with each of the elements of the experimental set-up highlighted.**

The impeller was driven via a EC-Max Brushless DC motor controlled using a EPOS2 motor controller ((Maxon Motor UK, Berkshire, UK) which was powered by a CPX400A 60 v 20 A DC power supply (TTid, Cambridgeshire, UK). A 25 mm OD and 6 mm ID clamp style jaw coupling with torque disk was used to couple the motor to the pump shaft (Ruland Manufacturing Company, Inc., Marlborough, UK).

A TS410 flow meter (Transonic Systems Inc., New York, USA) was attached to the outlet tubing to determine the fluid flow rate within the system in ml/min. This ultrasonic device is commonly deployed in clinical practice.

TSD104A Blood pressure transducers (BIOPAC Systems Inc., California, USA) were positioned at the inlet to (pre-load) and outlet from (after-load) the pump. Pressure values were recorded in (mmHg). The pump system and pressure monitors were primed with 0.9 % saline solution (Baxter, Berkshire, UK) prior to running the motor.

Temperature measurements were taken at the inlet to and at the outlet from the integrated system and at the outlet from the arterial reservoir and at the inlet to the venous reservoir using MT-29/1 T type hypodermic needle microprobes (Physitemp Instruments Inc., Clifton, NJ, USA). Measurements were recorded at a rate of 1 per minute for 6 hours using a TC-08 USB data logger (Pico Technology, Cambridgeshire, UK).

The heat exchanger was controlled using a NI control system (National Instruments, Austin, Texas, USA) and a custom made temperature controller, which controlled the peltier temperatures in response to changing system temperatures always aiming to maintain fixed temperature conditions.

Oxygen was provided via pressurised cylinder and the flow rate was measured by a gas flow meter (SECHRIST Industries Inc., California, USA). A gas flow ratio of 1:1 was employed in these studies.

The circuit was closed with the pump feeding from a reservoir positioned slightly lower than the inlet pumping fluid to a raised reservoir, which drained by gravity back to the lower reservoir. An 8 French cannula was placed at the outlet of and a 10 French at the inlet to the integrated system. A gate clamp on the feed to the upper reservoir was used to restrict flow and induce a pressure. A gate clamp was also used on the gravity drain

from the upper (arterial) reservoir to balance the flow rates to the lower (venous) reservoir. Initially the system was run without oxygen or heat provided to obtain control values. The system was run for 15 minutes and then oxygen, temperature and pressure measurements were taken. The pump speed was set at 6000 r.p.m and a gate clamp prior to the upper reservoir was adjusted to achieve a flow rate of approximately 350 ml/min. The system was run for 6 hours with flow rate and oxygen values taken every 30 minutes. Temperature and pressure values were recorded automatically every minute. The complete experiment was repeated three times.

### 6.7.3. Results

The main performance characteristics measured within this experiment were the pressure and temperature at the inlet to and outlet of the ECMO system and the oxygen partial pressure in the saline. As this was an endurance test the performance characteristics were plotted against time. Figure 309, Figure 310 and Figure 311 show pressure and temperature at the inlet and outlet of the system and oxygen partial pressure against time respectively. Figure 312 shows flow rate against time to show the range in which flow rate was maintained throughout the experiment.

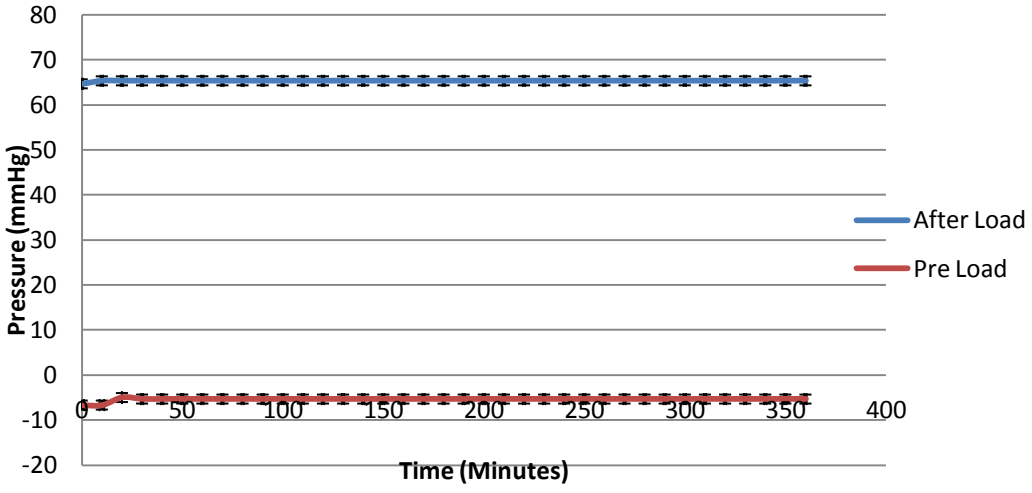


**Figure 309: Pressure at the inlet (pre-load) and outlet (after-load) of the integrated system against time. ± 1 Standard Deviation.**

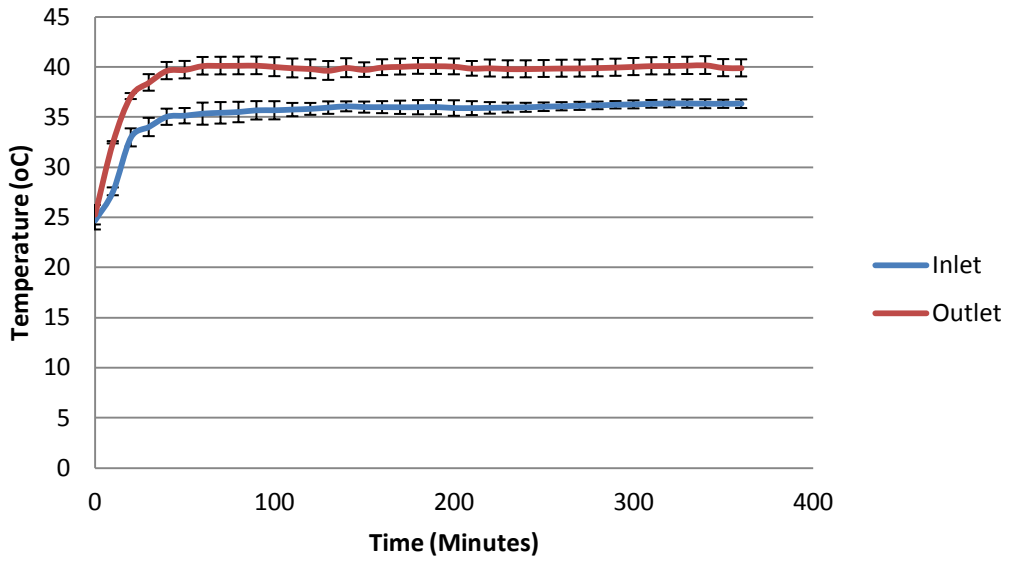


**Figure 310: Temperature at the inlet and outlet of the integrated system against time. ± 1 Standard Deviation.**

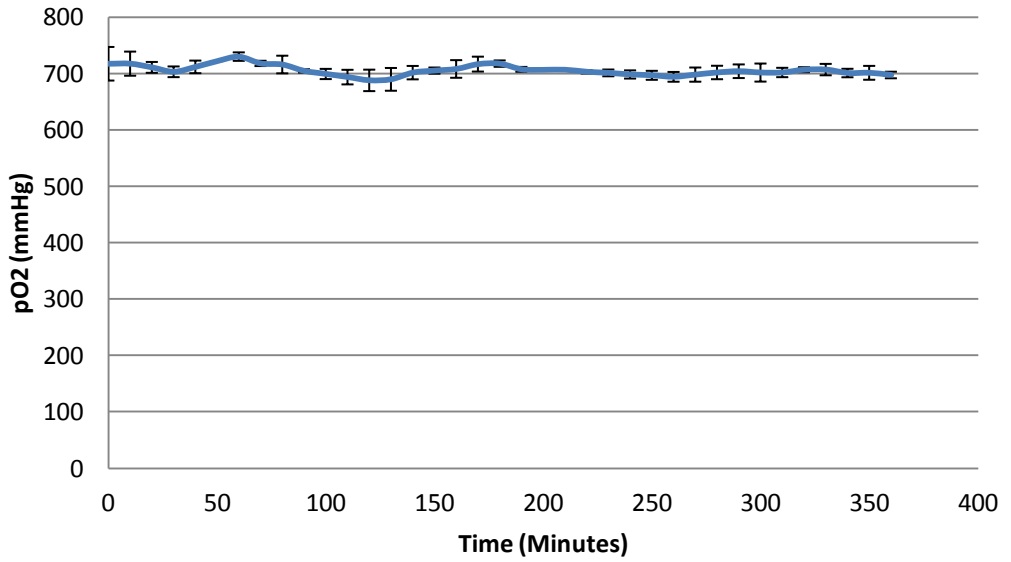


**Figure 311: Oxygen partial pressure of the saline used in the integrated system test circuit against time. ± 1 Standard Deviation.**

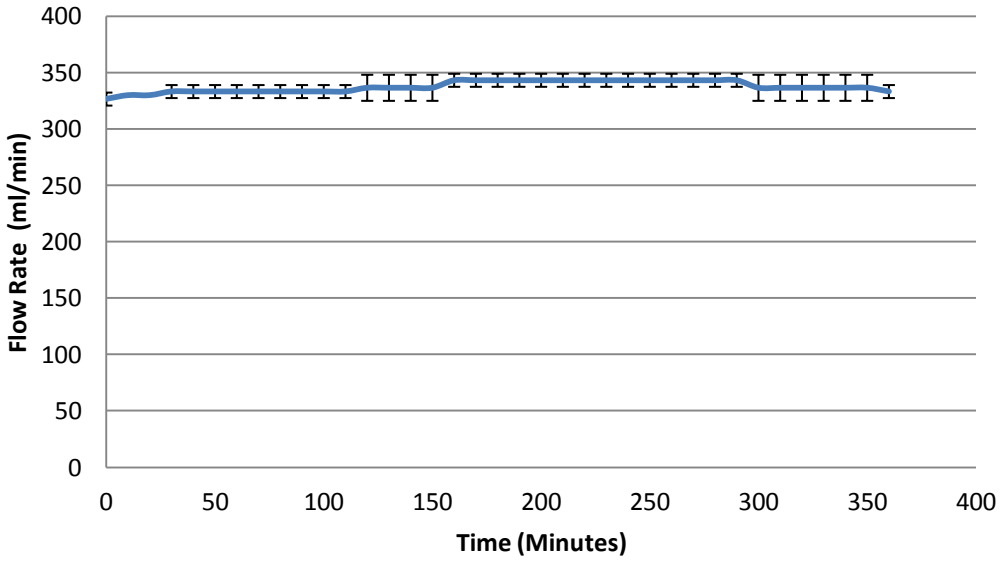


**Figure 312: Flow rate within the integrated system test circuit against time. ± 1 Standard Deviation.**

### 6.7.4. Discussion

This experiment was designed to replicate the conditions that apply to a live animal experiment in the closest manner possible. This experimental set-up has allowed for an effective evaluation of the miniaturised and integrated system developed and has provided feedback not only on the performance of the system but also on the manufacturing method and of the final integrated configuration. The performance characteristics of the integrated system can be compared to the individual performance characters in all cases except for the oxygenator as saline was used instead of blood. In this case the performance of the oxygenator was assumed to be unaffected by the integration configuration as the geometry of the oxygenator was unmodified. Table 6 below compares the performance characteristics of the heat exchanger and axial flow pump endurance testing against the results of the integrated system testing.

| | **Heat Exchanger** | *± 1 STD* | **AFP** | *± 1 STD* | **Integrated System** | *± 1 STD* |
|---|---|---|---|---|---|---|
| | | | | | | |
| **Temperature Difference** | | | | | | |
| *(oC)* | 2.51 | 0.46 | N/A | N/A | 2.43 | 0.4 |
| **Pressure** | | | | | | |
| ***Pre-Load*** | | | | | | |
| *(mmHg)* | N/A | N/A | 23.85 | 0.36 | -6.12 | 0.6 |
| ***After-Load*** | | | | | | |
| *(mmHg)* | N/A | N/A | 120.97 | 1.28 | 65.92 | 0.4 |
| **Flow Rate** | | | | | | |
| *(ml/min)* | 300 | 0 | 414.11 | 13.63 | 342.5 | 9.89 |

**Table 6: Table comparing the results of the heat exchanger and pump component testing to the results of the integrated system testing.**

Comparing the endurance test of the heat exchanger to the integrated results the difference can be attributed to the difference in flow rate and the additional heat loss that occurred within the pump and oxygenator, which were not included in the heat exchanger component testing. This comparison shows that the integration strategy has had no significant effect on the performance of the heat exchanger.

Comparing the overall pressure head it can be seen that there is a difference of approximately 25 mmHg between the two systems with the individual component producing a higher pressure head and flow rate. The differences between the systems can be attributed to differences in the heights of the reservoirs used in the experiments; however the main factor to have influenced the performance characteristics is more likely due to the inclusion of a 10 French cannula at the inlet to the device in the integrated system. The reduced cross-sectional area of the cannula restricts the flow into

the device and as a result a slightly negative pressure at the device inlet is observed. This negative pressure indicates that the pump has to provide suction in order to remove fluid from the lower reservoir. Reducing this cross-sectional area, through the use of a smaller cannula or through occlusion of the cannula tip by the vein wall, is likely to reduce the pressure further. If the pressure becomes excessively negative cavitation could occur, which could result in haemolysis (Bluestein and Mockros 1969; Reul and Akdis 2000). Furthermore the cross-sectional area at the inlet will limit the potential flow rate through the device. In a situation in which the maximum flow rate is reached increasing the r.p.m of the pump to induce more flow will simply result in a higher negative pressure at the inlet and increased haemolysis around the impeller.

It can therefore be seen that the venous pressure plays a key role in controlling an ECMO system and that the cannula has a major impact on this. Placing the largest bore cannula possible and ensuring that the tip is un-occluded is paramount to achieving the required performance. The size and placement of the cannula are dependent upon the vessels of the patient and the skill of the physician respectively.

### 6.7.5. Conclusions

This experiment has shown that the miniaturized and integrated system developed can satisfactorily perform under clinically relevant conditions for an extended period of time. The results show that the system results are comparable to the results obtained from testing of the individual components, indicating that the integration strategy has been successful. This work therefore suggests that the system is ready to move on to testing within a live animal experiment.

## 6.8. Chapter Conclusions

The fundamental components previously developed were shown to individually meet the requirements of a miniaturized and integrated ECMO system. The final stage in the development of the complete device was in the integration of these components. The work within this chapter focused on producing an integration strategy that met the following requirements:

- Optimization of system miniaturization through efficient integration without compromise in performance.
- Design manipulation to introduce safety features such as bubble traps.
- Design for ease of assembly, accessibility and reproducibility.
- Design for practicality to allow the system to be easily tested within a live animal experiment.

The development method used in this section relied heavily upon computational simulation. The models previously established and validated for each component were used to simulate the integration process, allowing several design iterations to be tried and tested prior to physical prototyping. This design approach was particularly essential in this phase of the system development as the manufacturing and assembly of the entire system was both time consuming and costly. The integrated ECMO system met all of the design criteria without compromising on performance. The system as a whole produced results that were comparable to those achieved by the individual components. The integration process therefore had no measureable negative impact upon the combined chain of technologies in terms of overall performance. The test conditions used to evaluate the design replicated the conditions of a live animal experiment as closely as possible. The results of the work conducted in this chapter have shown that the ECMO system produced is easy to assemble, safe to use, is reliable and can meet the performance requirements of a live animal experiment.

# 7. Animal Studies

## 7.1. Deployment of Integrated ECMO system in an animal model of partial circulatory support

The primary objective of this element of the work was to investigate the function of the integrated ECMO system under near-clinical conditions. A porcine model was employed and the work was undertaken after ethical and Home Office approval, under the animal license number 70/4660, for an acute support procedure on a series of 8 pigs. The approach was at all times similar to that employed in the clinical setting using fully anaesthetized animals which were sacrificed in accordance with Home Office regulations after a period of 6 hours of partial support. The partial support model in 10kg farmyard pigs was employed due to difficulties in achieving effective cannulation in a prior mini-pig model. The cannulation of the mini-pig was complicated by a vessel/body mass size mismatch which resulted in cannulae of insufficient size to support full circulatory support being deployed. This problem of vessel size mismatch was overcome when larger farmyard pigs were employed; however this led to a compromise in the level of cardiopulmonary support delivered which was restricted by the inherent performance envelope of the support technology that was designed for smaller animal deployment. The experimental procedure was as follows;

## 7.2. Anaesthesia and surgical procedure

Eight male farmyard pigs of between 8.5 and 13kg (10.7 +/- 2.8kg) were employed in these experiments. The animals were housed in the animal house for a period of at least 4 days prior to the procedures to ensure hydration levels and stress reduction. On the day of the experimental procedure the animals were pre-medicated with 17mg/kg Zoletil 100, and then transported to the operating room where anaesthesia was induced using Isofluorane (1-2%) and maintenance anaesthesia provided with Propofol (10mg/ml) at 4-

6mg/kg/hr and Fentanyl (0.035mg/kg/hr). A rectal temperature probe was inserted to monitor central temperature and a cannula inserted into the femoral vein for drug and fluid administration. After anaesthesia the animals were placed on their left flank, permitting access to the right external jugular vein and carotid artery. These vessels were exposed and slings were placed around them to aid insertion of arterial and venous cannulae and to control blood loss as shown within Figure 313.

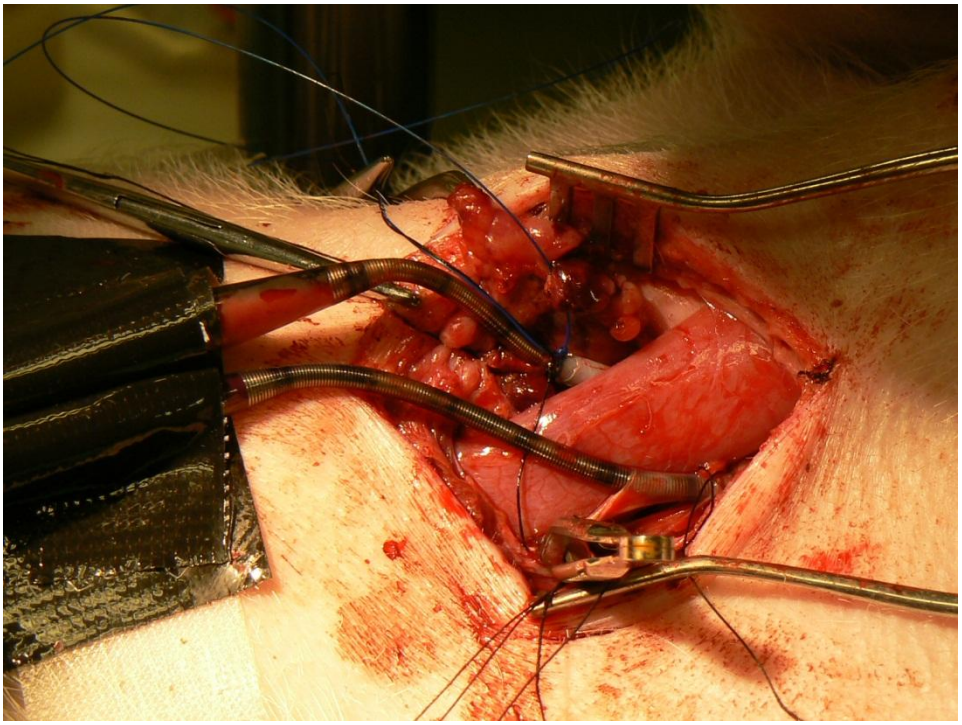

**Figure 313: Venous and arterial cannulae inserted and secured for attachment to the ECMO system.**

Heparin (5000IU) was then administered via the femoral vein. Additional heparin was added throughout the experiment to maintain an ACT of 400 seconds. A venous cannula (10 F, Bio-Medicus, Medtronic, Minneapolis, USA) was first inserted into the jugular vein and advanced several cm. The cannula was then tied in place using a nylon tie and secured to the surrounding tissues to prevent cannula migration. The cannula was then allowed to fill with venous blood, the cannula clamped and connected to the venous inlet

of the ECMO system via a ¼" connector. Air was purged from the cannula/tube interface using a saline filled syringe to displace air whilst making the connection. Once the venous system had been established, an arterial cannula (8F) was inserted into the carotid artery and advanced to the aortic margin. The cannula was withdrawn one cm upon feeling resistance to further advance. The cannula was primed by slowly releasing a tubing clamp until it was filled to the ¼" connector which would be used to connect to the ECMO system. The connection was made in the same manner as that described for venous cannula deployment. The system loop was at this point completed and the primed device remained clamped until ECMO was initiated. Figure 314 and Figure 315 show the system at initiation of the procedure and connected to the animal immediately prior to initiation respectively.

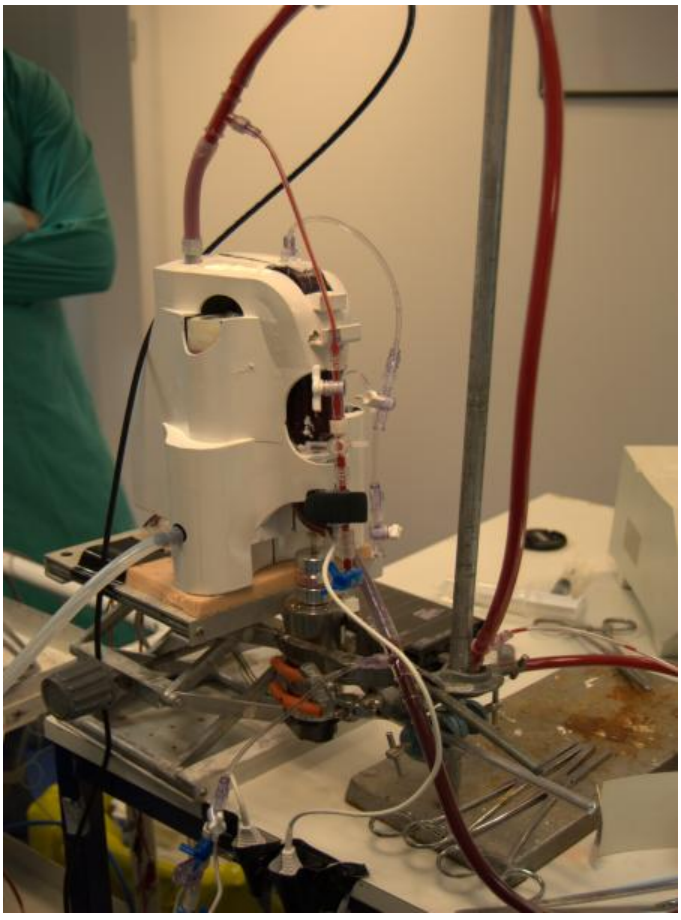

**Figure 314: The ECMO system shown at initiation of the ECMO procedure.**

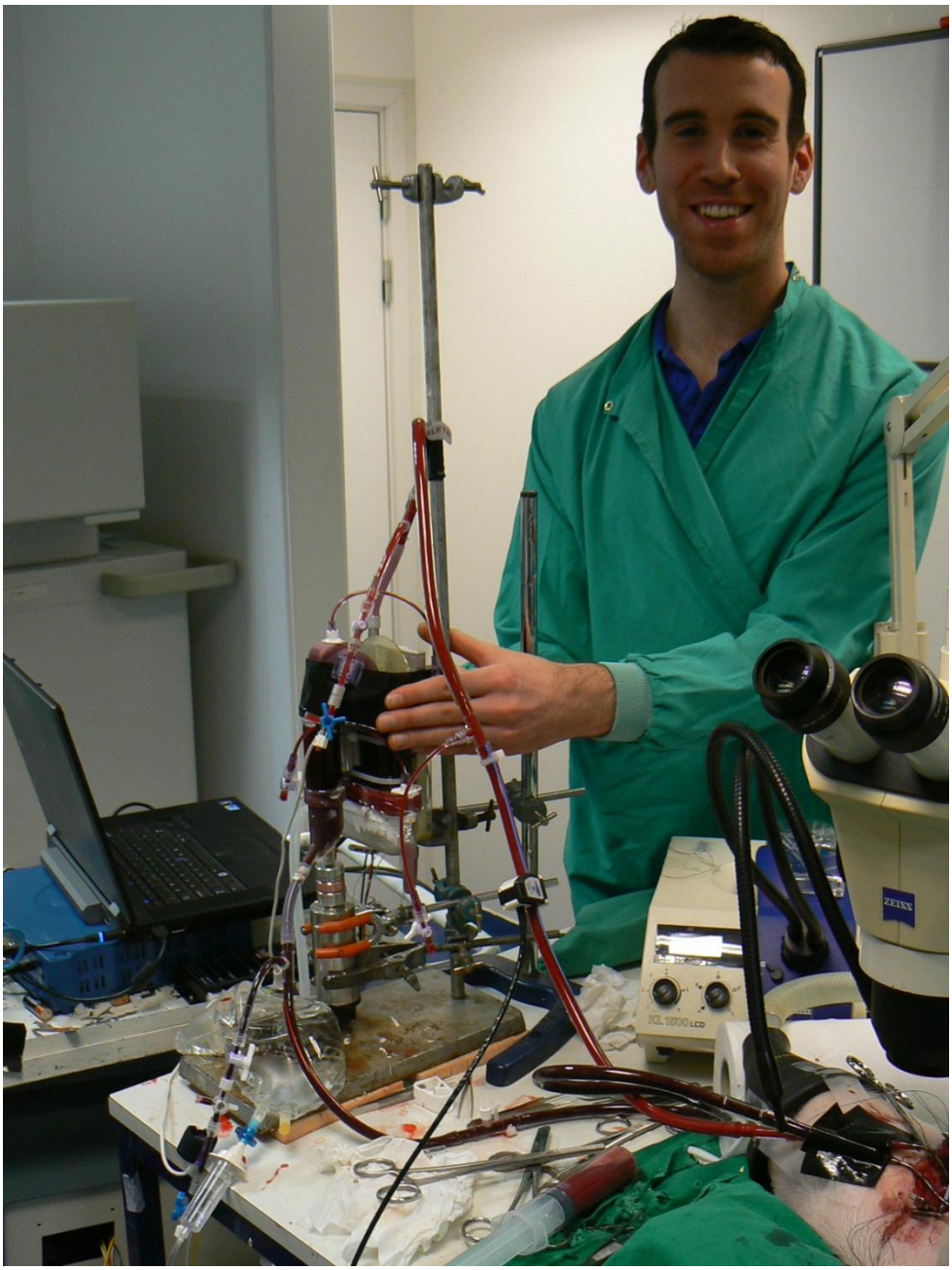


**Figure 315: ECMO system shown connected to the animal immediately prior to initiation of ECMO support.**

## 7.3. ECMO system assembly

The integrated ECMO system was assembled and a breakaway circuit constructed to permit both system priming and ultimately connection to the animal as shown within Figure 316.

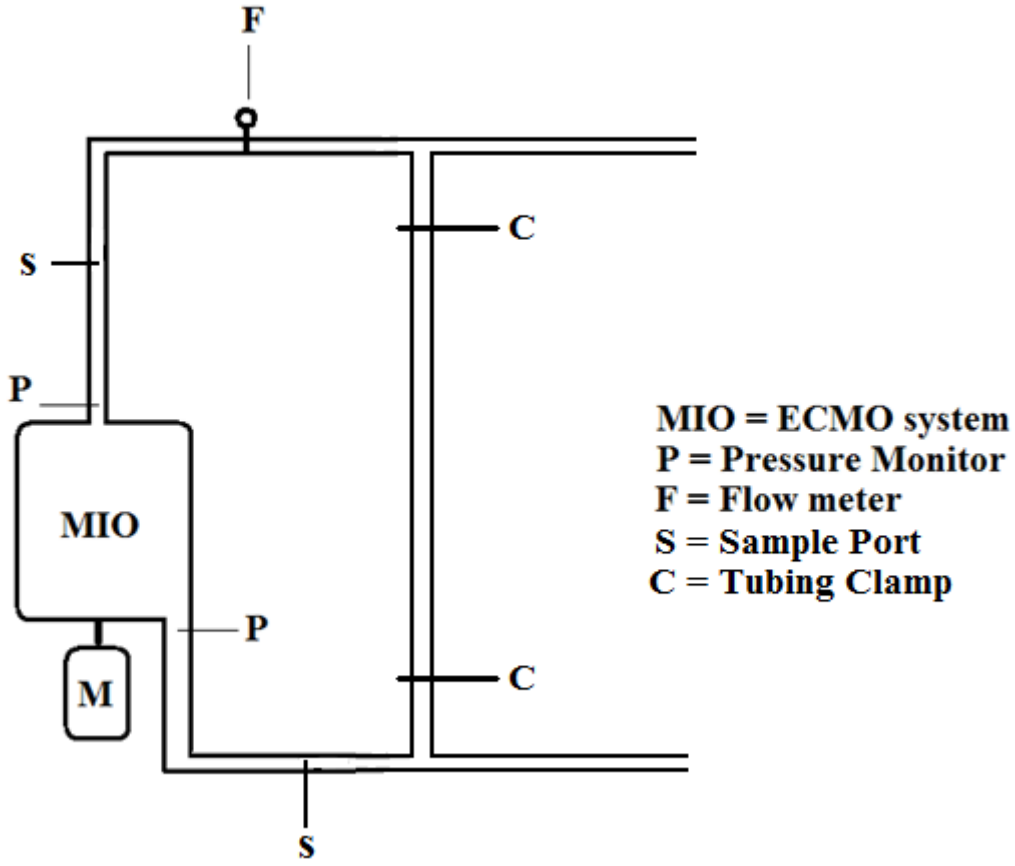


**Figure 316: Diagram of circuit showing the position of the monitoring devices and the breakaway loop used for priming purposes.**

The system was primed with Ringer's solution, and 5000 IU of Heparin administered to ensure anti-coagulation. The circuit was re-circulated whilst the surgical procedure was being undertaken, and once primed and de-aired using the in-built purge ports, the system was clamped off with tubing clamps and the break-away portion divided for attachment to the arterial and venous cannulae. Throughout the reperfusion phase the

circuit temperature was maintained at 37 degrees Celsius using the Peltier heat exchange system. An ultrasonic TS410 flow meter (Transonic Systems Inc., New York, USA) was attached to the arterial outlet of the system throughout the priming stage and remained in place for initiation and conduct of ECMO support. The circuit pressures were measured at the arterial and venous aspects of the circuit using TSD104A pressure transducers (BIOPAC Systems Inc., California, USA) to monitor these important functional characteristics. All system measurements were recorded either manually or using a data acquisition system throughout the procedure for future analysis.

## 7.4. Conduct of circulatory support

Once the cannulae had been successfully placed and the ECMO system primed and completely de-aired, circulatory support was initiated. The procedure was as follows;

1. The pump was gradually increased to a rotational rate of 2000 RPM
2. Gas flow was initiated at a 1:1 ratio to required blood flow rate (300ml/min)
3. The venous and arterial clamps were removed.
4. Blood flow and blood flow direction were monitored using the ultrasonic blood flowmeter.
5. Venous and arterial pressures were monitored.
6. Blood flow was increased by increasing the rotational rate of the pump to a positive displacement of 300ml/min
7. Venous pressure was closely monitored to ensure that excessive negative pressure was avoided (less than -10mmHg)
8. Once the system was stable, the first of a series of blood samples were taken for the assessment of Blood Gasses.
9. An ACT measurement was taken to ensure that an ACT in the range of 350-500seconds was maintained throughout the procedure.
10. Pressures, flow rate and temperature were recorded continually.

Once the desired flow rate was achieved, blood flow was adjusted to maintain a venous inlet pressure not exceeding -10mmHg. In this series of experiments blood flow adjustment was carried out manually in response to measured venous pressures. In general terms the rotational rate of the pump was increased or reduced in 500RPM steps in response to a change in venous pressure of 2mmHg around a fixed projected mean of -8mmHg. Clearly the size of the inflow and outflow cannulae has an effect upon the pressure profile of the device in use, and this factor was studied throughout this series of experiments as the maximum size of cannula for each vessel was deployed. Therefore in an attempt to maintain the predicted 300ml/min flow rate in these animals, there were occasions where the venous pressure was permitted to exceed -10. The effects of this will be discussed in the latter part of this chapter. During the conduct of the support procedure blood gas samples were taken from the venous and arterial lines of the system for determination of oxygenator performance. In addition blood pressures and central temperature were recorded at regular intervals. The blood flow was monitored continuously during the experimental period. In addition, observations regarding the general performance of the system were recorded, together with any technical failures. After the experimental period, the animals were sacrificed in accordance with Home Office scheduled methods (by exsanguinations and delivery of Uthenol).

## 7.5. Results and observations

The focus of this element of the study was to demonstrate the functionality of the integrated device in terms of the maintenance of partial cardiopulmonary support in an animal model. The factors which were studied largely reflected this focus, blood flow, blood gases, circuit pressures and temperature. Given that the system was providing only partial support, in the region of 15% of the total requirements of these animals, systemic parameters were given less consideration unless there was an apparent systemic problem.

### 7.4.1. Maintenance of clinically acceptable blood oxygenation.

Typical A-V colour difference seen during the ECMO procedures is shown in Figure 317. The clarity of difference in observed red colour intensity between venous (inlet) and arterial (outlet) blood is used by clinical teams as a first indicator of the adequacy of oxygenation, and although not a scientific measure of adequacy of oxygenation represents a first pass qualitative assessment.

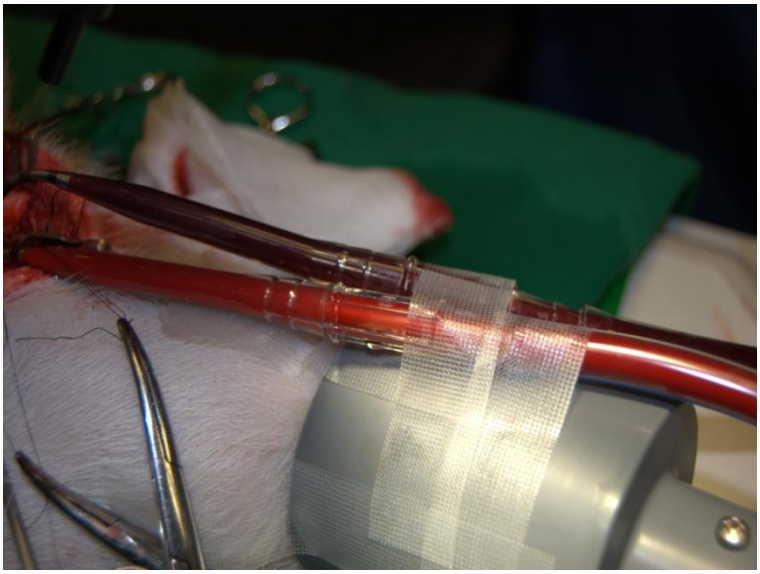

**Figure 317: Inlet and outlet tubes of the ECMO system during use. The clear A-V difference demonstrates that the system is oxygenating.**

More formal analysis of the oxygenation performance of the ECMO system was carried out and the results are shown in Figure 318. The red box indicates acceptable range of oxygen and carbon dioxide partial pressures, which were defined by Gourlay et al (Gourlay, Fleming et al. 1990).

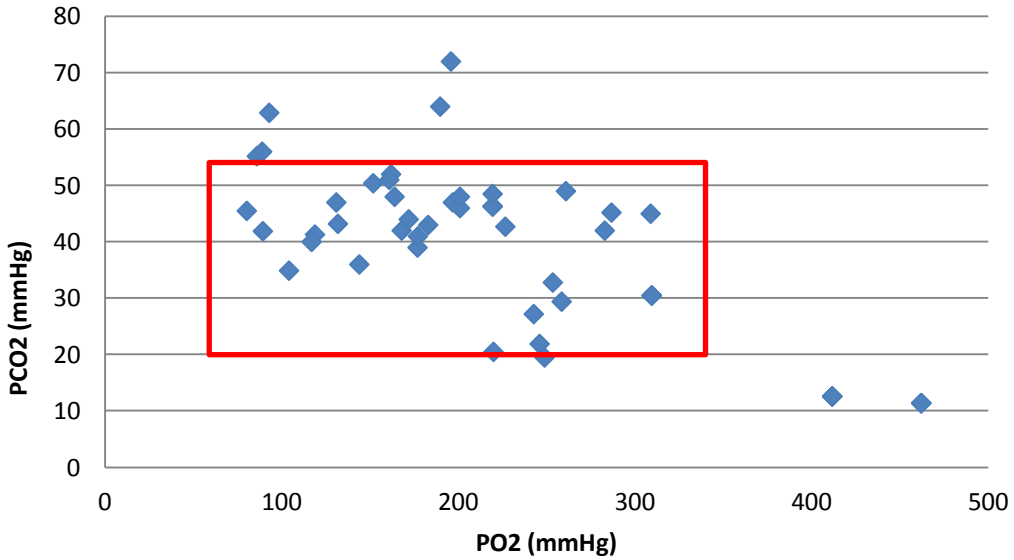


**Figure 318: The PO2 of samples taken from the ECMO system at random intervals are shown and put into context of the acceptable range (red box).**

### 7.4.2. Blood Flow

The blood flow generated by the ECMO system varied in response to the inlet and outlet conditions. This was particularly apparent in relation to the inlet conditions. The effect of inlet pressure on blood flow in this series of experiments is shown in Figure 319 and Figure 320.

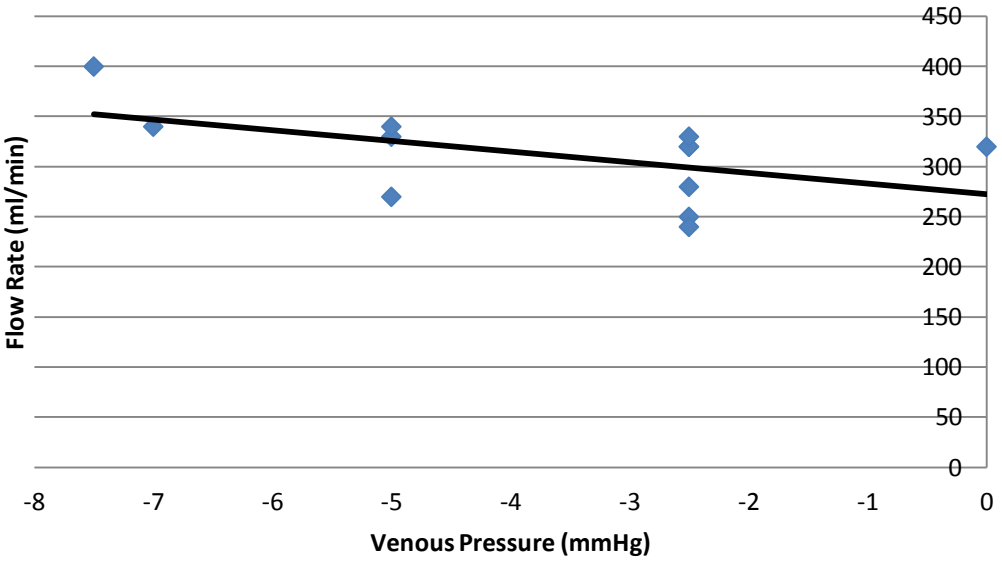


**Figure 319: The relationship between blood flow and inlet pressure across the expressed normal range of inlet conditions (-1—8mmhg).**

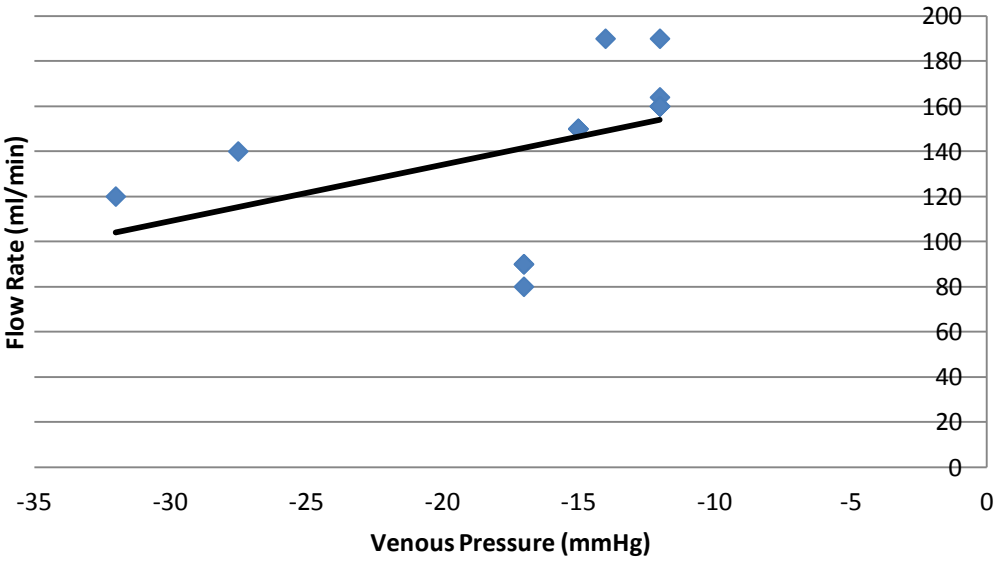


**Figure 320: The relationship between blood flow and inlet pressure beyond the normal range of inlet conditions.**

The relationship between blood flow and inlet pressure was largely as anticipated. Over the range 0 to -8mmHg there was a near linear increase in blood flow which rapidly

dropped as the venous inlet pressure fell beyond -8mmHg. These results clearly demonstrate the "clinical" range of inlet conditions for the integrated device suggesting that the acceptable range is indeed 0 to -8mmHg under the cannulation conditions employed. The reason for the reduction in blood flow associated with the lower venous pressures is most likely interaction between the RA wall and the cannula tip, resulting from some degree of vascular collapse as the system generates increasing levels of negative pressure.

### 7.4.3. Maintenance of Temperature

Body temperature was investigated to ascertain whether the system as capable of compensating for heat loss from the animal during the experimental procedure. A typical example of the temperature profile observed s shown in Figure 321.

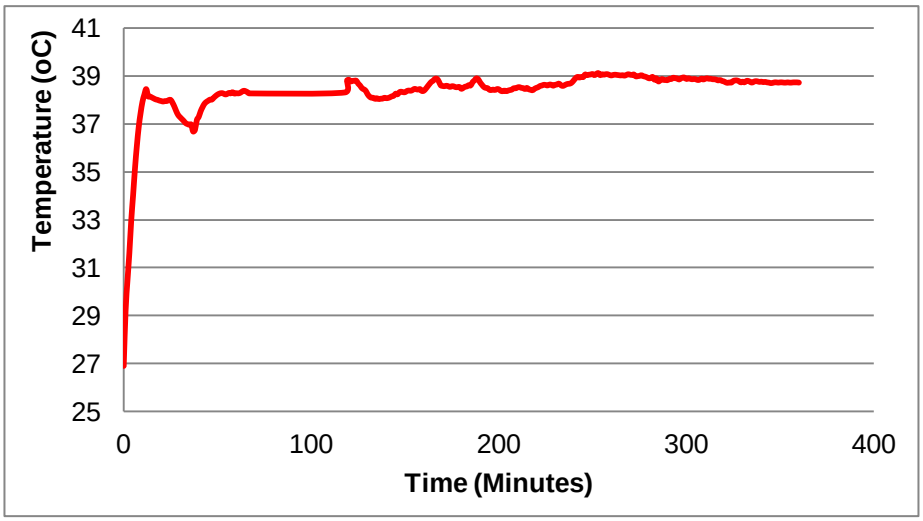


**Figure 321: The temperature profile observed in one animal over the experimental period.**

It was clear that the level of heat loss associated with the partial support procedure was small and that there was very little by way of variation in central temperature. There was in fact little or no need to deploy the heat exchanger during these experiments. The example shown represents the experiment during which there was the greatest temperature variation. The system had no difficulty in maintaining body temperature

during this procedure. A more critical challenge would be presented if the experiments included a period of hypothermia; however, this is not normal clinical practice and was thought to be inappropriate in this series of experiments.

## 7.6. Discussion

The animal experiments have in general confirmed the efficacy of the novel integrated ECMO technology. These experiments were carried out in a small group of animals, with the objective of evaluating the general performance of the device under "near-clinical" conditions. The device was associated with a good and reproducible performance profile, in terms of blood gas exchange, body temperature maintenance and blood flow delivery. Latterly, once the study moved to a larger pig model, there were no technical problems with the deployment of the device, but there were some unexpected challenges in earlier studies in which the device was deployed in mini-pigs of 3kg or less. In this early series of experiments it became clear that there was an issue of body mass/vessel diameter mismatch, which was not anticipated. In these mini-pigs it was not possible to deploy an arterial cannula of more than 4F and venous cannula size was restricted to 6F or less. The anticipated flow rate for mini-pigs of around 3kg is in the region of 300ml/min, well within the performance envelope of the ECMO system, however, this level of blood flow was not possible using cannulae of these dimensions. It was therefore decided to move on to a partial support model in larger pigs. This approach was considered to be appropriate as the objective was to test the performance of the device under free flowing conditions rather than to investigate the pathophysiological impact of its deployment on the subject animals, and such a partial model would permit the deployment of cannulae of normal clinical proportions in keeping with the flow range of interest. Once the experiment moved to this model, the device performed well and there were no technical failures.

Overall, the device proved to be capable of performing partial support in the large animal model in terms of all major functions. The prototypes were found to robust and predictable in performance.

## 7.7. Conclusion

The conclusions from these studies are as follows;

1. The integrated ECMO device was capable of providing acceptable gas exchange performance.

2. The pump was capable of generating predictable and reliable blood flow.

3. The Peltier heat exchanger system was capable of maintaining body temperature under the test conditions.

4. The device was robust and was associated with no technical failures.

5. There is a clear relationship between the venous inlet pressure conditions and the blood flow generated by the system.

6. There appears to be a clear “acceptable” range for venous inlet pressure for the safe and reliable function of the pumping component of the system.

# 8. Discussion and Conclusions

Life support systems have been employed in the clinical setting for many years (Gibbon 1954). Advancements in technology have resulted in systems that can temporarily replace the function of the heart and lungs allowing surgeons to perform surgery on a stationary platform over short periods of time (CPB) or to provide support for critically ill patients over extended periods of time (ECMO). ECMO has been responsible for saving the lives of many thousands of patients, particularly in the neonatal population. Despite this technical success, ECMO is associated with high morbidity and mortality rates. The ELSO findings up to 2008 report average mortality rates of approximately 35 % for VA ECMO and 74 % for VV ECMO. In general terms, the complications associated with ECMO deployment fall into 2 categories; 1 Patient related complications; 2 Technical complications and failures.

One of the most significant factors leading to complications of ECMO therapy is the technical complexity of the systems currently utilized in clinical practice. This complexity has been shown to contribute to complications such as, clot formation, oxygenator failure and failure of the connectors which are generally manually inserted into the ECMO system to interconnect the various parts of the system. Upp and Zwischenberger very elegantly described these challenges (Upp, Bush et al. 1994). Patient, rather than technical complications are also commonplace in ECMO therapy, but many of these are attributable to the technology and the long-term invasive nature of the procedure. Typically these include, the consumption of clotting factors leading to excessive bleeding, the activation of inflammatory processes due to the large blood contacting foreign surface area of typical ECMO systems and emboli production related to both clotting disruption and inflammatory processes. Gourlay described the impact of blood contacting surface area on the activation of inflammatory processes, confirming that there is a near linear relationship between surface area and the level of expression of

adhesion molecules on neutrophils under extracorporeal conditions (Gourlay, Stefanou et al. 2001).

A second, and significant challenge presented by the use of complex, high surface area devices for ECMO deployment, particularly in the neonatal setting, is the need to utilize large priming volumes to prepare the systems for clinical deployment. The impact of this priming requirement is a substantial dilution of the patient's blood, leading to low hematocrit and dilution of clotting factors etc. Gourlay et al confirmed that this haemodilution also results in further activation of inflammatory processes, a finding which Habib et al confirmed under clinical conditions (Gourlay, Samartzis et al. 2003; Habib, Zacharias et al. 2003; Hamrick, Gremmels et al. 2003). These issues assume much greater significance when ECMO is deployed in small children, where the surface area/body mass ratio is much higher leading to lower hematocrit levels during ECMO deployment.

The ECMO system complexity and large footprint render it both expensive and difficult to deploy for emergency use, and indeed limit its widespread use in general clinical practice despite clear evidence that delay in deployment has been shown to result in considerable negativity with regard to the success of ECMO therapy and its associated outcomes ((Schumacher, Roloff et al. 1993; Gill, Neville et al. 2002; Hamrick, Gremmels et al. 2003; Chaturvedi, Macrae et al. 2004; Brown and Goldman 2008)). In general terms the complexity of the ECMO system and its very large footprint has resulted in this intervention being available only in specialist centers which, in times of stressed need such as swine flu or other epidemics, results in an imbalance between supply and demand for this high end life saving technique.

A review of the literature suggests that the major challenges to maximizing the safe and effective widespread delivery of ECMO are as follows:

1. Complexity and size of the current systems.

2. Large footprint
3. Access to rapid deployment
4. Access to diagnostic tools whilst on ECMO support.

In this thesis we considered a possible strategy to mitigating some of these significant challenges, miniaturization and integration of the components of the ECMO system. To further enhance this strategy we considered some degree of independence from mains supplies to the system, particularly with regard to water supply for heat exchange purposes. It was thought that such an approach might lead to a smaller disposable component, smaller overall footprint and as a result enhance deployment capability through some degree of mobility achieved through independence form mains or tank water supplies. This concept appeared to be both logical and achievable, but required considerable understanding of the ECMO environment, patient and clinical needs and the design and performance requirements of the individual circuitry components. This work had a broad focus, incorporating design, evaluation and ultimately near-clinical deployment of novel technology for this highly specialist clinical technique. However, in designing such a system it is essential that due consideration of performance requirements and the impact of miniaturization on device safety be borne in mind.

Clearly such an approach to mitigating the challenges faced in the ECMO setting is not simply to make things smaller. Gourlay described that in some respects making devices smaller, with low priming volumes, in some respects, compromise safety, particularly with regard to the propagation of air emboli through extracorporeal systems (Gourlay 2012). In this respect small is not necessarily beautiful. This is a serious consideration in terms of the primary objectives of this thesis.

The design, development and testing process employed in this work has been described in the early chapters of this thesis. The performance and environmental requirements of the technology under development informed the design process and the level of

acceptance of the developed devices, in terms of clinical perspective, must be assured by investigation under clinically mimetic conditions, rather than simply clinician input. The design of ECMO devices and their components is a costly and iterative process which takes considerable time for validation and refinement. In this work we took the view that the many iterative steps involved in conventional physical design and testing process of ECMO/CPB technologies was both inelegant and time consuming. In recent years, complex computational models have evolved to aid in the design of complicated technologies, and these have been applied to CPB/ECMO design, particularly with regard to the pumping system. Burgreen et al suggested that the use of these modern design and modeling tools can both improve and speed up the design process by reducing the number of physical modeling iterations (Burgreen 2001). The benefits of this design strategy has been recognized and adopted by several other authors (Matsuda 1999; Gage 2002; Chimenti 2004; Qian 2006; Dehbahani 2009; Graefe, Borchardt et al. 2010). Given the budgetary constraints of this project a reduction in physical model production would be of great benefit to the process and would increase the possible horizons for achievement. In the present work this suggestion was well founded as we were able to test only a limited number of design iterations, but having performed fairly complex computer simulations, these iterations were in all cases, very close to acceptable and predicted performance levels when tested on the bench. Ultimately, we were able to construct an integrated device, modeled and proven to be of acceptable performance under computerized conditions, which were deployed in the animal environment. There must be some doubt as to whether this position could have been reached without the use of modern computational tools.

There are 3 core elements of the ECMO system; the oxygenator, blood pump and heat exchanger. Each of these components presented a different set of challenges in terms of the modeling and design process. Beyond this, the integration of all 3 presented another set of challenges.

The oxygenator was in many ways the least complex design challenge, but had the most stringent performance demands in terms of regulatory requirements and clinical performance. There are many differing configurations of oxygenator in current clinical practice, but by far the most common configuration is the extra-luminal blood flow configuration. There are a number of reasons for this, but Toomasian et al described both the safety and performance advantages of this configuration in an animal model and Khoshbin et al under clinical settings, leading to its general clinical uptake (Khoshbin, Roberts et al. 2005; Toomasian, Schreiner et al. 2005). Although, from the perspective of modeling, the simplicity of the blood inside the fiber configuration represents a smaller challenge the extra-luminal blood flow configuration offers both higher performance and safety which were the driver features for us adopting this type of device.

The modeling of this configuration represents a real challenge and to overcome this we adopted a porous media model, described by Graefe et al (Graefe, Borchardt et al. 2010). Whilst fully recognizing that this approach is at best a compromise solution, it is the most commonly employed model for the design of oxygenator devices and was within the modeling capability of the Bioengineering department. Ideally we would wish to model the device by replicating the actual physical conditions in the device, including the hollow fibers themselves, but the computational requirements to achieve this are beyond our current capability. However the model utilized proved to be valuable and reproducible, enabling the design and in particular, performance improvement of the device under development. Physical modeling of the oxygenator facilitated performance testing, but did not shed light on the underlying reasons for any lack of performance. This is where the use of computational modeling was of greatest use to the work. Through computational modeling we were able to identify issues such as shunting and stasis which are known to contribute to both inadequate performance of oxygenators and some activation of formed blood elements. In this regard, given the inability to identify underlying mechanisms of poor performance in physical models, the computer modeling was the primary design, diagnostic and testing tool. Indeed the quality of the modeling

and the information derived from it considerably reduced the number of device iterations required to reach our ultimate configuration. In this way physical modeling and testing was ultimately used as a method of confirmation of the computer design.

Conventionally, the pumps employed for ECMO applications consist of either roller pumps or centrifugal pumps. The 2011 review of ELSO registered hospitals indicate that 82.5 % of institutions use a roller pump and 17.5 % a centrifugal pump (Lawson, Ellis et al. 2011). Both offer a number of advantages and disadvantages under clinical conditions, but there is over 30 years of experience in using both types, and both are considered to be acceptable under normal conditions. However, neither the roller pump nor centrifugal pump lends themselves to the minimized integrated approach to ECMO.

The roller pump is essentially a non-disposable technology and the profile of conventional centrifugal pumps presents a challenge for integration. With this in mind we adopted an alternative approach, the axial flow pump. This configuration, so well described as a VAD device (Wieselthaler, Schima et al. 2000; Fraizier, Myers et al. 2002; Goldstein 2003), offers a more suitable form for integration. Its tubular profile sits very conveniently within an integrated ECMO device. The characteristics of this pump configuration are well understood and described in the literature, resulting in little need for reconfiguration for this application. There are some characteristics of the axial flow configuration which must be borne in mind when incorporation into an integrated technology are being considered, not least the fact that, like the centrifugal pump, it is an essentially non-occlusive circuit component resulting in a need for external flow monitoring. Apart from its “shape”, the axial flow device functions rather like a centrifugal device, being both pre-load and after-load dependent to some degree. This raises little concern, as the long clinical ECMO experience with such non-occlusive kinetic pumping solutions has generated a degree of conceptual familiarity. The design of the axial flow pump for blood pumping applications does present some challenges. Uppermost of these is the need to perform the blood perfusion role without causing damage to formed blood elements. The haemolytic effect of such a system is associated

with the sheer stresses caused by the shape and attitude of the impeller and the interface between the impeller and the outer housing. The critical issue of rotor design was apparent very early in the design and evaluation process, where we identified the effect of rotor pitch and rotor/casing gap on haemolysis generation and flow generation. These critical elements were the focus of much research and design effort in this thesis resulting in a device which had both an acceptable physical form and adequate function. Although the axial flow pump is not the convention in the ECMO setting, our experience in this present work suggests that is it suitable for this application. We were able to demonstrate under near-clinical conditions that this pump configuration lends itself well to the ECMO setting. This is the first time, to our knowledge, that this pump configuration has been used for ECMO applications. The reasons for this are many fold, but revolve principally around the cost of current axial flow devices which are generally designed for long term VAD support applications. We overcame the cost restraints by utilizing a novel direct drive mechanism which proved suitable for the fairly short-term requirements of the ECMO setting, thus avoiding the need for costly and technically complex rotor levitation technology. Although we recognize the technical superiority of the levitation system, the fixed-axis arrangement offered by the direct drive mechanism has some advantages, particularly with regard to the capability to manually drive the system with ease under power failure conditions and the assurance that direct drive provides with regard to maintenance of a fixed, non-eccentric axis. The use of direct drive did however introduce some additional design challenges, not least the fact that the flow path through the device could not be linear. The need to compensate for the presence of a drive mechanism resulted in an angled inlet to permit the introduction of the shaft. This orientation, although somewhat less than ideal, proved to be of little consequence in terms of device function or safety, but it is an area where some improvement will be required in future iterations of the device. Overall, we found that the axial flow configuration was easily incorporated into our integrated device and was associated with acceptable hydrodynamic and haemodynamic performance. Ultimately, we were able to examine the performance of our pump under near-clinical large animal conditions and were able to derive considerable information from this exercise. The

critical relationship between pre-load and after-load was apparent in this aspect of the work. We were able, for example to describe quite clearly the inlet conditions required for safe and effective delivery of blood flow under these experimental conditions. These data, in tandem with other data generated in this work, has confirmed that we have a clinically useable technology, which both lends itself to integration and, critically, meets the needs of the clinical ECMO community without introducing a radical change in policy.

The heat exchange element of the conventional ECMO circuit is the part of the system which limits mobility and is responsible for a large part of the extensive footprint of these complex technologies. The reliance of conventional ECMO systems on a water reservoir, water pump and blood/water heat exchanger positioned into the arterial line of the system, with a need for access to mains power and water supplies represents a considerable challenge if the system is to be deployed in less intensive or mobile environments. The drive to miniaturize and integrate the three major components of the ECMO system as the focus of the present work required that the approach to providing thermal control be reconsidered. A number of attempts at providing alternative thermal control interfaces were considered and studied in this work, although only the final approach was reported. An early attempt to provide temperature control by controlling the temperature of the ventilating gas to the oxygenator, using the oxygenator hollow fiber membranes themselves as the heat exchange interface with the blood, proved unsuccessful. This was largely due to the poor specific heat properties of the gas and the poor thermal conductance of the gas exchange fibers. However, there was some evidence that temperature could be maintained by this method in the face of low heat loss conditions in the system. It was however quite clear that this approach was not going to offer any degree of patient hypothermic/hyperthermic control. Another approach was therefore required to enable patients to be maintained in a controllable hypothermic/hyperthermic state, which may be required for some clinical settings. To achieve this without reliance on mains water supplies to the heat exchanger we investigated the use of Peltier temperature control chips as the blood temperature control

interface. These devices commonly employed in industrial and consumer goods industries have a number of desirable characteristics in terms of their potential inclusion in an integrated ECMO system. They can be manufactured in a wide range of sizes and have a very small cross sectional area, they can be interfaced with a heat conducting surface using thermally conductive adhesive and they are inexpensive, to the extent that they might be considered to be a disposable item. These characteristics suggest that the Peltier approach may be suitable for our application. In addition it is possible to control the temperature of the Peltier surface across a wide temperature range, affecting a cooling/heating effect by reversing the polarity of the power supply to the device. We therefore used these devices, coupled to the surface of an aluminium blood channeling chamber to control blood temperature during mock laboratory ECMO conditions and ultimately during the large animal testing. Although the Peltier devices proved not be as efficient as conventional large surface area/priming volume fluid devices in terms of heat exchange efficiency (Darling, King et al. 1994) it was apparent that this technology was perfectly capable of maintain blood temperature under normal operating conditions and of providing blood cooling and heating functions, albeit that this would take a little longer than normal with these prototype devices. The time for warming/cooling is of less importance in the ECMO setting where the modern trend is for a normothermic perfusion, or in some clinical situations, moderate hypothermic conditions (Ichiba, Killer et al. 2003; Guenther, Varelmann et al. 2009). The Peltier device was perfectly capable of maintaining normothermia under normal heat loss conditions, and this became perfectly clear during the large animal testing where normothermia was maintained in all experiments using this approach. The Peltier approach to thermal control therefore appears to be the ideal solution to the heat exchanger used in the integrated ECMO system, both in terms of performance and physical attributes, lending itself to integration in a miniaturized system.

The integration of the various components of the system presented particular challenges. The order of the component parts in the train of the integrated device was clear from the outset insofar as it should follow the conventional clinical sequence, pump, oxygenator,

heat exchanger. However, interfacing these components in a safe and effective manner, with a low priming volume and little "dead space" was challenging. The interfacing conduits, carrying the blood from one component to another in the sequence were designed to perform two functions; 1: To convey blood around the system and 2: To remove any air bubbles circulating through the device. This important air separation function was achieved by introducing areas of low velocity in the conduits between the primary components. This air separation element introduced between the pump and the oxygenator component also enabled more efficient distribution of blood into and through the oxygenator. Computer modeling of the flow path configuration and dimensions of these parts informed the design process and proved to be effective once the component parts were prototyped and tested in the laboratory. This process was repeated for all major components of the system and a design was completed for the integrated system which offered safety without compromising performance. Verification of this was achieved when the system was tested under near clinical ex-vivo conditions. However, it is clear that the performance of the technology as a whole could be improved in the future. The computer design and modeling was very effective in highlighting areas where the performance of the device, in particular where associated with blood flow, sheer stress and blood/material interaction could be enhanced. In general suggested iterative changes to the design were found to be appropriate, however, considerably greater improvement in performance should be possible if the manufacturing process and materials used to construct the device components were improved. Rapid prototyping of the component concepts, although convenient in producing working designs quickly, introduced some challenges relating to the quality of the prototype polymer. Latterly we moved to a "biocompatible" prototype printing polymer which offered improved biocompatibility of the overall system, but still introduced issues associated with flexibility of the printed components, particularly under higher temperature and pressure conditions. In effect, when using the printed polymer components, when the perfusate temperature was raised above 38 degrees Celsius, the polymer became flexible and we encountered problems of oxygenator bowing and of subsequent shunting of the flow. The influence of temperature on the structure of the

rotor had a similar effect, leading to either rotor failure by decoupling or material breakdown which led to macro-particulate emboli within the system. This did not present a significant problem in the animal trials as temperature was controlled within the limitations of the polymer and reinforcement of the components was introduced to offset the thermal challenge. However, when bowing did occur it was found to significantly reduce the performance of the oxygenator in particular through shunting in the region of bowing. These observations suggest that in future work, perhaps a move towards another more robust prototype manufacturing process could benefit the latter stages of such a device development program. The process developed to manufacture the fiber bundles also introduced some performance errors. The need to encapsulate (pot) the ends of the fibers using our centrifuge system without vacuum assistance resulted in excessive regions of potting at both ends of the device. Although this offers increased security in terms of the sealing of the fiber bundle, the reduction in the length of the fibers available for gas exchange had something of a negative impact upon the performance of the device. Enhancement of the potting process, using higher speeds and better control of compound introduction would resolve this and lead to an improvement in overall performance of the device as a gas exchanger. Overall however the integration process worked very well and the device performed largely as predicted by computer modeling, confirming the viability of the computer design and modeling protocol and the correlation between the computer design and the laboratory testing.

The objective of this work was to design, develop and test a new low footprint ECMO life support technology for neonatal applications. The design was informed by clinical and regulatory requirements, but a novel approach was required to integrate and miniaturize the size of the component parts which make up the system. Although a conventional approach was taken to the configuration of the oxygenator in the device, in the form of gas exchange fibers using blood outside of the fibers, novelty was required in designing the other components of the system and to achieving full integration. A formal design protocol was employed in designing the individual components of the system, and to achieving usable integration. This process consisted of concept-computer

design-computer modeling – physical modeling-physical testing, iterative steps. In this regard, we are able to produce a formal design for our device, based upon computer simulation and testing, but support this with physical testing of component parts, produced using rapid prototyping techniques. An additional benefit of this design protocol was that we were able to investigate the conformity between expected performances derived from computer modeling with physical testing. Early conceptualization of the proposed system, focused on the challenge of reducing the footprint of the conventional ECMO system and its reliance on central services, such as mains water and electricity. One of the major challenges faced by clinicians in the ECMO environment is the need for a water supply to provide thermal control of ECMO patients through an in-line heat exchanger system. Elimination of this element of the system would considerably reduce the footprint in one step. We investigated two approaches to this, the use of thermal control of the ventilating gas and the use of Peltiers as a thermal control interface. The use of thermal control of the ventilating gas proved ineffective, but the Peltier approach proved to be viable. This success enabled a radical redesign of the ECMO system for integration purposes. Keeping the device profile small and low volume was the prime aim of the integration process and largely informed the component design. We derived an axial flow pump solution which offers a very versatile form in terms of integration into the system. This together with a somewhat conventional, but geometrically novel oxygenator configuration, designed to minimize the effect of shunting, enabled the realization of a small footprint independent ECMO system. Critically we were able to demonstrate a high level of conformity in terms of function between the computer models and the results of physical testing. We had anticipated that there would be a disparity in this respect between the two approaches; however, we found that there was a fairly significant correlation between the two, suggesting that the formal design approach was inherently valid. The residual disparity between the expected and derived results was most likely due to the manufacturing process and the use of sub-optimal materials in the construction of the physical devices undergoing testing. However, we found that even taking into consideration our limited manufacturing and quality control capabilities, driven largely

by budget the final devices had acceptable performance. The final step in the work, when the device was deployed in a large animal model of ECMO, confirmed the performance and suitability of the technology for this critical setting. Further development work is of course required, but this has been identified and falls out with the scope of this research thesis. The following are the main achievements of this work;

1) The use of computational models to reduce the iterative load associated complex device development was confirmed as viable.

2) We were able to utilize an integrated rapid prototyping approach to develop working prototypes of individual components for laboratory testing.

3) There was a clear correlation between the results predicted by computational methods and those obtained in the laboratory.

4) We were able to employ computational design approach to optimizing integration thereby reducing the number of rapid prototypes required for testing.

5) It is possible to produce a fully integrated low foot print, low prime and low surface EMCO system with adequate performance characteristics suitable for clinical use.

6) The integrated ECMO system was proven computationally and in the lab was compatible with deployment under near clinical conditions.

7) The integrated ECMO design was proven capable of partially supporting a large animal under clinically mimetic conditions over an extended period of time.

8) A novel heat exchange technology was developed that allows the miniaturized and integrated system to be independent of a mains water supply

# 9. Limitations

The overriding objective of the present work was to produce a miniaturized and integrated ECMO system that will meet the operative requirements of the neonatal setting. The ultimate aim of the work was to test the technology concepts originating from this research in an animal model that is representative of the clinical setting. The overall objectives of this project were met, indeed surpassed in some respects, but there were some limitations which impacted upon aspects of scope and quality of the work. These limitations include;

- Rapid prototype material quality

The complexity of the component designs produced was such that rapid polymer prototyping was essential throughout the project. Initially the prototyping was conducted in house as the geometry and configuration of the products were frequently changing due to the iterative nature of the design process, and fast turnaround was essential to ensure the successful progression of the designs to meet the time constraints of the project.

Although fast turnaround was essential compromise was made in the quality of the products due to the properties of the material used in the rapid prototyping process. Specifically the hardness deflection temperature of the material was incapable of accommodating the conditions to which it was exposed during experimentation and as a result several prototypes failed or performed to a lower standard than was expected. During the later stages of the project with the configuration and geometry of the designs established this issue was addressed by sourcing a sub-contractor who could produce the rapid prototypes with a more appropriate material. This was a very important lesson for

similar future development work and although a limitation to the progression of the work, introduced a better understanding of the need for near manufacturing quality prototyping.

- Experimental batch sizes.

Throughout the project the batch sizes of prototypes used in the experimental work were typically small (n = 3). Ideally large batch sizes would be used to ensure consistency in the results; however it was not possible to produce large batches of prototypes within the financial constraints of the project. Additionally, testing the emerging technologies in the near-clinical animal model setting was seen as a key objective of this work. Such testing is by its very nature very expensive and limited the scope of the current project to some degree. Sacrificing numbers of prototypes for the sake of obtaining genuine clinical quality data was considered to be worthwhile in this instance.

Rapid prototyping is also a particularly expensive process and so the number of prototypes used in experimental work was limited. To compensate for the lack of physical prototypes the approach adopted throughout the project focused on producing computational simulations of the testing environment. This allowed a great deal of the design development and optimization to be carried out computationally prior to physical prototyping. As a result fewer physical iterations were required saving both time and money.

- Adherence to ISO standards.

The ISO standards provide standardized conditions and protocols to be used in the experimental evaluation of medical devices. Following these protocols allows for a

quantitative analysis of the developed products to internationally recognized standards and facilitates direct comparison with competitive devices.

Although the benefits of following the ISO standards are fully recognized the laboratory equipment and resources available to this project were such that strict adherence was not possible in all cases; however each experiment was conducted under as close an approximation to the standards as was possible and in several instances this resulted in conditions that were more taxing. For example the ISO standards for testing of a membrane oxygenator suggest an inlet blood saturation of approximately 60 % but the conditions of the blood used in the evaluation of the membrane oxygenators in this project were typically at around 20 %. However, in terms of contextualizing some of the data presented in this work non-adherence to international standards must be considered to be a limitation irrespective or any increase in challenge associated with the protocols utilized.

- Limited Departmental Resources

The laboratory in which the majority of the experimental work throughout the project was conducted had no dedicated technicians. All of the laboratory methods and techniques used had to be learnt and this increased the time required to ultimately test the product. This limitation increased the time constraints on the project but learning the relevant laboratory skills and methods lead to a deeper knowledge of the devices developed. This knowledge was fed into the design process improving the concepts and ultimately reducing the number of iterations required. Time and resource constraints frequently resulted in the need for creative “out of the box” thinking to produce fast and efficient ways to manufacture the products. An example of this creative thinking is in the adaptation of a washing machine to produce an enclosed centrifuge that allowed the oxygenation modules to be safely constructed in the lab.

# 10. Future Work

This project was essentially a proof of concept project in which demonstration of the feasibility of a highly miniaturized and integrated ECMO system was required. With the concept successfully demonstrated future work on the system is likely to focus on design for manufacturability. Further development of each of the aspects of the system is required to allow the concept to evolve into a system that is ready to be taken to clinical trials and ultimately to become a commercial device.

- Monitoring and Control Systems

In an ECMO system the following are required to be monitored to provide feedback as to the performance of the system and condition of the patient:

1. Venous saturation
2. Pre and post membrane pressure
3. Blood temperature
4. Blood flow rate
5. Bubble detection
6. Pump rotational speed
7. Peltier temperature

Throughout the project external systems were used to monitor these properties. Integration of the monitoring devices into the design of the system is required. Suitable components must be sourced; as the bulk of the system is to be disposable the components must be cheap, small, lightweight and adaptable to allow them to be efficiently integrated in to the system.

The ECMO system design should be analyzed to determine the most appropriate position for placement of the monitoring devices such that the miniaturization and integration of the system is not compromised.

- Development of a suitable holder/control interface

The disposable ECMO unit will interface with a non-disposable holder/controller. The control system will contain the motor for the blood pump, the main control circuitry, user interface and power supply for the device. Ideally the disposable ECMO unit when orientated correctly will click fit into the holder. Once in place the monitoring devices of the system should automatically interface with the controller and the motor and pump drive should also connect. The device will contain a touch screen and monitor to allow a user to control and observe the ECMO system.

- Optimization of the blood pump

Optimization of the blood pump is required to improve both haemodynamic and hydrodynamic performance. A detailed analysis of the straightener, impeller and diffuser geometries is required along with the pump geometry, orientation and impeller to casing gap size.

One of the drawbacks with the current design is the angled inlet. By changing the location of the drive to be based at the outlet it would allow the inlet to be made parallel to the pump axis. This would improve the flow through the device and should result in an improved performance and so work on producing an inverted version of the current design is required. Figure 322 below shows a cross-section of a proposed inverted pump design with the fundamental components labeled.

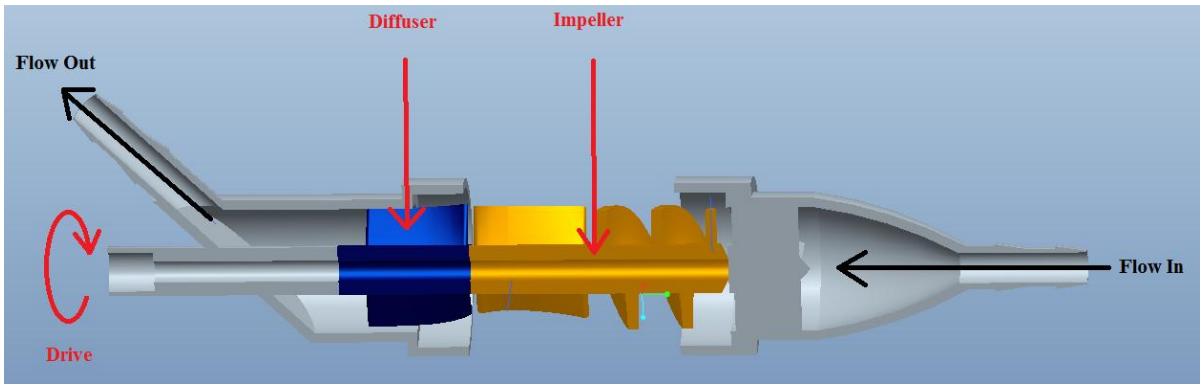


**Figure 322: ProEngineer model showing a proposed design for an inverted blood pump with the fundamental components labeled.**

Alternatives to the direct drive used in the current design should be investigated. Currently using a levitation based design is too expensive and would impact on the size of the ECMO system. Direct drive using a magnetic coupling was developed during the project; however with the resources available the prototypes developed were unreliable and time restrictions on the project meant that this concept was dropped. Further development into a magnetically coupled pump could result in a successful design. Such a system would make interfacing the system to the holder/controller a much simpler task when compared to a traditional direct drive.

The concept that was developed featured an impeller mounted onto a shaft, which had a ring of magnets at the base. The base was completely enclosed with the impeller and casing connected through diamond bearings. The inlet casing was made in two parts to allow standard bearings to be placed within the design to provide more stability and to prevent fluid passing into the lower chamber. The impeller and diffuser were connected via a second set of diamond bearings.

Figure 323and Figure 324 below show a cross-section of the model with the parts highlighted and an exploded view of the concept model.

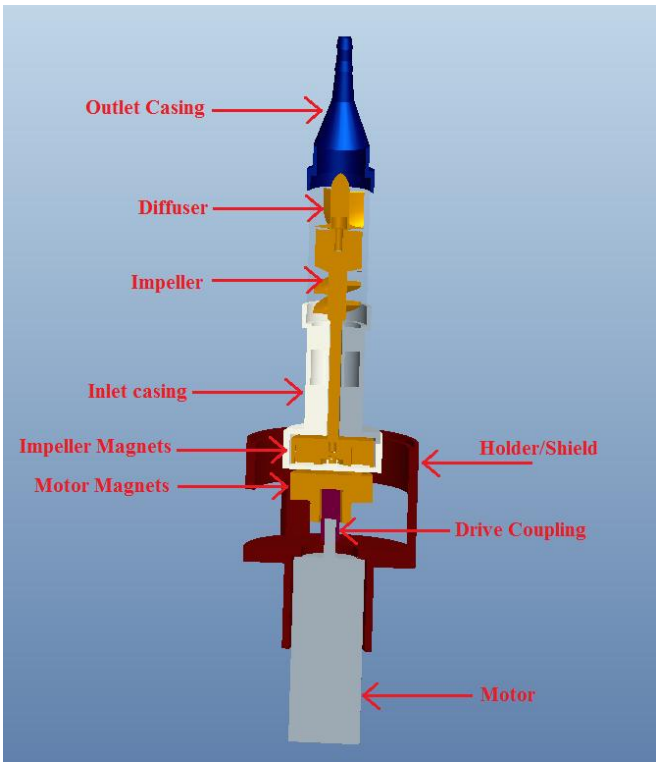


**Figure 323: Pro-engineer model showing the magnetically coupled direct drive concept with the major parts of the design labeled.**

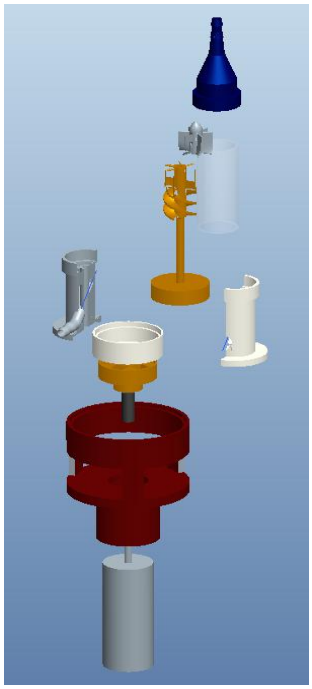

**Figure 324: Exploded view of the magnetically coupled direct drive concept.**

Figure 325and Figure 326 below show the magnets, spacers and the male diamond bearing in the base of an impeller shaft cut from aluminium and a selection of the rapid prototype parts used to construct the concept respectively.

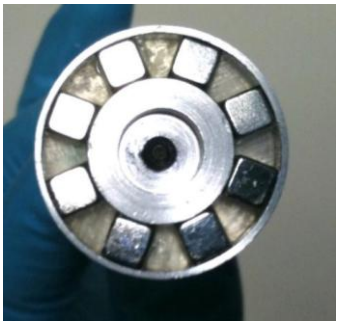

**Figure 325: Picture of an impeller shaft cut from aluminium with magnets, spacers and male diamond bearing in the base.**

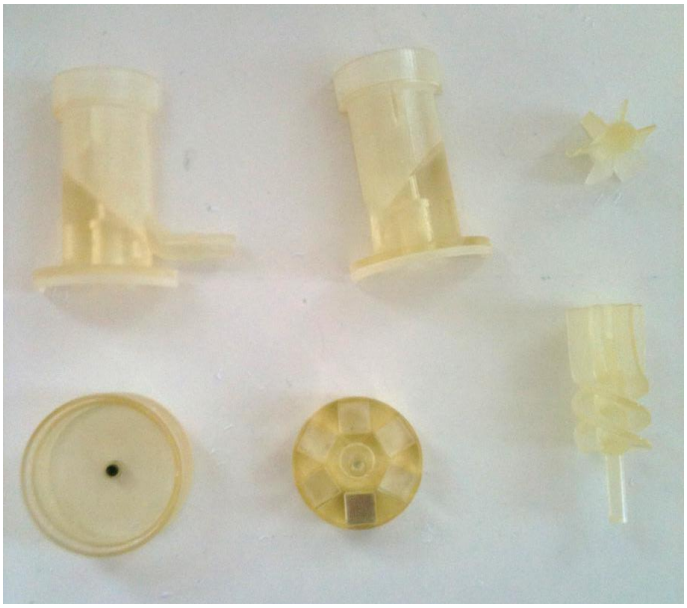

**Figure 326: Picture showing a selection of rapid prototype parts used to make the magnetically coupled direct drive axial flow blood pump.**

- Optimization of the Oxygenator

The manufacturing method used in the project to develop the oxygenator module was very basic and as a result consistency and quality issues arose. By addressing the manufacturing issues it will be possible to pack more fiber into the module increasing the quality, performance and reliability of the device.

With performance and reliability issues addressed the geometry of the oxygenator can be modified to allow for more efficient miniaturization and integration with the other components of the ECMO system.

- Optimization of the Heat Exchanger

A more detailed computational analysis into the most efficient flow path through the heat exchanger is required. The path must be optimized to make the best use of the peltier surface area and to increase the exposure time of the blood to the heat source as it passes through the device.

In general future work on any of the aspects of the system should look towards producing a solution that considers the manufacturability of the design. The configuration and integration strategy should be redesigned such that they meet the additional requirements of the manufacturing method used to create each aspect of the system. A balance must be made between the cost of device, ease of manufacturability, performance, aesthetics and ergonomics. Compromise in any one of these areas should be offset by a gain in another. An overall design strategy must be developed with the specific manufacturing methods for each aspect of the system determined. This should provide a further set of design requirements and allow for a further iteration of the design to evolve. This evolved design should be much closer to the final configuration and should have addressed the issues with the proof of concept design highlighted within this thesis.

# 11. References

Abrams, L. D. (1959). "The Practice of Total Cardio-Pulmonary By-Pass: A Short Review." Postgraduate Medical Journal: 144-148.

Aharon, A. S., D. C. Drinkwater, et al. (2001). "Extracorporeal membrane oxygenation in children after repair of congenital cardiac lesions." The Annals of Thoracic Surgery **72**: 2095-2101.

Anderson, H. I. and R. H. Bartlett (1993). "ELSO: Multicenter comparison of conventional venoarterial access versus venovenous double-lumen catheter access in newborn infants undergoing extracorporeal membrane oxygenation." Journal of Pediatric Surgery **28**: 530-535.

Andrew, M., B. Paes, et al. (1990). "Development of the hemostatic system in the neonate and young infant." American Journal of Pediatric Hematology Oncology **12**: 95-104.

Arens, J., H. Schnoring, et al. (2008). "Development of a Miniaturized Heart-Lung Machine for Neonates With Congenital Heart Defect." American Society for Artificial Intelegent Organs: 509-513.

Arlt, M., A. Philipp, et al. (2012). "Early experiences with miniaturized extracorporeal life-support in the chatheterization laboratory." European Journal of Cardiothoracic Surgery.

Armainsson, L. T., M. N. Ilbawi, et al. (1995). "Reconstruction of the Carotid Artery Following Extracorporeal Membrane Oxygenation (ECMO)." Vascular and Endovascular Surgery **29**: 345-349.

Bartlett, R. H. (2005). "Historical Perspectives: Extracorporeal Membrane Oxygenation (ECMO)." Neoreviews **6**: 251-254.

Bartlett, R. H., A. B. Gazzaniga, et al. (1976). "Extracorpreal membrane oxygenation (ECMO) cardiopulmonary support in infancy." Transactions of the American Society for Artificial Internal Organs **22**: 80-93.

Bartlett, R. H., J. Toomasian, et al. (1986). "Extracorporeal Membrane Oxygenation (ECMO) in Neonatal Respiratory Failure." Annals of Surgery **204**(3): 236-244.

Bernstein, E. F. and L. R. Gleason (1967). "Factors influencing hemolysis with roller pumps." Surgery **61**: 432-442.

Beurtheret, S., C. Mastroianni, et al. (2012). "Extracorporeal Membrane Oxygenation for 2009 Influenza A (H1N1) Acute Respiratory Distress Syndrome: Single-Centre Experience with 1-Year Follow-up." European Journal of Cardiothoracic Surgery **41**(3): 4.

Bluestein, M. and L. F. Mockros (1969). "Hemolytic effects of energy dissipation in flowing blood." Medical and Biological Engineering and Computing **7**(1): 16.

Brown, K. L. and A. P. Goldman (2008). "Neonatal extra-corporeal life support: Indications and limitations." Early Human Development **84**: 143-148.

Brown, W. R., D. M. Moody, et al. (2000). "Longer Duration of Cardiopulmonary Bypass Is Associated With Greater Numbers of Cerebral Microemboli." Stroke **31**: 707-713.

Burda, G., H. Trittenwein, et al. (2004). "Testing of Extracorporeal Membrane Oxygenation Circuit Related Hemolysis Using Long-term Stored Packed Red Cells and Fresh Frozen Plasma." Artificial Organs **28**(5): 496-517.

Burgreen, G. W., Antaki, J. F., Wu, Z. J., Holmes, A. J. (2001). "Computaitonal Fluid Dynamics as a Development Tool for Rotary Blood Pumps." Artificial Organs **25**(5): 4.

Catapano, G., H. D. Papenfuss, et al. (2001). "Mass and Momentum Transport in Extra-luminal flow (ELF) Membrane Devices for Blood Oxygenation." Journal of membrane Science **184**: 123-135.

Chang, A. C. (1998). Pediatric cardiac intensive care, Lippincott Williams & Wilkins.

Chaturvedi, R. R., D. Macrae, et al. (2004). "Cardiac ECMO for biventricular hearts after paediatric open heart surgery." Heart **90**: 545-551.

Chenoweth, D. (1987). "Complement Activation in Extracorporeal Circuits." Annals of the New York Academy of Sciences **516**: 306-313.

Chimenti, M., Varela, L., de Forteza, E., Favaloro, R. (2004). "Computational Fluid Dynamics Analysis of a Novel Axial Flow Blood Pump with Two Counter-Rotating Impellers." Mecanica Computacional **23**: 7.

Cianchi, G., M. Bonizzoli, et al. (2011). "Ventilatory and ECMO treatment of H1N1-induced severe respiratory failure: results of an Italian referral ECMO center." BMC Pulmonary Medicine **11**(2).

Cloherty, J. P., E. C. Eichenwald, et al. (2012). Manual of Neonatal Care, Lippincott Williams and Wilkins.

Clowes, G. H. (1960). "Extracorporeal Maintanence of Circulation and Respiration." Physiology Review **40**(4): 826-919.

Clowes, G. H. and W. E. Neville (1958). "Membrane oxygenator." Extracorporeal Circulation: 81-100.

Cohn, L. H. (2003). "Fifty Years of Open-Heart Surgery." Circulation **107**: 3.

Cooley, D. A. (1987). "Development of the roller pump for use in cardiopulmonary bypass." Texas Heart Institute Journal **14**(2): 113-118.

Cornish, J. D., D. R. Gerstmann, et al. (1986). "Inflight use of extracorporeal membrane oxygenation for severe neonatal respiratory failure." Perfusion **1**: 281-287.

Courtney, J. M., N. M. K. Lamba, et al. (1994). "Biomaterials for blood-coating applications." Biomaterials **15**(10): 7.

Crane, K. A., D. Brown, et al. (1983). "Further decrease in subclinical hemplysis utilizing 12.7 mm tubing in arterial roller head." The Annals of Thoracic Surgery **35**: 463-465.

Cross, F. S., R. M. Berne, et al. (1956). "Evolution of a rotating disc type reservoir oxygenator." Proceedings of the Society for Experimental Biology and Medicine **93**: 210-214.

Curtis, J. J., C. C. Wagner-Mann, et al. (1994). "In Vitro Evaluation of Five Commercially Available Perfusion Systems." International Journal of Angiology **3**: 128-133.

Dalton, H. J., P. T. Rycus, et al. (2005). "Update on Extracorporeal Life Support 2004." Seminars in Perinatology **29**: 24-33.

Darling, E. M., C. L. King, et al. (1994). "Comparison of four stainless steel heat exchangers for neonatal ECMO applications." The Journal of Extra-corporeal Technology **26**(2): 5.

Davies, A., D. Jones, et al. (2009). "Extracorporeal Membrane Oxygenation for 2009 Influenza A(H1N1) Acute Respiratory Distress Syndrome." The Journal of the American Medical Association **302**(17): 7.

DeAngelis, G. A., D. G. Mitchell, et al. (1992). "Right Common Carotid Artery Reconstruction in Neonates after Extracorporeal Membrane Oxygenation: Color Doppler Imaging." Radiology **182**: 521-525.

Dehbahani, M., Behr, M., Hormes, M., Steinseifer, U., Arora, D., Coronado, O., Pasquali, M. (2009). "A Review of Computational Fluid Dynamics Analysis of Blood Pumps." European Journal of Applied Mathematics **20**: 28.

Delius, R., H. Anderson, et al. (1993). "Venousvenous compares favorably with venoarterial access for extracorporeal membrane oxygenation." The Journal of Thoracic and Cardiovascular Surgery **106**(2): 329-338.

DeWall, R. A. (2003). "The evolution of the helical reservoir pump-oxygenator system at the University of Minnesota." The Annals of Thoracic Surgery **76**: 2210-2215.

DeWall, R. A. (2003). "Origin of the helical reservoir bubble oxygenator heart-lung machine." Perfusion **18**: 163-169.

Di Bella, I., F. Pagani, et al. (2000). "Results with the Novacor assist system and evaluation of long-term assistance." European Journal of Cardio-thoracic Surgery **18**: 112-116.

Di Russo, G. B. and G. R. Martin (2005). "Extracorporeal Membrane Oxygenation for Cardiac Disease: No Longet a Mistaken Diagnosis." Pediatric Cardiac Surgery Annual **8**: 34-40.

Diettert, G. A., B. A. Bercu, et al. (1958). "A disposable screen oxygenator." Annals of Surgery **148**(6): 959-967.

Dobell, A. R. C., M. Mitri, et al. (1965). "Biological Evaluation of Blood After Prolonged Recirculation Through Film and Membrane Oxygenators." Annals of Surgery **161**(4): 6.

Drummond, M., D. M. Braile, et al. (2005). "Technological evolution of membrane oxygenators." Brazillian Journal of Cardiovascular Surgery **20**(4): 432-437.

Duncan, B. W., A. E. Ibrahim, et al. (1998). "Use of rapid-deployment extracorporeal membrane oxygenation for the resuscitation of pediatric patients with heart disease after cardiac arrest." The Journal of Thoracic and Cardiovascular Surgery **116**: 305-309.

Eash, H. J., H. M. Jones, et al. (2004). "Evaluation of Plasma Resistant Hollow Fiber Membranes For Artificial Lungs." American Society of Artificial Internal Organs **50**: 491-497.

ELSO (2007). "International Summary." Extracorporeal Life Support Organisation.

Estafanous, F. G., P. G. Barash, et al. (2001). Cardiac anesthesia: Principles and clinical practice, Lippincott Williams & Wilkins.

Fortenberry, J. D., V. Bhardwaj, et al. (1996). "Neutrophil and cytokine activation with neonatal extracorporeal membrane oxygenation." The Journal of Paediatrics **128**(5): 8.

Fraizier, O. H., T. J. Myers, et al. (2002). "Initial Clinical Experience With the Jarvik 2000 Implantable Axial-Flow Left Ventricular Assist System." Circulation **105**: 2855-2860.

Frenckner, B. and P. Radell (2008). "Respiratory failure and extracorporeal membraneoxygenation." Seminars in Pediatric Surgery **17**: 34-41.

Gage, K. L. G., M. J.; Burgreen, G. W.; Wagner, W. R; (2002). "Predicting Membrane Oxygenator Pressure Drop Using Computational Fluid Dynamics." Artificial Organs **27**(7): 8.

Gariboldi, V., D. Grisoli, et al. (2011). "Mobile extracorporeal membrane oxygenation unit expands cardiac assist surgical programs." Annals of Thoracic Surgery **90**(5): 1548-1552.

Gaylor, J. D. S., S. Hickey, et al. (1994). "Membrane oxygenators: influence of design on performance." Perfusion **9**: 173-180.

Gaylor, J. D. S. and L. F. Mockros (1978). "Novel method for fabricating capillary membrane oxygenators." Medical and Biological Engineering and Computing **16**: 369-378.

Gershfeld, N. L. and M. Murayama (1988). "Thermal Instability of Red Blood Cell Membrane Bilayers: Temperature Dependence of Hemolysis." Journal of Membrane Biology **101**: 5.

Gibbon, J. H. J. (1954). "The application of a mechanical heart and lung apparatus to cardiac surgery." Minnesota Medicine **37**: 171-180.

Gibbon, J. H. J. (1997). "The first 20 years of the heart and lung machine." Texas Heart Institute Journal **24**(1): 1-8.

Gill, B. S., H. L. Neville, et al. (2002). "Delayed instituation of Extracorporeal Membrane Oxygenation Is Associated With Increased Mortality Rate and Prolonged Hospital Stay." Journal of Pediatric Surgery **37**: 7-10.

Goldstein, D. J. (2003). "Worldwide Experience With the MicroMed DeBakey Ventricular Assist Device as a Bridge to Transplantation." Circulation **108**: 272-277.

Gourlay, T. (2012). Historical Development of Minimized Cardiopulmonary Bypass. Oxford, Woodhead Publishing Ltd.

Gourlay, T., J. Fleming, et al. (1990). "Evaluation of a Range of Extracorporeal Membrane Oxygenators." Perfusion **5**(2): 16.

Gourlay, T., I. Samartzis, et al. (2003). "Inflammatory Response of Rat and Human Neutrophils Exposed to Di-(2-ethyl-hexyl)-phthalate-Plasticized Polyvinyl Chloride." Artificial Organs **27**(3): 256-260.

Gourlay, T., I. Samartzis, et al. (2003). "The effect of haemodilution on blood-biomaterial contact-mediated CD11b expression on neutrophils: ex vivo studies." Perfusion **18**: 87-93.

Gourlay, T., D. Stefanou, et al. (2001). "The Effect of Circuit Surface Area on CD11b(mac-1) Expression in a Rat Recirculation Model." Artificial Organs **26**(6): 4.

Gourlay, T., D. Stefanou, et al. (2002). "The Effect of Methanol Washing of Plasticized Polyvinyl Chloride on Biomateral-Contact-Mediated CD11b (mac-1) Expression in a Rate Recirculation Model." Artificial Organs **26**(1): 5-9.

Graefe, R., R. Borchardt, et al. (2010). "Improving Oxygenator Performance Using Computational Simulation and Flow Field-Based Parameters." Artificial Organs **34**(11): 6.

Graulich, J., J. Sonntag, et al. (2002). "Complement activation by invivo neonatal and in vitro extracorporeal membrane oxygenation." Mediators of Inflammation **11**(4): 69.

Graves, D. F., J. M. Chernin, et al. (1996). "Anticoagulation practices during neonatal extracorporeal membrane oxygenation: survey results." Perfusion **11**: 461-466.

Guenther, U., D. Varelmann, et al. (2009). "Extended therapeutic hypothermia for several days ducting extracorporeal membrane-oxygenation after drowning and cardiac arrest: Two cases of survival with no neurological sequelae." Resuscitation **80**: 3.

Habib, R. H., A. Zacharias, et al. (2003). "Adverse Effects of Low Hematocrit During Cardiopulmonary Bypass in the Adult: Should current practice be changed?" The Journal of Thoracic and Cardiovascular Surgery **125**: 12.

Haines, N. M., P. T. Rycus, et al. (2009). "Extracorporeal Life Support Registry Report 2008: Neonatal and Pediatric Cardiac Cases." American Society of Artificial Internal Organs **55**: 111-116.

Hamada, Y., T. Kohtani, et al. (2001). "Blood transfusion under cardiopulmonary bypass is a possible inducer for inflammation?" Kyobu Geka **54**(10): 4.

Hamrick, S. E. G., D. B. Gremmels, et al. (2003). "Neurodevelopmental Outcome of Infants Supported With Extracorporeal Membrane Oxygenation After Cardiac Surgery." Pediatrics **111**: 671-675.

Haworth, W. S. (2003). "The Development of the Modern Oxygenator." The Annals of Thoracic Surgery **76**: 2216-2219.

Heimbecker, R. O. (1977). "Letter to Editor. Atraumatic perfusion and the membrane lung; a quiet revolution." European Surgical Research **9**(1): 1-2.

Herron, D. M., R. Grabowy, et al. (1997). "The Limits of Bloodwarming: Maximally Heating Blood with an Incline Microwave Bloodwarmer." The Journal of Trauma **43**(2): 2.

Hill, J. D. (1977). "Acute pulmonary failure: treatment with extracorporeal oxygenation." Medical Instrumentation **11**: 198-201.

Hill, J. D., T. G. O'Brien, et al. (1972). "Prolonged extracorporeal oxygenation for acute post-traumatic respiratory failure (shock-lung syndrome). Use of the Bramson membrane lung." New England Journal of Medicine **286**(12): 629-634.

Hintz, S. R., D. M. Suttner, et al. (2000). "Decreased Use of Neonatal Extracorporeal Membrane Oxygenation (ECMO): How New Treatment Modalities Have Affected ECMO Utilization." Pediatrics **106**: 1339-1343.

Horton, A. M. and W. Butt (1992). "Pump-induced haemolysis: is the constrained vortex pump better or worse than the roller pump?" Perfusion **7**: 103-108.

Hoshi, H., J. Asama, et al. (2005). "Disposable Magnetically Levitated Centrifugal Blood Pump: Design and In Vitro Performance." Artificial Organs **29**(7): 520-526.

Hoshi, H., S. Takatani, et al. (2005). "Development of Magnetically Levitated Centrifugal Blood Pump System." Papers of Technical Meeting on Linear Devices **05**(44): 5-10.

Ichiba, S., H. M. Killer, et al. (2003). "Pilot investigation of hypothermia in neonates receiving extracorporeal membrane oxygenation." Archives of Diseases in Childhood - Fetal and Neonatal Edition **88**: 128-133.

Iwahashi, H., K. Yuri, et al. (2004). "Development of the Oxygenator: Past, Present and Future." Journal of Artificial Organs **7**: 111-120.

Karle, V. A., B. L. Short, et al. (1997). "Extracorporeal membrane oxygenation exposes infants to the plasticizer, di(2-ethylhexyl)phthalate." Critical Care Medicine **25**(4): 696-703.

Kawahito, K. and Y. Nose (1997). "Hemolysis in Different Centrifugal Pumps." Artificial Organs **21**(4): 323-326.

Kawahito, S., T. Maeda, et al. (2002). "Hemolytic Characteristics of Oxygenators During Clinical Extracorporeal Membrane Oxygenation." American Society of Artificial Internal Organs **48**(6): 636-639.

Kawahito, S., T. Motomura, et al. (2002). Annals of Thoracic and Cardiovascular Surgery **8**(5): 268-274.

Kawahito, S., T. Motomura, et al. (2002). "Development of a New Hollow Fiber Silicone Membrane Oxygenator for ECMO: The Recent Progress." Annual of Thoracic Cardiovascular Surgery **8**(5): 268-274.

Khoshbin, E., N. Roberts, et al. (2005). "Poly-Methyl Pentene Oxygenators Have Improved Gas Exchange Capability and Reduced Transfusion Requirements in Adult Extracorporeal Membrane Oxygenation." American Society of Artificial Internal Organs **51**: 281-287.

Kim, W. G. and C. J. Yoon (1998). "Roller Pump Induced Tubing Wear of Polyvinylchloride and Silicone Rubber Tubing: Phase Contrast and Scanning Electron Microscopic Studies." Artificial Organs **10**(22): 892-897.

Kirkpatrick, A. W., R. Chun, et al. (1999). "Hypothermia and the Trauma Patient." Canadian Journal of Surgery **42**(5): 10.

Klotz, S., M. C. Deng, et al. (2004). "Left Ventricular pressure and volume unloading during pulsatile versus nonpulsatile left ventricular assist device support." The Annals of Thoracic Surgery **77**: 143-149.

Kolff, W. J. (1997). "The Artificial Kidney: A Dialyzer with great area." Journal of the American Society of Nephrology **8**(12): 1959-1965.

Kolff, W. J., B. Watschinger, et al. (1956). "Results in patients treated with the coil kidney (disposable dialyzing unit)." Journal of the American Medical Association **11**(16): 1433-1437.

Kolobow, T. and R. L. Bowman (1963). "Construction and Evaluation of an Alveolar Membrane Artificial Heart-Lung." Transactions of the American Society for Artificial Internal Organs **9**: 238-243.

Kolobow, T., R. G. Spragg, et al. (1971). "Extended Term (To 16 Days) Partial Extracorporeal Blood Gas Exchange with the Spiral Membrane Lung in Unanesthetized

Lambs." Transactions of the American Society for Artificial Internal Organs **17**: 350-354.

Kurusz, M., E. W. Christman, et al. (1980). "Roller Pump Induced Tubing Wear: Another Argument in Favour of Arterial Line Filtration." The Journal of Extra-Corporeal Technology **12**(2): 49-59.

Langenbacher, D., T. Nield, et al. (2001). "Neurodevelopmental Outcome of ECMO Survivors at Five Years of Age: The Potential for Academic and Motor Difficulties." The Journal of Special Education **35**(3): 156-160.

Lawson, S., C. Ellis, et al. (2011). "Neonatal extracorporeal membrane oxygenation devices, techniques and team roles: 2011 survey results of the United States' Extracorporeal Life Support Organization centers." The Journal of Extra-corporeal Technology **43**(4): 8.

Lee, S. S., K. H. Ahn, et al. (2004). "Shear Induced Damage of Red Blood Cells Monitored by the Decrease of their Deformability." Korea-Austraila Rheology Journal **16**(3): 5.

Leonard, R. J. (2003). "The transition from the bubble oxygenator to the microporous membrane oxygenator." Perfusion **18**: 179-183.

Lequier, L. (2004). "Extracorporeal Life Support in Pediatric and Neonatal Critical Care: A Review." Journal of Intensive Care Medicine **19**: 243-258.

Lequier, L. and A. Chan (2005). "Anticoagulation during extracorpreal life support." Progress in Pediatric Cardiology **21**: 81-85.

Leshchinskii, B. M., G. P. Itkin, et al. (1990). "Centrifugal pumps for blood forcing: Technical Aspects." Meditsinskaya Tekhnika **1**: 28-31.

Levy, M. S., J. C. Share, et al. (1995). "Fate of the Reconstructed Carotid Artery After Extracorporeal Membrane Oxygenation." Journal of Pediatric Surgery **30**(7): 1046-1049.

Mahoney, C. B. (1998). "Heparin-bonded circuits: clinical outcomes and costs." Perfusion **13**: 192-204.

Marasco, S., G. Lukas, et al. (2008). "Review of ECMO Support in Critically Ill Adult Patients." Heart, Lung and Circulation **17**: 41-47.

Martini, F. (2005). "Fundamentals of Anatomy and Physiology." Pearson Education **(7th Edition)**.

Matsuda, N. N., M.; Sakai, K.; Kuwana, K.; Tahara, K. (1999). "Theoretical and Experimental Evaluation for Blood Pressure Drop and Oxygen Transfer Rate in Outside Blood Flow Membrane Oxygenator." Journal of Chemical Engineering of Japan **32**(6): 8.

Melrose, D. G. (1953). "A Mechanical Heart-Lung for use in Man." British Medical Journal **2**: 57-62.

Melrose, D. G. (1959). "Pumping and Oxygenating Systems." The British Journal of Anaesthesia **31**: 393-400.

Meyns, B., L. Vercaemst, et al. (2005). "Plasma leakage of oxygenators in ECMO depends on the type of oxygenator and on patient variables." The international Journal of Artificial Organs **28**(1): 1-5.

Moen, O., E. Fosse, et al. (1994). "Roller and centrifugal pumps compared in vitro with regard to haemolysis, granulocyte and complement activation." Perfusion **9**: 109-117.

Mongero, L. B., J. R. Beck, et al. (1998). "Clinical evaluation of setting pump occlusion by the dynamic method: effect on flow." Perfusion **13**: 360-368.

Montgomery, V. L., J. M. Strotman, et al. (2000). "Impact of multiple organ system dysfunction and nosocomial infections on survival of children treated with extracorporeal membrane oxygenation after heart surgery." Critical Care Medicine **28**(2): 526-531.

Moon, Y. S., S. Ohtsubo, et al. (1996). "Comparison of centrifugal and roller pump hemolysis rates at low flow." Artificial Organs **20**(6): 579-581.

Morgan, I. S., M. Codispoti, et al. (1998). "Superiority of centrifugal pump over roller pump in paediatric cardiac surgery: prospective randomised trial." The European Journal of Cardio-Thoracic Surgery **13**: 526-532.

Motomura, T., T. Maede, et al. (2003). "Development of Silicone Rubber Hollow Fiber Membrane Oxygenator for ECMO." Artificial Organs **27**(11): 1050-1056.

Muntean, W. (1999). "Coagulation and Anticoagulation in Extracorporeal Membrane Oxygenation." Artificial Organs **23**(11): 979-983.

Murakami, T., L. R. Golding, et al. (1979). "Nonpulsatile biventricular bypass using centrifugal blood pumps." Japanese Journal of Artificial Organs **8**: 636-639.

Nakata, K., T. Maeda, et al. (2000). "Development of a new silicone membrane oxygenator for ECMO." annals of Thoracic and Cardiovascular Surgery **6**(6): 373-377.

Nixon, P. G. F., V. A. Grimshaw, et al. (1960). "Clinical Experience with the Melrose oxygenator at normal and reduced temperature." Thorax **15**: 193-197.

Noon, G. P., L. E. Kane, et al. (1985). "Reduction of Blood Trauma in Roller Pumps for Long-term Perfusion." World Journal of Surgery **9**: 65-71.

Nose, Y. and P. S. Malchesky (1981). "Therapeutic membrane plasmapheresis." In: Therapeutic plasmapheresis. Oda, T (ed) Stuttgart: F.K. Schattauer.: 3-14.

Olsen, D. B. (2000). "The History of Continuous-Flow Blood Pumps." Artificial Organs **6**(24): 401-404.

Paparella, D., T. M. Yau, et al. (2002). "Cardiopulmonary bypass induced inflammation: pathophysiology and treatment. An update." European Journal of Cardio-thoracic Surgery **21**: 12.

Pedersen, T., V. Videm, et al. (1997). "Extracorporeal Membrane Oxygenation Using a Centrifugal Pump and a Servo Regulator to Prevent Negative Inlet Pressure." The Annals of Thoracic Surgery **63**: 1333-1339.

Peek, G. J., K. Wong, et al. (1999). "Tubing failure during prolonged roller pump use: a labratory study." Perfusion **14**: 443-452.

Perepechkin, L. P. and N. P. Perepechkina (1999). "Hollow Fibres for Medical Applications. A Review." Fibre Chemistry **31**(6): 411-420.

Qian, K. X., Wang, F. Q., Zeng, P., Ru, W. M., Yuan, H. Y., Feng, Z. G. (2006). "Computational Fluid Dynamics Verified the Advantages of Streamlined Impeller Design in Improving flow patterns and Anti-Haemolyisis Properties of Centrifugal Pump." Journal of Medical Engineering and Technology **30**(6): 4.

Rais-Bahrami, K., S. Nunez, et al. (2004). "Follow-Up Study of Adolescents Exposed to Di(2-Ethylhexyl) Phthalate (DEHP) as Neonates on Extracorporeal Membrane Oxygenation (ECMO) Support." Environmental Health Perspectives **112**(1339-1340): 1339.

Rais-Bahrami, K., A. E. Wagner, et al. (2000). "Neurodevelopmental Outcome in ECMO Vs Near-Miss ECMO Patients at 5 Years of Age." Clinical Pediatrics **39**: 145-152.

Rais-Bahrami, K., D. M. Walton, et al. (2002). "Improved oxygenation with reduced recirculation during venovenous ECMO: comparison of two catheters." Perfusion **17**: 415-419.

Reul, H. M. and M. Akdis (2000). "Blood pumps for circulatory support." Perfusion **15**: 295-311.

Reul, H. M. and M. Akdis (2000). "Blood Pumps for Circulatory Support." Perfusion **15**: 16.

Rinder, C. S., J. L. Bonan, et al. (1992). "Cardiopulmonary Bypass Induces Leukocyte-Platelet Adhesion." Blood **79**(5): 4.

Robertson, C. M. T., N. N. Finer, et al. (1995). "Neurodevelopmental Outcome After Neonatal Extracorporeal Membrane Oxygenation." Canadian Medical Association Journal **152**(12): 1981-1988.

Roncon-Albuquerque, R., C. Basilio, et al. (2012). "Portable miniaturized extracorporeal membrane oxygenation systems for H1N1-related severe acute respiratory distress syndrome: A case series." Journal of Critical Care: 1-10.

Roy, B. J., P. T. Rycus, et al. (2000). "The Changing Demographics of Neonatal Extracorporeal Membrane Oxygenation Patients Reported to the Extracorporeal Life Support Organization (ELSO) Registry." Pediatrics **106**: 1334-1338.

Saito, S. and T. Nishinaka (2005). "Chronic nonpulsatile blood flow is compatible with normal end-organ function: implications for LVAD development." Journal of Artificial Organs **8**: 143-148.

Saito, S., S. Westaby, et al. (2002). "End-organ function during chronic nonpulsatile circulation." The Annals of Thoracic Surgery **74**: 1080-1085.

Sakaki, M., Y. Taenaka, et al. (1994). "Influences of nonpulsatile pulmonary flow on pulmonary function: Evaluation in a chronic animal model." The Journa of Throracic and Cardiovascular Surgery **108**: 495-502.

Sallam, A. M., Hwang. N. H. (1984). "Human Red Blood Cell Hemolysis in a Turbulent Shear Flow: Contribution of Reynolds Shear Stresses." Biorheology **21**(6): 783-797.

Schneider, B., J. Schena, et al. (1989). "Exposure to di (2-ethylhexyl) phthalate in infants receiving extracorporeal membrane oxygenation." New England Journal of Medicine **320**: 1563.

Schumacher, R. E., D. Roloff, et al. (1993). "Extracorporeal Membrane Oxygenation in Term Newborns: A Prospective Cost-Benefit Analysis." American Society of Artificial Internal Organs **39**: 873-879.

Segers, P. A., J. F. Heida, et al. (2001). "Clinical evaluation of nine hollow-fibre membrane oxygenators." Perfusion **16**: 95-106.

Setz, K., K. Kesser, et al. (1992). "Comparison of a New Venous Control Device with a Bladder Box System for Use in ECMO." American Society of Artificial Internal Organs **38**(4): 835-840.

Shanley, C. J., R. B. Hirschl, et al. (1994). "Extracorporeal Life Support for Neonatal Respiratory Failure: A 20-Year Experience." Annals of Surgery **220**(3): 269-282.

Sharp, K. M., Mohammad, F. S. (1998). "Scaling of Hemolysis in Needles and Catheters." Annals of Biomedical Engineering **26**: 9.

Sinard, J. M. and R. H. Bartlett (1990). "Review Articles: Extracorporeal membrane oxygenation (ECMO): Prolonged bedside cardiopulmonary bypass." Perfusion **5**: 239-249.

Sirotkina, M. G., O. A. Osipov, et al. (1970). "Review and Analysis of Membrane Oxygenators." Meditsinskaya Tekhnika(3): 43-51.

Skeggs, L. T. (2000). "Persistence ... and Prayer: From the Artificial Kidney to the AutoAnalyzer." Clinical Chemistry **46**(9): 1425-1436.

Slater, J. P., E. A. Rose, et al. (1996). "Low Thromboembolic Risk Without Anticoagulation Using Advanced-Design Left Ventriculat Assist Devices." The Annals of Thoracic Surgery **62**: 1321-1327.

Smith, C. E. and K. Wagner (2008). "Principles of Fluid and Blood Warming in Trauma." International TraumaCare **18**(1): 8.

Smith, J. H. (2007). "ECMO, VAD and Circulatory Support." Procedures of the Paediatric Intensive Care Unit: 1-105.

Snyder, E. J., S. Weckerly, et al. (1989). "A positive/negative pressure monitor for use in neonatal extracorporeal membrane oxygenation." Perfusion **4**: 283-289.

Stolar, C. J. H., M. A. Crisafi, et al. (1995). "Neurocognitive Outcomes for Neonates Treated With Extracoporeal Membrane Oxygenation: Are Infants With Congenital Diaphragmatic Hernia Different?" Journal of Pediatric Surgery **30**(2): 366-372.

Suma, K., T. Tsuji, et al. (1981). "Clinical performance of microporous polypropylene hollow-fiber oxygenator." The Annals of Thoracic Surgery **32**: 558-562.

Sutera, S. P., Mehrjardi, M.H. (1975). "Deformation and Fragmentation of Human Red Blood Cells in Turbulent Shear Flow." Biophysical Journal **15**: 1-10.

Takahashi, T. and W. R. J. (1983). "Thermal Shock Hemolysis in Human Red Cells. The Effect of Temperature, Time and Osmotic Stress." Cryobiology **20**(5): 13.

Taylor, K. M., W. H. Bain, et al. (1979). "Peripheral vascular resistance and angiotensin II levels during pulsatile and no-pulsatile cardiopulmonary bypass." Thorax(34): 594-598.

Thiara, A. P. S., T. N. Hoel, et al. (2007). "Evaluation of oxygenators and centrifugal pumps for the long-term pediatric extracorporeal membrane oxygenation." Perfusion **22**: 323-326.

Toomasian, J. M., R. J. Schreiner, et al. (2005). "A Polymethylpentene Fiber Gas Exchanger for Long-Term Extracorporeal Life Support." American Society for Artificial Intelegent Organs **51**: 7.

UCSF, M. C. (2004) Intensive Care Nursery House Staff Manual.

Undar, A. (2004). "Myths and Truths of Pulsatile and Nonpulsatile Perfusion During Acute and Chronic Cardiac Support." Artificial Organs **5**: 439-443.

University of Michigan and Section of Pediatric Surgery (2007). "Procedures: Extracorporeal Membrane Oxygenation."

Upp, J. R., P. E. Bush, et al. (1994). "Complications of neonatal extracorporeal membrane oxygenation." Perfusion **9**: 241-265.

Utley, J. R. (1990). "Pathophysiology of Cardiopulmonary Bypass: Current Issues." Journal of Cardiac Surgery **5**(3): 12.

Vasku, J., J. Wotke, et al. (2007). "Acute and chronic consequences of non-pulsatile blood flow pattern in long-term total artificial heart experiment." Pathophysiology **14**: 87-95.

Visser, C. and D. S. de Jong (1997). "Clinical evaluation of six hollow-fibre membrane oxygenators." Perfusion **12**: 357-368.

von Segesser, L. K. (1999). "Cardiopulmonary support and extracorporeal membrane oxygenation for cardiac assist." The Annals of Thoracic Surgery **68**: 672-677.

Wagner, K., G. K. Sangolt, et al. (2008). "Transportation of critically ill patients on extracorporeal membrane oxygenation." Perfusion **23**: 101-106.

Wan, S., J.-L. LeClerc, et al. (1997). "Inflammatory Response to Cardiopulmonary Bypass: Mechanisms Involved and Possible Therapeutic Strategies." Chest **112**: 16.

Westaby, S., T. Katsumata, et al. (1998). "Jarvik 2000 Heart: Potential for Bridge to Myocyte Recovery." Circulation **98**: 1568-1574.

Wieselthaler, G. M., H. Schima, et al. (2000). "First Clinical Experience With the DeBakey VAD Continuous-Axial-Flow Pump for Bridge to Transplantation." Circulation **101**: 356-359.

Wilson, B. J., H. S. Heiman, et al. (2002). "A 16-Year Neonatal/Pediatric Extracorporeal Membrane Oxygenation Transport Experience." Pediatrics **109**: 189-193.

Wilson, J. M., L. K. Bower, et al. (1996). "ECMO in Evolution: The Impact of Changing Patient Demographics and Alternative Therapies on ECMO." Journal of Pediatric Surgery **31**(8): 1116-1123.

Wolfson, P. J. (2003). "The development and use of extracorporeal membrane oxygenation in neonates." The Annals of Thoracic Surgery **76**: 2224-2229.

Yamasaki, Y., T. Hayashi, et al. (2006). "Early experience with low-prime (99ml) extracorporeal membrane oxygenation support in children." American Society of Artificial Internal Organs **52**(1): 5.

Zwischenberger, J. B., T. T. Nguyen, et al. (1994). "Complications of neonatal extracorporeal membrane oxygenation: Collective experience from the Extracorporeal Life Support Organization." The Journal of Throracic and Cardiovascular Surgery **107**: 838-849.